**GEORGIA DOT RESEARCH PROJECT 22-20**

Final Report

# QUALITY MANUAL FOR STEEL BRIDGE FABRICATION

**Office of Performance-Based Management and Research**
600 West Peachtree Street NW | Atlanta, GA 30308

**March 2026**

## TECHNICAL REPORT DOCUMENTATION PAGE

| 1. Report No.<br>FHWA-26-2220 | 2. Government Accession No.<br>N/A | 3. Recipient's Catalog No.<br>N/A |
|---|---|---|
| 4. Title and Subtitle<br>QUALITY MANUAL FOR STEEL BRIDGE FABRICATION | | 5. Report Date<br>March 2026 |
| | | 6. Performing Organization Code<br>N/A |
| 7. Authors<br>Ryan J. Sherman, PhD, PE, (ORCID 0000-0001-7525-4775),<br>Lauren K. Stewart, PhD, PE, (ORCID 0009-0001-5188-0285),<br>Matthew L. Phillips (ORCID 0000-0002-0605-6094) | | 8. Performing Organization Report No.<br>22-20 |
| 9. Performing Organization Name and Address<br>Georgia Institute of Technology<br>790 Atlantic Drive<br>Atlanta, GA 30332 | | 10. Work Unit No.<br>N/A |
| | | 11. Contract or Grant No.<br>PI #0019329 |
| 12. Sponsoring Agency Name and Address<br>Georgia Department of Transportation (SPR)<br>Office of Performance-based Management and Research<br>600 West Peachtree Street NW<br>Atlanta, GA 30308 | | 13. Type of Report and Period Covered<br>Final Report Nov 2022 – Mar 2026 |
| | | 14. Sponsoring Agency Code<br>N/A |
| 15. Supplementary Notes<br>Conducted in cooperation with the U.S. Department of Transportation, Federal Highway Administration. | | |


16. Abstract

The American Association of State Highway and Transportation Officials (AASHTO) and the American Welding Society (AWS) provide extensive guidance documents that govern the welding of steel bridge members; however, none of the documents provide guidance regarding the number of times a welding nonconformance can be repaired without penalty or rejection, leading to uncertainty in the fabrication industry and potentially costly member rejections. While a few studies have investigated the effects of multiple weld repairs, none have studied the effects of multiple repair welds on members and practices common in the steel bridge industry. As such, there is currently insufficient data to determine whether multiple repair welds affect the material properties or the fatigue life of welded joints on bridge members. The goal of the current study is to investigate the effects of multiple repair welds on complete joint penetration (CJP) butt-splice welds and suggest an appropriate limit to GDOT and the steel bridge industry on the number of repair welds that can be performed at a single location. To accomplish this goal, the current study is comprised of three main research thrusts: (a) gather existing industry data and knowledge on welding nonconformances and repairs through a literature review and survey, (b) generate novel experimental data through a suite of material characterization tests on CJP joints with up to five weld repairs, and (c) generate novel experimental data through large-scale fatigue life tests on CJP butt-splice joints with up to five weld repairs. The results of this research show that up to five weld repairs can be performed at a joint without significant changes to the material properties or fatigue life of the CJP joint. The significance of these findings is that the data suggest: (a) there are no mechanistic or fatigue life indications that a CJP butt splice joint with up to five weld repairs will perform significantly differently than a CJP joint with no repairs, and (b) the repaired joint should still meet all applicable strength and fatigue design requirements.


| 17. Key Words<br>Welding nonconformance, repair weld, complete joint penetration (CJP) joint, experimental tests, fatigue, material characterization | 18. Distribution Statement<br>No restrictions. This document is available through the National Technical Information Service, Springfield, VA 22161. |
|---|---|

| 19. Security Classification (of this report)<br>Unclassified | 20. Security Classification (of this page)<br>Unclassified | 21. No. of Pages<br>227 | 22. Price<br>Free |
|---|---|---|---|

**Form DOT 1700.7 (8-72)** Reproduction of completed page authorized.

GDOT Research Project 22-20

Final Report

# QUALITY MANUAL FOR STEEL BRIDGE FABRICATION

By

Matthew Phillips
Graduate Research Assistant

Lauren K. Stewart, Ph.D., P.E.
Professor

Ryan J. Sherman, Ph.D., P.E.
Associate Professor

Georgia Institute of Technology

Contract with
Georgia Department of Transportation

In cooperation with
U.S. Department of Transportation, Federal Highway Administration

March 2026

# SI* (MODERN METRIC) CONVERSION FACTORS

## APPROXIMATE CONVERSIONS TO SI UNITS

| Symbol | When You Know | Multiply By | To Find | Symbol |
|---|---|---|---|---|
| | | **LENGTH** | | |
| in | inches | 25.4 | millimeters | mm |
| ft | feet | 0.305 | meters | m |
| yd | yards | 0.914 | meters | m |
| mi | miles | 1.61 | kilometers | km |
| | | **AREA** | | |
| $in^2$ | square inches | 645.2 | square millimeters | $mm^2$ |
| $ft^2$ | square feet | 0.093 | square meters | $m^2$ |
| $yd^2$ | square yard | 0.836 | square meters | $m^2$ |
| ac | acres | 0.405 | hectares | ha |
| $mi^2$ | square miles | 2.59 | square kilometers | $km^2$ |
| | | **VOLUME** | | |
| fl oz | fluid ounces | 29.57 | milliliters | mL |
| gal | gallons | 3.785 | liters | L |
| $ft^3$ | cubic feet | 0.028 | cubic meters | $m^3$ |
| $yd^3$ | cubic yards | 0.765 | cubic meters | $m^3$ |
| | | NOTE: volumes greater than 1000 L shall be shown in $m^3$ | | |
| | | **MASS** | | |
| oz | ounces | 28.35 | grams | g |
| lb | pounds | 0.454 | kilograms | kg |
| T | short tons (2000 lb) | 0.907 | megagrams (or "metric ton") | Mg (or "t") |
| | | **TEMPERATURE (exact degrees)** | | |
| °F | Fahrenheit | 5 (F-32)/9<br>or (F-32)/1.8 | Celsius | °C |
| | | **ILLUMINATION** | | |
| fc | foot-candles | 10.76 | lux | lx |
| fl | foot-Lamberts | 3.426 | $candela/m^2$ | $cd/m^2$ |
| | | **FORCE and PRESSURE or STRESS** | | |
| lbf | poundforce | 4.45 | newtons | N |
| $lbf/in^2$ | poundforce per square inch | 6.89 | kilopascals | kPa |

## APPROXIMATE CONVERSIONS FROM SI UNITS

| Symbol | When You Know | Multiply By | To Find | Symbol |
|---|---|---|---|---|
| | | **LENGTH** | | |
| mm | millimeters | 0.039 | inches | in |
| m | meters | 3.28 | feet | ft |
| m | meters | 1.09 | yards | yd |
| km | kilometers | 0.621 | miles | mi |
| | | **AREA** | | |
| $mm^2$ | square millimeters | 0.0016 | square inches | $in^2$ |
| $m^2$ | square meters | 10.764 | square feet | $ft^2$ |
| $m^2$ | square meters | 1.195 | square yards | $yd^2$ |
| ha | hectares | 2.47 | acres | ac |
| $km^2$ | square kilometers | 0.386 | square miles | $mi^2$ |
| | | **VOLUME** | | |
| mL | milliliters | 0.034 | fluid ounces | fl oz |
| L | liters | 0.264 | gallons | gal |
| $m^3$ | cubic meters | 35.314 | cubic feet | $ft^3$ |
| $m^3$ | cubic meters | 1.307 | cubic yards | $yd^3$ |
| | | **MASS** | | |
| g | grams | 0.035 | ounces | oz |
| kg | kilograms | 2.202 | pounds | lb |
| Mg (or "t") | megagrams (or "metric ton") | 1.103 | short tons (2000 lb) | T |
| | | **TEMPERATURE (exact degrees)** | | |
| °C | Celsius | 1.8C+32 | Fahrenheit | °F |
| | | **ILLUMINATION** | | |
| lx | lux | 0.0929 | foot-candles | fc |
| $cd/m^2$ | $candela/m^2$ | 0.2919 | foot-Lamberts | fl |
| | | **FORCE and PRESSURE or STRESS** | | |
| N | newtons | 0.225 | poundforce | lbf |
| kPa | kilopascals | 0.145 | poundforce per square inch | $lbf/in^2$ |

* SI is the symbol for the International System of Units. Appropriate rounding should be made to comply with Section 4 of ASTM E380.
(Revised March 2003)

## TABLE OF CONTENTS

## LIST OF FIGURES

## LIST OF TABLES

## LIST OF ABBREVIATIONS AND SYMBOLS

AASHTO .....American Association of State Highway and Transportation Officials

AHT .....Asymmetric Hyperbolic Tangent

AISC .....American Institute of Steel Construction

AISI.....American Iron and Steel Institute

AMPF.....Advanced Manufacturing Pilot Facility (GA Tech)

ARP.....Approved Repair Plan

ASME .....American Society of Mechanical Engineers

ASTM .....American Standard for Testing Materials

AWS.....American Welding Society

CAFT .....Constant Amplitude Fatigue Threshold

CJP .....Complete Joint Penetration

CVN .....Charpy V-Notch

COMP .....Committee on Materials and Pavement

DIC.....Digital Image Correlation

DOR .....Direction of Roll

EGW .....Electrogas Welding

ESW .....Electroslag Welding

FCAW .....Flux Cored Arc Welding

FHWA.....Federal Highway Administration

FL.....Fusion Line (of Weld Metal and HAZ)

GDOT .....Georgia Department of Transportation

GMAW .....Gas Metal Arc Welding

HAZ .....Heat Affected Zone

HI .....Heat Input (welding parameter)

HPS .....High Performance Steels

HPU.....Hydraulic Power Unit

HV.....Vickers Hardness

INBA.....Inelastic Nonlinear Buckling Analysis

LPRM.....Load Path Redundant Member

LRFD .....Load Resistance Factor Design

MTR.....Material Test Reports

MT.....Magnetic Particle Testing (NDT)

NCHRP .....National Cooperative Highway Research Program

NDT .....Nondestructive Testing

NSBA.....National Steel Bridge Alliance

NSTM .....Nonredundant Steel Tension Member

OMAT.....Office of Materials and Testing (GDOT)

PJP.....Partial Joint Penetration

PQR.....Procedure Qualification Record

PTFE .....Polytetrafluoroethylene

PT.....Dye-Penetrant Testing (NDT)

QA.....Quality Assurance

QC .....Quality Control

QPL .....Qualified Products List

RMSE.....Root Mean Square Error

RT .....Radiographic Testing (NDT)

S-N .....Stress-Life

SAW.....Submerged Arc Welding

SEML.....Structural Engineering and Materials Laboratory (GA Tech)

SFQM.....Standard Fabrication Quality Manual

SMAW .....Shielded Metal Arc Welding

TS.....Travel Speed (welding parameter)

US .....United States

UTM.....Universal Testing Machine

VT .....Virtual Testing (NDT)

WFS .....Wire Feed Speed (welding parameter)

WPS .....Welding Procedure Specification

$\Delta\sigma$ or $(\Delta F)n$ .....Stress Range

$(\Delta F)_{TH}$.....Constant Amplitude Fatigue Threshold (per AASHTO LRFD-10)

$\varepsilon_y$.....Strain Corresponding to the Yield Strength

$A$ .....Fatigue Detail Constant (per AASHTO LRFD-10)

$m$.....Slope of the AASHTO Fatigue Resistance Curve in the Finite Life Region

$N$.....Fatigue Life Corresponding to the Stress Range

$t_f$.....Flange Thickness

$T$ .....Thickness

# EXECUTIVE SUMMARY

The American Association of State Highway and Transportation Officials (AASHTO) and the American Welding Society (AWS) organizations provide a multitude of standards and guidance documents that govern the welding of steel bridge members and components. Even so, welding nonconformances (i.e., defects or discontinuities) still occasionally appear during fabrication and must be repaired before final acceptance, with some nonconformances requiring multiple repair attempts before the nonconformance is adequately addressed. Currently, governing agencies provide no guidance to owners and fabricators on how many repair attempts can be made at a single location. This lack of guidance leads to ambiguity and disagreement between owners and fabricators about the number of repairs allowed before a member must be rejected.

Few existing studies have investigated the effects of multiple weld repairs on the behavior or fatigue life of a complete joint penetration (CJP) weld. Among these, none have directly targeted the materials, member sizes, and shop fabrication practices common to the bridge industry. As such, there is currently a lack of experimental data to determine the effects that multiple repair welds have on the behavior and fatigue life of CJP joints in bridge members. The goal of the current study is to investigate the effects of multiple repair welds on complete joint penetration (CJP) butt-splice welds and suggest an appropriate limit and quality acceptance system to GDOT and the steel bridge industry on the number of repair welds that can be performed at a single location. The objectives of the current research program to accomplish this are: (1) gather existing data and practices used in the steel bridge industry to address welding nonconformances and repairs, (2) generate novel experimental data to characterize the material properties of CJP welded joints that have been subjected to a varying number of repair welds,

(3) generate novel large-scale experimental data to characterize the fatigue performance of CJP welded joints that have been subjected to a varying number of repair welds, and (4) develop recommendations regarding quality acceptance and limits for repairing welding nonconformances. The findings from this study will be used in tandem with other relevant GDOT documents to create the first draft of the GDOT Steel Fabrication Quality Manual.

The current study is comprised of three main research thrusts: (a) gathering of existing knowledge and practices regarding welding nonconformances and repairs, (b) a material characterization experimental program, and (c) a large-scale experimental fatigue life testing program. The gathering of existing knowledge and practices for welding nonconformances and repairs consists of interviews with fabricators, a literature review, and a survey sent to representative AASHTO members in state owner agencies across the US. The material characterization experimental program consists of a suite of tests conducted on 12 specimens with CJP butt-splice welds repaired 0 - 5 times. The fatigue life experimental program consists of four large-scale tests that target built-up I-section members. Each test girder was comprised of either 3/4 in. or 1-1/2 in. flanges, and each flange contained four CJP butt-splice test joints that were repaired 0 - 5 times. The test girders were loaded in a pure tension, four-point bending configuration, with four CJP joints concurrently tested to failure or runout at a constant amplitude stress range of 24 ksi. Both the material characterization and fatigue life tests targeted A709-50W and A709-HPS70W steels.

The literature review and AASHTO member survey show that approximately half of the states surveyed use a state-specific quality manual for fabrication and implement some form of restriction on the number of allowable weld repairs, although no standard suggests this. The material characterization tests show that the number of weld repairs has little to no effect on the

ductility, yield strength, tensile strength, and impact energy of the CJP joints and the surrounding heat-affected zone (HAZ) base metals. All repaired specimens tested met the minimum strength requirements of the steel bridge industry and performed similarly to the CJP joints tested without repairs. The large-scale fatigue life tests show that the repaired CJP joints met or exceeded the design-life predictions from AASHTO, and there was no discernable trend between the number of repair welds and fatigue life of the CJP joints. Based on these findings, there appears to be no significant change in the material properties or fatigue life performance of CJP butt-splice welded joints up through five repairs.

# CHAPTER 1. INTRODUCTION

Built-up steel members are used extensively in bridges throughout the United States (US) for their shape and economic efficiencies. These members are fabricated by joining multiple steel plates by welding to form the desired cross section and member length. Many variables can influence the quality and performance of a welded joint, including the weld filler metal, welding parameters, joint type, and base material. To ensure a minimum criterion of quality and uniformity, the American Welding Society (AWS) and American Association of State Highway and Transportation Officials (AASHTO) developed standards and guidance documents for welding, with the most common document used in bridge fabrication being the *AASHTO/AWS D1.5: Bridge Welding Code* (2020). AWS D1.5 provides extensive guidance and standards for welding steel bridge members and components, including workmanship, technique, qualification, and inspection requirements. Even with this guidance, welding nonconformances (i.e., defects or discontinuities) will occasionally be found during fabrication that must be repaired, with some joints requiring multiple repair welds before being sound and passing inspection requirements.

While AASHTO/AWS D1.5 and other bridge fabrication standards from AASHTO and the Federal Highway Administration (FHWA) offer guidance on detecting and repairing welding nonconformances, little to no guidance is provided to fabricators, engineers, and owners regarding the number of repairs that can be made at a single location. This lack of guidance often leads to ambiguity and disagreements between owners and fabricators over how many repairs should be allowed, with the most extreme result being the rejection of entire bridge members for seemingly excessive repair welds at a single joint. Such disputes add significant cost and time to the project.

Limited prior research exists on multiple repair welds. Currently, no studies directly investigate the effects of multiple repair welds on the material properties and fatigue performance of ASTM A709 (ASTM 2021b) grade steels, the most commonly used grade for built-up steel bridge members in the US. As such, data are lacking to determine whether multiple repair welds at a single location influence the overall strength or expected fatigue life of built-up steel bridge members.

### 1.1. Research Goal and Objectives

The goal of the proposed research is to recommend a quality acceptance system and limits for GDOT and the steel bridge industry for relevant nonconformances (as indicated by GDOT) in fabricated steel bridge members and components. In the current research program, weld repairs—specifically, repeated weld repairs required to address welding nonconformances at the same complete joint penetration (CJP) joint—are the focus. The findings from this research are summarized and used in tandem with other relevant GDOT documents to create the first draft of a GDOT Steel Fabrication Quality Manual (SFQM). The objectives targeted to accomplish the proposed research goal are as follows:

- **Objective 1**: Gather data from national standards, governing owner agencies, and fabricators to determine the current standards, practices, and restrictions used in the steel bridge industry to detect and address various fabrication nonconformances.
- **Objective 2**: Generate and synthesize data from a suite of experimental material property tests to characterize any changes in the material properties of CJP welded joints that have been subjected to a varying number of repair welds.

- **Objective 3**: Generate and synthesize data from large-scale experimental fatigue tests to characterize any changes in the fatigue performance of CJP welded joints that have been subjected to a varying number of repair welds.
- **Objective 4**: Develop recommendations regarding quality acceptance and limits for repairing welding nonconformances and implement said recommendations in the first draft of the GDOT Steel Fabrication Quality Manual (SFQM).

### 1.2. Report Layout

To investigate the influence of multiple repair welds on the material properties and fatigue performance of ASTM A709 grade steels, a research program has been developed, and the research program and results are discussed in this report. Chapter 2 discusses relevant background on welding and bridge fabrication, welding nonconformances and repairs, previous studies on the effects of multiple repair welds, and pertinent fatigue-life design parameters for bridge members. Chapter 3 presents the findings from a literature review and survey that explored current industry practices and testing methods for detecting and correcting welding nonconformances. Chapter 4 discusses the material characterization experimental testing program, and Chapter 5 discusses the material characterization test results. Chapter 6 discusses the fatigue life experimental testing program, and Chapter 7 discusses the fatigue life test results. Chapter 8 summarizes the findings from the material characterization and fatigue life tests and presents final recommendations for quality acceptance and repair limits for welding nonconformances. Notably, the first draft of the GDOT Steel Fabrication Quality Manual was also produced as part of the current research project. Appendix D discusses the development of the SFQM and provides context on the organization of the manual.

# CHAPTER 2. BACKGROUND

## 2.1. Welding

Welding is the process of fusing two different components by heating the materials to the welding temperature using either heat or pressure, and although not always necessary, it usually includes a filler material. In the steel bridge industry, welding typically uses an electric arc to heat the components and a filler metal to form the joints needed to create built-up plate member sections and splice components. The most commonly used welds fall into two general categories: groove welds and fillet welds. Groove welds are typically used when high-strength welds or joints are needed (e.g., butt splices) and can be complete joint penetration (CJP) or partial joint penetration (PJP) welds, depending on the required penetration. Fillet welds are economical welds typically used to fabricate built-up members or to attach components to main members, for which the full strength of a groove weld is not required.

### *2.1.1. Welding Processes*

Various welding processes can be used to create welds, with some of the more common ones being shielded metal arc welding (SMAW), submerged arc welding (SAW), gas metal arc welding (GMAW), flux cored arc welding (FCAW), electrogas welding (EGW), and electroslag welding (ESW) (AASHTO/AWS 2020). Each process has its advantages and disadvantages, and they are approved for different fabrication uses by AASHTO/AWS D1.5 and state owners. Of the processes listed, SAW and SMAW are the most commonly used for bridge members. GMAW is allowed with the permission of the owner, but this process is only reliable in a contained environment when the protective gas shield can be reliably maintained. FCAW is often not allowed for welding main bridge members due to historical weld quality issues when not

carefully controlled, but it can be used to fabricate secondary bridge members, such as cross-frames in some bridge types. EGW and ESW are less common but are allowed with the permission of the owner.

SAW is an arc welding process that uses an arc between the weld pool and a bare metal electrode. This process is often mechanized or automated and uses a blanket of granular flux to protect the arc during welding (AASHTO/AWS 2020). The typical SAW process uses a welding machine, a wire feeder, a flux delivery system, and a travel carriage or gantry. During the welding process, welding wire is continuously fed through a nozzle and melted by the welding arc to fuse the components being joined, while the granular flux provides a protective coating. The flux shields the weld from atmospheric contamination and helps to stabilize the arc (AWS 2025). Additionally, flux helps protect the deposited weld metal by forming a protective coating that is removed shortly after each pass, resulting in a smooth, concentrated weld bead with minimal spatter. For these reasons, SAW is ideal for long, continuous welds in high-volume production environments, including in the bridge industry for fillet welds and CJP / PJP butt-splice joints.

SMAW, commonly referred to as stick welding, is a welding process that uses an arc between the weld pool and a covered metal electrode (i.e., welding rods) (AASHTO/AWS 2020). The typical SMAW process includes a welding machine and welding rods. During welding, the arc is struck between the weld pool and the welding rod, which melts the flux coating on the rod and forms a concentrated layer of shielding gas that protects the arc. The metal electrode is then deposited onto the weld pool to form the weld bead. SMAW is ideal for joints with limited access and for short, targeted welds. SMAW is commonly used in the bridge

industry, when SAW is not feasible, to attach components to main members (e.g., stiffeners, gusset plates, etc.), and to perform targeted repair welds.

### *2.1.2. Weld Regions*

During the welding process, new weld metal is deposited, and the base metals in the surrounding region are subjected to a severe thermal cycle. The surface of the base metal directly adjacent to the weld experiences a phase change and is heated to the point of melting; however, the base metal near the weld, although not heated to the melting point, is also affected by the rapid heating and cooling cycle. The surface layer of base metal that is melted and fused with the filler weld metal is called the fusion line (FL), and the base metal region immediately surrounding the welded location is referred to as the heat-affected zone (HAZ). Figure 2-1 shows the profile of a typical CJP butt-splice weld and the resulting welded regions of interest.


**Figure 2-1. Illustration. Typical CJP weld profile showing weld metal, HAZ, and base metal regions.**

The HAZ often exhibits mechanical properties that differ from those of the base metal due to the severe heating and cooling cycles induced by the welding process. The grain structure within the HAZ region varies from that of the base metal, typically being coarser near the fusion line and normalizing to the finer base metal grain size over the length of the HAZ region. The

coarser grain structure and embrittlement of the HAZ region can lead to a decrease in yield and/or fracture toughness, which can increase the chance of fatigue cracks forming and propagating in the HAZ because of the more intense stress concentrations typically found in the boundaries of the coarser grains. As such, the most significant discrepancies in mechanical properties between the base metal and HAZ generally occur within the coarse-grain structure near the fusion line (Easterling 1992).

Recently, Collins and Yount (2023) investigated the toughness of the HAZ resulting from various welding processes, conducting a suite of tests including microhardness, Charpy V-notch (CVN) impact, and full fracture tests. For the SAW process, they found that the highest microhardness values were measured within 1-2 millimeters of the weld fusion line; however, all peak values remained below the recommended maximum hardness threshold of 280 Vickers hardness specified in AASHTO/AWS D1.5. Additionally, they found that the CVN specimens directly next to the fusion line consistently resulted in the lowest (i.e., worst) results; therefore, notching specimens close to the fusion line is critical. For almost all the tested specimens, the HAZ CVN values were lower than those of the base metals, but they still met the minimum impact requirements of ASTM A709 (ASTM 2021b). This study confirms that the HAZ generally exhibits material behavior that differs from that of the base metal. Still, these changes are not substantial enough to cause the HAZ created from a SAW process to perform below the relevant minimum standards in AASHTO/AWS D1.5 or A709.

### *2.1.3. Welding Nonconformances and Repairs*

During fabrication, welding nonconformances may occasionally occur. Welding nonconformances are defects or discontinuities in the welded region that result in the welded

joint not meeting the required standards or specifications. Some typical welding nonconformances include cracking, porosity, spatter, undercut, overlap, inclusions, incomplete fusion, and incomplete penetration (AASHTO/AWS 2020). Depending on the severity of the nonconformance, a weld repair can be performed using an approved procedure.

AWS and AASHTO have developed extensive guides and standards that detail how to detect and repair typical weld nonconformances. Some of the more prominent guides include AASHTO/NSBA G2.2 – Resolutions of Steel Bridge Fabrication Errors (2016), AASHTO Steel Bridge Fabrication Specification (2023), FHWA Bridge Welding Reference Manual (2019), and AASHTO/AWS D1.5 (2020). These guides and specifications outline the procedures to follow for an effective repair. If a subsurface defect or major flaw is found, the nonconformance is generally repaired using the following steps:

1. Identify the severity of the nonconformance and determine if a repair is feasible.
2. Excavate the defect, ensuring that the defect and a portion of the immediate surrounding region are removed.
3. Reweld the excavated region following an approved welding procedure specification (WPS).
4. Perform nondestructive testing (NDT) to check the soundness of the weld. If a defect is detected, repeat Steps 1 to 3 until the weld is sound per the NDT.

If a nonconformance is severe enough, the fabricator may need to replace the member or component in kind. If a surface defect is found, the nonconformance can often be repaired by grinding and additional welding, with no effect on the integrity of the original weld or the surrounding metals.

Currently, neither AWS nor AASHTO limits the number of repair welds that can be made on a member or at the same joint. While repair procedures and methodologies are discussed extensively in AASHTO/AWS D1.5 (2020), there is no mention of the number of repairs allowed for either nonredundant steel tension members (NSTMs) or load path redundant members (LPRMs). The omission has resulted in ambiguity and nonuniformity among state owners and steel fabricators, with no agreed-upon number of acceptable repair welds. The only reference to a limit on the number of repair welds is in the FHWA Bridge Welding Reference Manual (2019), which states that no limit is currently placed on the number of allowable weld repairs based on fatigue-life experimental data from Kelly (1997). The Kelly (1997) and other relevant studies involving multiple repair welds are discussed in the next section.

## 2.2. Previous Studies Targeting Multiple Repair Welds

### *2.2.1. Fatigue-Life Assessment Studies*

A limited number of previous studies directly target the effects of multiple repair welds. The study most applicable to the steel bridge industry is from Kelly (1997). In this study, large-scale fatigue tests were conducted on nine built-up I-section members with different types of welded butt-splices located at discrete locations along the top and bottom flanges. No material characterization tests were performed. The study targeted ASTM A131 (2019) and API-2W grade steels, which are typically used in naval vessels. Seven girders had flanges that were 3/8 in. thick, and two girders had flanges that were 1 in. thick. The specimens were loaded using a fully reversed loading pattern (i.e., R = -1) at a stress range of 120 MPa (~18 ksi) until a crack was detected. The cracks were tested until “failure,” which corresponded to a through-thickness crack that propagated halfway through the flange width. Upon failure, the crack was repaired by

gouging and welding, followed by additional cycling until a new crack was found. The process was repeated until all joints had been cracked and repaired multiple times. The results indicated that the number of weld repairs had no appreciable influence on the fatigue life of the joint.

While trends can be drawn from the Kelly (1997) study, there are some notable differences between the specimens in the study and modern bridge members. One notable difference is the grade of material. The flanges tested were composed of A131 grade steels, whereas bridge members are composed of A709 grade steels. Aside from the chemical compositions, which vary slightly based on the grades of steel, both standards have a variety of grades that cover similar ranges of yield and tensile strengths. The main difference between the two standards is that A131 requires all steel grades to be killed, whereas A709 does not. Killing steel results in a more uniform chemical composition and a finer grain pattern that is less susceptible to grain growth during heat treatments than typical non-killed steels, which improves overall weldability and reduces defects. However, although it is not explicitly defined in A709, the majority of A709 steels used in bridge fabrication are subjected to some form of grain refinement process, which makes them comparable to A131 steels.

Another difference is the thickness of the flanges tested. Bridge flanges are typically much thicker than the flanges tested in Kelly (1997), with typical bridge girder flange thicknesses exceeding one inch. Specimen thickness plays a crucial role in fatigue as the probability of a critical flaw being present increases with the bulk volume of a sample, particularly in cases where the joint is being welded so many times (Bannantine 1990). Given that Kelly (1997) focused predominantly on 3/8 in. thick flange members, data are currently lacking on the effects of these weld repairs on thicker flange members. Furthermore, the repair welds performed during the Kelly (1997) study are in-situ repairs, which are more akin to in-

field repairs than shop repairs performed during the initial fabrication phase. Some key repair differences include the repair procedures used, the level of quality control, and the quality of the repair welds, which vary due to different orientations and available weld processes. Although some of these factors may be more impactful than others, it is essential to recognize that the results from Kelly (1997) may not directly represent the fatigue performance of welded joints constructed with A709 grade steels that have been repaired various times in a shop setting.

### *2.2.2. Material Property Characterization Tests*

Other studies have also investigated the effects of multiple repair welds (AghaAli et al. 2014; Carpenter et al. 2021; Jiang et al. 2013; Lin et al. 2012). However, these studies focused exclusively on material characterization tests rather than fatigue tests. Also, all the studies investigated steel grades that are not typical of the steel bridge industry, namely, stainless steels. The results and recommendations from these studies often varied based on the material being tested. AghaAli et al. (2014) investigated AISI 316L stainless steel and found that the number of weld repairs had little impact on yield and tensile strength; however, they found that weld repairs had significant negative impacts on impact toughness and pitting corrosion resistance. Jiang et al. (2013) and Lin et al. (2012) investigated AISI 304L stainless steel and found that the number of weld repairs had no significant effect on impact strength, but weld repairs did affect fracture characteristics. Ultimately, AghaAli et al. (2014) and Lin et al. (2012) recommended no limit on the number of repair welds (when corrosion was not an issue). In contrast, Jiang et al. (2013) recommended a limit of two repairs based on observed changes in microstructure and residual stresses. Carpenter et al. (2021) investigated the effects of multiple repair welds on quench and tempered (Q&T) steel for naval vessels and found that multiple repair welds led to no significant decrease in the toughness or microstructure.

In addition to the fatigue life and material characterization tests, several studies have investigated the influence that multiple repair welds have on the residual stress profile of the joint. One such study from Schasse et al. (2015) investigated the impacts of multiple repair welds on the residual stress profiles of high-strength S690QL structural steel using X-ray diffraction techniques. They found that the longitudinal and transverse residual stresses in the HAZ increased with the number of weld repairs, often reaching the yield strength of the material. This is significant as it indicates that multiple repair welds may influence limit states sensitive to residual stresses, such as buckling or flexural limit states. However, it should be noted that the observed increase in residual stresses would not significantly impact the fatigue limit state of bridge members. Tensile residual stresses are typically additive to the loading stresses, which do not influence the fatigue stress range but do increase the mean stress. As the AASHTO design standards are largely based on data tested under pure tension loading, they inherently account for a positive mean stress (Keating and Fisher 1986).

Similar to the Kelly (1997) study, these studies provide valuable trends that can be drawn and related to the performance of A709 steels. However, most of these studies targeted stainless steels, which behave differently from A709-grade steels because of their different chemical compositions. Additionally, none of these welds or repair welds were performed in accordance with the fabrication practices typical of the steel bridge industry. Differences in joint details and welding practices can significantly affect overall results, particularly in multi-pass welds due to allowable interpass temperatures and preheating requirements.

## 2.3. AASHTO Fatigue Design

Because of cyclic loading of bridges, AASHTO requires that all fatigue-sensitive details on steel bridge members and components be designed to have a fatigue life that meets or exceeds the design life of the bridge. These fatigue-sensitive details include base materials, welded connections parallel and perpendicular to the stress flow, and bolt holes, among others. During the design phase, the bridge is subjected to specific loading patterns, and the resulting member stresses at each detail location are then checked against standardized stress-life (S–N) fatigue resistance curves.

The AASHTO fatigue resistance curves were developed as part of a significant research effort in the late 1900s funded by the National Cooperative Highway Research Program (NCHRP). The experimental results from this research program, summarized in NCHRP Report 286 (Keating and Fisher 1986), were synthesized and used to create the mean fatigue resistance curves for details used in bridges. Currently, AASHTO utilizes eight fatigue resistance curves to represent the detail categories: A, B, B′, C, C′, D, E, or E′. The AASHTO S-N design fatigue resistance curves, shown in Figure 2-2, are plotted in a log–log format. In this figure, the ordinate represents the design stress range ($\Delta\sigma$), and the abscissa corresponds to the design life (i.e., the number of cycles, $N$) expected before failure. The fatigue life of a detail is considered adequate if its design stress range and required fatigue life plot below the appropriate S-N fatigue resistance curve. Notably, the design fatigue resistance curves used in AASHTO LRFD-10 (2024) represent the 95% confidence limit of the mean fatigue resistance curves developed as part of the NCHRP projects, which corresponds to the design fatigue resistance curves being approximately two standard deviations below the mean of the experimental data (Modjeski and Masters, Inc. et al. 2014).

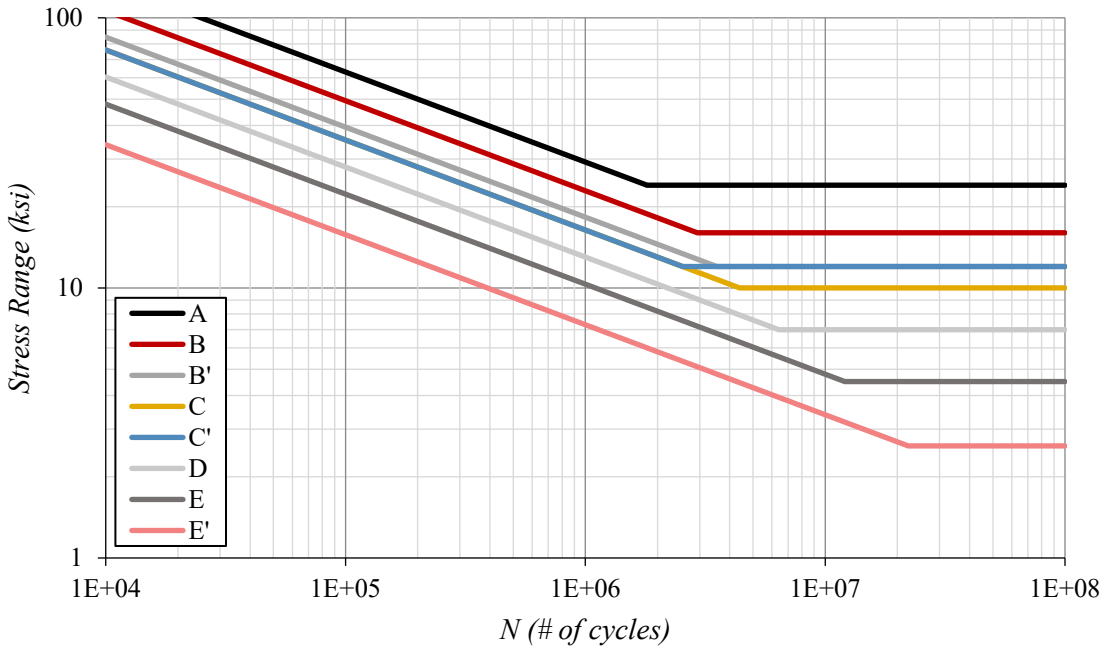


**Figure 2-2. Graph. AASHTO S–N fatigue resistance design curves.**

The AASHTO S–N fatigue resistance curves are defined by two main regions: the finite life region and the infinite life region. The finite life region corresponds to the high stress range portion of the S–N fatigue curves, where a detail will fail from fatigue within a finite number of loading cycles; the infinite life region corresponds to the lower stress range portion of the S-N fatigue curves, where a detail will theoretically never fail from fatigue. The finite life region of the S–N curves is defined by Equation 1, and the infinite life region of the S–N curves is defined by Equation 2.

$$(\Delta F)_n = \left(\frac{A}{N}\right)^{\frac{1}{m}} \quad \text{(Eq. 1)}$$

$$(\Delta F)_n = (\Delta F)_{TH} \quad \text{(Eq. 2)}$$

In these equations, $(\Delta F)_n$ is the stress range, $A$ is a constant defined in AASHTO LRFD-10 Table 6.6.1.2.3-1 that pertains to the detail category, $N$ is the fatigue life (i.e., cycle count) corresponding to the stress range, $m$ is the slope of the S–N curve in the finite life region, and

$(\Delta F)_{TH}$ is the constant amplitude fatigue threshold (CAFT) limit defined in AASHTO LRFD-10 Table 6.6.1.2.3-1 that pertains to the detail category. In the finite life region, the S-N curves are parallel and have a slope of -3. For all S–N curves, the infinite life region begins at the cycle count ($N$) corresponding to when $(\Delta F)_n = (\Delta F)_{TH}$ in Eq. 1.

# CHAPTER 3. CURRENT INDUSTRY PRACTICES FOR QA/QC DOCUMENTATION, NONCONFORMANCES, AND NONDESTRUCTIVE TESTING

The first research objective targets the review and assessment of all standards, practices, and limits currently used in the United States for the fabrication of steel bridge members and components, in particular those related to the detection and repair of fabrication nonconformances. This objective was accomplished through two main research tasks: (a) a literature review of available documents and (b) a survey of owners. The literature review and owner survey are discussed in detail in the following sections. The data and insights gathered were used to inform the development of the experimental testing program and to ensure that the GDOT SFQM is a comprehensive document that meets or exceeds industry standards.

## 3.1. Literature Review of Existing Standards

A thorough literature review was conducted to compile all available information on standards and references that provide guidance and/or restrictions on QA/QC documentation, the detection and repair of welding nonconformances, and commonly used nondestructive testing methods for different nonconformances. The key standard and reference documents found were:

- ASTM A6 – Standard Specification for General Requirements for Rolled Structural Steel Bars, Plates, Shapes, and Sheet Piling (ASTM 2021a)
- AWS D1.1 – Structural Welding Code – Steel (AWS 2020)
- AASHTO/AWS D1.5 – Bridge Welding Code (AASHTO/AWS 2020)
- AASHTO/NSBA S2.1 – Steel Bridge Fabrication Guide Specification (AASHTO/NSBA 2018)
- AASHTO/NSBA G2.2 – Guidelines for Resolution of Steel Bridge Fabrication Errors (AASHTO/NSBA 2016)

- AASHTO/NSBA G4.1 – Steel Bridge Fabrication QC/QA Guide Specification (AASHTO/NSBA 2019)
- AASHTO/NSBA G4.4 – Sample Owners Quality Assurance Manual (AASHTO/NSBA 2006)
- AASHTO – LRFD Bridge Construction Specifications (AASHTO 2017)
- AASHTO – LRFD Bridge Design Specifications (AASHTO 2024)
- AASHTO – LRFD Steel Bridge Fabrication Specifications (AASHTO 2023)
- ANSI/AISC 303 – Code of Standard Practice for Steel Buildings and Bridges (AISC 2022a)
- AISC 360 – Specification for Structural Steel Buildings (AISC 2022b)
- FHWA – Bridge Welding Reference Manual (FHWA 2019)

These standard and reference documents were used to develop the survey discussed in the following section and the first draft of the GDOT SFQM. Notably, the only standard or reference document found that explicitly addresses a limit on the number of allowable weld repairs is the FHWA Bridge Welding Reference Manual.

### 3.2. Survey of Owners

A survey was conducted of owners across the United States. The goals of the survey were to: (a) gain a better understanding of the quality assurance / quality control (QA/QC) standards typically used in steel bridge fabrication, (b) gather resources and sample quality manual utilized by owners, and (c) gather industry knowledge and concerns regarding nondestructive testing (NDT) methods and the effects of multiple weld repairs. The survey, titled “GDOT Steel Bridge Quality Manual for Fabrication Survey,” was created using the online-based survey software

Qualtrics, which allowed for the creation of a more sophisticated and streamlined survey than a traditional paper-based survey. All survey questions were either short-answer written responses or multiple-choice grids where respondents could select all applicable answers. The survey was distributed to representative members of the AASHTO Committee on Materials and Pavement (COMP) in owner agencies via an email from the GDOT State Materials Engineer. The email contained a brief description of the survey and instructions on access and completion. A PDF copy of the survey and the email used to distribute it are provided in Appendix A.

### *3.2.1. Survey Details and Results*

The GDOT Steel Bridge Quality Manual for Fabrication Survey was distributed to relevant AASHTO members on March 6, 2023, and the survey closed (i.e., no further responses accepted) on June 2, 2023. During the survey period, Georgia Tech received 30 completed surveys representing 27 different states (including Georgia). Occasionally, multiple survey responses were received from the same state. As survey topics are generally handled on a statewide basis, the survey results are also grouped by state. Therefore, if multiple responses were received from the same state, the data from both surveys were combined into a single data point for that state.

The GDOT Steel Bridge Quality Manual for Fabrication Survey consists of five major sections: (a) general information, (b) steel bridge QA/QC fabrication, (c) steel bridge fabrication nonconformances and repairs, (d) NDT methods, and (e) concluding questions. A breakdown of the main goals, questions, and results for each of the five major sections is provided in the following subsections. Multiple standards and references are repeatedly shown in an abbreviated form for many of the survey results discussed and presented below. See Section 3.1 for a list of

all the abbreviated standards and references. Additionally, the answer choice GDOT selected in their survey is shown in the relevant figures below to compare GDOT's practice at the time of the survey with those of other states. As noted earlier, a PDF copy of the survey is provided in Appendix A, so all questions discussed below can be found there.

#### *3.2.1.1. QA/QC Fabrication Documents*

The first major section of results involves QA/QC fabrication documents. The main goal of this section was to collect data on the QA/QC documents and standards the owner agency uses for steel bridge fabrication; as such, the core question of the fabrication documents section was whether the owner agency had a quality manual for steel bridge fabrication. Depending on the response, a series of follow-up questions focused on which documents and references were used to create the owner's QA/QC standards and who the intended audience was for those standards (e.g., inspectors, fabricators, etc.).

Of the 27 states that completed the survey, 12 reported having a dedicated QA/QC manual for steel bridge fabrication, and 15 reported not having a QA/QC manual but using other documents instead. Of the 12 that reported having a QA/QC manual, eight provided copies of the QA/QC documents for reference. Figure 3-1 shows a map and list of all states that completed a survey, with those states further broken down into those that used a QA/QC manual and those that did not. Note that states that sent in multiple responses are indicated in the list of states provided in the figure via a "(x2)" marker. Overall, survey responses were uniformly distributed across the continental United States, with the northwestern region the only area without responses. Of the 12 states indicating they had a QA/QC manual, six noted that their manuals

were for internal use only (i.e., inspectors only), and six indicated that their manuals were open for internal and external use (i.e., inspectors and fabricators).

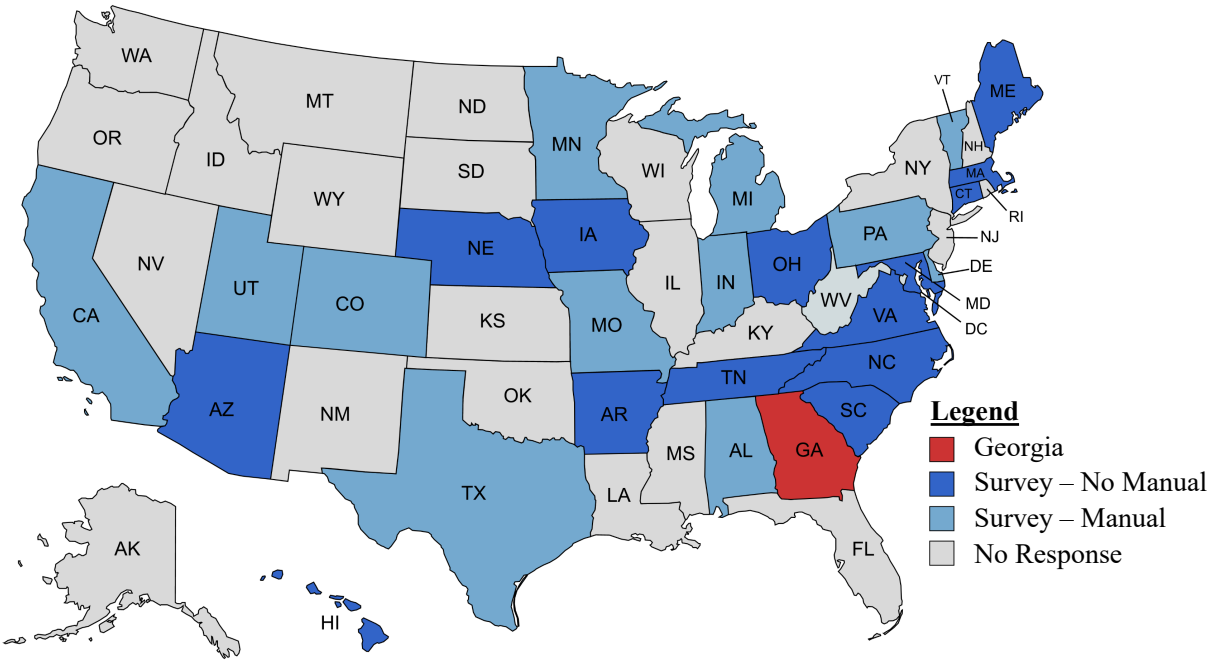


| | | | | | |
|---|---|---|---|---|---|
| Alabama (x2) | Connecticut | Iowa | Minnesota | Ohio | Texas |
| Arizona | Delaware | Maine | Missouri | Pennsylvania | Utah |
| Arkansas (x2) | Georgia | Maryland | Nebraska | South | Vermont |
| California (x2) | Hawaii | Massachusetts | North | Carolina | Virginia |
| Colorado | Indiana | Michigan | Carolina | Tennessee | |

**Figure 3-1. Illustration. Map and list of survey responses per state.**

As discussed previously, one of the main goals of the survey was to gather data on the resources and standards that states either use for their QA/QC or use to create their QA/QC manual. As such, there were a couple of multiple-choice questions throughout the survey that asked participants to select the standards and references used by their organization, with a few short-answer slots for write-in answers if needed. The results from these questions are compiled and shown in Figure 3-2.

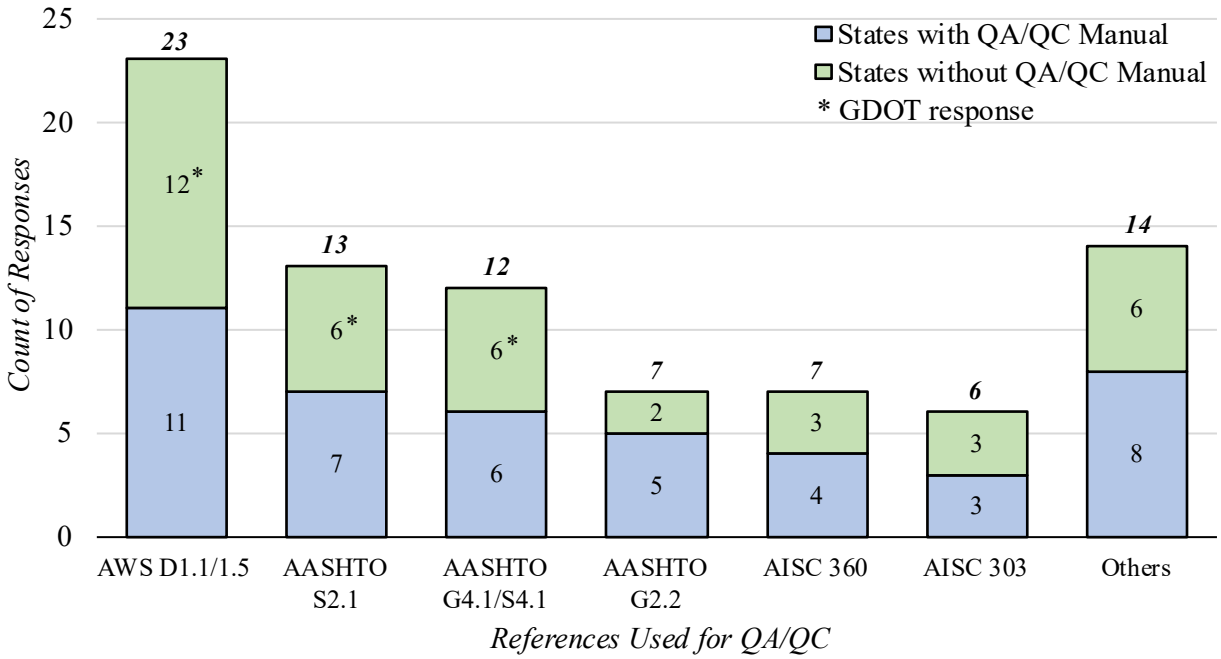


**Figure 3-2. Graph. References used for QA/QC standards or to create QA/QC manual.**

In Figure 3-2, the multiple-choice answers in the survey questions are listed along the abscissa, and the number of times each answer was selected is shown on the ordinate. Furthermore, the total tally for each answer choice is broken down into two subcategories: responses from states with a QA/QC manual and responses from states without one. Notably, these questions allowed multiple answers to be selected; therefore, the total tally does not necessarily sum to 27. In addition to the standards and references listed, multiple respondents noted that their state uses other documents for QA/QC. Some of the most common write-in documents included the AASHTO LRFD Bridge Construction Manual (AASHTO 2017), their specific state Standard Specifications for Roadway Construction document, contract documents, and other in-house documents (e.g., memoranda, standard operating procedures).

*3.2.1.2. Nonconformances*

The second major section of results involves nonconformances. The main goal of this section was to collect data regarding how the different owner agencies handle nonconformances. More specifically, the focus was on the resources used to repair different common nonconformances and the restrictions (if any) the owner agency has on repairing these specific nonconformances. To limit the section scope, the nonconformances were grouped into five general categories: Improper/Errant Holes, Minor Weld Defects, Major Weld Defects, Base Material Defects, and Other Defects. Targeted questions were then asked regarding each major group rather than about specific nonconformances. The questions included resources used to repair the nonconformances and whether any limits were placed on the number of allowable repairs. The repair limit question was critical because one of the primary focuses of the current research is understanding how multiple weld repairs influence the behavior of a welded joint. As such, there were targeted follow-up questions focused on the number of allowable repairs and the reasoning/justification for the owner agency's restriction on the number of allowable repairs. The main survey question on nonconformances is Question 2, which was a multiple-choice grid-style question. The results from the nonconformances question are compiled and shown in Figure 3-3.

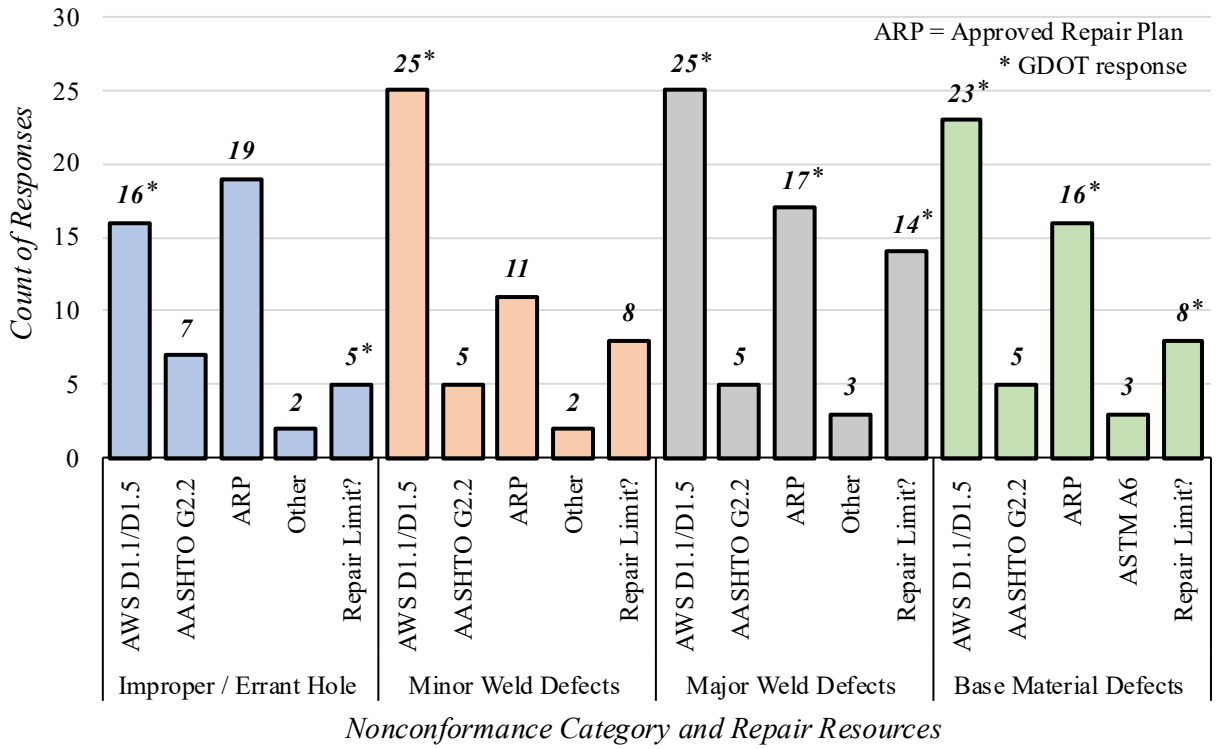


**Figure 3-3. Graph. Resources and restrictions for nonconformance repairs.**

In Figure 3-3, the multiple-choice answers from Question 2 are listed along the abscissa in groupings representing the major nonconformance categories discussed above, and the number of times each answer was selected is tallied for each answer choice and shown on the ordinate. The first four options in each group are a standard or requirement that the owner uses or requires to repair the specific nonconformance, with the ARP option being an approved repair plan. The fifth option is simply an indication of any limit that the owner imposes on the number of allowable repairs of a particular nonconformance. Notably, the questions allowed multiple responses; as such, the total number of tallies does not necessarily sum to 27. Because the final major category, "Other Defects," is broad, the results are not shown in the figure above. Instead, the category was explored via a follow-up question that requested the participant to describe any other common defects not listed. The responses to the follow-up "Other Defects" question included:

- Corrosion from storage
- In-transport damage
- Incorrect base metal
- Incorrect welding consumable or welding parameters
- Dimensional deviation
- Flatness
- Camber
- Blasting
- Cleaning and coating application
- Geometrical tolerance errors
- Mislocated weldments
- Machining tolerances
- Arc strikes
- Heat cambering
- Laminations

An important question stemming from the results shown in Figure 3-3 is the repair limit for each major nonconformance category. A major thrust of the current research effort is the development of the GDOT SFQM, which considers the effects of multiple repair welds and the limits (if any) on weld repairs. Due to the importance of understanding industry practice for allowable weld repair, a follow-up question requested the participant to elaborate on their repair limit response from Question 2, namely, the repair limit used for each nonconformance category. The responses are shown in Figure 3-4.

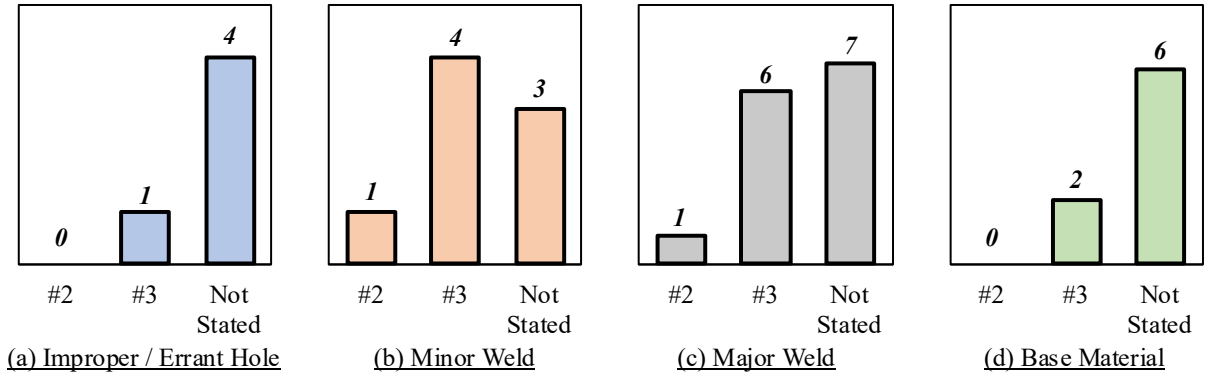


**Figure 3-4. Graph. Number of allowable repairs for each nonconformance category: (a) Improper / Errant Hole, (b) Minor Weld, (c) Major Weld, and (d) Base Material.**

Figure 3-4 has four subfigures, each representing one of the four major nonconformance categories displayed in Figure 3-3. For each subfigure, the number of allowable repairs is plotted along the abscissa, and the number of times it was listed is tallied and shown on the ordinate. Note that the total number of answers for each major nonconformance category corresponds to the total number of responses shown for the repair limit question in Figure 3-3. Of the responses that stated a repair limit, the reasoning behind the limit was generally attributed to AASHTO/AWS D1.5 restrictions. This finding is noteworthy because, to the knowledge of the authors, no editions (current or previous) of AASHTO/AWS D1.5 impose any limit on the number of allowable repairs, given that the proposed repair is within the specified parameters. Additionally, many responses did not provide a specific number of allowable repairs but stated that the permissible limit was handled on a case-by-case basis. These responses were tallied under the "Not Stated" option in Figure 3-4.

*3.2.1.3. Nondestructive Testing (NDT) for Welds*

The third major section of results involves NDT for welds. The main goal of the NDT section was to collect data on the NDT methods used to inspect various weld types. As such, the questions focused on the different NDT methods required for PJP, CJP, and longitudinal/transverse fillet welds. The results from these questions are compiled and shown in Figure 3-5. Figure 3-5a shows the results from Question 3, which focused on the different methods used for each weld type. Figures 3-5b and 3-5c show the results from Questions 3-1 and 3-2, which focused on the most commonly used NDT method for groove and fillet welds, respectively. In Figure 3-5, the multiple-choice answers to Question 3 are listed along the abscissa, grouped by the welding categories discussed above. Within each weld category subgroup, the various standard NDT methods are listed, with the associated acronyms at the top

of the figure. Figures 3-5b and 3-5c list the NDT methods from the short-answer responses along the abscissa. For all three subfigures, the number of times each option was selected is tallied and shown on the ordinate. Notably, these questions allowed multiple responses; as such, the total tally will not necessarily sum to 27.

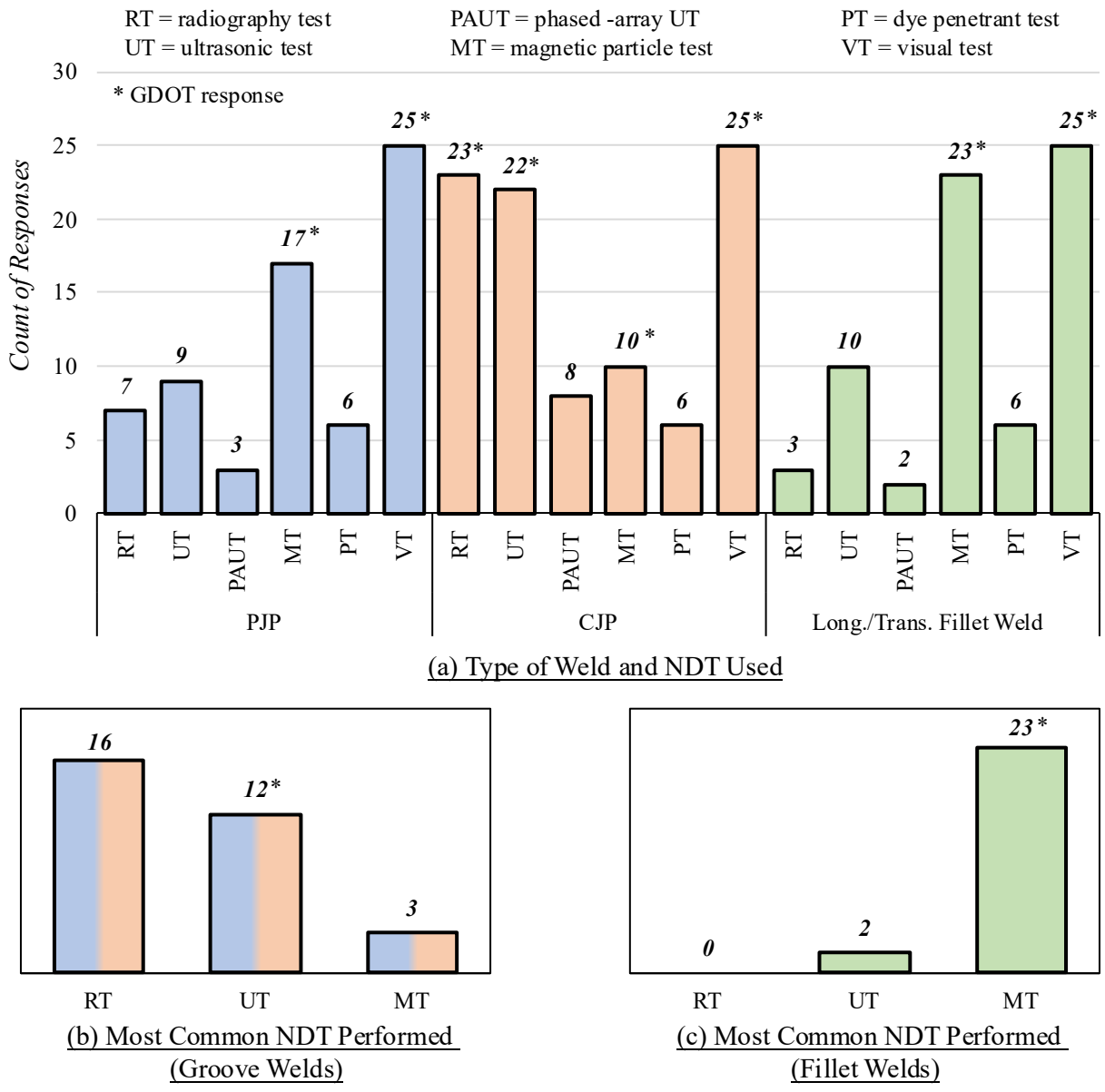


**Figure 3-5. Multiple Graphs. Nondestructive testing (NDT) used for welds. (a) Type of Weld and NDT Used, (b) Most Common NDT Performed (Groove Welds), and (c) Most Common NDT Performed (Fillet Welds).**

*3.2.1.4. Fabricator Consequences for Noncompliance and Suggested Areas of Study*

The fourth major section involves concluding questions focused on the fabricator consequences of recurring nonconformances and suggested areas for study. The main goal of the concluding questions section was to gain a better understanding of the consequences typically imposed on fabricators for recurring nonconformances and to identify other areas of fabrication that could benefit from further study. The main survey questions that pertained to these topics were Questions 4 and 5, which addressed fabricator consequences and suggested areas for study, respectively. Both questions asked for a short-answer response.

Regarding recurring nonconformances, many respondents indicated that they had little-to-no experience with fabricators that had recurring nonconformances to the point where they needed to be addressed. However, some owners indicated that their perceived route forward would be to meet with the fabricator, have the specific welder removed from the project, or remove the fabricator from their Qualified Products List (QPL), and to file a complaint with AISC if the nonconformances continued after the meeting. Additionally, many respondents indicated that they would impose more stringent inspection requirements (e.g., increased inspection frequency, additional hold points, etc.) on the work being performed if recurring nonconformances became an issue.

While many respondents answered “no” to the question about additional areas of study, some offered insightful responses, including:

- More specific beam sweep and straightness tolerances outside of A6
- Repair of in-field/transportation damage
- Errant holes in splices

- CNC drilling tolerances
- Warpage, heat damage, and straightness effects from numerous repairs
- Mill laminations in plates / flange lamellar tearing
- Effects of multiple repairs and the impact on the steel and HAZ (x2)

The additional research responses were interesting because multiple answers addressed the effects of multiple repair welds, indicating an industry need. Other suggested topics concerned geometric tolerances or flange lamellar tearing, which could also be related to weld repairs, depending on the joint.

# CHAPTER 4. MATERIAL CHARACTERIZATION EXPERIMENTAL PROGRAM

The second research objective targets the characterization of the material properties of CJP welded joints that have been repaired multiple times. To accomplish this, a material characterization experimental program has been developed to generate a full suite of novel material property data for these repaired joints. This data was then examined to determine whether these repairs alter or negatively affect the strength, ductility, and fracture toughness of the joint. The material characterization experimental program is discussed in the following subsections, and the material characterization testing results are discussed in Chapter 5.

## 4.1. Experimental Material Testing Matrix

Two grades of steel are targeted in the current research program: ASTM A709-50W and ASTM A709-HPS70W. A709-50W has a minimum yield strength of 50 ksi, and the "W" indicates it is a weathering steel. A709-50W and A709-50 behave similarly, with the weathering variant typically chosen when atmospheric corrosion resistance is required. A709-HPS70W has a minimum yield strength of 70 ksi, and the "HPS" stands for high-performance steel, which was developed for higher strength, improved weldability, and higher toughness than equivalent strength non-HPS steels (Wilson 1999). These two grades of steel are selected for the current study because they, or an equivalent strength grade of steel in ASTM A709, comprise the majority of steel specified for primary bridge members in the US and are readily available from most steel producers.

Using insights from previous studies on weld repairs (see Section 2.2) and discussions with industry fabricators, the current study sets a maximum threshold of five weld repairs. Although instances may exist in which more than five repairs have been performed, most owners

and fabricators generally limit the number of weld repairs at a single location to two or three before rejecting the member. As such, five repairs at a single location represent an extreme for most owners and will provide sufficient data to demonstrate any trends in material behavior resulting from the weld repairs. Based on the targeted steel grades and weld repair limit, an experimental test matrix has been developed and is shown in Table 4-1, including the sample groups, steel grades, and the number of repair welds for each sample group. The 50-B and 70-B groups represent the base material samples for the respective steel grades, and the 50-R# and 70-R# groups represent samples with varying numbers of repair welds, where the # represents the number of repairs each group received. For example, 50-R0 has zero repair welds, representing a typical CJP welded joint in A709-50W grade material with no repairs, and 70-R3 has three repairs, representing a CJP welded joint in A709-HPS70W grade material that has been repaired three times. Including the base material, 12 different sample groups are evaluated.

**Table 4-1. Material characterization experimental matrix.**

| *Sample Group* | *Steel Grade* | *#Repair Welds* | *Sample Group* | *Steel Grade* | *#Repair Welds* |
|---|---|---|---|---|---|
| 50-B | 50W | - | 70-B | HPS70W | - |
| 50-R0 | 50W | - | 70-R0 | HPS70W | - |
| 50-R1 | 50W | 1 | 70-R1 | HPS70W | 1 |
| 50-R2 | 50W | 2 | - | - | - |
| 50-R3 | 50W | 3 | 70-R3 | HPS70W | 3 |
| 50-R4 | 50W | 4 | - | - | - |
| 50-R5 | 50W | 5 | 70-R5 | HPS70W | 5 |

To characterize any changes introduced by the numerous repair welds, a comprehensive suite of material tests was conducted for each sample group listed in Table 4-1, including tension tests, bend tests, Charpy V-notch (CVN) impact tests, microhardness tests, and macroetches. The selected tests are essential for providing insight into the strength, ductility, and fracture toughness of each sample group. Comparing results across sample groups and against

appropriate standards provides an understanding of the effects of multiple repair welds on joint performance. A breakdown of the material tests and the respective number of specimens tested in each sample group is provided in Table 4-2. Note that the microhardness and macroetch sample count are shown as one because the respective test(s) were conducted on a single specimen.

**Table 4-2. Material testing specimens per sample group.**

| *Sample Group* | *Tension* | *Bend* | *CVN* | *Microhardness* | *Macroetch* |
|---|---|---|---|---|---|
| 50-B | 3 | - | 36 | - | - |
| 50-R0, R1, R2, R3, R4, R5 | 3 | 2 | 18 | 1 | 1 |
| 70-B | 3 | - | 36 | - | - |
| 70-R0, R1, R3, R5 | 3 | 2 | 18 | 1 | 1 |
| **Total** | **36** | **20** | **252** | **10** | **10** |

## 4.2. Plate Specimens

A procedure inspired by the standard welding procedure specification (WPS) qualification tests described in AASHTO/AWS D1.5 (2020) was implemented to obtain test specimens for material characterization testing. This procedure involved creating a material characterization plate for each sample group using the specific welding procedure, plate material, and number of repairs. The test specimens (e.g., tensile tests, bend tests, etc.) were cut from the material characterization plates. Note that all repair welds were performed on the material characterization plates at the shop soon after the base CJP weld or previous repair weld was performed to mimic the procedure and effects of typical fabrication shop repairs. A detailed description of the design and layout of the material characterization plates, base material properties, fabrication and welding processes used, and specimen sampling techniques is provided in the subsections below.

### *4.2.1. Plate Design and Layout*

The material characterization plates fabricated for the current study are based on the typical WPS qualification test plate layouts found in AASHTO/AWS D1.5 (2020). Each material characterization plate consists of two 12” x 20” x 1” plates that were welded together along their length (i.e., the 20” edge) using a single 60° V-groove weld detail, resulting in a 24” x 20” x 1” plate. The only exception was the base material samples (i.e., 50-B and 70-B), which are only 12” x 20” x 1” plates with no welding. For the material characterization plates, the two 12” x 20” x 1” plates were always oriented such that the direction of roll (DOR) was perpendicular to the weld, replicating the plate and weld orientations found in typical welded CJP joints.

Because of the plate size and the large amount of required welding, plate distortion was essential to control during fabrication to ensure the final material characterization plates were relatively flat for subsequent test specimen extraction. Based on conversations with fabricators, the common technique to help control distortion in the fabrication shop is to alternate the side of the plate where the repair weld is performed every couple of repairs. Using this knowledge, a welding repair plan was developed:

- For material characterization plates with one, two, or three repairs, all repair welds were performed on the back plate face.
- For material characterization plates with four or five repairs, the first three or four repairs were performed on the back plate face, and the final repair (i.e., repair four or repair five) was performed on the front plate face.

For all repairs, a hypothetical “defect” was assumed to be located along the center of the CJP weld at the mid thickness of the plate (i.e., at 0.5T, where T is thickness), and the excavations and repairs always exceeded this depth by approximately 1/16 of an inch. This methodology

ensured that the center of the plate and the surrounding material were subjected to the correct number of repairs while minimizing plate distortions. Figure 4-1 shows the layout of a typical material characterization plate and illustrates the different repair plans discussed.

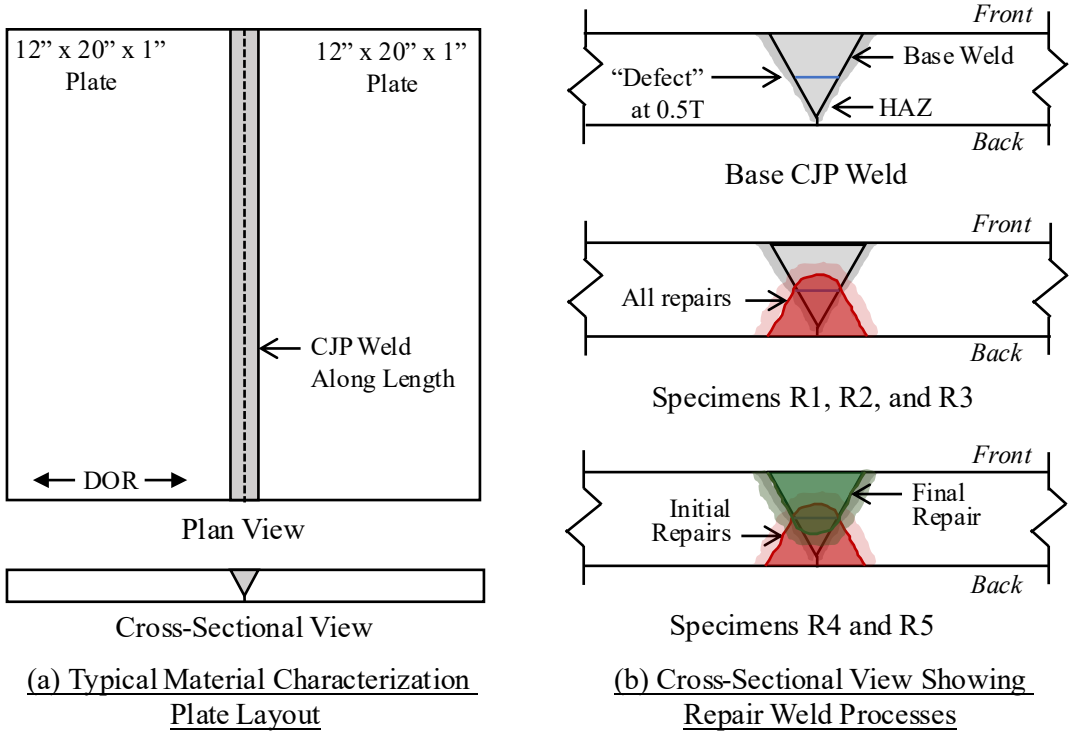


**Figure 4-1. Multiple Illustrations. Layout of material characterization plates and illustration of different repair processes. (a) Typical material characterization plate layout and (b) Cross-sectional view showing repair weld processes**

### *4.2.2. Plate Base Material Properties and Information*

All base material plates used to create the material characterization plates are either A709-50W or A709-HPS70W grades of steel. All base material plates for each steel grade were from the same heat and underwent the same post-treatment processes and storage conditions. The A709-50W plates were from heat D8027, and the A709-HPS70W plates were from heat 4506400. Notably, the A709-HPS70W plates were strengthened to their final strength through the quench-and-temper heat treatment process. The chemical compositions and material

properties (i.e., yield and tensile strengths, elongations, and CVN impact energies) reported in the manufacturer's material test reports (MTRs) for both heats are provided below in Table 4-3. Additional testing was performed on these materials as part of the current research program, and all these testing results are reported in Chapter 5.

**Table 4-3. Material properties and chemical composition from MTRs for base material plates.**

| | ***Heat #*** | **D8027** | **4506400** |
|---|---|---|---|
| | *Grade of Material* | A709-50W | A709-HPS70W |
| | *Plate Thickness (in.)* | 1 | 1 |
| *Material Properties* | *Yield Strength (ksi)* | 57, 58 | 88.1 |
| | *Tensile Strength (ksi)* | 82, 82 | 101.5 |
| | *Elongation (%)* | | |
| | *2 in. Gage* | - | 52.7 |
| | *8 in. Gage* | 22, 22 | - |
| | *CVN Impact (ft-lb)* | | |
| | *-25°F* | - | 188, 151, 142 |
| | *40°F* | 130, 135, 136, 158, 160, 164 | - |
| *Chemical Composition (Weight %)* | *Carbon, C* | 0.120 | 0.100 |
| | *Manganese, Mn* | 1.010 | 1.320 |
| | *Phosphorus, P* | 0.008 | 0.012 |
| | *Sulfur, S* | 0.001 | 0.001 |
| | *Silicon, Si* | 0.350 | 0.430 |
| | *Copper, Cu* | 0.310 | 0.270 |
| | *Nickel, Ni* | 0.360 | 0.270 |
| | *Chromium, Cr* | 0.550 | 0.480 |
| | *Molybdenum, Mo* | 0.070 | 0.030 |
| | *Vanadium, V* | 0.036 | 0.074 |
| | *Aluminum, Al* | 0.013 | 0.030 |
| | *Columbium, Cb* | 0.001 | - |
| | *Calcium, Ca* | - | 0.000 |
| | *Nitrogen, N* | - | 0.011 |
| | *Niobium, Nb* | - | 0.005 |
| | *Titanium, Ti* | - | 0.003 |
| | *Boron, B* | - | 0.000 |
| | *Tin, Sn* | - | 0.011 |

### *4.2.3. Plate Fabrication and Welding Information*

The material characterization plates used in the current study were fabricated by High Steel Structures in Lancaster, PA. All material characterization plates were fabricated by the same group of certified welders and followed the same repeatable fabrication process, as

discussed in detail below. The CJP weld used for all plates is a single 60° V-groove weld with no backing, and all welds were performed using submerged arc welding (SAW). The single 60° V-groove weld was chosen because it is the most common CJP groove weld detail for plates less than 2.0 in. thick. The SAW process was selected as it is the most common process used on steel bridge members. Runout tabs were used on all plates to ensure no discontinuities or defects were introduced by the start and termination of the weld, and a combination of arc gouging and mechanical grinding was used for all weld excavations. After the final repair, all CJP groove welds were ground smooth and checked for soundness using radiographic testing (RT).

For all joints, the base CJP welds required eight to ten passes, and the repair welds required six to eight passes. All base CJP joints and repair welds in the 50-grade plates were welded using 3/32 in. Lincoln LA-75 / 960 wire (F8A2-ENi1K-NI1-H8), and all base CJP joints and repair welds in the 70-grade plates were welded using 3/32 in. Lincoln LA-85 / MIL800 wire (F9A4-ENi5-G-H2). Both wires are nickel-bearing electrodes suitable for weathering steels.

Table 4-4 shows all pertinent welding information for each material characterization plate, including the welding parameters, calculated heat input, and preheat / interpass temperatures. The welding parameters shown were used for all CJP welds performed on that particular plate, and all the welding parameters fall within the ranges specified in the WPSs. Copies of the WPSs used for both grades of steel are provided in Appendix B. Notably, material characterization plates 70-R1 and 70-R5 were fabricated later than the others due to a fabrication discrepancy with the original plates; hence, the welding parameters differ slightly. Steel plates from the same heat as the original plates were used for the final 70-R1 and 70-R5 plates, and the fabrication processes were consistent with the earlier plates. The fabrication process used to create all the material characterization plates is as follows:

1. All 12” x 20” x 1” plates were cut and prepped for the single V-groove weld joint per the requirements of the WPS. The plates were then tack-welded along the root of the joint to hold them in place during the initial weld passes.
2. The material was preheated to the required minimum temperature. The base CJP weld was then performed on the front of the plate using the SAW process. The plate was then flipped, and the tack welds and leg of the initial joint were arc gouged out. Finally, the gouged region was welded using the same welding parameters as the base CJP weld.
3. A “defect” was assumed to be located at 0.5T of the CJP weld. The weld material was then removed via carbon arc gouging and mechanical grinding to a depth of ~1/16 in. beyond the “defect” (i.e., ~0.56T). Careful attention was given to restricting excavations to the weld material to minimize the disturbance or removal of the surrounding HAZ.
4. A repair weld was then performed to restore the welded joint. The face on which the repair weld was performed depends on the specimen and repair count (see Section 4.2.1).
5. Steps 3 and 4 were repeated until the plate received the required number of repairs.
6. Once the final repair weld was completed, it was mechanically ground smooth with a grinder, and RT was then performed over the entire CJP weld to ensure there were no defects or discontinuities.
7. Steps 1 to 6 were repeated until all plates were fabricated.

Figures 4-2 and 4-3 illustrate the fabrication process and show photos of the final material characterization plates, respectively.

**Table 4-4. Welding parameters used in the fabrication of material characterization plates.**

| *Material Characterization Plate* | *Weld Pass* | *WFS (in./min)* | *Amp. (A)* | *Volt. (V)* | *TS (in./min)* | *HI (kJ/in.)* | *Temp. Range* | |
|---|---|---|---|---|---|---|---|---|
| | | | | | | | *Min. (°F)* | *Max. (°F)* |
| 50-R0, R1, R2, R3, R4, R5 | 1 | 92 | 448 | 30 | 16 | 50.4 | 100 | 550 |
| | 2+ | 105 | 495 | 32 | 16 | 59.4 | 100 | 550 |
| 70-R0, R3 | 1 | 92 | 448 | 30 | 16 | 50.4 | 125 | 450 |
| | 2+ | 105 | 495 | 32 | 16 | 59.4 | 125 | 450 |
| 70-R1, R5 | 1+ | 104 | 480 | 33 | 16 | 59.4 | 125 | 450 |

WFS = wire feed speed || TS = travel speed || HI = Heat Input
Note: The welding parameters shown were used for all CJP welds and repair welds on that particular plate.

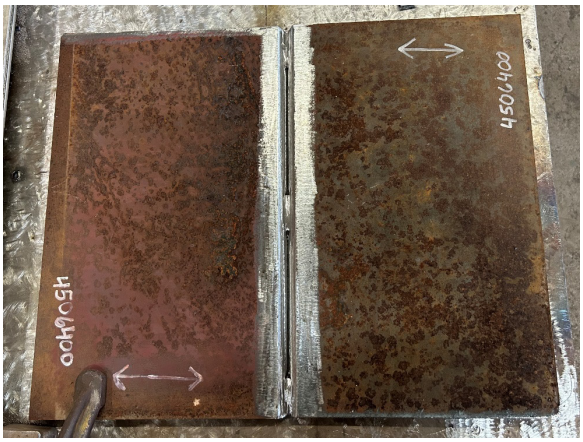

Step 1: Prep and align plates.

Step 2: Perform base CJP weld using SAW.

Step 3: Excavate "defect" by arc gouging and grinding.

Step 4: Perform repair weld using SAW.

**Figure 4-2. Multiple Photos. Photos showing the material characterization plate fabrication process.**

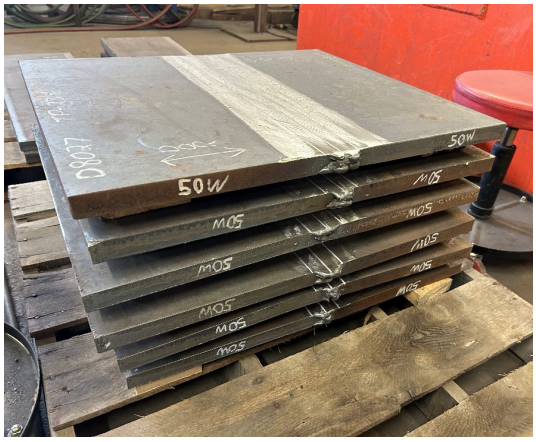


All 50W Plates After Fabrication


Plan View of HPS70W Plate After Fabrication

**Figure 4-3. Multiple Photos. Photos of material characterization plates after fabrication.**

All plates passed the first round of RT inspection, and no additional repairs were required. Figure 4-4 shows representative RT results for the material characterization plates 50R3 and 70R3. The RT results confirmed that all the final material characterization plate welds were sound and contained no defects or discontinuities that would influence the subsequent material test results.

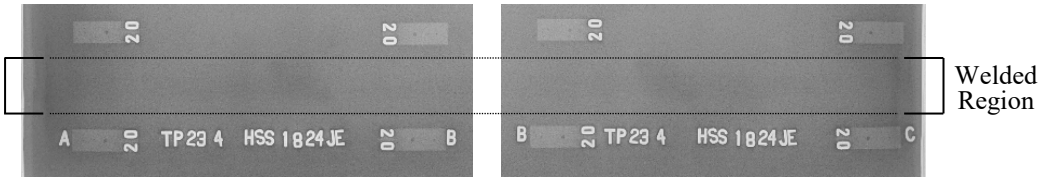


RT Results from Material Characterization Plate 50-R3
(no defects detected)

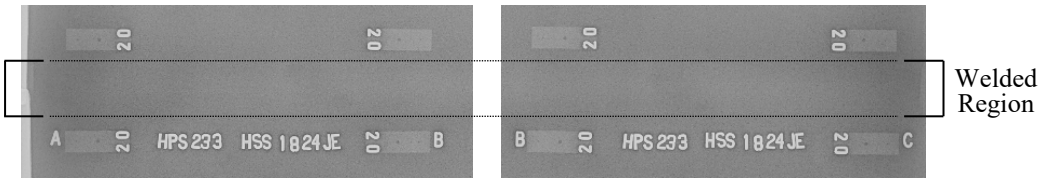


RT Results from Material Characterization Plate 70-R3
(no defects detected)

**Figure 4-4. Multiple Photos. Radiographic testing (RT) NDT results from 50-R3 and 70-R3 material characterization plates showing no defects.**

After all repair welds and final NDT inspections were complete, the material characterization plates were shipped to the Georgia Tech Structural Engineering and Materials

Laboratory (SEML). Upon arrival, all plate heat numbers were confirmed, and the distortion of each material characterization plate, generally a slightly V-shaped plate, was measured along the weld length at each end and the middle of the plate. The distortion measurements were performed by tensioning a string across the plate edges (along the 24" length) and measuring the distance from the string to the top of the CJP weld using a pair of calipers. The measured plate distortions are shown in Table 4-5. The measured distortions show that the alternating-face technique used for multiple repairs effectively controlled the overall plate distortions.

**Table 4-5. Measured material characterization plate distortions along the weld length.**

| *Material Characterization Plate* | *Top (in.)* | *Middle (in.)* | *Bottom (in.)* | *Avg. (in.)* |
|---|---|---|---|---|
| 50-B | - | - | - | - |
| 50-R0 | 0.359 | 0.355 | 0.349 | 0.354 |
| 50-R1 | 0.450 | 0.438 | 0.452 | 0.447 |
| 50-R2 | 0.324 | 0.335 | 0.332 | 0.330 |
| 50-R3 | 0.200 | 0.180 | 0.200 | 0.193 |
| 50-R4 | 0.153 | 0.148 | 0.165 | 0.155 |
| 50-R5 | 0.104 | 0.127 | 0.138 | 0.123 |
| 70-B | - | - | - | - |
| 70-R0 | 0.180 | 0.166 | 0.169 | 0.172 |
| 70-R1 | 0.245 | 0.255 | 0.243 | 0.248 |
| 70-R3 | 0.185 | 0.170 | 0.184 | 0.180 |
| 70-R5 | 0.232 | 0.220 | 0.220 | 0.224 |

### *4.2.4. Sampling of Specimens from Plates*

The excess base material was trimmed from the material characterization plates to make them more manageable and suitable for specimen extraction. All material characterization plates were trimmed to 10" x 20" x 1," with the CJP weld centered along the 10" width. Rectangular blanks of distinct thicknesses were cut along the weld length to produce tensile, bend, CVN, and macroetch / microhardness specimens. Careful consideration was given to the cutting pattern to ensure that the different specimens were sampled from regions across the entire weld length,

providing unbiased results. Additionally, all specimens were cut a minimum of 1.0 in. from the plate edges to ensure that the weld start and termination points did not influence the test results. Figure 4-5 shows the typical specimen extraction pattern and a photo of one cut material characterization plate. Note that the CVN blanks are displayed as large rectangular blocks, and the actual CVN specimens were later machined from the blocks. In total, the following specimens were removed from each material characterization plate:

- Tension Specimens (x3)
- Side-Bend Specimens (x2)
- CVN Blocks (x3)
- Macroetch / Microhardness Block (x1)

The layout, machining, testing details, and testing results for the tension, side-bend, CVN, and macroetch/microhardness specimens are discussed in Chapter 5.

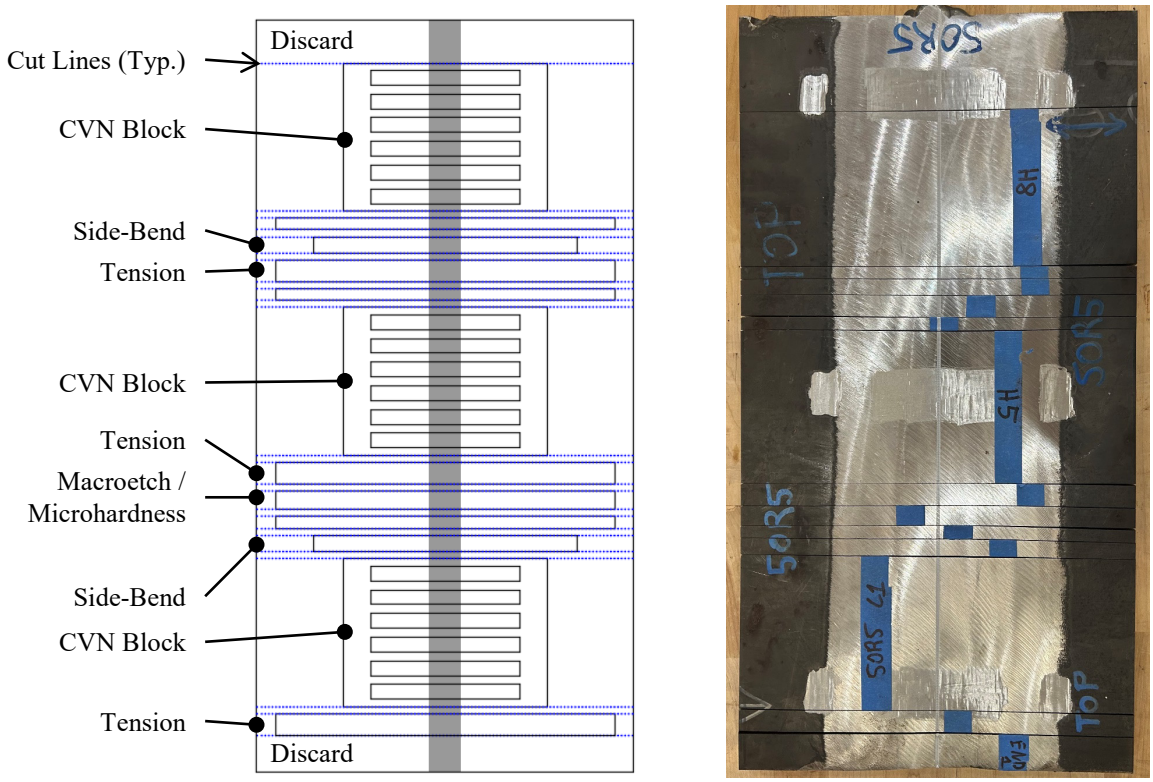


(a) Typical Sampling Pattern

(b) 50-R5 Material Characterization Plate After Cutting

**Figure 4-5. Multiple Elements. Typical specimen sampling pattern for the material characterization plates. (a) typical sampling pattern and (b) photo of 50-R5 sample plate after cutting.**

# CHAPTER 5. MATERIAL CHARACTERIZATION TESTING RESULTS

The material characterization tests conducted target the properties of the joint and the HAZ regions as appropriate. As discussed in Section 2.1, the weld metal is generally removed and replaced during weld repairs; hence, there is little concern about its material properties (since it is new after every repair) or about the base metal well outside the welded joint (since it remains largely unaffected). However, the HAZ metals surrounding the weld remain throughout the repairs and undergo repetitive thermal cycles from the nearby welding process, which could negatively influence material property changes and alter joint performance.

The suite of material characterization tests conducted includes tension tests, side-bend tests, CVN impact tests, macroetches, and microhardness tests. The tension and side-bend tests provide insights into the overall performance of the joint, while the CVN impact tests and microhardness tests provide insights into the performance of individual weld regions, such as the HAZ. The macroetches offer insights into the weld geometry and allow identification of the different weld regions. Each of these test programs, including the specimens, testing setup, and testing results, is discussed in detail in the following subsections.

## 5.1. Tension Tests

### *5.1.1. Specimen Information and Testing Setup*

Three tension tests were conducted for each material characterization plate, resulting in a total of 36 tension tests. These tests are significant because they provide insights into the yield strength, tensile strength, and ductility of the joints. The tension specimens were machined from the rectangular blanks cut from the material characterization plates per the geometrical requirements of the sheet-type specimen in ASTM E8 (ASTM 2022a) and the surface finish

requirements of AASHTO/AWS D1.5 (2020). All tension specimens are 1/2-inch thick and were machined by Chicago Spectro in Chicago, IL. Figure 5-1 shows a typical tension specimen. Figure 5-1a shows roughly how the tension specimen was positioned in the rectangular blank, and Figure 5-1b shows the geometrical and surface finish requirements. Note that the tension specimens were always positioned in the rectangular blank such that the gage region was centered on the CJP weld and at 0.5T.

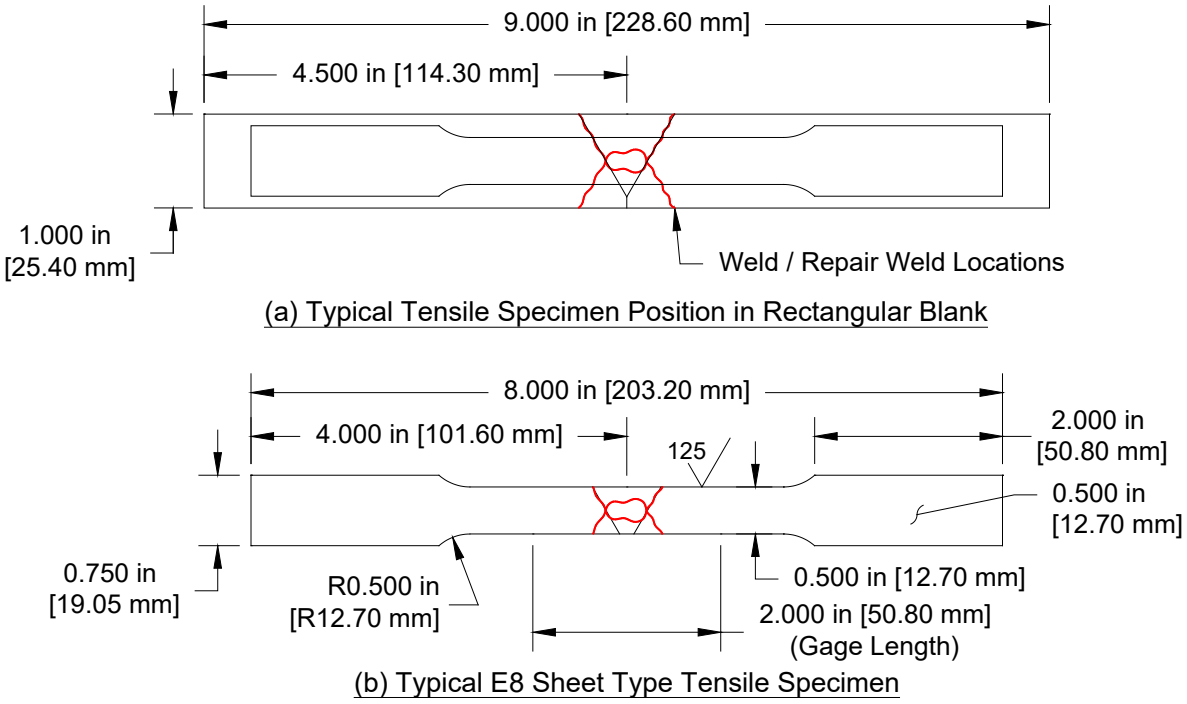


**Figure 5-1. Illustration. Typical tension specimen. (a) Typical tensile specimen position in rectangular blank, and (b) typical E8 sheet-type tensile specimen.**

All tension tests were conducted at the Georgia Tech SEML using an MTS, hydraulically controlled 55-kip universal testing machine (UTM). The UTM was equipped with a centering fixture to ensure no eccentricity was introduced into the specimen, and the UTM was calibrated and certified by MTS within the year before testing. All tension tests were conducted per the requirements of ASTM E8 (ASTM 2022a) in displacement control at a constant rate of 0.03 in./min to determine the yield properties. After the specimen reached yield, the loading rate

was increased to 0.2 in./min to determine the tensile strengths and to bring the specimens to rupture.

All loads were captured using the calibrated load cell within the UTM, and all strains/displacements were captured using a Correlated Solutions digital image correlation (DIC) system. Using the DIC system enabled the use of a digital extensometer, which offers more flexibility in positioning than a traditional clip-on extensometer. A digital extensometer ensured it was correctly positioned at the location of failure, which could be anywhere along the gage length due to the influence of the welded joint. Additionally, the DIC system captured the strain field of the entire welded joint, providing insights into the behavior of the different weld regions. Figure 5-2 shows an overview of the testing setup used for all the tension tests.

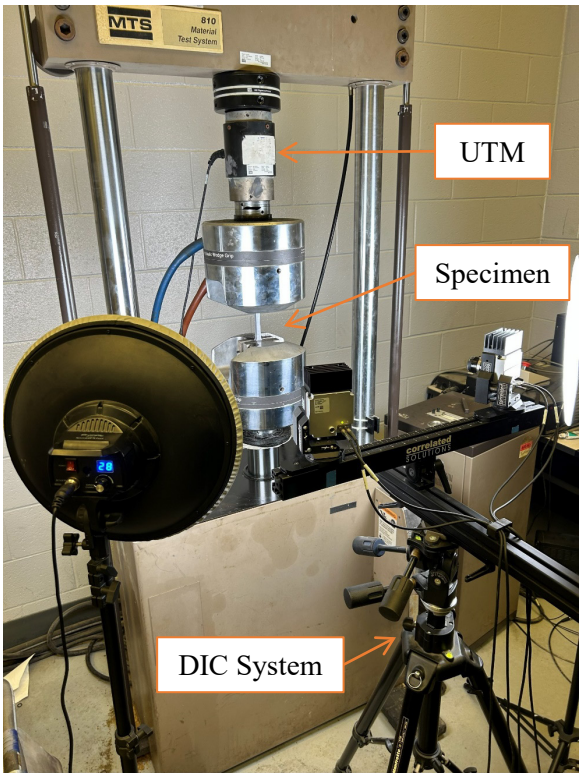


**Figure 5-2. Photo. Overview of tension testing setup.**

### *5.1.2. Testing Results*

Before testing, all tension coupons were chemically etched using a 5% nital solution to expose the different weld regions, and the fusion lines of the welded joints were marked for visual clarity. These specimens were then tested to rupture, and the failure location (i.e., necking / rupture) and test results for each specimen were tracked and recorded. The yield strength of all specimens was determined using the 0.2% offset method described in ASTM E8 (ASTM 2022a). All tensile strengths were taken as the maximum stress achieved during testing, and the elongation values were recorded at the point of fracture, signified by a sudden drop in strength after necking. Figure 5-3 shows a photo of the specimens after testing. As shown in the figure, all 50-grade specimens failed within the weld metal, and all 70-grade specimens failed in the base metal directly outside the welded joint.

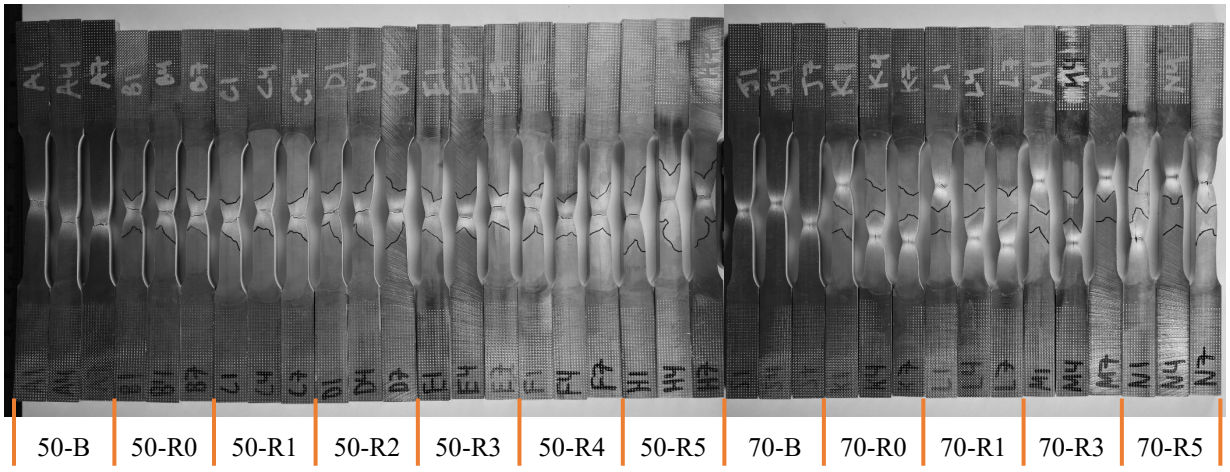


**Figure 5-3. Photo. Photo of tension specimens after testing.**

The DIC strain fields were used to visualize the welded joints and to confirm whether the welded joints influenced the failure. Figure 5-4 shows two representative strain fields captured using DIC for specimens 50-R3-T2 and 70-R3-T2 at various loading stages. In this figure, a color gradient maps the strain field over a range of 0 to 0.1 in./in., and two different loading

stages are shown: $10\varepsilon_y$ and $26\varepsilon_y$, where $\varepsilon_y$ is the strain corresponding to the yield stress. The loading stages were arbitrarily chosen because they represent intermediate points beyond the yield and tensile strengths and exhibit distinct strain fields that show the different weld regions. At both loading stages shown, the weld metal, HAZ, and base metal are clearly visible due to the different strain rates of each. At $26\varepsilon_y$, the necking location of the specimen is shown in red, indicating the point of maximum strain. As shown, the point of failure is entirely in the weld metal for 50-R3-T2 and in the base metal for 70-R3-T2. This behavior is typical across all specimens of each grade and confirms that the necking locations are always either entirely in the weld metal or in the base metal.

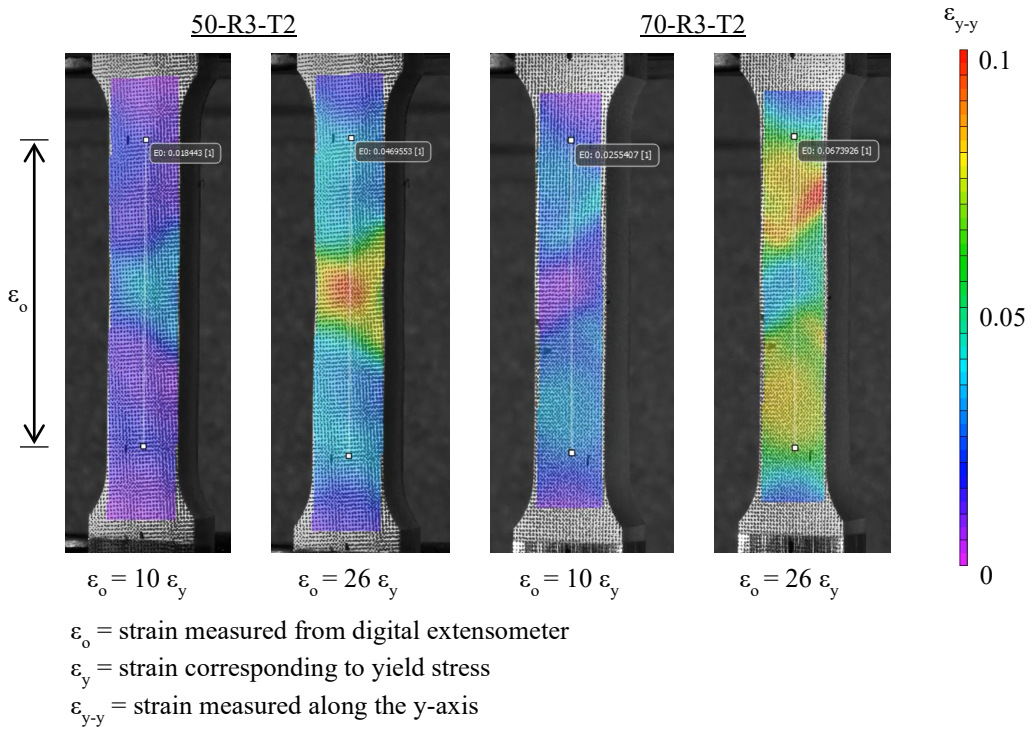


**Figure 5-4. Multiple Photos. DIC data showing strain fields of 50-R3-T2 and 70-R3-T2 at various loading stages.**

Figures 5-5 through 5-16 show the stress-strain curves for all tension tests conducted for each sample group. In these figures, the strain is plotted on the abscissa and the stress on the

ordinate. Note that each figure includes a subfigure showing a close-up of the yield region, demonstrating the 0.2% offset method used to determine the yield strengths. Figures 5-17 and 5-18 show the resulting stress-strain curves for all tension tests conducted for the 50-grade and 70-grade sample groups, respectively. The yield strength, tensile strength, and elongation values for all the tension tests are tabulated in Table 5-1, and the averages for each sample group are tabulated in Table 5-2.

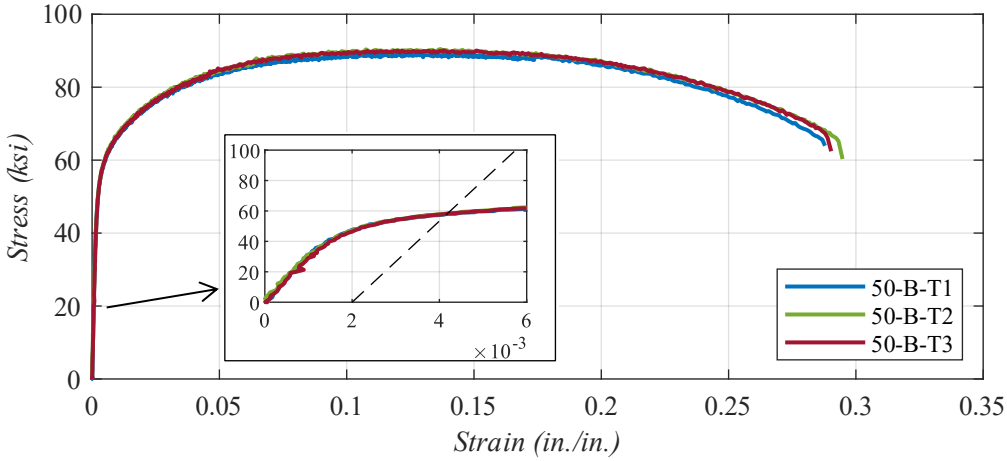


**Figure 5-5. Graph. Stress-strain plots for 50-B.**

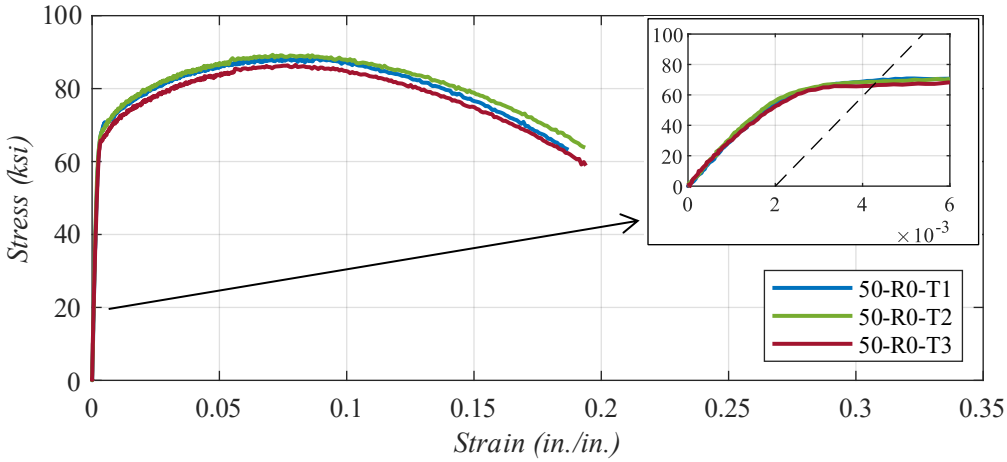


**Figure 5-6. Graph. Stress-strain plots for 50-R0.**

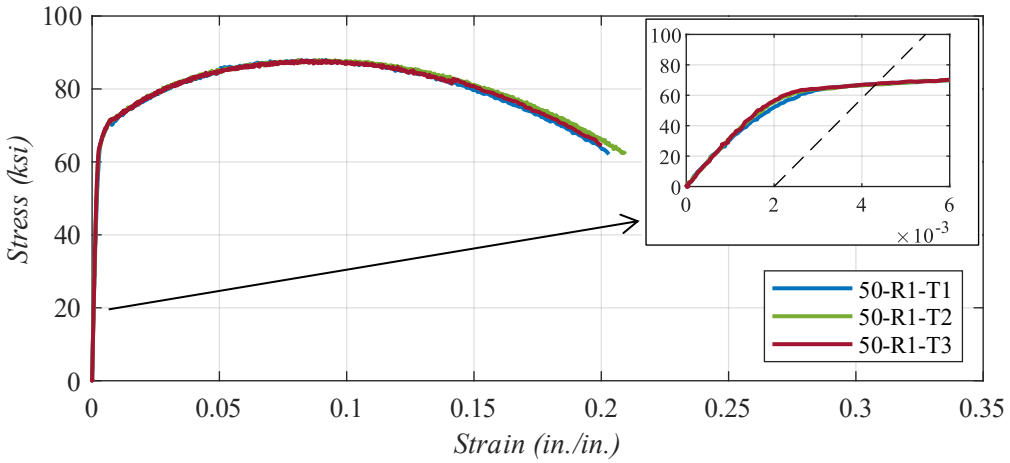


**Figure 5-7. Graph. Stress-strain plots for 50-R1.**

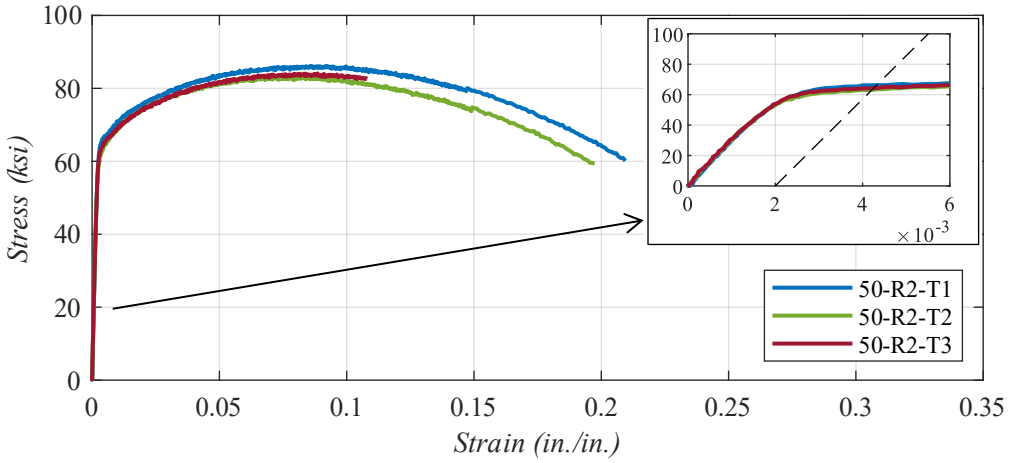


**Figure 5-8. Graph. Stress-strain plots for 50-R2.**

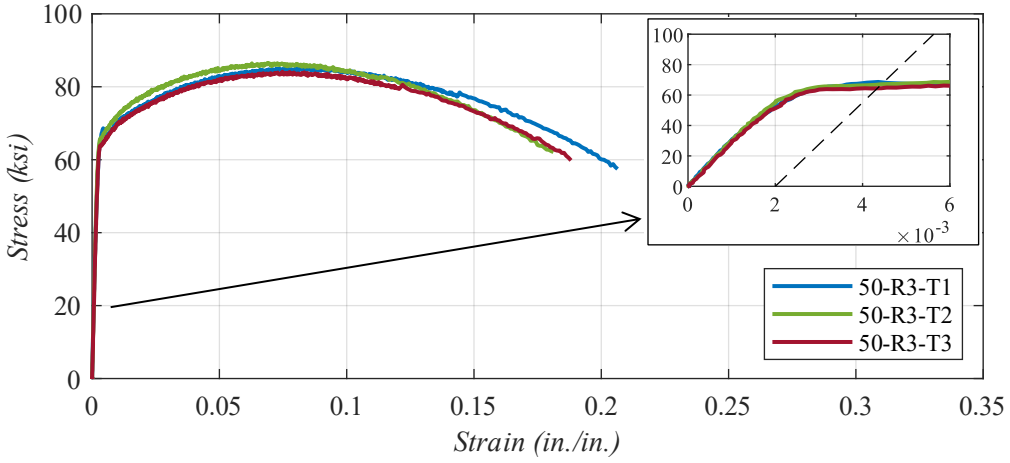


**Figure 5-9. Graph. Stress-strain plots for 50-R3.**

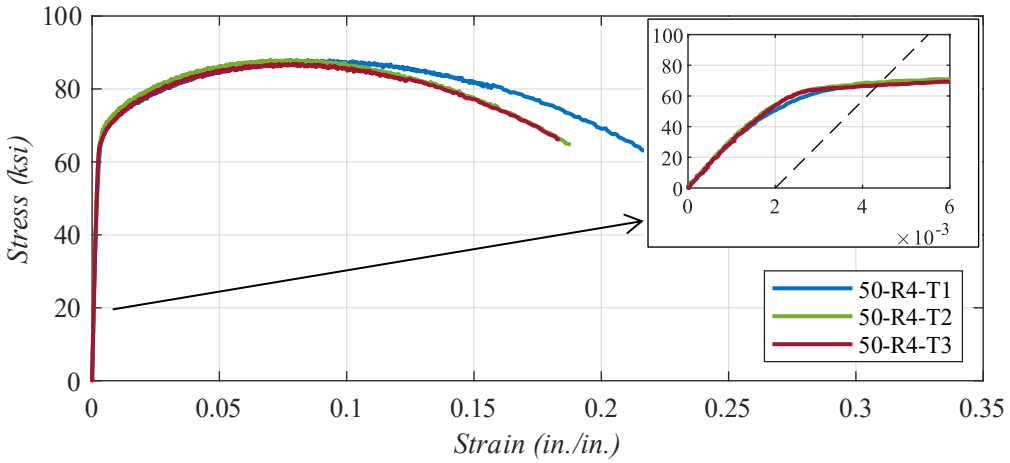


**Figure 5-10. Graph. Stress-strain plots for 50-R4.**

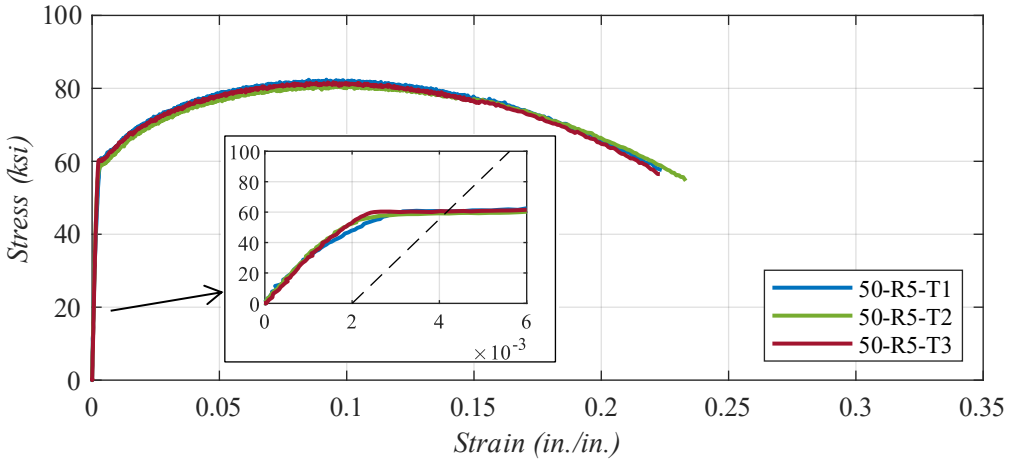


**Figure 5-11. Graph. Stress-strain plots for 50-R5.**

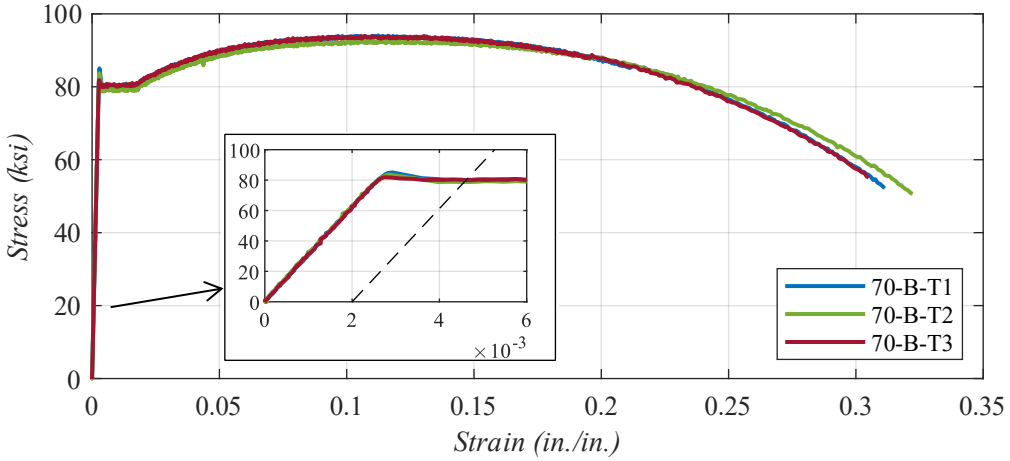


**Figure 5-12. Graph. Stress-strain plots for 70-B.**

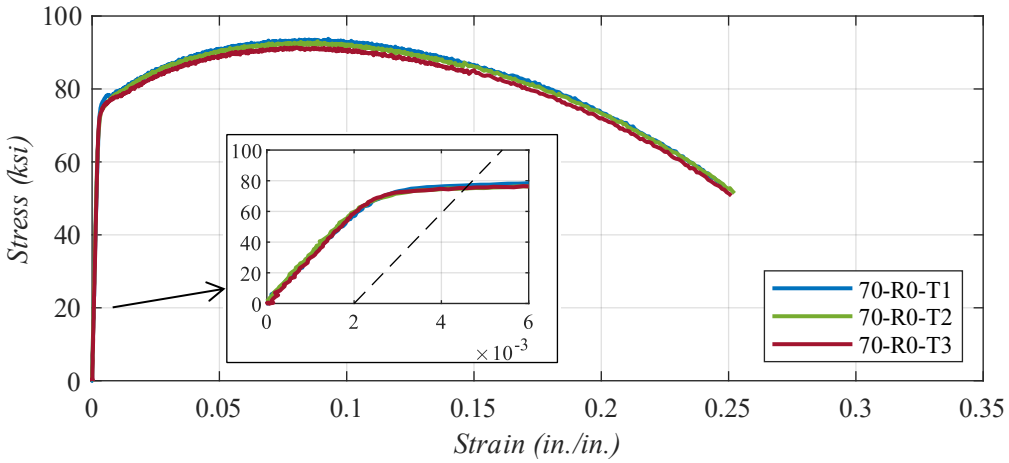


**Figure 5-13. Graph. Stress-strain plots for 70-R0.**

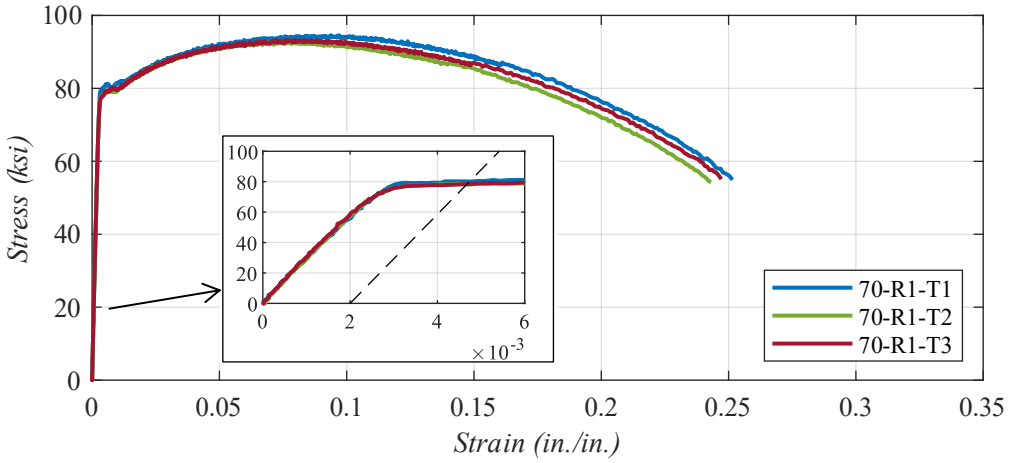


**Figure 5-14. Graph. Stress-strain plots for 70-R1.**

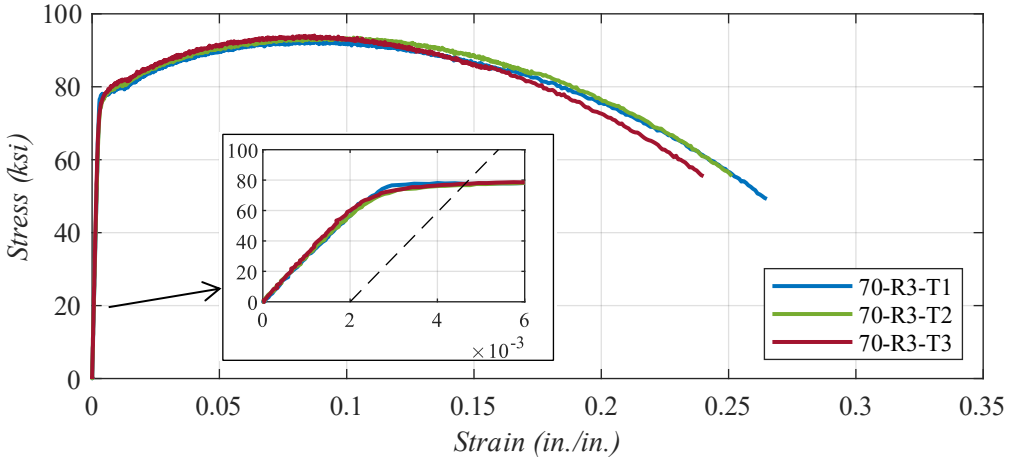


**Figure 5-15. Graph. Stress-strain plots for 70-R3.**

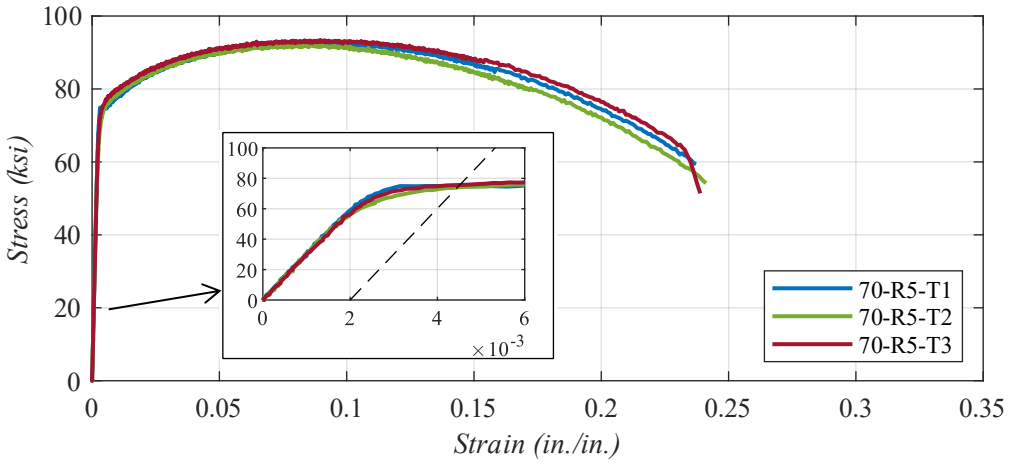


**Figure 5-16. Graph. Stress-strain plots for 70-R5.**

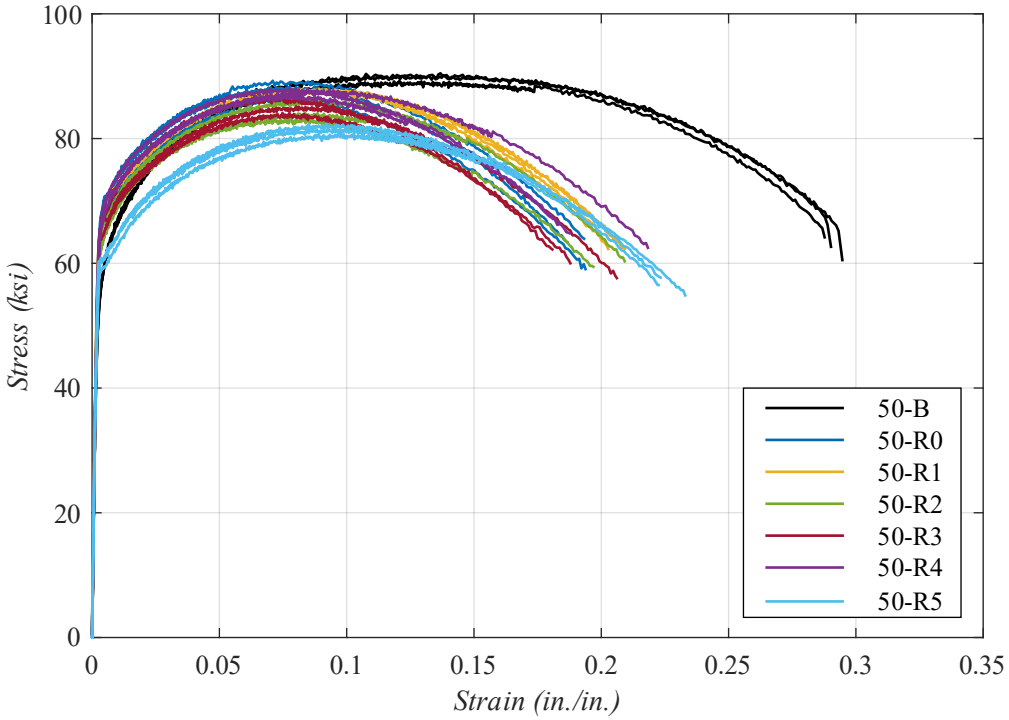


**Figure 5-17. Graph. Stress-strain plots for all 50-grade specimens.**

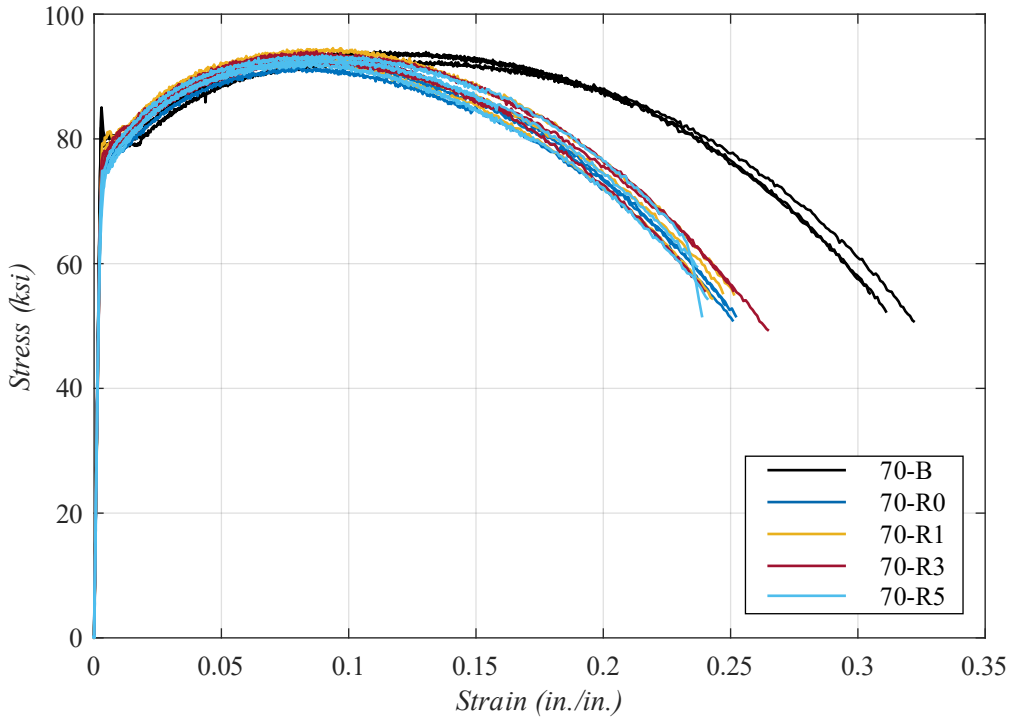


**Figure 5-18. Graph. Stress-strain plots for all 70-grade specimens.**

**Table 5-1. Yield stress, tensile stress, and elongation values for all tension tests.**

| *Specimen* | *Yield (ksi)* | *Tensile (ksi)* | *Elong. (in./in.)* | *Specimen* | *Yield (ksi)* | *Tensile (ksi)* | *Elong. (in./in.)* |
|---|---|---|---|---|---|---|---|
| 50-B-T1 | 57.6 | 89.2 | 0.288 | 70-B-T1 | 80.0 | 94.1 | 0.311 |
| 50-B-T2 | 58.4 | 90.5 | 0.295 | 70-B-T2 | 78.7 | 92.6 | 0.322 |
| 50-B-T3 | 58.3 | 90.1 | 0.290 | 70-B-T3 | 80.3 | 93.9 | 0.305 |
| 50-R0-T1 | 69.2 | 88.3 | 0.187 | 70-R0-T1 | 77.2 | 93.8 | 0.248 |
| 50-R0-T2 | 68.7 | 89.3 | 0.194 | 70-R0-T2 | 74.9 | 93.1 | 0.252 |
| 50-R0-T3 | 66.6 | 86.5 | 0.194 | 70-R0-T3 | 75.2 | 91.4 | 0.251 |
| 50-R1-T1 | 67.5 | 88.0 | 0.203 | 70-R1-T1 | 80.1 | 94.6 | 0.251 |
| 50-R1-T2 | 66.9 | 88.0 | 0.209 | 70-R1-T2 | 78.1 | 92.9 | 0.243 |
| 50-R1-T3 | 67.4 | 87.9 | 0.200 | 70-R1-T3 | 78.4 | 93.3 | 0.247 |
| 50-R2-T1 | 66.2 | 86.2 | 0.209 | - | - | - | - |
| 50-R2-T2 | 63.6 | 83.2 | 0.197 | - | - | - | - |
| 50-R2-T3 | 64.2 | 84.1 | 0.108 | - | - | - | - |
| 50-R3-T1 | 68.0 | 85.2 | 0.206 | 70-R3-T1 | 77.6 | 92.7 | 0.265 |
| 50-R3-T2 | 67.1 | 86.5 | 0.181 | 70-R3-T2 | 76.7 | 93.5 | 0.251 |
| 50-R3-T3 | 64.5 | 84.1 | 0.188 | 70-R3-T3 | 77.5 | 94.1 | 0.240 |
| 50-R4-T1 | 67.8 | 87.9 | 0.218 | - | - | - | - |
| 50-R4-T2 | 68.9 | 88.0 | 0.188 | - | - | - | - |
| 50-R4-T3 | 67.0 | 86.9 | 0.184 | - | - | - | - |
| 50-R5-T1 | 60.6 | 82.4 | 0.224 | 70-R5-T1 | 74.9 | 92.8 | 0.237 |
| 50-R5-T2 | 59.2 | 80.8 | 0.233 | 70-R5-T2 | 73.7 | 92.3 | 0.241 |
| 50-R5-T3 | 60.7 | 81.7 | 0.223 | 70-R5-T3 | 75.7 | 93.5 | 0.239 |

**Table 5-2. Average yield stress, tensile stress, and elongation values for each sample group.**

| *Sample Group* | *Yield (ksi)* | *Tensile (ksi)* | *Elong. (in./in.)* | *Sample Group* | *Yield (ksi)* | *Tensile (ksi)* | *Elong. (in./in.)* |
|---|---|---|---|---|---|---|---|
| 50-B | 58.1 | 89.9 | 0.291 | 70-B | 79.7 | 93.6 | 0.313 |
| 50-R0 | 68.2 | 88.0 | 0.192 | 70-R0 | 75.8 | 92.7 | 0.251 |
| 50-R1 | 67.3 | 87.9 | 0.204 | 70-R1 | 78.9 | 93.6 | 0.247 |
| 50-R2 | 64.7 | 84.5 | 0.172 | - | - | - | - |
| 50-R3 | 66.5 | 85.3 | 0.192 | 70-R3 | 77.3 | 93.4 | 0.252 |
| 50-R4 | 67.9 | 87.6 | 0.197 | - | - | - | - |
| 50-R5 | 60.2 | 81.6 | 0.227 | 70-R5 | 74.7 | 92.9 | 0.239 |

As the figures and tables show, all the tension specimens from each sample group agree well with one another, with the measured properties generally varying by no more than 5% across the three specimens. Additionally, Figures 5-17 and 5-18, and the summary tables show that the different welded sample groups exhibit similar stress-strain curves and comparable strengths and ductility, regardless of the number of repairs. In general, the welded specimens have strengths comparable to those of the base material, but the ductility of the welded specimens is significantly less than that of the base material.

### *5.1.3. Discussion of Results*

To evaluate what, if any, influence numerous weld repairs have on the yield, tensile, and ductility of a CJP butt-splice joint, data from the tension tests from each grade of material were compiled and compared across all the different numbers of weld repairs. Figures 5-19 and 5-20 compare the measured elongations from the 50-grade and 70-grade tension tests, respectively. In these figures, the abscissa is the number of weld repairs, and the ordinate is the measured elongation. Additionally, the base metal minimum requirements specified in ASTM A709 (ASTM 2021b) and the weld metal minimum requirements specified in AWS A5.23 (AWS 2021) are shown for reference.

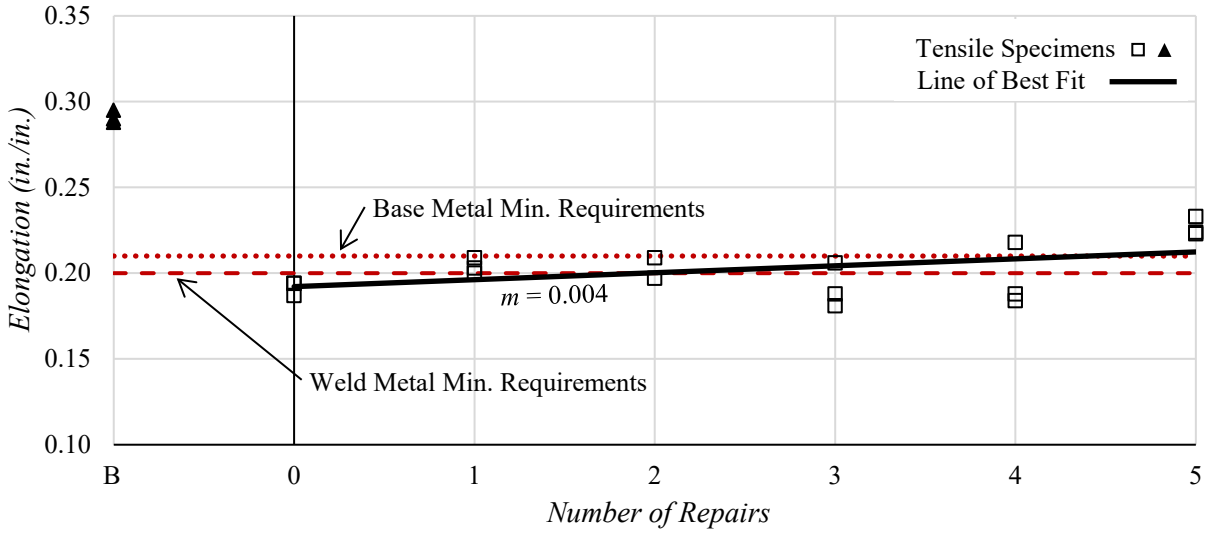


**Figure 5-19. Graph. Comparison of measured elongations for 50-grade tensile specimens.**

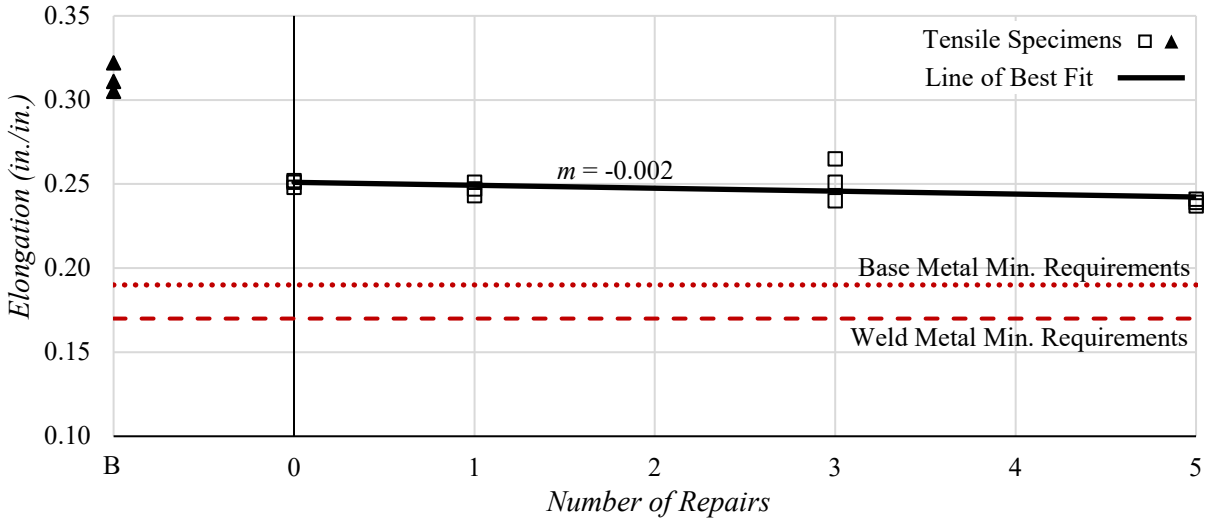


**Figure 5-20. Graph. Comparison of measured elongations for 70-grade tensile specimens.**

Figure 5-19 shows that not all the 50-grade welded specimens met the A709 minimum ductility requirements, and all the welded specimens have a lower measured elongation than the base metal specimens. Only the 50-grade welded specimens with five repairs met the A709 minimum requirements; however, because the majority of the specimens were close to or just below the A709 minimum requirements, this observation appears more indicative of the 50-grade joint performance itself than of the influence of weld repairs. Looking at overall trends,

the measured elongation of the 50-grade specimens has a positive relationship with the increasing number of weld repairs, increasing at a rate of 0.004 in./in. per weld repair. Figure 5-20 shows that all 70-grade specimens exceed the A709 minimum ductility requirements. Looking at overall trends, the measured elongation of the 70-grade specimens has a negative relationship with the increasing number of weld repairs, decreasing at a rate of 0.002 in./in. per weld repair. However, the negative relationship is not significant because the measured elongations are well above the A709 minimum requirements, and the trend is essentially flat, with no repaired joint having a measured ductility less than 5% below the baseline R0 joint with no repairs.

Figures 5-21 and 5-22 compare the measured yield strengths from the 50-grade and 70-grade tension tests, respectively. In these figures, the abscissa is the number of weld repairs, and the ordinate is the measured yield stress. Additionally, the base metal minimum requirements specified in ASTM A709 and the weld metal minimum requirements specified in AWS A5.23 are shown for reference.

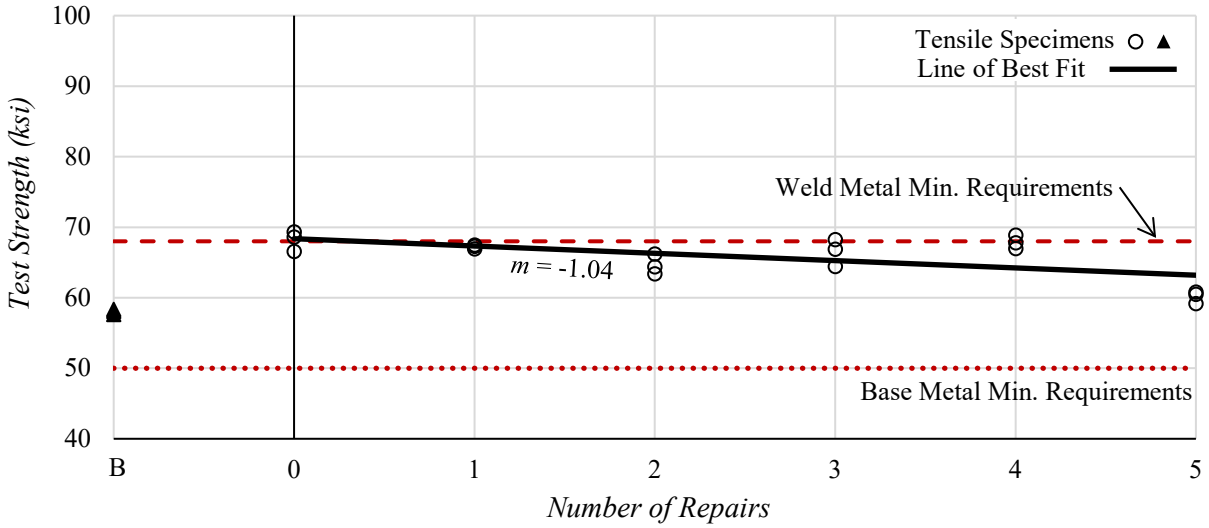


**Figure 5-21. Graph. Comparison of yield stresses for 50-grade tensile specimens.**

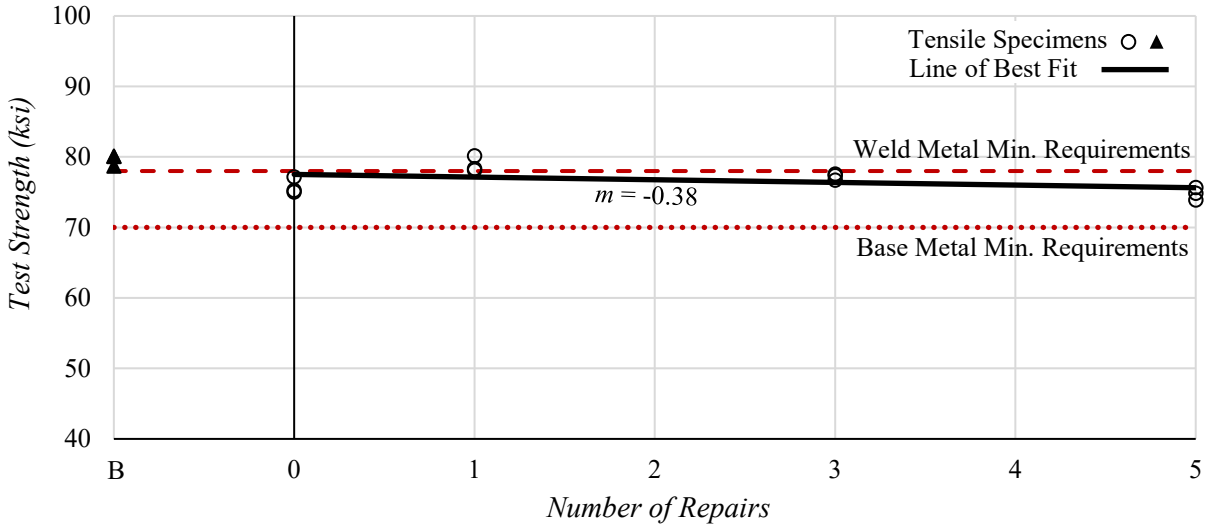


**Figure 5-22. Graph. Comparison of yield stresses for 70-grade tensile specimens.**

Figure 5-21 shows that all 50-grade welded specimens exceed the A709 minimum yield requirements and have a slightly larger yield stress than the base metal specimens. Looking at overall trends, the measured yield strength of the 50-grade specimens shows a negative relationship with the number of weld repairs, decreasing by 1.04 ksi per weld repair. On average, the 50-grade specimens exhibited a decrease in yield strength of approximately 12% from R0 to R5, and the lowest strength specimen still exceeded the A709 minimum requirements by 17%. Similarly, Figure 5-22 shows that all 70-grade welded specimens exceed the A709 minimum yield requirements and have slightly lower yield stresses than the base metal specimens. Looking at overall trends, the measured yield strength of the 70-grade specimens shows a negative relationship with the number of weld repairs, decreasing by 0.38 ksi per weld repair. On average, the 70-grade specimens exhibited a decrease in yield strength of approximately 2% from R0 to R5, and the lowest strength specimen still exceeded the A709 minimum strength requirements by approximately 7%. While a negative trend was found for both grades of material, these negative trends were not significant, and all specimens exceeded the minimum A709 yield strength requirements.

Figures 5-23 and 5-24 compare the measured tensile strengths from the 50-grade and 70-grade tension tests, respectively. In these figures, the abscissa is the number of weld repairs, and the ordinate is the measured tensile stress. Additionally, the base metal minimum requirements specified in ASTM A709 and the weld metal minimum requirements specified in AWS A5.23 are shown for reference.

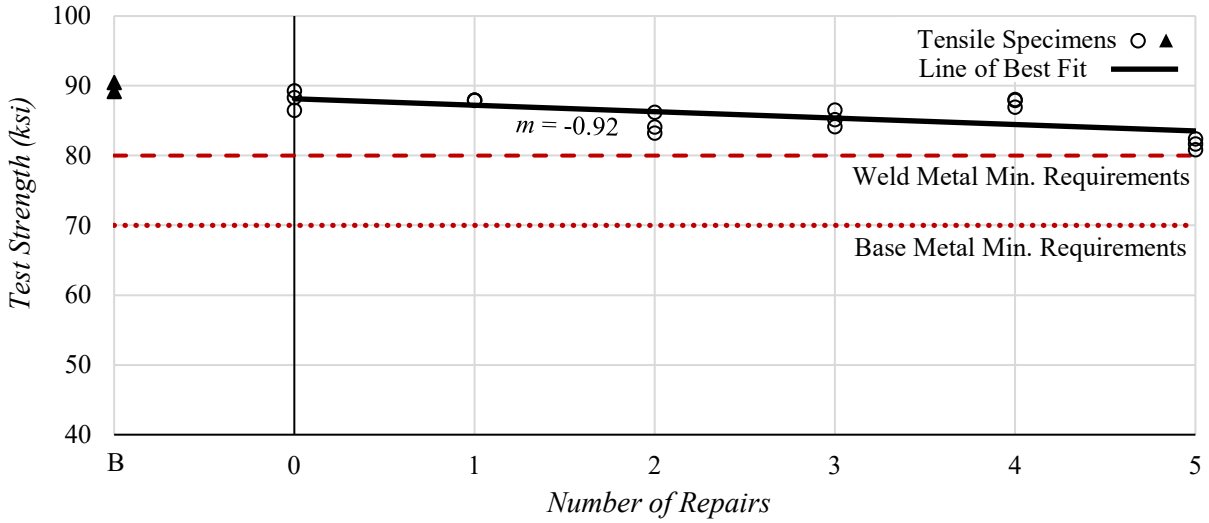


**Figure 5-23. Graph. Comparison of tensile stresses for 50-grade tensile specimens.**

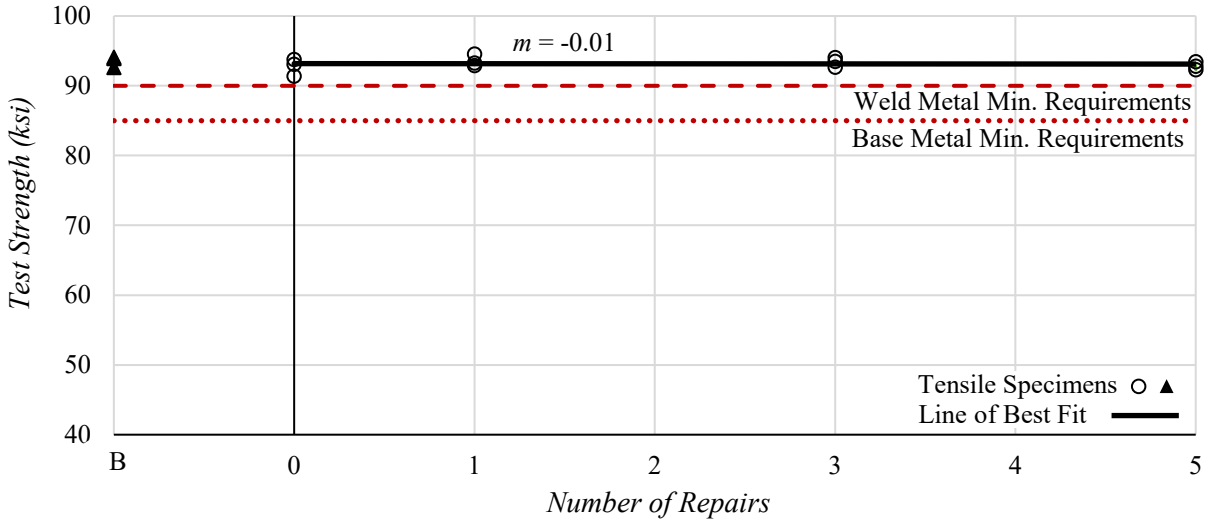


**Figure 5-24. Graph. Comparison of tensile stresses for 70-grade tensile specimens.**

Figure 5-23 shows that all 50-grade welded specimens exceed the A709 minimum tensile strength requirements and have slightly lower tensile stress than the base metal specimens. Looking at overall trends, the measured tensile strength of the 50-grade specimens has a negative relationship with the number of weld repairs, decreasing by 0.92 ksi per weld repair. On average, the 50-grade specimens exhibited a decrease in tensile strength of approximately 7% from R0 to R5, and the lowest strength specimen still exceeded the A709 minimum requirements by 17%. Figure 5-24 shows that all 70-grade welded specimens exceed the A709 minimum tensile strength requirements and have tensile strengths comparable to those of the base metal specimens. Looking at overall trends, the measured yield strength of the 70-grade specimens shows a negative relationship with the number of weld repairs, decreasing by 0.01 ksi per weld repair. The low trend rate indicates that there is essentially no relationship between tensile strength and the number of weld repairs for the specimens, and all specimens exceeded the A709 minimum tensile strength requirements by 9%. Similar to the yield strengths, a negative trend was found for both grades of material. However, these negative trends were not significant, and all specimens exceeded the minimum A709 tensile strength requirements.

Based on the discussions above, the following conclusions can be drawn:

- The measured elongations of the welded specimens indicated that the weld repairs have little effect on the overall ductility of the joint.
- The measured yield and tensile stresses of the welded specimens exceeded the A709 minimum requirements, and the weld repairs had little effect on the yield and tensile strengths of the joint. Although a negative relationship between the yield / tensile stresses and the number of weld repairs was observed, the trends were insignificant because the

rate of change was always low, and all specimens always exceeded the A709 minimum strength requirements by at least 7%.

- As such, there appears to be no significant change in the ductility, yield strength, or tensile strength of the CJP butt-splice welded joints up through five repairs.

## 5.2. Side-Bend Tests

### *5.2.1. Specimen Information and Testing Setup*

Two side-bend tests were conducted for each material characterization plate, resulting in a total of 20 side-bend tests. These tests are significant as they are common ductility checks performed as part of WPS qualification tests in fabrication shops. The side-bend specimens were machined from the rectangular blanks cut from the material characterization plates per the geometrical requirements of ASTM E190 (ASTM 2021c) and the surface finish requirements of AASHTO/AWS D1.5 (2020). All side-bend specimens were 3/8-inch thick and machined at Georgia Tech. Figure 5-25 shows the typical side-bend specimen. Note that ASTM E190 specifies a minimum length of six inches, and AASHTO/AWS D1.5 specifies a length of ten inches. The seven-inch length was chosen as it is a convenient, intermediate length that worked well with the testing jigs used.

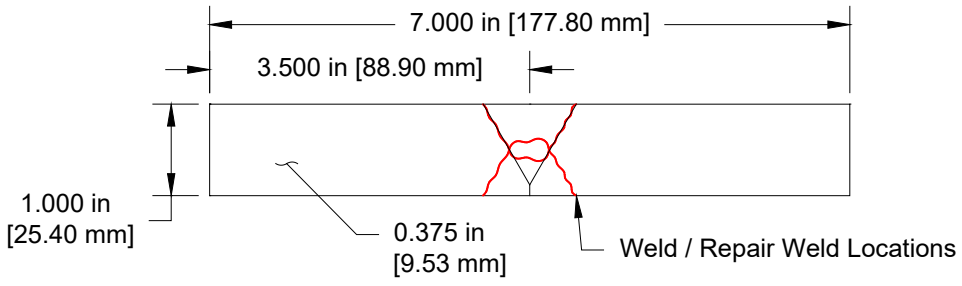


**Figure 5-25. Illustration. Typical side-bend specimen.**

Per the requirements of AASHTO/AWS D1.5 (2020) and ASTM E190 (ASTM 2021c), two different guided bend test jigs were needed to accommodate the material grades being tested: a 50-grade jig and a 70-grade jig. These testing jigs are almost identical, except that the 70-grade testing jig has slightly larger dimensions than the 50-grade testing jig to account for the reduced ductility expected from higher-strength materials. All 50-grade side-bend specimens were tested at the GDOT Office of Materials and Testing (OMAT) Facility using a testing jig that meets the dimensional requirements of AASHTO/AWS D1.5 for 50-grade materials. All 70-grade side-bend specimens were tested at the Local 387 Iron Worker Training Facility using a testing jig that meets the dimensional requirements of AASHTO/AWS D1.5 for 70-grade materials. All side-bend tests were conducted per the requirements of ASTM E190 using a hydraulically controlled plunger system that operated at a constant displacement rate. Figures 5-26 and 5-27 show an overview of the 50-grade and 70-grade testing jigs, respectively.

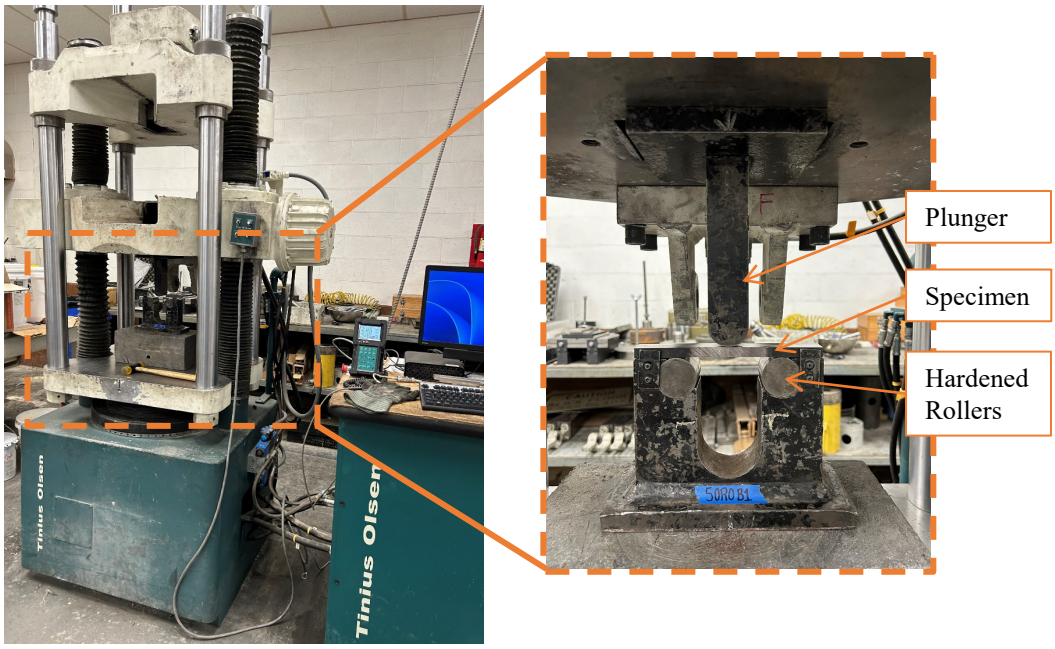


**Figure 5-26. Multiple Photos. Overview of 50-grade side-bend testing setup.**

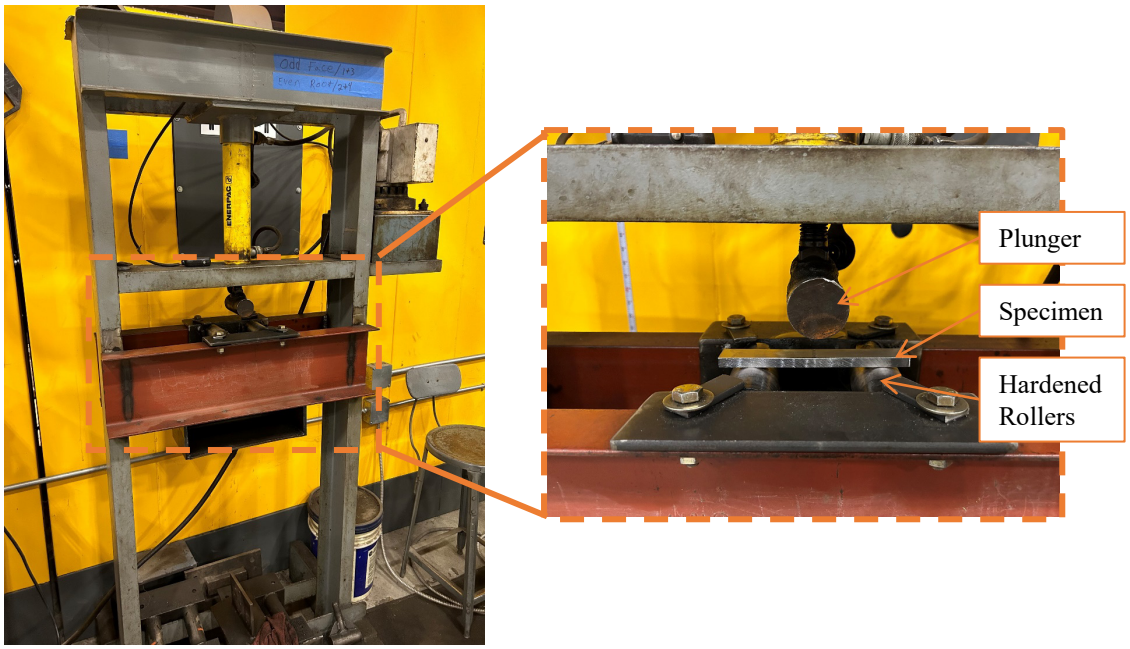


**Figure 5-27. Multiple Photos. Overview of 70-grade side-bend testing setup.**

### *5.2.2. Testing Results*

All side-bend specimens were bent to the designated U-shape specified in ASTM E190 (ASTM 2021c), and the specimens were inspected for cracks using visual testing (VT) and dye-penetrant testing (PT) inspection methods. If cracks were found in the weld metal or surrounding HAZ, the specimen was labeled as "Fail," and if no cracks were found, the specimen was labeled as "Pass." If cracks were found in the base metal but not in the weld metal, the specimen was labeled as "Pass*." Post-testing photos of representative specimens are shown in Figure 5-28, and the final testing results for all specimens are shown in Table 5-3. Figure 5-28a is representative of all specimens designated as "Pass," and Figure 5-28b is representative of all specimens designated as "Pass*." No specimens were designated as a "Fail," so no representative photo is provided. Photos of all the side-bend specimens after testing are in Appendix C.

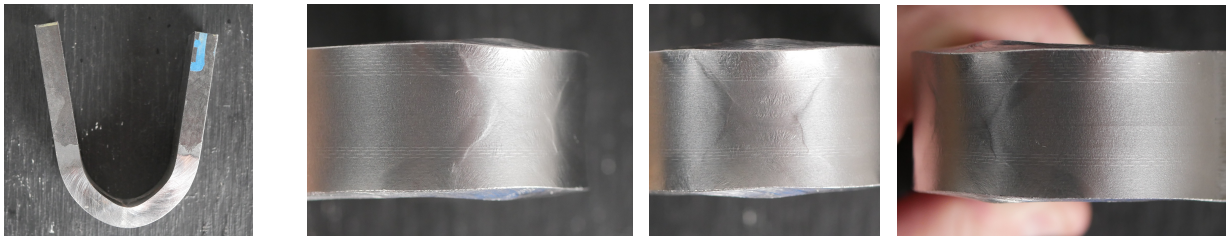

Overview Left-Side Center Right-Side

(a) Photos of 50-R1-B1 side-bend test (Pass)

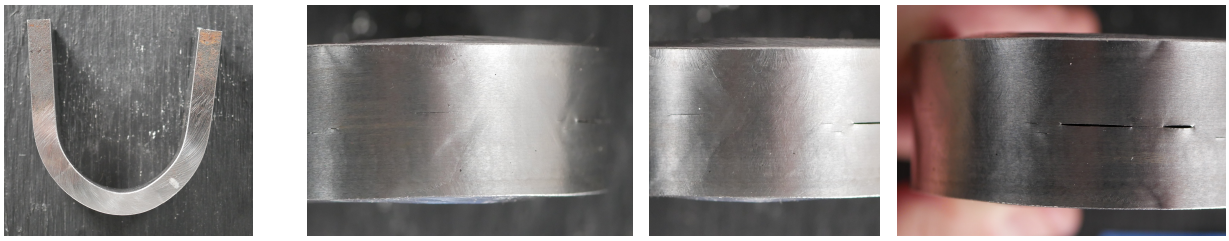

Overview Left-Side Center Right-Side

(b) Photos of 70-R1-B1 side-bend test (Pass*)

**Figure 5-28. Multiple Photos. Representative photos of tested side-bend specimens. (a) Photos of 50-R1-B1 side-bend test (Pass) and (b) Photos of 70-R1-B1 side-bend test (Pass*)**

**Table 5-3. Side-Bend Test Results**

| *Specimen* | *Result* | *Specimen* | *Result* |
|---|---|---|---|
| 50-R0-B1 | Pass | 70-R0-B1 | Pass |
| 50-R0-B2 | Pass | 70-R0-B2 | Pass |
| 50-R1-B1 | Pass | 70-R1-B1 | Pass* |
| 50-R1-B2 | Pass | 70-R1-B2 | Pass* |
| 50-R2-B1 | Pass | - | - |
| 50-R2-B2 | Pass | - | - |
| 50-R3-B1 | Pass | 70-R3-B1 | Pass |
| 50-R3-B2 | Pass | 70-R3-B2 | Pass |
| 50-R4-B1 | Pass | - | - |
| 50-R4-B2 | Pass | - | - |
| 50-R5-B1 | Pass | 70-R5-B1 | Pass* |
| 50-R5-B2 | Pass | 70-R5-B2 | Pass* |

* weld metal and HAZ pass, base metal fail

As Table 5-3 shows, all specimens passed the bend test, meaning no cracks were found in the weld metal of any of the specimens. However, some specimens showed cracks in the base metal along the center of the plate. Upon inspection, the cracks were contained within the base metal and appeared to have no interaction with the weld metal or HAZ. As such, these specimens

are also classified as Pass, but with the note that the base metal experienced cracking due to lamination issues (designated as Pass* in Table 5-3). Interestingly, all the plates that experienced base metal cracking were from the plates that were refabricated after the original plates.

As all of the Pass* specimens were from the refabricated plates, the cracking that occurred was further investigated. A close examination of the 70-R1 and 70-R5 bend specimens shows that the cracks are almost directly in the middle of the plate and appear to be the result of lamellar tearing of the base metal plates. The plate fabricator and plate producer were consulted for further clarification regarding why these particular plates experienced lamellar tearing, whereas the other plates from the same heat did not. The plate producer indicated that it is not uncommon for the lamellar tearing observed to occur during extreme ductility checks on specimens pulled from the end of the heat, due to impurities that aggregate near the middle of the plate during cooling. As such, the lamellar tearing is directly related to the base metal in these two plates and is not an indication of poor weld quality or ductility. Additionally, the plate producer indicated that the difference in the sampling location of the heat should not have a significant impact on the tests being performed, which was confirmed by the other material characterization tests that showed the 70-R1 and 70-R5 specimens exhibited no signs of lamellar tearing and no significant deviations from the 70-R0 or 70-R3 specimens.

## 5.3. CVN Impact Tests

### *5.3.1. Specimen Information and Testing Setup*

In total, 252 CVN impact tests were performed as part of the material characterization research effort: 36 for the base metal groups and 18 for each material characterization plate. These tests are significant as they give insights into the fracture toughness of the HAZ around the

welded joint being tested. Oversized CVN blanks were machined from the CVN blocks cut from the material characterization plates, and all CVN blanks were taken from 0.5T. All oversized CVN blanks were oriented perpendicular to the weld, and six CVN blanks were taken from each CVN block. The oversized CVN blanks were 0.394 x 0.394 x 3.937 in. [10 x 10 x 100 mm] and machined within the geometrical and surface finish requirements specified in ASTM E23 (ASTM 2018), except for having a length of 3.937 in. [100 mm] rather than 2.165 in. [55 mm]. All specimens not meeting the cross-sectional allowances indicated in ASTM 23 were marked as defective and not tested. All oversized CVN blanks were machined by Chicago Spectro in Chicago, IL, and shipped to the Georgia Tech SEML for notching and testing.

The oversized CVN blanks were chemically etched with a nital solution to expose the different weld regions, and the weld fusion lines were marked with a marker. As the HAZ metals are the primary region of concern, all welded specimens were then notched in the HAZ following the findings from Collins and Yount (2023) and guidance from the American Society of Mechanical Engineers (ASME) Boiler and Pressure Vessel Code Section VIII Division 1 (ASME VIII-1) (2023) standards. For V-shape weld profiles, the ASME VIII-I (2023) standard recommends that specimens be notched at a horizontal distance of two millimeters from the fusion line. Collins and Yount (2023) found that the lowest (i.e., worst) impact results for SAW typically occurred for specimens with notches within two millimeters of the fusion line, with the results becoming increasingly worse the closer the notch was to the fusion line.

Based on the literature, the notch locations in the current study were set at a horizontal distance of one millimeter from the fusion line near the middle of the CVN specimen and always consisted of at least 70% HAZ material along the notch length. The distance of one millimeter was chosen to set the notch as close to the fusion line as possible. The “double-V” shaped weld

profile formed from the base and repair welds made it impossible for the notch to consist of 100% HAZ material at the targeted offset; therefore, the 70% rule used was chosen as a baseline based on the geometrical ratios observed in the first few specimens notched in the 50-R0 specimens. The notching parameters ensured that the worst-case regions were targeted and that the notch location was primarily HAZ material rather than weld metal.

All specimens were broached at the Georgia Tech SEML, and all notches were checked for compliance using a caliper gauge designed to check the notch depth per ASTM E23 (ASTM 2018) requirements. Once all the specimens were notched and checked, they were cut to their final length of 2.165 in. [55 mm]. Figure 5-29 illustrates the machining process described above and shows a typical CVN specimen. Figures 5-29a and 5-29b show the layout of the oversized CVN blanks within the CVN blocks, and Figure 5-29c shows the layout of the typical CVN specimen within the CVN blank. Note that all CVN specimens were notched on the face orthogonal to the weld profile, which corresponds to the face shown in Figure 5-29c, with a surface finish of 63 microinches (μin). Figure 5-30 shows photos of a specimen in the broaching machine and being checked with the caliper gauge.

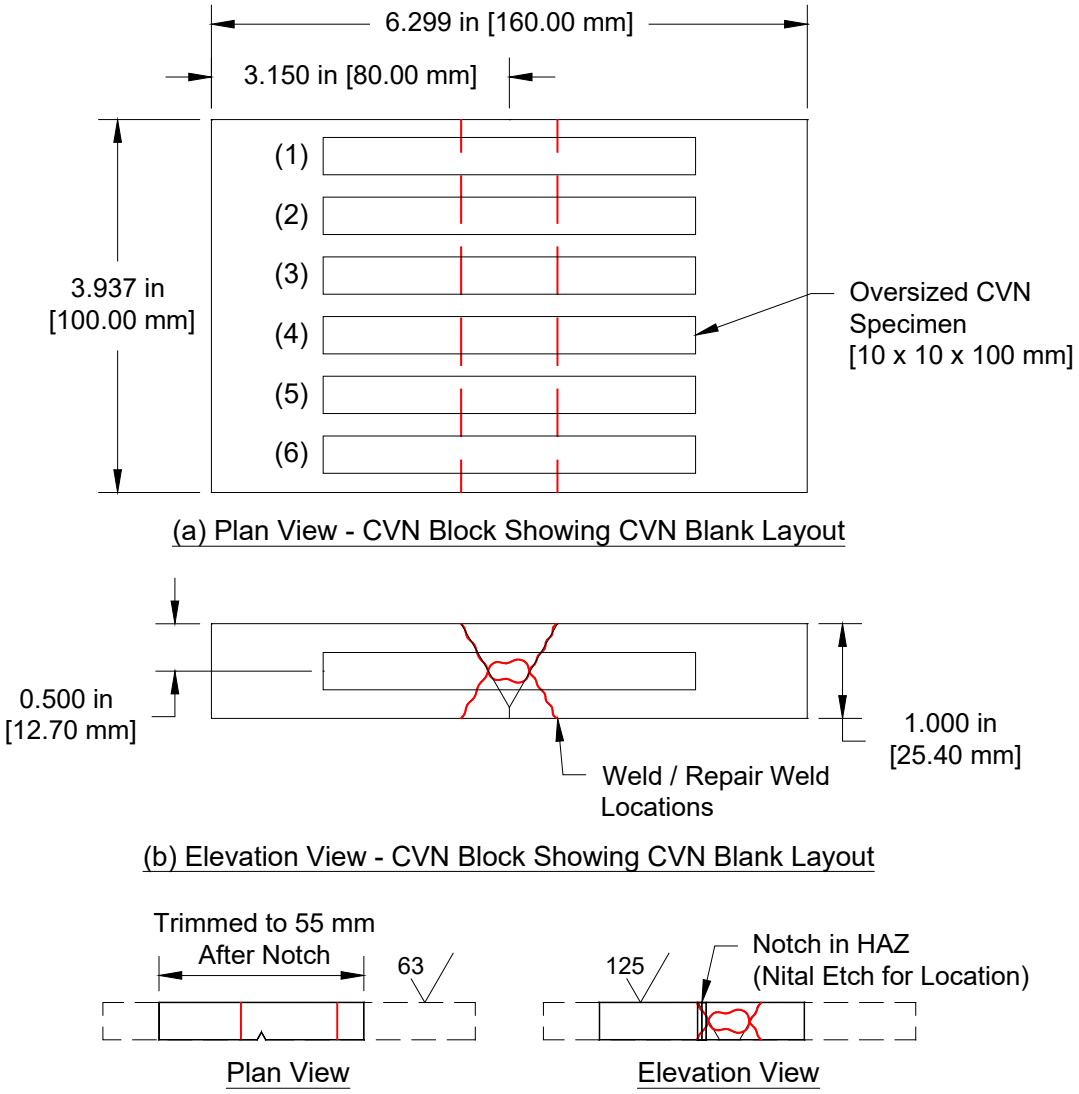


**Figure 5-29. Illustration. Typical CVN impact specimen. (a) Plan View – CVN block showing CVN blank layout, (b) Elevation View – CVN block showing CVN blank layout, and (c) Typical CVN specimen**

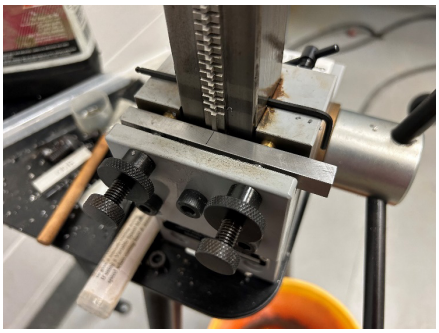

(a) Photo of CVN specimen being notched

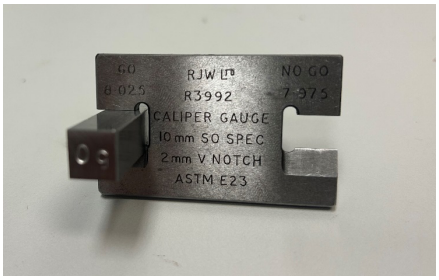


(b) Photo of CVN specimen in caliper gauge

**Figure 5-30. Multiple Photos. Photos showing the broaching and checking of the CVN specimen. (a) Photo of CVN specimen being notched, and (b) photo of CVN specimen in caliper gauge.**

All CVN impact tests were conducted at the Georgia Tech SEML per the requirements of ASTM E23 using an Instron Impact Testing Machine equipped with a 750-joule impact hammer. The impact tester was calibrated and certified approximately six months before any testing. All CVN specimens were cooled or heated to the testing temperatures in a methanol bath, and all specimens were bathed at the testing temperature for a minimum of five minutes before testing. Figure 5-31 shows an overview of the testing setup used for all the CVN impact tests.


**Figure 5-31. Photo. CVN impact tester.**

### *5.3.2. Testing Results*

36 CVN specimens were tested for each base metal sample group: 18 from the 50-B and 70-B material characterization plates, and 18 from the excess base materials of 50-R3 and 70-R3. For the base metal specimens, the CVN specimens were tested at temperatures ranging from 110°F [-79°C] to 120°F [49°C] to generate full temperature transition curves. 18 CVN specimens were tested for each welded sample group, with 15 specimens targeting the HAZ and three specimens targeting the weld metal. When 18 CVN specimens were unavailable for testing, the HAZ specimen count was prioritized. For the HAZ specimens, three CVN specimens were tested at five temperatures: -110°F [-79°C], -60°F [-51°C], -30°F [-34°C], 0°F [-18°C], and 60°F [-16°C]. For the weld metal specimens, all three CVN specimens were tested at 0°F [-18°C].

Figure 5-32 shows the CVN impact test results for the base metal sample groups. Figures 5-33 and 5-34 show the CVN impact test results for the 50-grade sample groups (i.e., 50-R0, R1, R2, R3, R4, and R5) and 70-grade sample groups (i.e., 70-R0, R1, R3, and R5), respectively. In these plots, the bottom abscissa shows the test temperature in Fahrenheit, and the left ordinate shows the absorbed CVN impact energy in foot-pounds (ft-lb). Similarly, the top abscissa is the test temperature in Celsius, and the right ordinate is the absorbed CVN impact energy measured in joules (J). The CVN data in each subplot have been fit with an asymmetric hyperbolic tangent (AHT) best-fit curve (Wallin 2011). The AHT best-fit curve was determined using the following equation:

$$Y = \frac{LS + US}{2} + \frac{US - LS}{2} * \tanh\left(\frac{T_o - DBTT}{C + D * T_o}\right) \quad \text{(Eq. 3)}$$

where, $LS$ is the lower shelf value (in joules), $US$ is the upper shelf value (in joules), $T_o$ is the temperature (°C), $DBTT$ is the ductile to brittle transition temperature (°C), $C$ corresponds to the

half-width transition region (°C), and *D* quantifies the asymmetry of the curve. The root mean square error (RMSE) between each AHT fit curve and the CVN data is provided in each subplot. Additionally, the ASTM A709 minimum impact energies for 50W and HPS70W nonredundant steel tension members (NSTM) and load path redundant members (LPRM) are plotted.

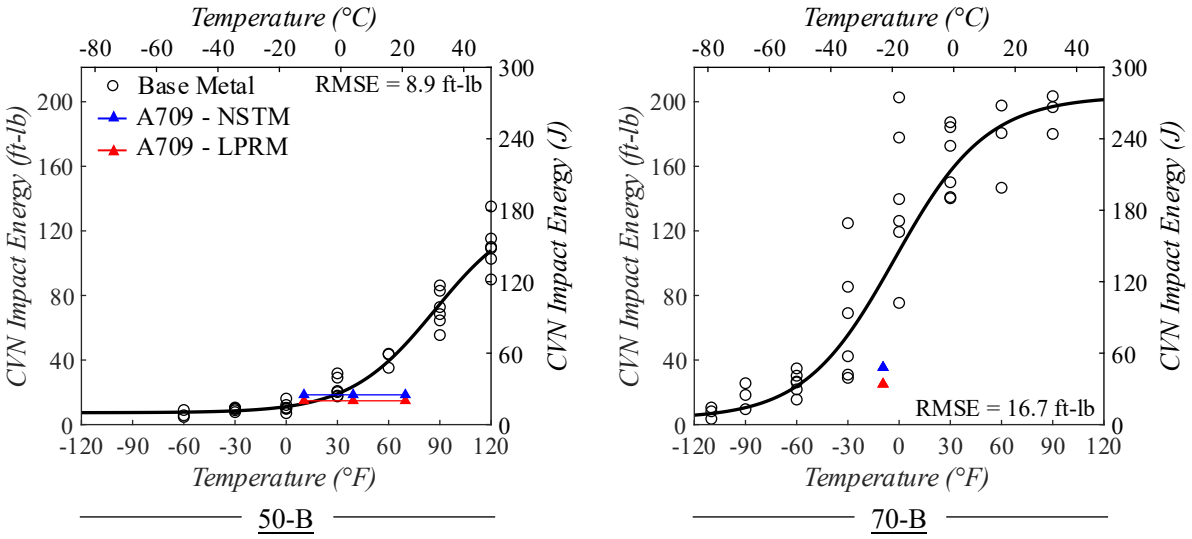


**Figure 5-32. Multiple Graphs. CVN impact test results for base metal sample groups.**

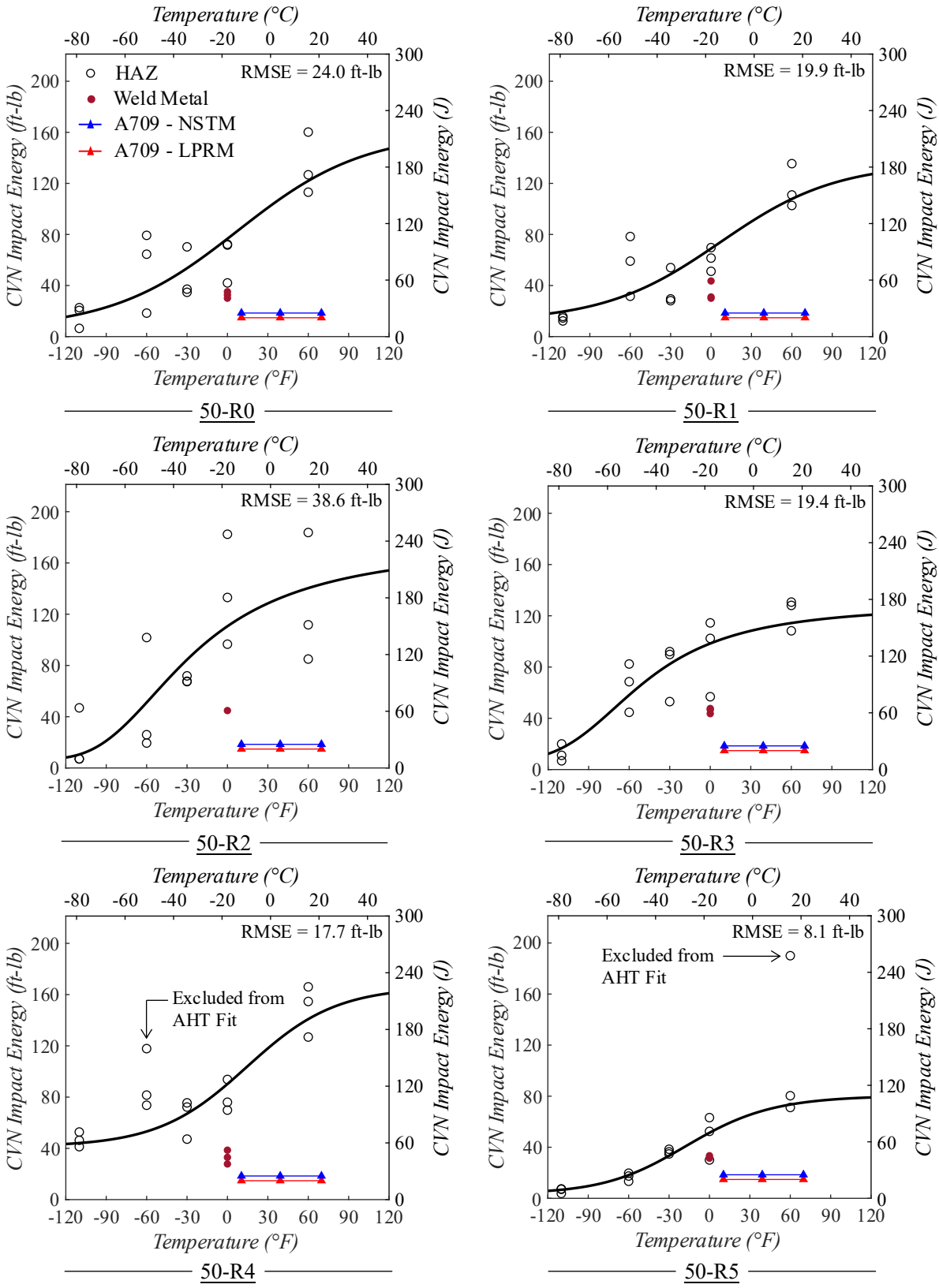


**Figure 5-33. Multiple Graphs. CVN impact test results for 50-grade welded sample groups.**

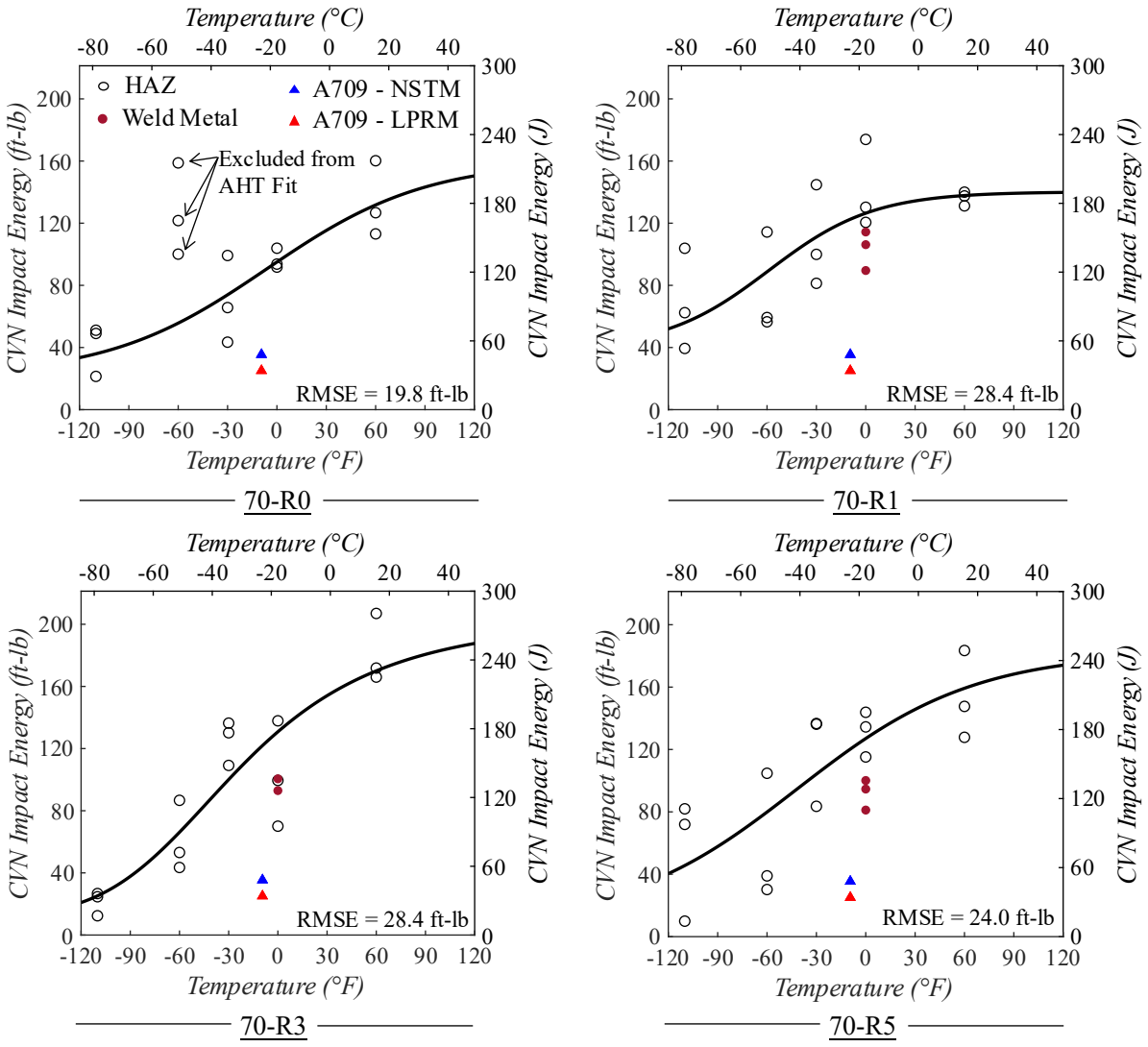


**Figure 5-34. Multiple Graphs. CVN impact test results for 70-grade welded sample groups.**

As the figures show, there is a fair amount of scatter over most temperatures tested for all sample groups, with the degree of scatter quantified by the RMSE scores in each plot. When the welded sample groups are compared to the base metal sample groups, these RMSE scores show that all the welded sample groups exhibit greater scatter than is typical for base metals; however, there is no apparent trend between the number of repairs and the degree of scatter. While it is normal to have a large amount of scatter throughout the transition zone, the majority of the HAZ sample groups tested exhibit neither a clear upper nor a lower shelf region. This large degree of

scatter and the lack of clear shelf regions result in the AHT fit curves varying drastically from sample group to sample group. Despite the scatter, all HAZ specimens from the welded sample groups met or exceeded the ASTM A709 minimum impact energies for 50W and HPS70W NSTMs and LPRMs.

### *5.3.3. Discussion of Results*

The AHT fit curves varied from sample group to sample group because of the large data scatter and the lack of well-defined upper and lower bound shelves. As such, it was not reasonable to compare these different AHT fit curves to evaluate the influence of multiple weld repairs on the CVN impact data. Instead, the CVN impact data for all sample groups were compiled and examined at each temperature tested, allowing comparison of the CVN impact data at each temperature as a function of the different weld repairs. Figures 5-35 and 5-36 show the CVN impact test results for all temperatures and sample groups tested for the 50-grade and 70-grade specimens, respectively. In these figures, the bottom abscissa shows the test temperature in Fahrenheit, and the left ordinate shows the CVN impact energy in foot-pounds (ft-lb). Similarly, the top abscissa is the test temperature in Celsius, and the right ordinate is the CVN impact energy measured in joules (J). Additionally, the ASTM A709 minimum impact energies for 50W and HPS70W NSTM and LPRM are plotted. For both grades of material tested, confirmatory specimens were also broken in the weld metal of each sample group to assess the weld metal impact energy; these values are shown in the figures.

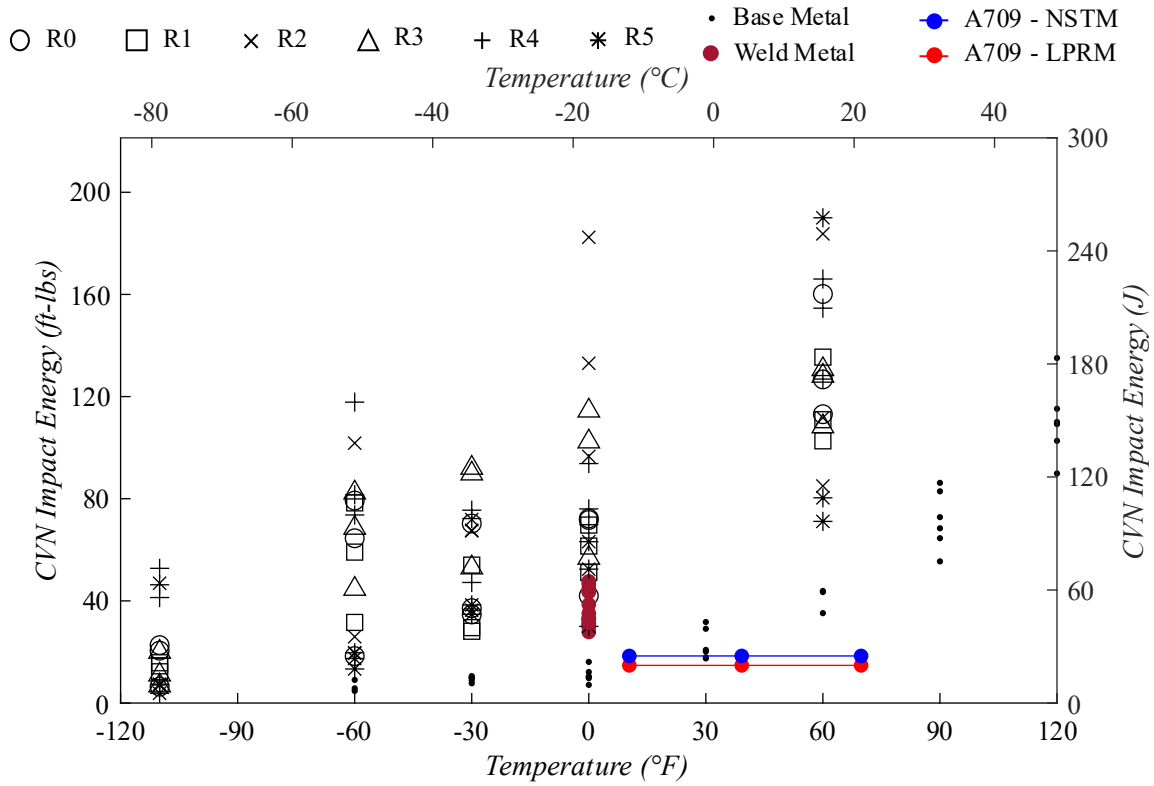


**Figure 5-35. Graph. CVN impact test results for all 50-grade specimens.**

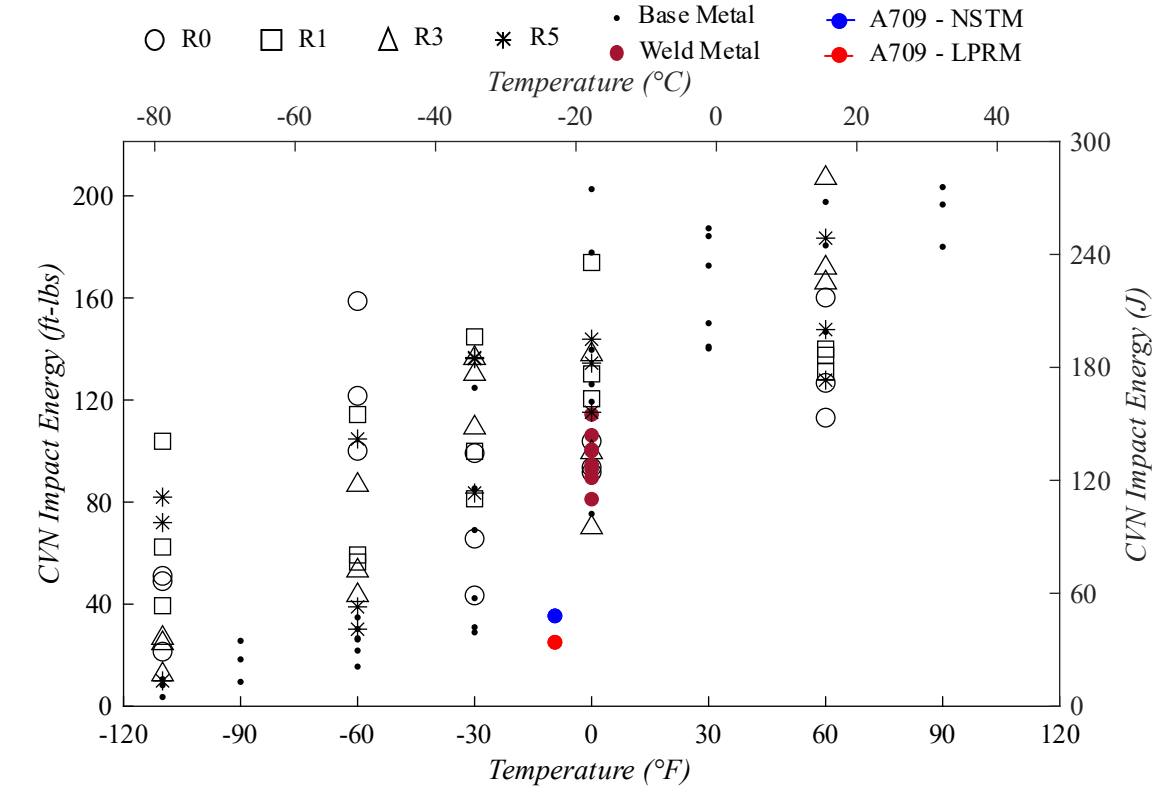


**Figure 5-36. Graph. CVN impact test results for all 70-grade specimens.**

Figure 5-35 shows that although there is scatter in the collective dataset, the 50-grade welded sample group specimens all follow the expected trend of increasing CVN impact energy with increasing test temperature. On average, the welded sample group specimens exhibit a higher CVN impact energy than the base metal. In all cases, all the CVN impact tests for the welded sample groups exceed the A709 minimum impact energy requirements for all three temperature zones. Similarly, Figure 5-36 shows that all 70-grade welded sample group specimens follow the expected trend of increasing CVN impact energy with increasing test temperature. On average, the welded sample group exhibits a CVN impact energy similar to that of the base metal. In all cases, all the CVN impact tests for the welded sample groups and the base metal exceed the A709 minimum impact energy requirement at the required temperature zone. Additionally, the weld metal impact energies are shown at 0°F in each plot. All weld metal samples exhibited consistent impact energy across all sample groups and were comparable to the respective HAZ impact energies.

To directly investigate whether the number of repair welds influences CVN behavior, the CVN impact energies for each material grade were compiled and plotted as a function of the number of repair welds. Figures 5-37 and 5-38 show plots for the 50-grade and 70-grade materials, respectively. In each figure, five subfigures plot all the tests performed at the following temperatures: -110°F, -60°F, -30°F, 0°F, and 60°F. In each of these subfigures, the abscissa is the number of repairs, and the ordinate is the measured CVN impact energy in ft-lb.

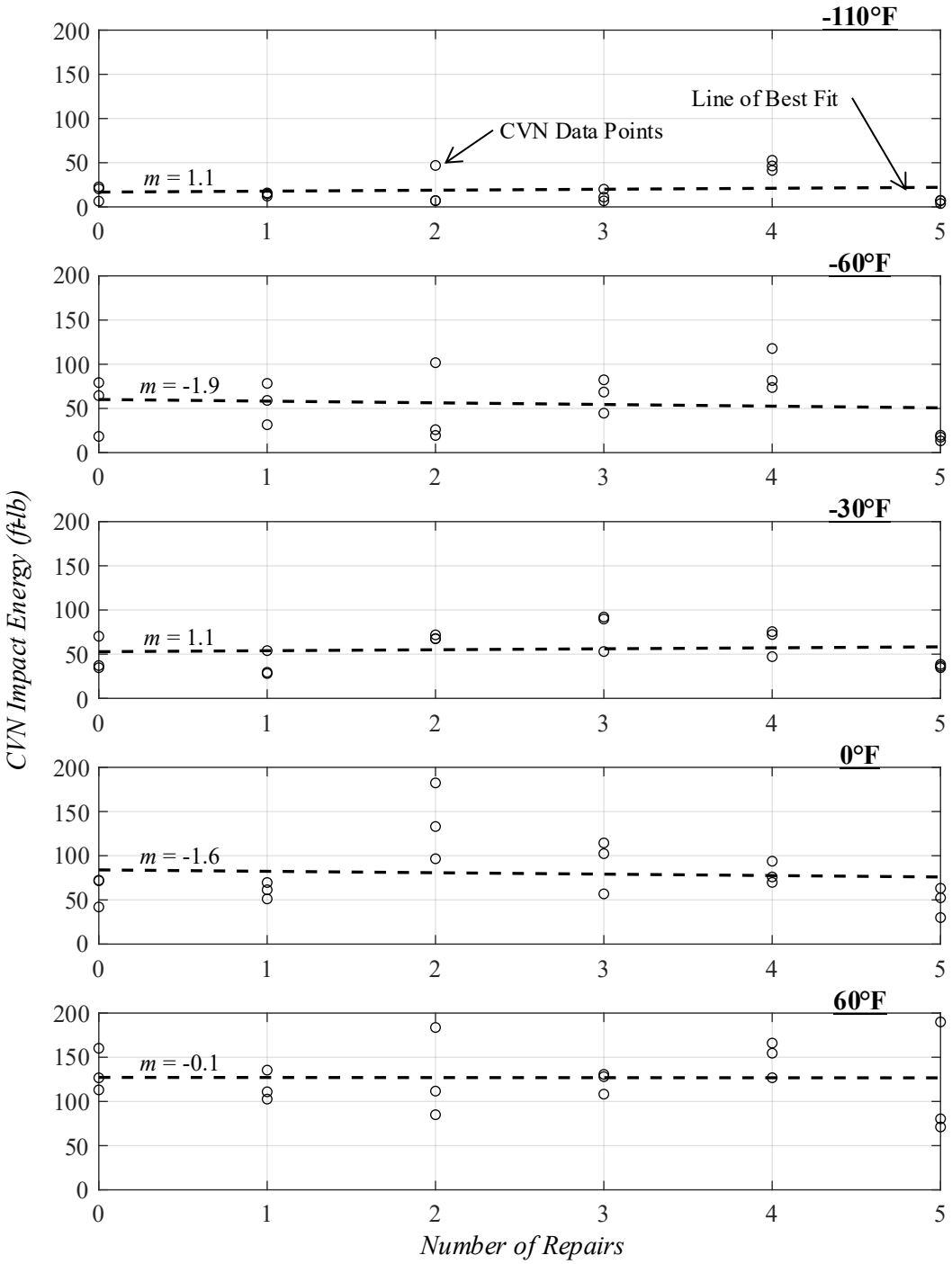


**Figure 5-37. Multiple Graphs. Comparison plots showing the 50-grade CVN impact energies versus the number of weld repairs for each test temperature.**

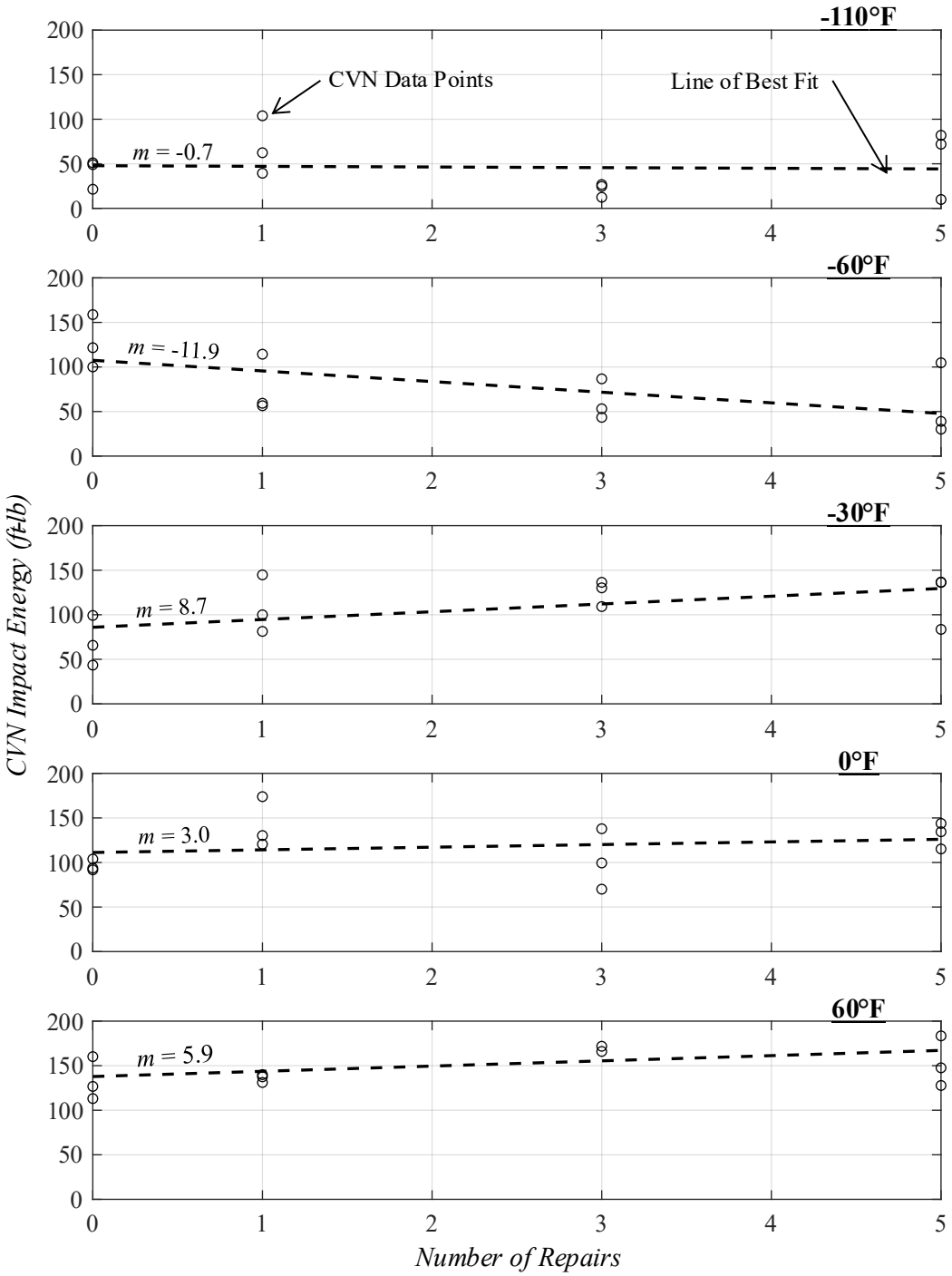


**Figure 5-38. Multiple Graphs. Comparison plots showing the 70-grade CVN impact energies versus the number of weld repairs for each test temperature.**

For the 50-grade specimens, Figure 5-37 shows that, on average, there is little to no change in the CVN impact energy with the number of repair welds at any tested temperature, as demonstrated by the slopes of the best-fit trend lines in each subfigure. This slope represents the relationship between the CVN impact energies and the number of repair welds, with a positive value indicating an increase in impact energy with increasing number of repair welds and a negative value indicating the opposite. As shown, all tested temperatures suggest that, on average, the CVN impact energies increased or decreased by less than 2 ft-lb per weld repair.

For the 70-grade specimens, Figure 5-38 shows a small change in the CVN impact energy across the number of repair welds at the different temperatures. As with the 50-grade specimens, the rates of change for each testing temperature are best represented by the slopes of the best-fit trend lines provided in each subfigure. As these slopes show, the largest change in impact energies occurs at -60°F and -30°F. At the -60°F test temperature, the best-fit line shows a negative relationship between the CVN impact energy and the number of repair welds, with the impact energy decreasing at a rate of 11.9 ft-lb per repair weld. At the -30°F test temperature, the best-fit line shows a positive relationship between the CVN impact energy and the number of repair welds, with impact energy increasing at a rate of 8.7 ft-lb per repair weld. While the decreasing impact energy observed at -60°F may be of initial concern, the trend was not observed at -60°F for the 50-grade materials, and it was not present at any of the other 70-grade testing temperatures, many of which actually showed an increase in impact energy.

Based on the discussions above, the following conclusions can be drawn:

- Although the CVN data for both grades of material showed substantial scatter, the comparative best-fit trend lines indicate that, on average, there is no appreciable change in CVN impact energy across the different numbers of weld repairs studied.

- Regardless of the number of repairs, the measured CVN impact energies of the HAZ and weld metal all exceeded the A709 minimum impact energy requirements.
- As such, there appears to be no significant change in the impact energy of the HAZ near repaired CJP butt-splice welded joints up through five repairs.

## 5.4. Macroetches

### *5.4.1. Specimen Information and Testing Setup*

Macroetches were taken of each welded sample group, yielding a total of 10 macroetches. These tests are significant because they show the welded profiles being studied and allow examination of the different weld regions. The specimens used to obtain the macroetches were 4” x 1” x 1/2"-thick rectangular blanks cut from the material characterization plates, milled to be plane within +/- 0.001 in., and polished to a surface roughness of ~2 μin. (0.05 microns) using silicon carbide sandpaper and polishing pads on a tabletop polishing machine. The different weld regions were exposed by using a 5% nital etch solution just before taking the macroetches. All macroetches were taken at the Georgia Tech Advanced Manufacturing Pilot Facility (AMPF) using a Zeiss optical microscope. Figure 5-39 shows a typical rectangular blank specimen before etching.

**Figure 5-39. Photo. Typical rectangular blank used for macroetches (before etching).**

### *5.4.2. Testing Results*

All macroetches were obtained and examined to visualize the different weld regions: namely, the weld metal, HAZ, and fusion lines. Figures 5-40 and 5-41 show the macroetches for the 50-grade and 70-grade specimens, respectively. Furthermore, the HAZ regions were measured using the built-in measurement tool in the Zeiss optical microscope to quantify the extent of the HAZ in each sample group, providing insights into the relationship between the size of the HAZ and the number of repair welds. Perpendicular measurements from the fusion line to the edge of the visible HAZ were taken throughout each profile from 0.25T to 0.75T, and the range of measured values is reported for each side of the weld of each specimen in Table 5-4. Additionally, the width of the weld profile at 0.5T, measured from fusion line to fusion line, is provided for context. Note that the directions left and right are indicated with respect to the macroetches shown in Figures 5-40 and 5-41.

As the figures show, all the welded specimens had similar double V-groove geometrical weld profiles, and the weld profiles were well maintained through all the repairs except sample group 50-R5, which is much larger than the other profiles. Based on the alignment, the final repair for 50-R5 was slightly off-center, resulting in an expanded weld profile compared to the other specimens. Table 5-4 shows that all specimens of each material had comparable weld widths and HAZs, except for 50-R5. For the 50-grade materials (excluding 50-R5), weld widths ranged from 9 to 11 millimeters, and HAZ widths ranged from 1.2 to 3.2 millimeters. For the 70-grade materials, weld widths ranged from 11.1 to 12.9 millimeters, and HAZ widths ranged from 1.8 to 4.4 millimeters.

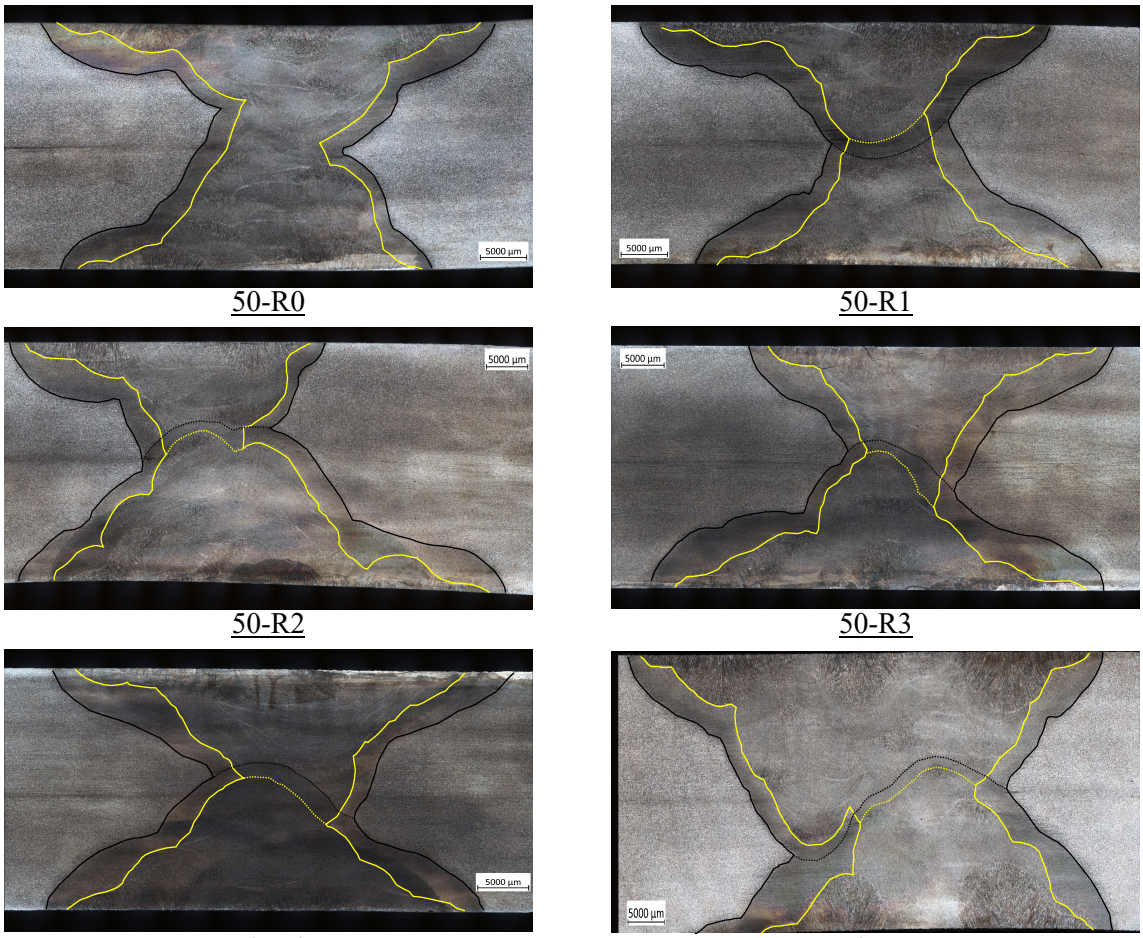


**Figure 5-40. Multiple Photos. Macroetches showing the weld regions of the 50-grade specimens. (yellow = fusion line, black = HAZ boundary )**

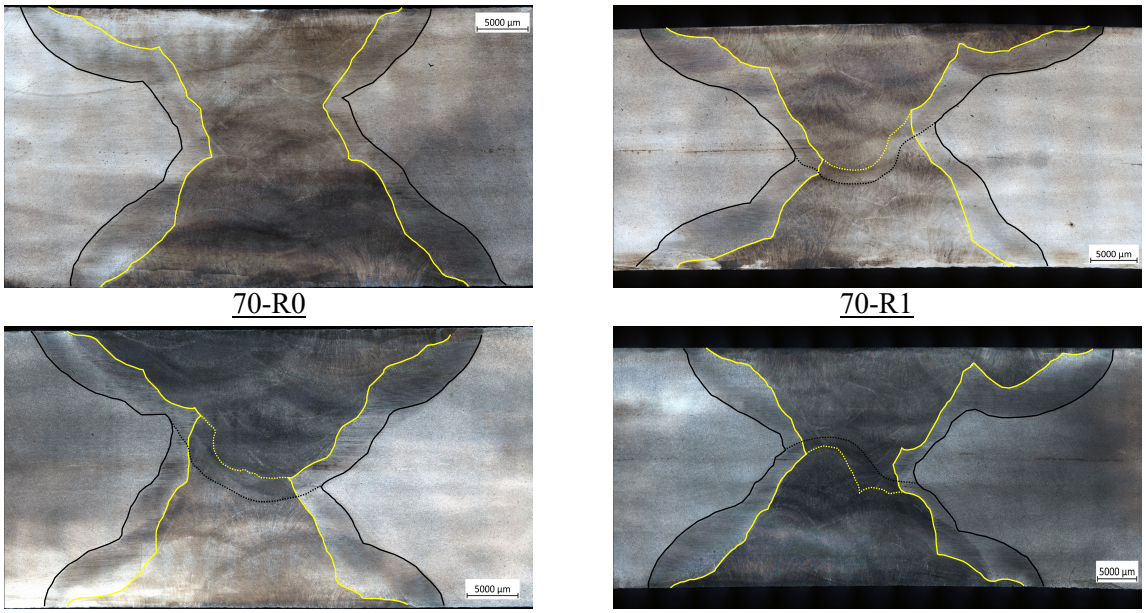


**Figure 5-41. Multiple Photos. Macroetches showing the weld regions of the 70-grade specimens. (yellow = fusion line, black = HAZ boundary)**

**Table 5-4. Range of measured weld and HAZ regions for each sample group.**

| *Sample Group* | *Weld @0.5T in. [mm]* | *HAZ-Left in. [mm]* | *HAZ-Right in. [mm]* | *Sample Group* | *Weld @0.5T in. [mm]* | *HAZ-Left in. [mm]* | *HAZ-Right in. [mm]* |
|---|---|---|---|---|---|---|---|
| 50-R0 | 0.393 [10.0] | 0.063 - 0.094 [1.6 - 2.4] | 0.055 - 0.083 [1.4 - 2.1] | 70-R0 | 0.508 [12.9] | 0.079 - 0.173 [2.0 - 4.4] | 0.102 - 0.118 [2.6 - 3.0] |
| 50-R1 | 0.354 [9.0] | 0.063 - 0.102 [1.6 - 2.6] | 0.098 - 0.110 [2.5 - 2.8] | 70-R1 | 0.461 [11.7] | 0.083 - 0.114 [2.1 - 2.9] | 0.079 - 0.098 [2.0 - 2.5] |
| 50-R2 | 0.409 [10.4] | 0.067 - 0.122 [1.7 - 3.1] | 0.047 - 0.122 [1.2 - 3.1] | - | | - | - |
| 50-R3 | 0.378 [9.6] | 0.063 - 0.091 [1.6 - 2.3] | 0.087 - 0.110 [2.2 - 2.8] | 70-R3 | 0.437 [11.1] | 0.087 - 0.106 [2.2 - 2.7] | 0.122 - 0.169 [3.1 - 4.3] |
| 50-R4 | 0.433 [11.0] | 0.071 - 0.102 [1.8 - 2.6] | 0.052 - 0.126 [1.3 - 3.2] | - | | - | - |
| 50-R5 | 1.126 [28.6] | 0.091 - 0.299 [2.3 - 7.6] | 0.087 - 0.193 [2.2 - 4.9] | 70-R5 | 0.461 [11.7] | 0.087 - 0.134 [2.2 - 3.4] | 0.071 - 0.102 [1.8 - 2.6] |

## 5.5. Microhardness Tests

### *5.5.1. Specimen Information and Testing Setup*

Microhardness tests were conducted on the welded regions for each sample group. Microhardness tests were performed in lieu of traditional hardness tests because they allow much smaller spacings between indentation tests, which are essential for properly characterizing the HAZ regions in the specimens. These tests are significant because they provide insights into how the material properties of the joint vary across the different weld regions, which, in turn, can be related back to the overall joint performance observed in the other material characterization tests. The microhardness tests were conducted on the same 4” x 1” x 1/2" polished rectangular blank that which the macroetches were obtained. After the macroetches were obtained, the rectangular blanks were repolished to a surface finish of ~8 μin. using a 1,200-grit silicon carbide sandpaper on a table-top polishing machine, and they were then lightly etched using a 5% nital etch solution. Although etching the surface before hardness testing is not desirable, etching was necessary to identify the different weld regions. Figure 5-39 (in Section 5.4) shows the typical rectangular blank used for microhardness tests.

All microhardness tests were conducted at the Georgia Tech AMPF lab using a Wilson VH3300 hardness tester. The hardness tester was installed and calibrated approximately one month before use, and it was checked for calibration daily. All microhardness tests were conducted per ASTM E384 (ASTM 2022b), and a 0.5-kg Vickers indenter was used for all tests. Figure 5-42 shows an overview of the testing setup used for all microhardness tests.

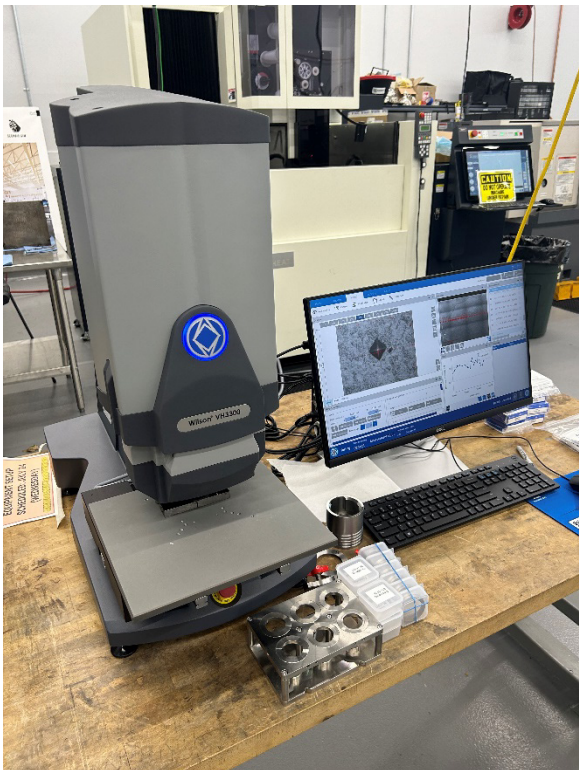

**Figure 5-42. Photo. Overview of microhardness test setup.**

### *5.5.2. Testing Results*

All microindentation tests were performed and measured per the requirements of ASTM E384 (ASTM 2022b). All hardness shot layouts were developed using the weld profile alignment tool in the Wilson hardness tester, which is a simple shot layout tool with preset, discretized regions for the different weld regions. Using this alignment tool, three rows of hardness shots were taken across the welded joint of each specimen at 0.25T, 0.50T, and 0.75T. Each row of shots was symmetrically performed across the welded joint as follows:

- (10) shots at 1 mm in the base metal,
- (#) shots at 0.5 mm in the visible HAZ, and
- (#) shots at 1 mm in the weld metal.

Since the HAZ and weld metal varied across the specimens, the symbol # above indicates that the number of shots taken in these regions varied from specimen to specimen, but the shots were consistently spaced at the listed spacings. Each row was generally comprised of 40 to 90 shots, depending on the size of the HAZ and weld metal. Figure 5-43 shows the macroetch of Specimen 50-R1 overlaid with the typical pattern. Note that the 0.5 mm spacing used in the HAZ was generally extended 1 to 2 millimeters beyond the visible HAZ boundary to ensure all HAZ measurements were obtained before increasing the spacing.

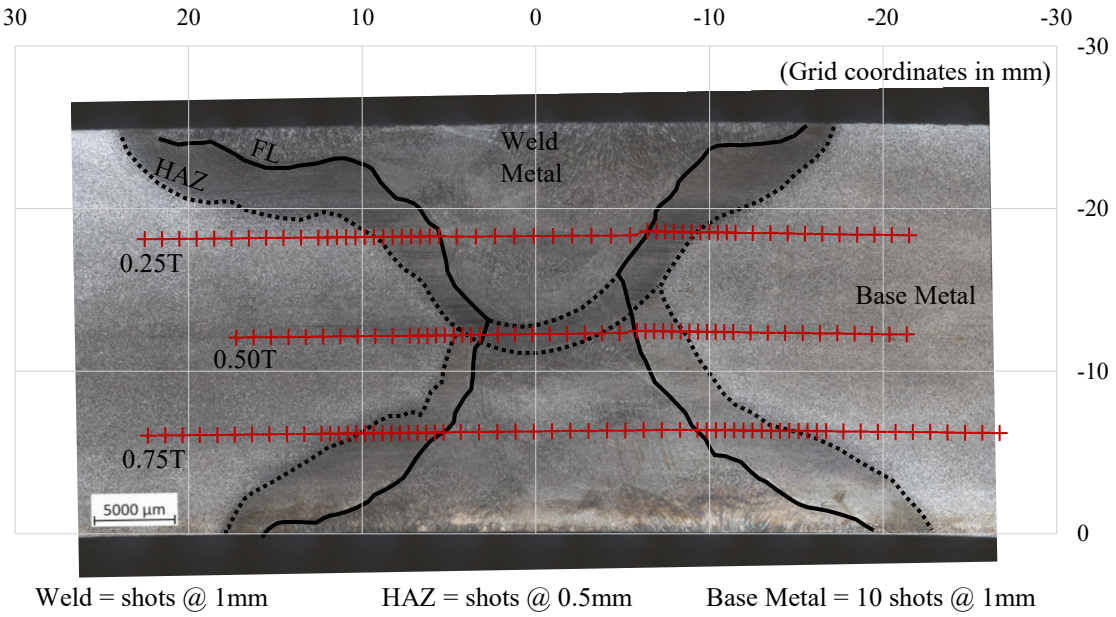


**Figure 5-43. Illustration. Typical microhardness layout, 50-R1 shown.**

After indentation, all indents were checked for symmetry per the ASTM E384 requirements, and all indents not meeting the requirements were marked as outliers in the results. Extreme cases were thrown out. Additionally, locations with repeat indents, which happened occasionally because of a software glitch, were marked as outliers in the results. The measured hardness values of each specimen are shown in Figures 5-44 through 5-53. In these figures, there is a subplot for each row of data collected (i.e., shots taken at 0.25T, 0.50T, and 0.75T). For all

three subplots, the abscissa is the horizontal distance along the weld, and the ordinate is the measured Vickers hardness values from the 0.5-kg indenter (HV 0.5). Additionally, the fusion lines and visible HAZ boundaries are indicated in the plots to give context to the data. Note that the zero-point along the abscissa represents the center of the weld metal for that row of data, meaning that this zero-point is local for each subplot and is not a global point of symmetry.

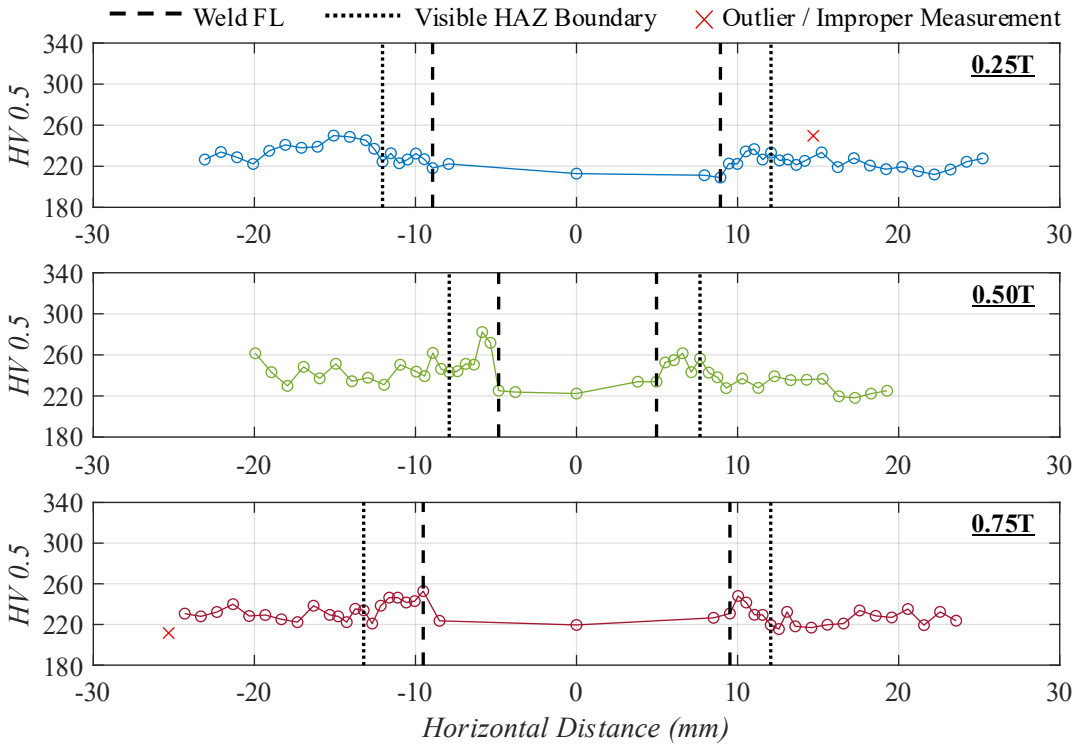


**Figure 5-44. Multiple Graphs. Hardness measurements for 50-R0.**

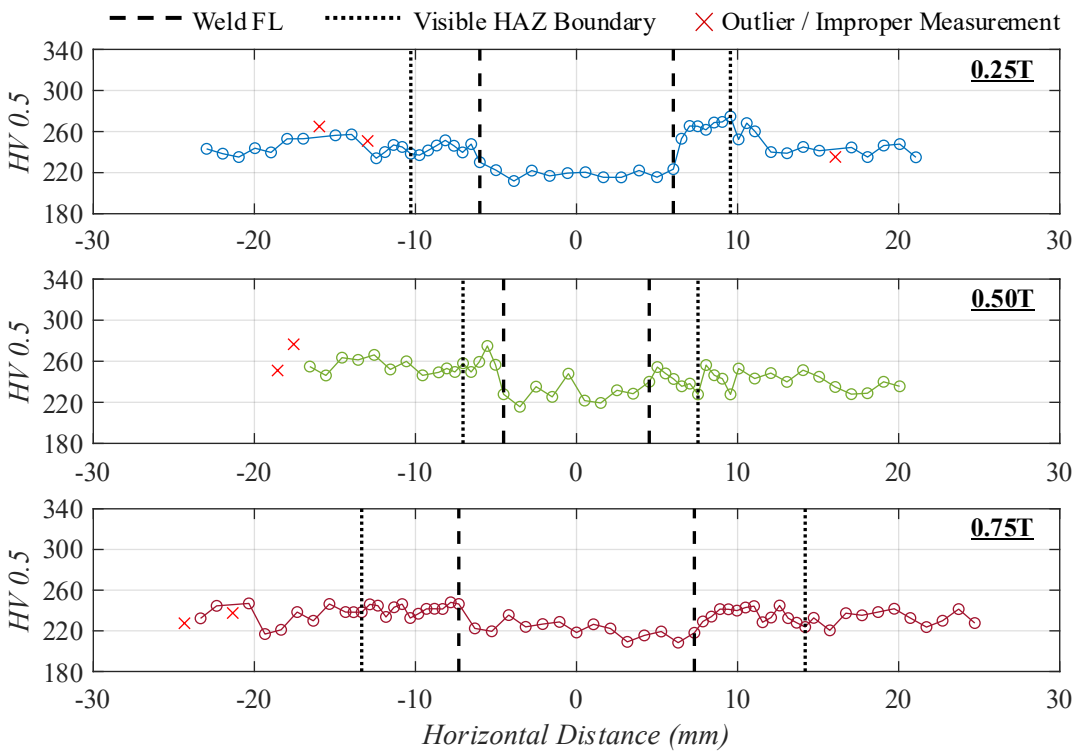


**Figure 5-45. Multiple Graphs. Hardness measurements for 50-R1.**

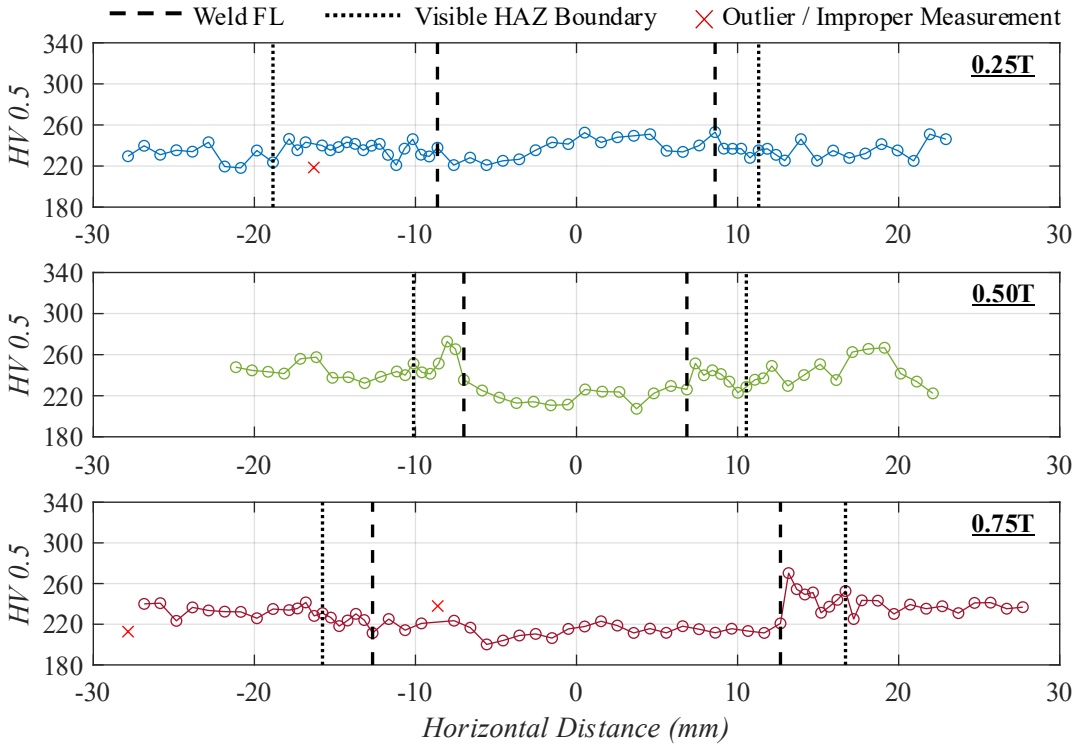


**Figure 5-46. Multiple Graphs. Hardness measurements for 50-R2.**

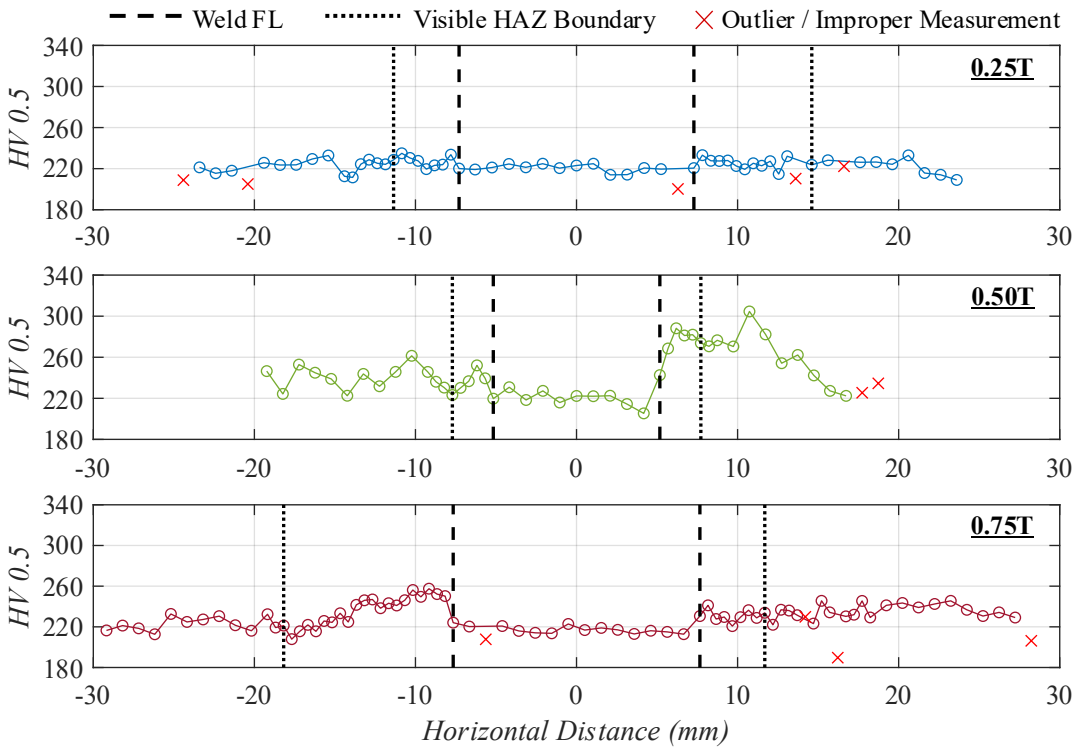


**Figure 5-47. Multiple Graphs. Hardness measurements for 50-R3.**

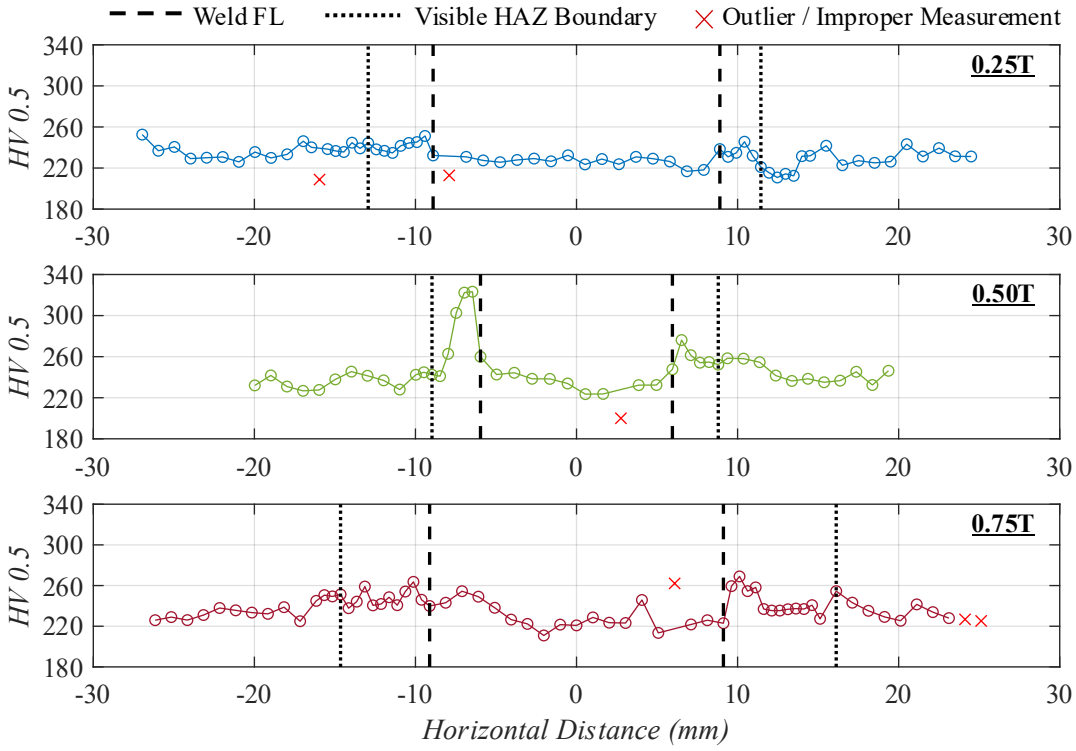


**Figure 5-48. Multiple Graphs. Hardness measurements for 50-R4.**

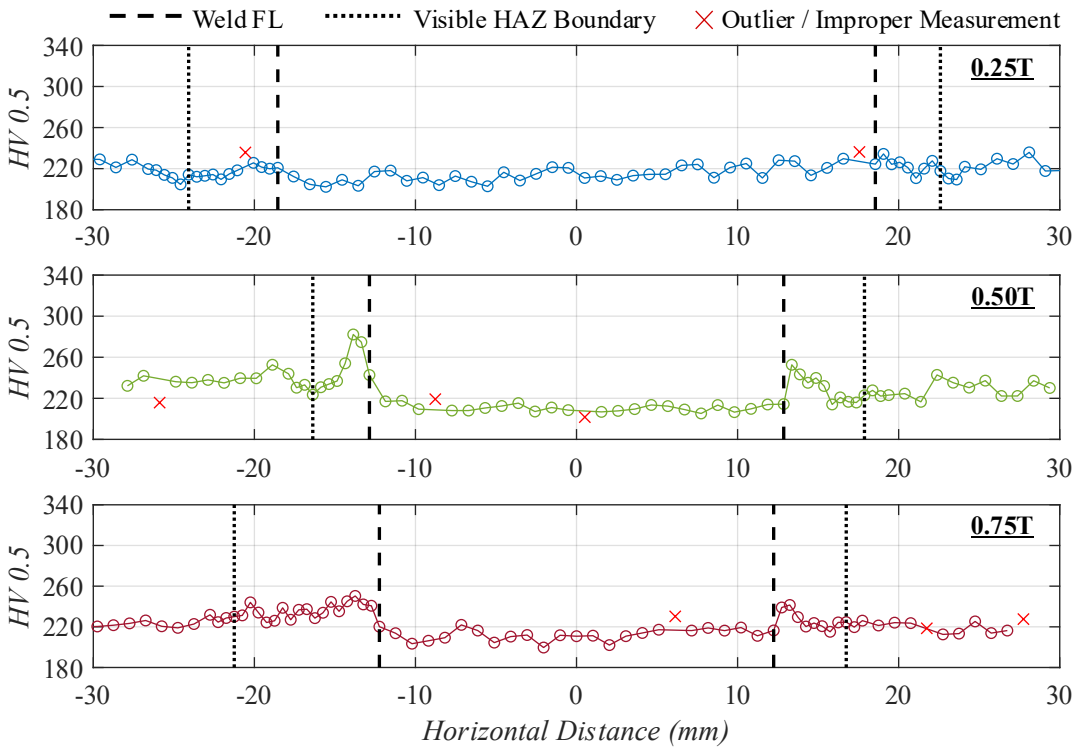


**Figure 5-49. Multiple Graphs. Hardness measurements for 50-R5.**

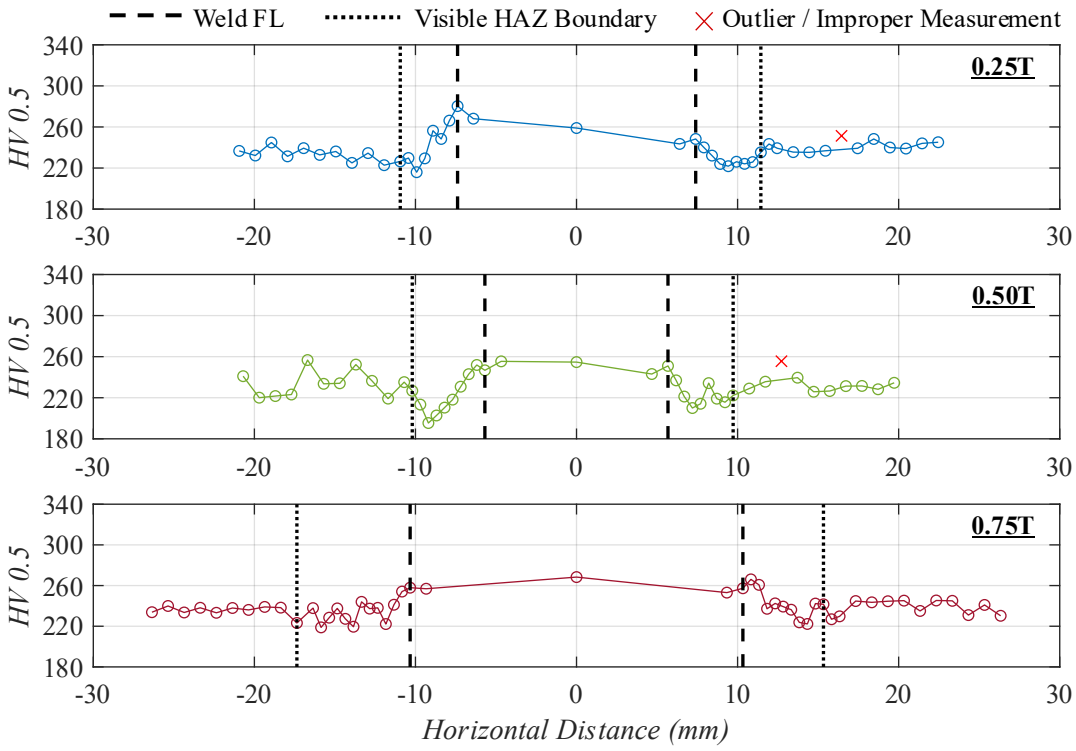


**Figure 5-50. Multiple Graphs. Hardness measurements for 70-R0.**

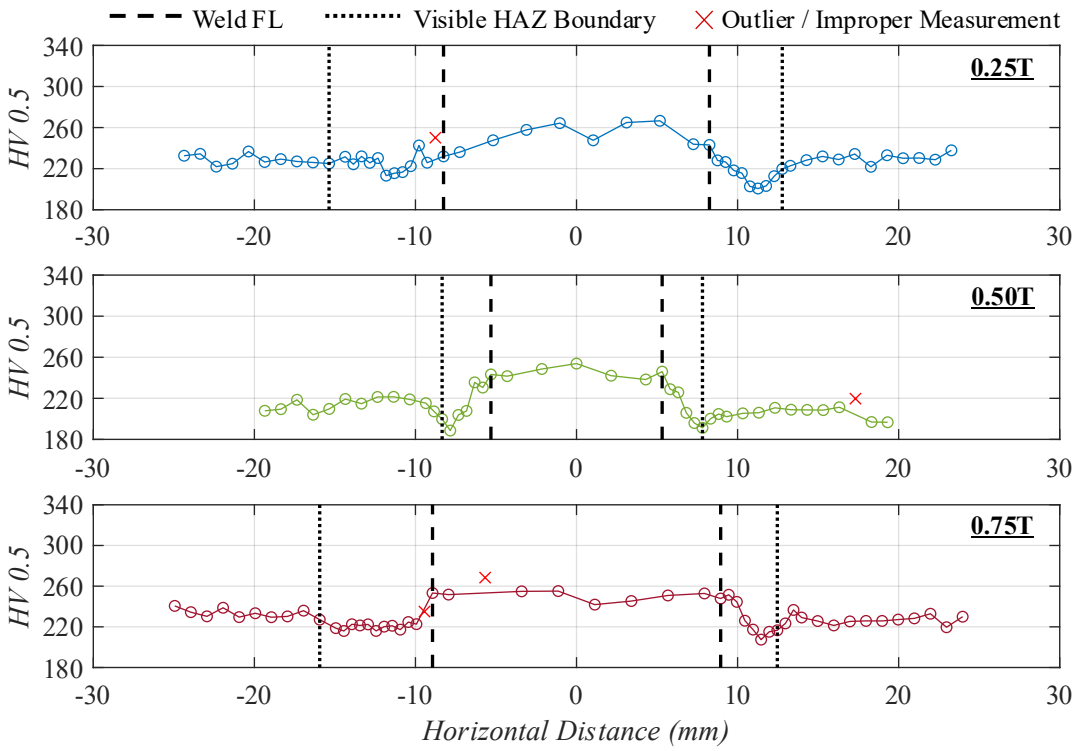


**Figure 5-51. Multiple Graphs. Hardness measurements for 70-R1.**

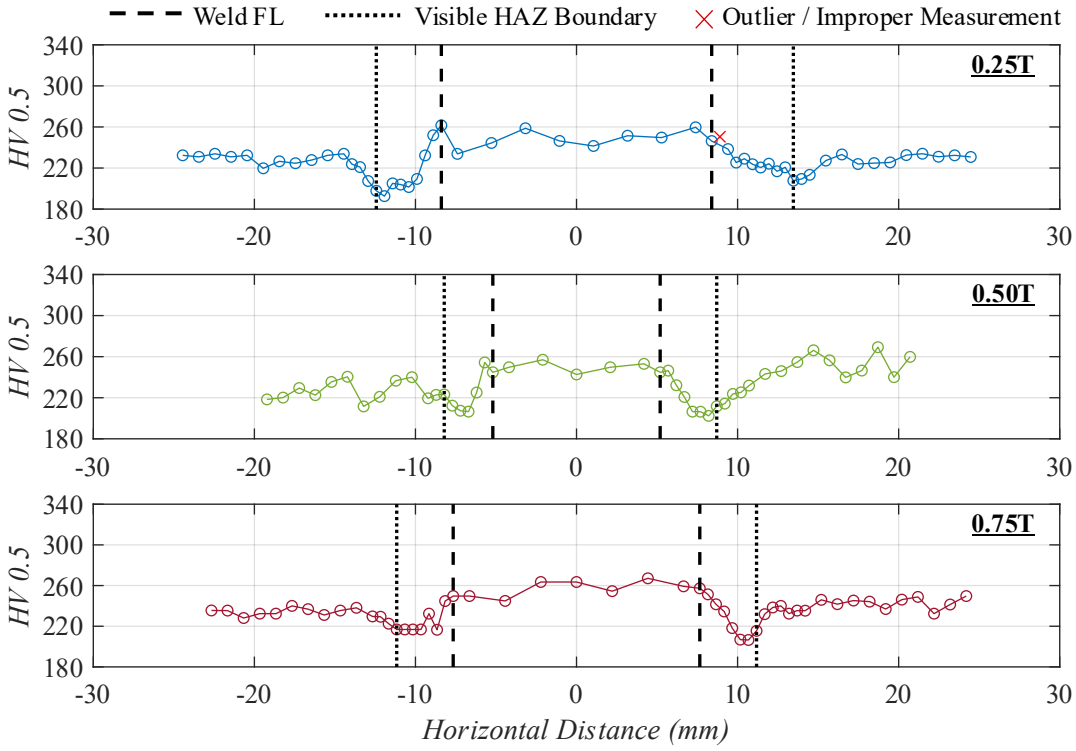


**Figure 5-52. Multiple Graphs. Hardness measurements for 70-R3.**

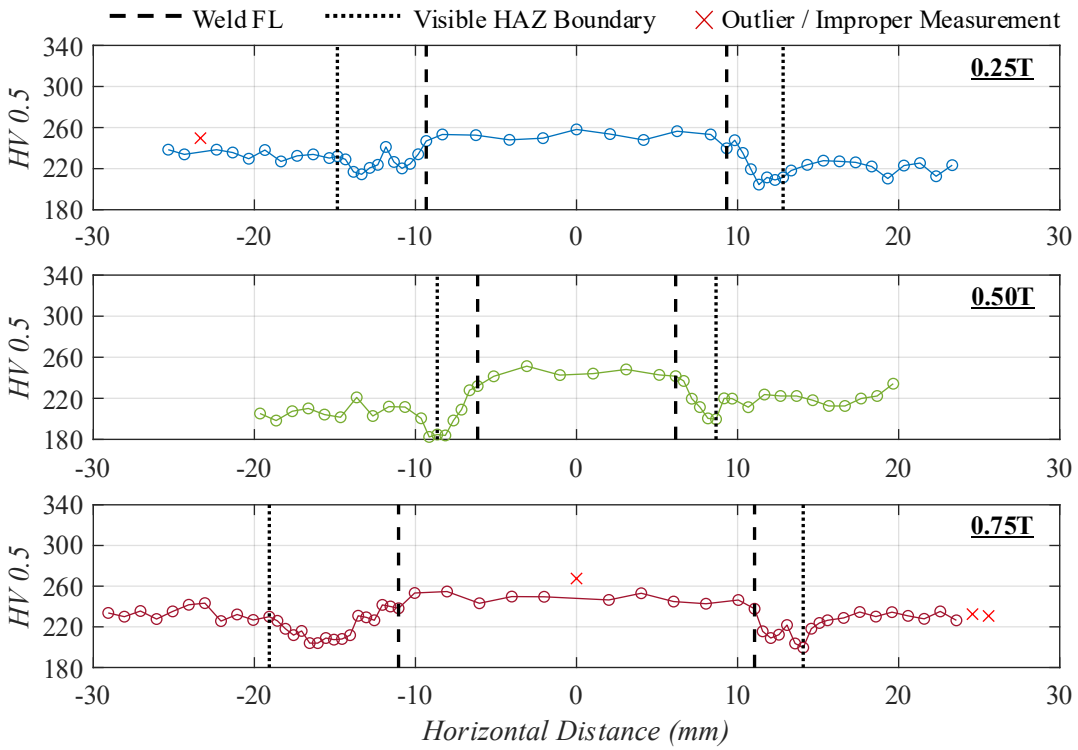


**Figure 5-53. Multiple Graphs. Hardness measurements for 70-R5.**

Looking at the figures, the different hardness values measured across the welded joint clearly depict the three weld regions analyzed (i.e., base metal, HAZ, and weld metal), and the largest hardness values and the greatest hardness changes across a section generally occurred at 0.50T. For the 50-grade specimens, the HAZ regions generally have a higher hardness than the weld metal and base metal regions, with hardness values typically spiking upward, then returning to base metal values over a 2–3 millimeter range outside the fusion line of the weld. Notably, all the 50-grade specimens at 0.5T either exceed or are close to the 280 Vickers hardness limit specified in AASHTO/AWS D1.5 for SAW (AASHTO/AWS 2020). Conversely, the HAZ regions of the 70-grade specimens generally have a lower hardness than both the weld metal and base metal regions, with the hardness values typically dropping downward, then returning to the base metal values over a 3–5 millimeter range outside the fusion line of the weld. Notably, all the

70-grade specimens at 0.5T are below the 280 Vickers hardness limit specified in AASHTO/AWS D1.5 for SAW.

### *5.5.3. Discussion of Data*

The hardness data at 0.5T for all sample groups were analyzed. The worst-performing HAZ (i.e., the side of the weld with the highest/lowest hardness) from each sample group was compared for each steel grade, allowing evaluation of the measured hardness to determine whether the number of repairs influences hardness across the CJP joint. The primary area of concern was the HAZ, which was the focus of the comparisons. However, some measurements from the nearby weld metal and base metals are also shown for context. Figure 5-54 shows the comparison plot for the 50-grade specimens, and Figure 5-55 shows the comparison plot for the 70-grade specimens. In both figures, the abscissa is the measured distance from the fusion line of the weld, where positive values represent moving away from the weld metal, negative values represent moving into the weld metal, and the ordinate is the measured Vickers hardness values (HV 0.5). The data were fit with a best-fit curve (generally a 3rd–5th-order polynomial), and these were used as the primary comparison tool across the different sample groups. For clarity, the individual data points are not shown. Because of the general scatter of the data and reliability of comparisons, no numerical trends or patterns were attempted for this data comparison; instead, general trends and observations are discussed.

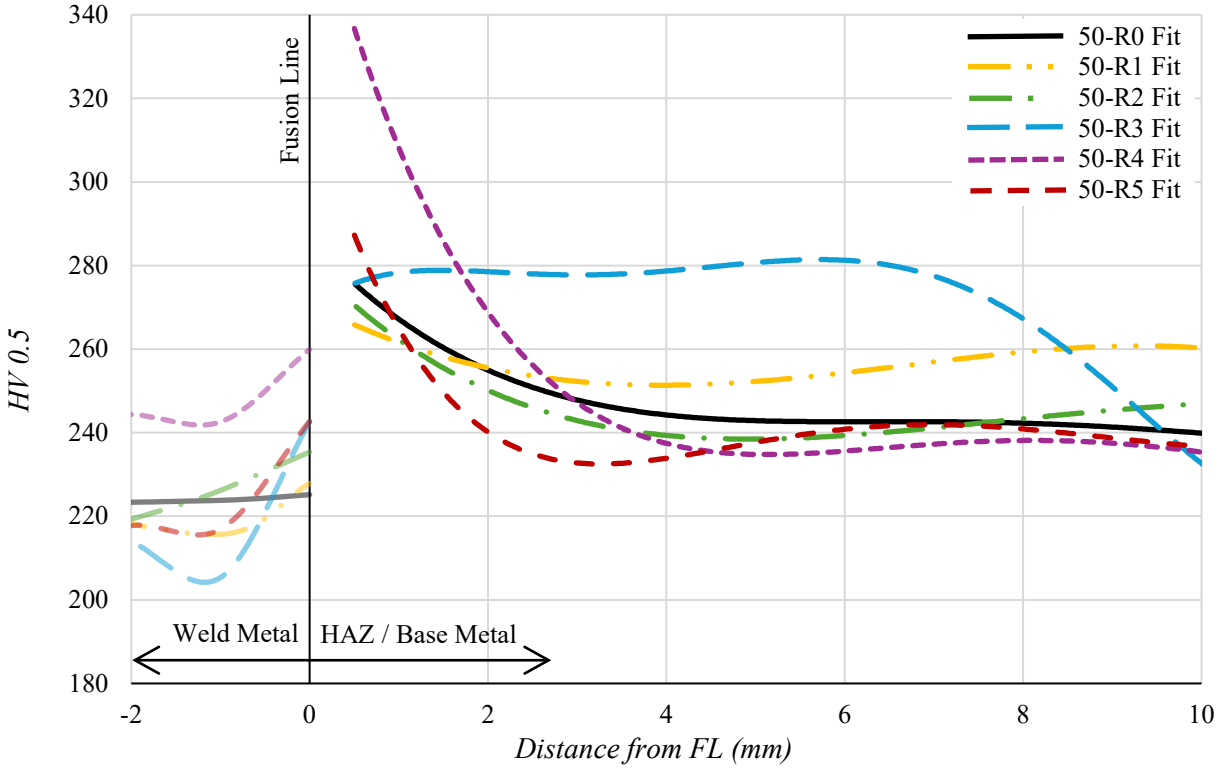


**Figure 5-54. Graph. Comparison of 50-grade hardness values within the HAZ.**

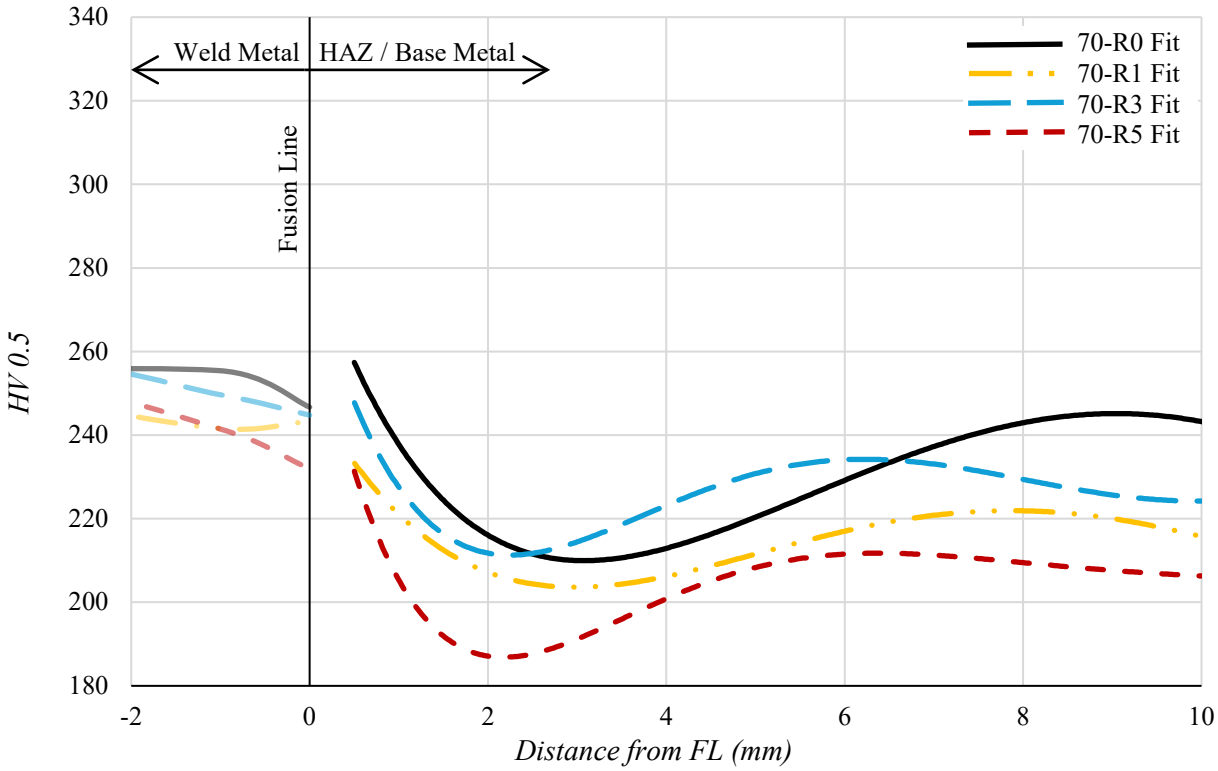


**Figure 5-55. Graph. Comparison of 70-grade hardness values within the HAZ.**

In Figure 5-54, all specimens show a spike in hardness directly adjacent to the fusion line, which returns to the typical base metal hardness after approximately 3 mm. The notable exception to this is 50-R3, which does not return to the typical base metal hardness until around 12 mm. Looking at the hardness values in this 3 mm region, 50-R1 and 50-R2 show hardness comparable to that of 50-R0 (i.e., a typical CJP joint with no repairs). 50-R3 has a maximum hardness equal to 50-R0, but it does not return to the base metal hardness as quickly as the other sample groups. 50-R4 shows the largest increase in hardness, reaching a maximum of 320 Vickers hardness. 50-R5 also has an increase in hardness, albeit not as large as the 50-R4 spike. Looking collectively at the different best-fit lines, a general trend indicates that more than three weld repairs may increase hardness in the HAZ.

Interestingly, Figure 5-55 shows the opposite for the 70-grade specimens. All the specimens show a decrease in hardness directly next to the fusion line that gradually returns to the typical base metal hardness after approximately 4 mm. A collective look at the different best-fit lines for the data in this 4 mm region shows a decreasing trend in hardness as the number of repairs increases. However, even for the 70-R5 specimen (which showed the largest decrease compared with 70-R0), the reduction in hardness is not substantial, with only 15–25 Vickers hardness units below the base metal.

Based on the discussions above, the following statements can be concluded:

- For the 50-grade specimens, the repaired specimens typically exhibited a hardness greater than or equal to that of the R0 specimen, with some hardness values exceeding the 280 Vickers hardness limit recommended by AASHTO/AWS D1.5 for SAW procedures.

- For the 70-grade specimens, the repaired specimens typically exhibited a hardness lower than that of the R0 specimen, but none of the hardness values were more than 15-25 Vickers hardness units less than the base metal.
- There appears to be an observable relationship between the hardness in the HAZ and the number of weld repairs, indicating that there is also an observable relationship between the tensile strength and the number of repair welds. However, this observable relationship was not observed in the tensile data gathered during the tension tests.
- As such, this data shows that the number of weld repairs does affect the hardness of the HAZ, but this effect does not translate into meaningful changes in the material properties measured using more macroscopic test specimens.

# CHAPTER 6. FATIGUE LIFE EXPERIMENTAL TESTING PROGRAM

The third research objective targets the assessment of the fatigue life of repaired CJP welded joints in bridge members. To accomplish this, a large-scale fatigue life experimental program has been developed to generate novel fatigue life data for repaired CJP welded butt-splice joints in bridge members. The resulting data were used to determine whether these repairs alter or negatively affect the fatigue life of the joint. The fatigue life experimental program is presented in the following subsections, and the test results are discussed in Chapter 7.

Unlike many strength-based tests, the thickness of the test specimen can influence its fatigue life. Therefore, fatigue results cannot always be directly extrapolated to thicker or thinner specimens, especially for thicker test specimens, which inherently have a higher probability of containing an internal defect because of their larger volume of material (Easterling 1992). Additionally, the number of weld passes required to fill the CJP joints increases with specimen thickness, thereby subjecting the nearby HAZ to an increasing number of thermal cycles during the initial and repair weld processes. As discussed in Section 2.1.2, thermal cycles can embrittle the HAZ, leading to potential fatigue issues due to stress concentrations in the coarse-grained HAZ. Additionally, the fabrication practices and specimen geometry can influence its fatigue life. Built-up steel members often require a combination of fillet and groove welds at varying orientations and in close proximity. The added constraint and residual stresses can significantly affect the fatigue life of the specimen (Keating and Fisher 1986). For these reasons, large-scale fatigue tests are necessary to properly assess the influence of multiple weld repairs on CJP joints used in bridge members.

## 6.1. Experimental Fatigue Life Testing Matrix

The large-scale fatigue tests were developed to complement the suite of material characterization tests conducted in the current study. As such, the same grades of steel and weld repair thresholds targeted in the material characterization tests were also investigated for the large-scale fatigue tests. Namely, ASTM A709-50W and A709-HPS70W grade steels and a threshold of five weld repairs were evaluated for the fatigue life studies.

The large-scale fatigue tests in the current study were conducted on built-up I-section members that had numerous repaired CJP welds along their flanges. To investigate whether thickness influences the fatigue life of repaired CJP joints, the current study targeted two flange thicknesses: 3/4 in. and 1-1/2 in. The 1-1/2 in. thickness was chosen because it is commonly used in bridge members, and the 3/4 in. thickness was selected because it represents a substantial step down from 1-1/2 in. Based on the targeted two materials and flange thicknesses, four girders were fabricated and tested. Table 6-1 shows a large-scale experimental fatigue testing matrix detailing the combinations of materials and flange thicknesses tested. Note that the flanges contain the welded CJP joints being tested; therefore, using a nonhomogeneous web material for Girders 3 and 4 had no influence on the testing program.

**Table 6-1. Large-scale fatigue experimental matrix.**

| *Specimen* | *Flange Material* | *Flange Thickness, $t_f$ (in.)* | *Web Material* | *Web Thickness, $t_w$ (in.)* |
|---|---|---|---|---|
| G1 | 50W | 1-1/2 | 50W | 1/2 |
| G2 | 50W | 3/4 | 50W | 1/2 |
| G3 | HPS70W | 1-1/2 | 50W | 1/2 |
| G4 | HPS70W | 3/4 | 50W | 1/2 |

## 6.2. Test Girders

The fatigue life test girders in the current study were designed with inspiration from the Kelly (1997) study, albeit with a few key differences to ensure that the member thicknesses and additional restraint typically found in bridge members were considered. The test girders used in the current study are built-up I-section members with numerous CJP welds along the flange lengths, each with a different number of repairs. All repair welds were performed at the shop soon after the base CJP weld or a previous repair weld was performed, to mimic the procedure and effects of typical fabrication shop repairs, meaning that all flange repair welds were performed before the web was attached to the girders.

### *6.2.1. Girder Design and Layout*

The fatigue life test girders were doubly symmetric, built-up I-section members. The top and bottom flanges were 6 in. x 3/4 in. or 6 in. x 1-1/2 in. rolled plates (depending on the girder), and the webs were 15 in. x 1/2 in. rolled plates. The girders consisted of two 4'-6" long end sections and one 6'-8" long middle section. The end sections were for loading purposes only, and the middle section was the testing region. In the middle section, four CJP joints were located in each flange, resulting in eight CJP joints per girder. Each CJP joint is uniquely identified as J1 to J8, and each joint was repaired 0, 1, 3, or 5 times. J1 and J5 correspond to zero repair welds, and J2 and J6 correspond to one repair weld. J3 and J7 correspond to three repair welds, and J4 and J8 correspond to five repair welds.

The CJP joints in the middle section were staggered such that no joints shared the same transverse cross section, and all CJP joints on the same flange were spaced 16 in. apart. The end CJP joints were positioned such that all joints were a minimum of 12 in. away from the bearing

stiffeners. Figure 6-1 shows the layout of the fatigue testing girders, and Table 6-2 breaks down the number of CJP joints tested for each flange thickness and repair count. The girder design accounted for the spacing between the different CJP joints to ensure no influence from nearby joints, whether from fabrication processes or cracks that may appear during testing. During the material characterization plate fabrication, it was observed that the base metal more than 6 in. from the weld always maintained a temperature below the interpass temperature limit. Additionally, Kelly (1997) found that small fatigue cracks that developed in the flanges during testing had no significant influence on the stress ranges of the other joints, provided the surrounding joints were at least 4 in. away. As such, the 16 in. spacing was sufficient to independently fabricate, test, and repair each joint without influencing the surrounding joints.

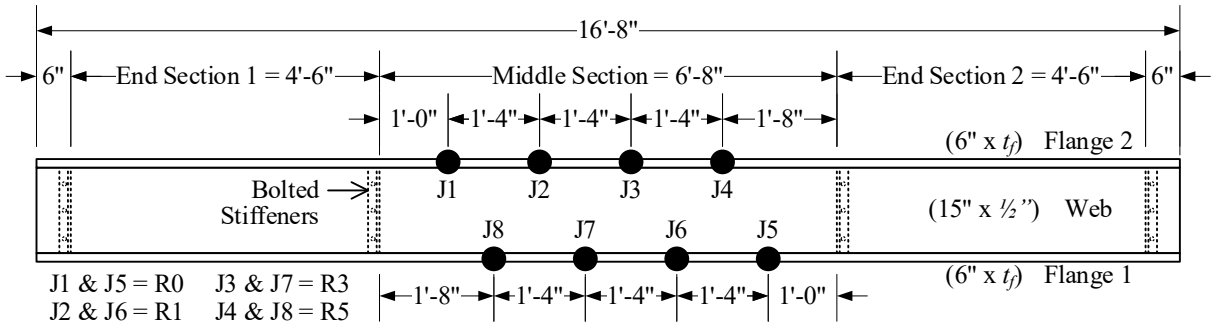


**Figure 6-1. Illustration. Layout of fatigue testing girders.**

**Table 6-2. Count of test joints by number of repair welds and grade of material.**

| | *50-Grade Joint Count* | | *70-Grade Joint Count* | |
|---|---|---|---|---|
| *# Repair Welds* | *1-1/2 in. Flange (Girder 1)* | *3/4 in. Flange (Girder 2)* | *1-1/2 in. Flange (Girder 3)* | *3/4 in. Flange (Girder 4)* |
| 0 | 2 | 2 | 2 | 2 |
| 1 | 2 | 2 | 2 | 2 |
| 3 | 2 | 2 | 2 | 2 |
| 5 | 2 | 2 | 2 | 2 |
| **Total** | **8** | **8** | **8** | **8** |

### *6.2.2. Girder Base Material Properties and Information*

All plates used to create the fatigue test girders are either grade A709-50W or A709-HPS70W. Five different heats of steel were used, each representing a unique combination of plate thickness and material grade. Table 6-3 shows the heats of steel used for each girder component. Notably, the A709-HPS70W plates were produced through the quench-and-temper heat treatment process. Table 6-4 provides the chemical compositions and material properties (i.e., yield and tensile strengths, elongations, and CVN energies) reported in the MTRs for all heats. Additionally, two tension coupons were cut and tested from extra stock for each unique heat of steel to confirm the material properties reported in the MTRs. The tension coupons were cut and tested following the processes described in Section 5.1.1. Figure 6-2 shows the resulting stress-strain curves for these tension tests, and the average yield strength, tensile strength, and elongation values for each sample group are tabulated in Table 6-5.

**Table 6-3. Heat numbers for each test girder component.**

| | *Flanges* | | *Web* | |
|---|---|---|---|---|
| *Girder* | *Grade* | *Heat #* | *Grade* | *Heat #* |
| G1 | 50W | A4F201 | 50W | 36033496 |
| G2 | 50W | 3604594 | 50W | 36033496 |
| G3 | HPS70W | 2606165 | 50W | 36033496 |
| G4 | HPS70W | 813Y70980 | 50W | 36033496 |

**Table 6-4. Material properties and chemical composition from MTRs for each girder plate.**

| | ***Heat #*** | **36033496** | **A4F201** | **3604594** | **2606165** | **813Y70980** |
|---|---|---|---|---|---|---|
| | *Girder / Component* | G1-G4 / Web | G1 / Flanges | G2 / Flanges | G3 / Flanges | G4 / Flanges |
| | *Plate Thickness (in.)* | 1/2 | 1-1/2 | 3/4 | 1-1/2 | 3/4 |
| *Material Properties* | *Yield Strength (ksi)* | 60, 55.9 | 51 | 52.3, 60.4 | 80.1 | 85.1 |
| | *Tensile Strength (ksi)* | 86.5, 82.9 | 78 | 77.6, 85.5 | 96.1 | 95.9 |
| | *Elongation (%)* | | | | | |
| | *2 in. Gage* | - | - | - | 53.7 | 40 |
| | *8 in. Gage* | 23, 24.1 | 23 | 20.5, 22.5 | - | - |
| | *CVN Impact (ft-lb)* | | | | | |
| | *-40°F* | 79, 53, 75, 133, 64, 112 | - | - | - | - |
| | *-25°F* | - | - | - | 134, 111, 114 | 99, 34, 29 |
| | *20°F* | - | - | 72, 74, 74, 119, 130, 101 | - | - |
| | *25°F* | - | 231, 253, 216 | - | - | - |
| *Chemical Composition (Weight %)* | *Carbon, C* | 0.050 | 0.070 | 0.160 | 0.080 | 0.090 |
| | *Manganese, Mn* | 1.310 | 1.260 | 1.040 | 1.280 | 1.160 |
| | *Phosphorus, P* | 0.011 | 0.008 | 0.008 | 0.011 | 0.005 |
| | *Sulfur, S* | 0.003 | 0.003 | 0.000 | 0.001 | 0.004 |
| | *Silicon, Si* | 0.320 | 0.310 | 0.330 | 0.390 | 0.403 |
| | *Copper, Cu* | 0.300 | 0.340 | 0.290 | 0.280 | 0.338 |
| | *Nickel, Ni* | 0.260 | 0.330 | 0.220 | 0.270 | 0.360 |
| | *Chromium, Cr* | 0.620 | 0.630 | 0.480 | 0.470 | 0.610 |
| | *Molybdenum, Mo* | 0.050 | 0.030 | 0.030 | 0.030 | 0.048 |
| | *Vanadium, V* | 0.066 | 0.075 | 0.029 | 0.073 | 0.058 |
| | *Aluminum, Al* | 0.023 | 0.031 | 0.026 | 0.031 | 0.034 |
| | *Columbium, Cb* | - | 0.054 | - | - | 0.003 |
| | *Calcium, Ca* | 0.002 | - | 0.001 | 0.002 | - |
| | *Nitrogen, N* | 0.012 | 0.009 | - | - | 0.006 |
| | *Niobium, Nb* | 0.004 | - | 0.005 | 0.003 | - |
| | *Titanium, Ti* | 0.002 | 0.008 | 0.002 | 0.002 | 0.002 |
| | *Boron, B* | 0.0002 | - | 0.0003 | 0.0002 | 0.0002 |
| | *Tin, Sn* | 0.011 | - | 0.010 | 0.011 | 0.002 |

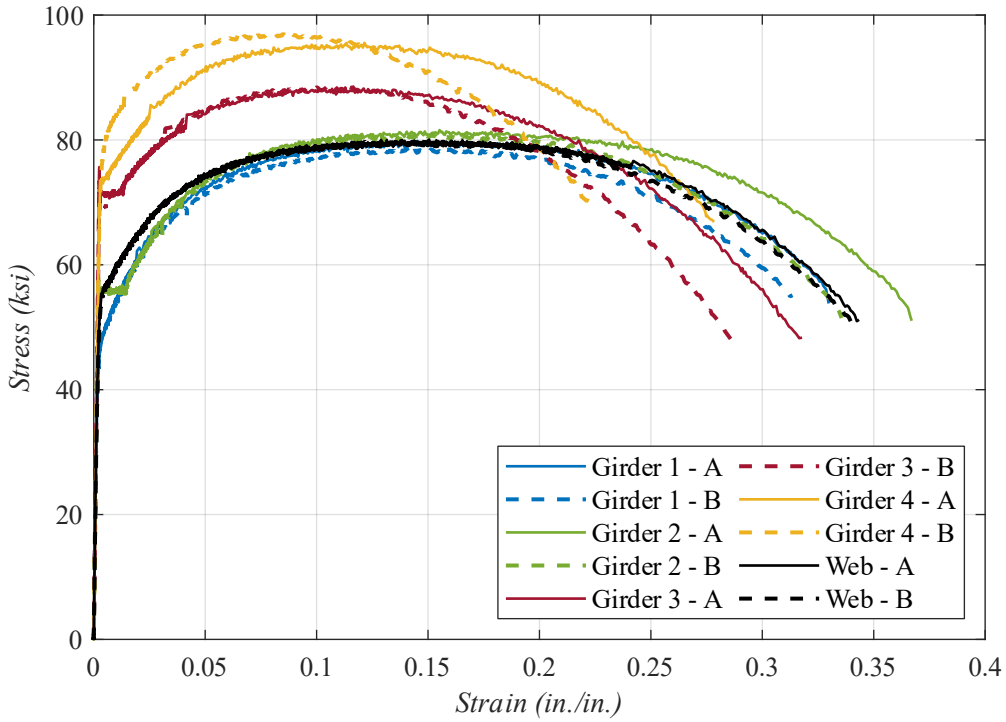


**Figure 6-2. Graph. Stress-strain plots for tension specimens taken from test girder components.**

**Table 6-5. Average yield stress, tensile stress, and elongation for each test girder component.**

| *Girder / Component* | *Heat #* | *Avg. Yield (ksi)* | *Avg. Tensile (ksi)* | *Avg. Elong. (in./in.)* |
|---|---|---|---|---|
| G1 / Flanges | A4F201 | 49.0 | 79.3 | 0.322 |
| G2 / Flanges | 3604594 | 56.1 | 81.3 | 0.351 |
| G3 / Flanges | 2606165 | 71.3 | 88.5 | 0.302 |
| G4 / Flanges | 813Y70980 | 76.1 | 96.3 | 0.251 |
| G1-G4 / Web | 36033496 | 55.7 | 79.9 | 0.343 |

### *6.2.3. Girder Fabrication and Welding Information*

The fatigue test girders were fabricated by High Steel Structures in Williamsport, PA. Each flange was fabricated by joining five plates with four CJP-welded butt-splice joints. Similar to the fabrication of the material characterization plates used in the material characterization tests, the CJP weld for all flange plates was a single 60° V-groove weld with no backing, and all base CJP and full-length repair welds were performed using the SAW process. Runout tabs were

used on all CJP and full-length repair welds, and a combination of arc gouging and mechanical grinding was used for all weld excavations. After the final repair was performed, all CJP groove welds were ground smooth and checked for soundness using RT. Once all flanges were fabricated, the girders were assembled using double-sided 5/16 in. fillet welds along the length of the flange-to-web junctions. All fillet welds were performed using SAW with 3/32 in. Lincoln LA-75/960 wire (F8A2-ENi1K-Ni1-H4) and checked using visual and magnetic particle testing (VT and MT) techniques per the requirements of AASHTO/AWS D1.5 (2020).

For Girders 1 and 3, the base CJP joints generally required 16 to 18 passes, and the repair welds generally required seven to nine passes. For Girders 2 and 4, the base CJP joints generally required four to seven passes, and the repair welds generally required four to six passes. All base CJP joints and repair welds in the 50W plates (i.e., Girders 1 and 2) were welded with 3/32 in. Lincoln LA-75/960 wire (F8A2-ENi1K-Ni1-H4), and all base CJP joints and repair welds in the HPS70W plates (i.e., Girders 3 and 4) were welded with 3/32 in. Lincoln LA-85/MIL800HPNi wire (F9A4-ENi5-G-H2). Both wires are nickel-bearing electrodes suitable for weathering steels.

Table 6-6 presents all pertinent welding information for the CJP welded joints in each girder, including welding parameters, calculated heat input, and preheat/interpass temperatures. Due to the large number of welds at each CJP joint, a range of similar welding parameters was used throughout fabrication. In lieu of creating an exhaustive list of parameters for each joint and weld pass, an envelope of the welding parameters used for each girder is provided in Table 6-6, reporting the minimum and maximum values recorded for each welding parameter across all CJP joints on each girder. All the welding parameters fell within the allowable ranges specified in the WPSs. Copies of the WPSs used for both grades of steel are provided in Appendix B. Note that the welding parameters for Girders 1 / 3 and 2 / 4 (i.e., girders with the same flange thicknesses)

are essentially the same, as the two welding procedures are nearly identical except for the consumable.

The fabrication process used to create all the welded CJP joints on the girder flanges was identical to the one used for the material characterization plates (see Section 4.2.3), except that the plate face on which the repair weld was performed alternated between the front and back plate faces each repair to help control the distortions (i.e., the flange plate was flipped each repair). Figure 6-3 shows some photos of the CJP welds being fabricated and the girders being assembled.

**Table 6-6. Welding parameters used in the fabrication of CJP welded joints in girder flanges.**

| *Girder* | *Weld* | *Weld Pass* | *WFS (in./min)* | *Amp. (A)* | *Volt. (V)* | *TS (in./min)* | *HI (kJ/in.)* | *Temp. Range* | |
|---|---|---|---|---|---|---|---|---|---|
| | | | | | | | | *Min. (°F)* | *Max. (°F)* |
| Girder 1 | Base | 1 | 90 | 400 | 31.5 | 16 | 47.3 | 70 | 550 |
| (All Joints) | | 2+ | 115 | 440 | 33 | 16 | 54.5 | 70 | 550 |
| | Repairs | 1+ | 90-125 | 400-440 | 31-34 | 16 | 46.5-56.1 | 70 | 550 |
| Girder 2 | Base | 1 | 90 | 400 | 31.5 | 16 | 47.3 | 70 | 550 |
| (All Joints) | | 2+ | 115 | 440 | 33 | 16 | 54.5 | 70 | 550 |
| | Repairs | 1+ | 90-125 | 400-440 | 31-34 | 16 | 46.5-56.1 | 70 | 550 |
| Girder 3 | Base | 1 | 110 | 410-420 | 32-33.5 | 18 | 43.7-46.9 | 125 | 450 |
| (All Joints) | | 2+ | 115-125 | 420-465 | 33-35 | 18 | 46.2-54.3 | 125 | 450 |
| | Repairs | 1+ | 95-125 | 410-470 | 32-35 | 18 | 43.7-54.8 | 125 | 450 |
| Girder 4 | Base | 1 | 100-110 | 415 | 30.5-32 | 18 | 42.2-44.3 | 125 | 450 |
| (All Joints) | | 2+ | 100-120 | 415-425 | 30.5-33.5 | 18 | 42.2-46.3 | 125 | 450 |
| | Repairs | 1+ | 100-125 | 415-435 | 32-34 | 18 | 44.3-49.3 | 125 | 450 |

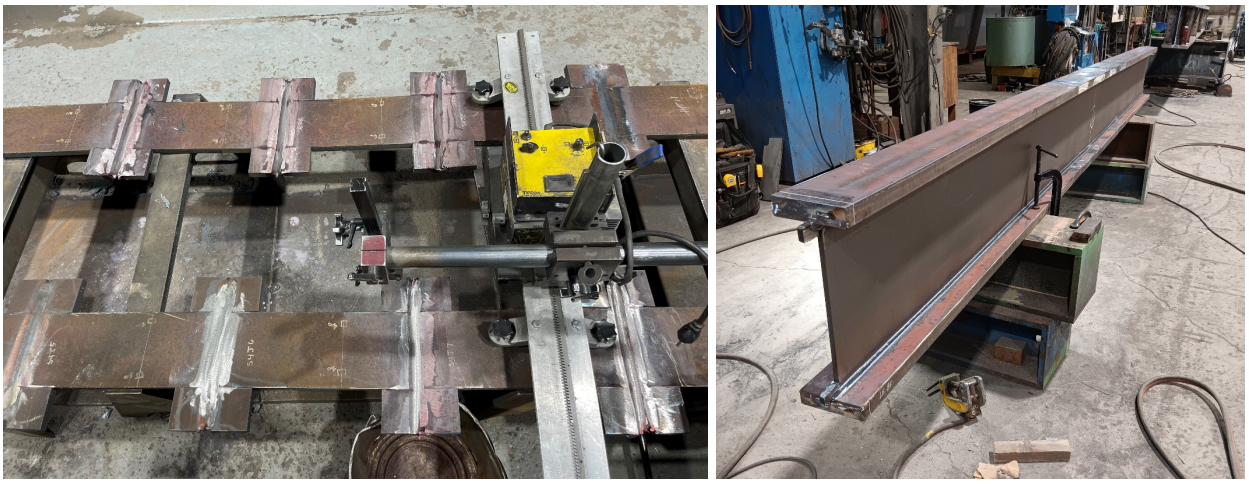

(a) Photo showing CJP joints being welded (G4 Shown)

(b) Photo showing assembled girder (G1 shown)

**Figure 6-3. Multiple Photos. Photos showing the fabrication of the fatigue life testing girders. (a) Photo showing CJP joints being welded, and (b) Photo showing assembled girder.**

All CJP joints from all girders passed the first round of RT inspection, except for Girder 1 – Joint 3 (G1-J3) and Girder 3 – Joints 1, 3, and 6 (G3-J1, G3-J3, G3-J6). For G1-J3, RT identified a slag inclusion ~0.10 in. below the surface and ~1.0 in. off the flange edge. For G3-J1, RT identified a slag inclusion ~0.07 in. below the surface near the flange edge. For G3-J3, RT identified slag inclusions ~0.07 in. and ~0.06 in. below the surface near the flange edges. For G3-J6, RT identified a slag inclusion ~0.13 in. below the surface near the flange edge. For each joint, the defect locations were excavated using the typical arc gouging and grinding procedure, and a repair weld was performed using shielded metal arc welding (SMAW) with a 5/32 in. E7018 electrode running at ~160 amps. Using SMAW for targeted repairs like these is common in the bridge industry, and SAW was not feasible in this instance because it was not a full-length repair. The RT results confirm that all the final CJP joints in the flanges are sound and contain no defects or discontinuities along the length of the joint that would negatively influence the fatigue life test results (discussed in Chapter 7). Figure 6-4 shows representative RT results

for G1-J3 that showcase an RT result with a detected defect and the final RT result that is defect-free.

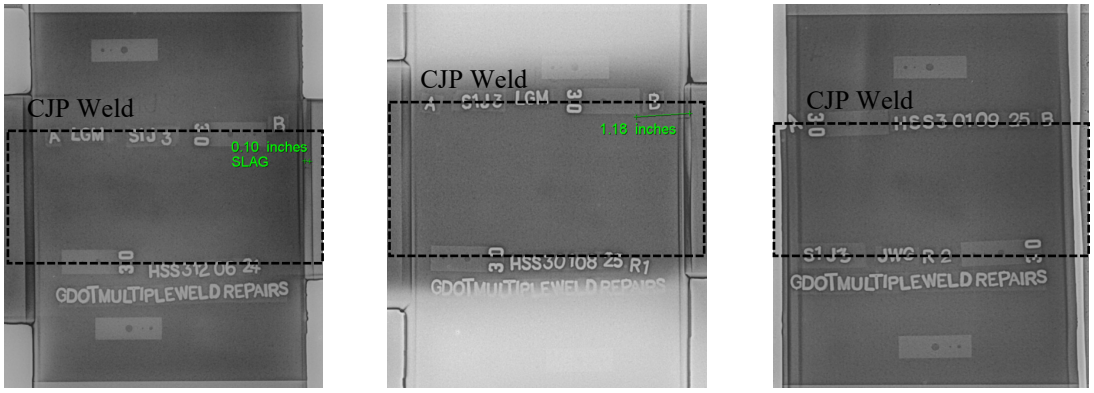


Girder 1 – J3 (R3) – 1
(initial – defect)

Girder 1 – J3 (R3) – 2
(repaired – defect)

Girder 1 – J3 (R3) – 3
(repaired – no defects)

**Figure 6-4. Radiographic testing (RT) NDT results from G1-J3 showing a detected defect and the final RT with no defects.**

### *6.2.4. AASHTO Fatigue Details*

The fatigue test girders have four relevant fatigue details: (a) ground smooth CJP groove welds, (b) longitudinal fillet welds, (c) bolted stiffeners with pretensioned bolts, and (d) noncoated weathering base metals. Given that AASHTO does not differentiate between a standard CJP groove weld and a CJP groove weld that has been repaired, all CJP groove welds in the specimens are classified the same. In accordance with Table 6.6.1.2.3-1 of AASHTO LRFD-10, all four details are Category B and are governed by the same S-N design curve, meaning they have the same design life and an equal chance of failing. Although the current study focuses on the fatigue performance of CJP joints, other fatigue details are unavoidable. Figure 6-5 shows the relevant AASHTO fatigue details on the test beam, and Table 6-7 summarizes the relevant AASHTO fatigue design parameters for each detail.

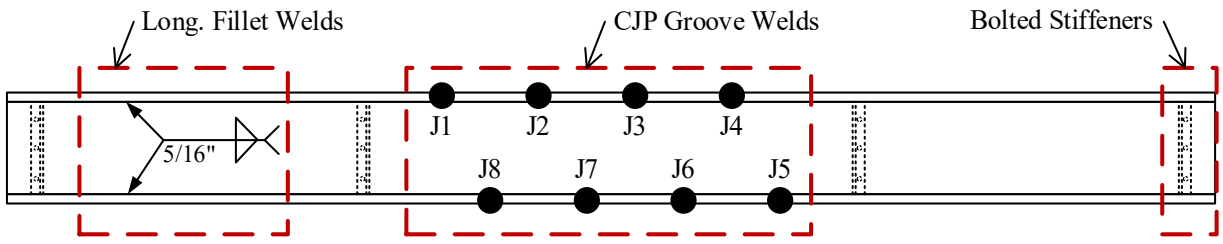


**Figure 6-5. Illustration. AASHTO fatigue details on the test girder.**

**Table 6-7. Summary of AASHTO fatigue details and design constants per AASHTO LRFD-10.**

| *AASHTO Detail* | *Detail Category* | *Constant, A ($ksi^3$)* | *CAFT, $(\Delta F)_{TH}$ (ksi)* |
|---|---|---|---|
| CJP Joint Transverse to Stress Flow (Ground Smooth) | B | $120 \times 10^8$ | 16 |
| Continuous Longitudinal Fillet Weld | B | $120 \times 10^8$ | 16 |
| Bolted Stiffeners w/ Pretensioned Bolts | B | $120 \times 10^8$ | 16 |
| Base Material (Noncoated Weathering Steel) | B | $120 \times 10^8$ | 16 |

CAFT = Constant Amplitude Fatigue Threshold

## 6.3. Experimental Testing Configuration

A four-point bending configuration was used for all large-scale fatigue tests, resulting in a theoretical constant-moment region across the middle segment and allowing concurrent testing of four CJP joints. Figure 6-6a shows the loading configuration and idealized boundary conditions. The loading beam, discussed in the next section, is shown for clarity. The resulting shear-moment diagrams are shown in Figure 6-6b. Notably, the "modified pin" used as an end boundary condition was a traditional pin machined to allow a slight longitudinal translation, providing restraint similar to a rocker until the point of fixity. The modified pin helped reduce the axial forces developed under a true pin–pin boundary condition while still ensuring that both the loading and testing beams had independent longitudinal restraint for safety. While the modified pin helped reduce some axial forces, a compressive axial force still developed during loading and had to be accounted for in calculations. As such, the modified pin was conservatively treated as a traditional pin for calculations. Note that longitudinal restraint for the

system is provided by the actuator and modified pin. Lateral bracing of the top and bottom flanges was applied approximately 12 in. inward of the end boundary conditions.

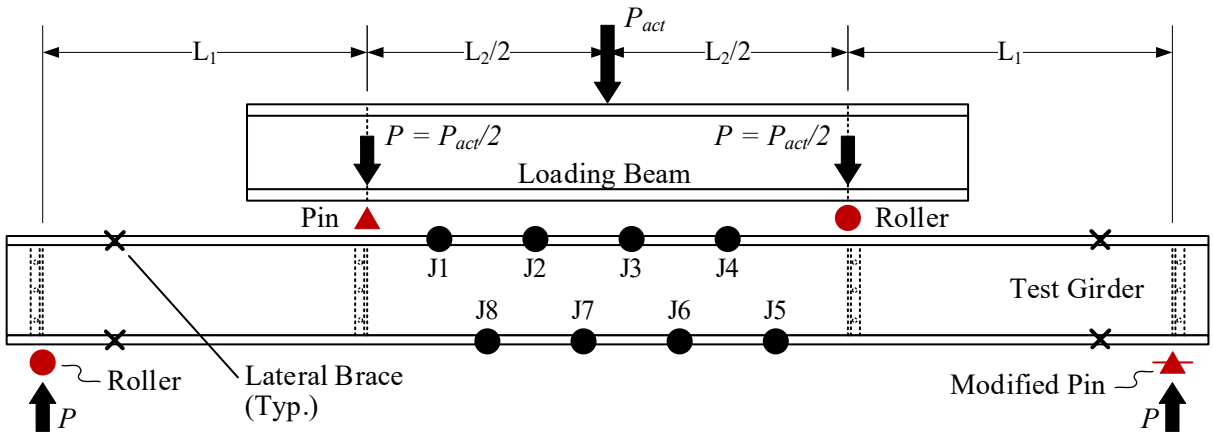


(a) Four-Point Bending Loading Configuration

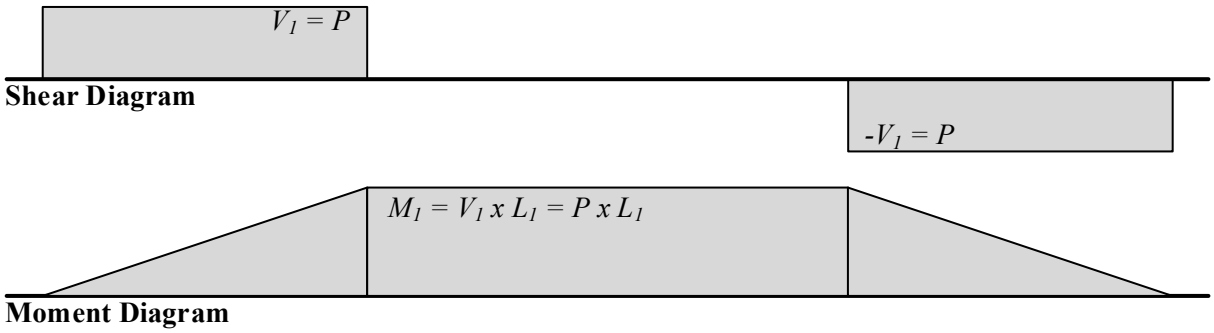


(b) Shear-Moment Diagrams

**Figure 6-6. Multiple Illustrations. Large-scale fatigue test loading configuration and resulting shear-moment diagrams. (a) Four-point loading configuration and (b) shear-moment diagrams.**

## 6.4. Experimental Testing Setup

The large-scale fatigue life tests were conducted at the Georgia Tech SEML. The experimental test setup consisted of a load frame, a 146-kip and 328-kip hydraulic actuator (equipped with 110-kip and 220-kip load cells, respectively), a loading beam, the test specimens, concrete pedestals, a lateral bracing system, and boundary conditions. The hydraulic actuators were MTS single-ended actuators, controlled by a FlexTest 60 Controller and Series 793 controller software. The actuators were connected to the hydraulic power unit (HPU) via high-

pressure hydraulic lines. The loading beam was a 10’-0” long W14x257 connected to the actuator via a clevis hook with four tensioned bolts. The loading beam was attached to the test girder via a pin-and-roller boundary condition at the top flange of the test girder and secured in place during testing with plates and bridge clamps. The boundary conditions kept the loading beam properly aligned with the testing girder and allowed it to consistently apply the two interior point loads at the intended locations.

The lateral bracing system and concrete pedestals supported the test girder, and the load frame supported the actuator. The lateral bracing system was comprised of L4-1/2 x 4-1/2 x 1/2 angles bolted and clamped into an interlocked triangular bracing system to prevent lateral movement of the girder flanges. The vertical angle used to brace the test girder was lined with a 3/8 in. thick polytetrafluoroethylene (PTFE) sheet to reduce friction and minimize unintended longitudinal restraint. The load frame and concrete pedestals were anchored to the strong floor via pretensioned DYWIDAG bars, and the end boundary conditions and end lateral bracing system were anchored to the concrete pedestals. All boundary conditions were constructed using 2-1/2 in. diameter round bars and ASTM A514 steel plates, which were machined to create the semi-circle inserts needed for the pin connections. All pin connections were lubricated during testing with white lithium grease to reduce friction. Figure 6-7 shows a schematic overview of the large-scale fatigue testing setup, and Figure 6-8 shows photos of the large-scale fatigue testing setup. Figure 6-9 provides close-up photos of the boundary conditions.

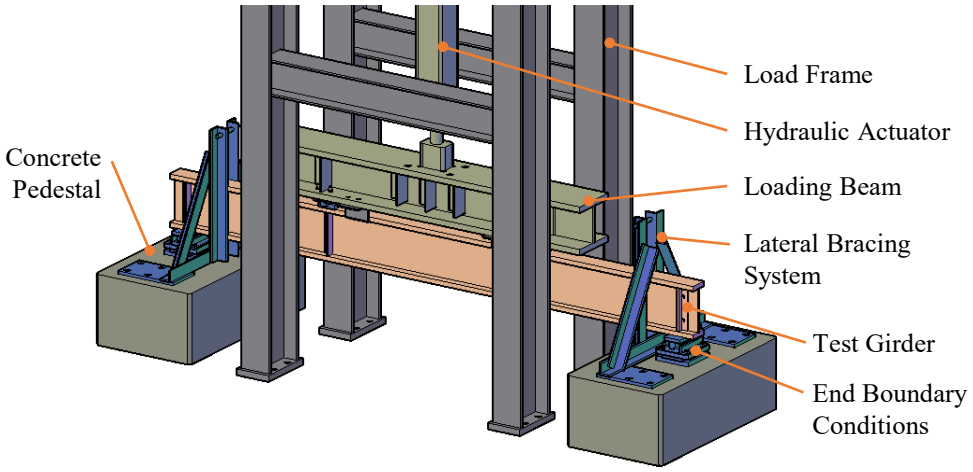


**Figure 6-7. Illustration. Schematic overview of the large-scale fatigue testing setup.**

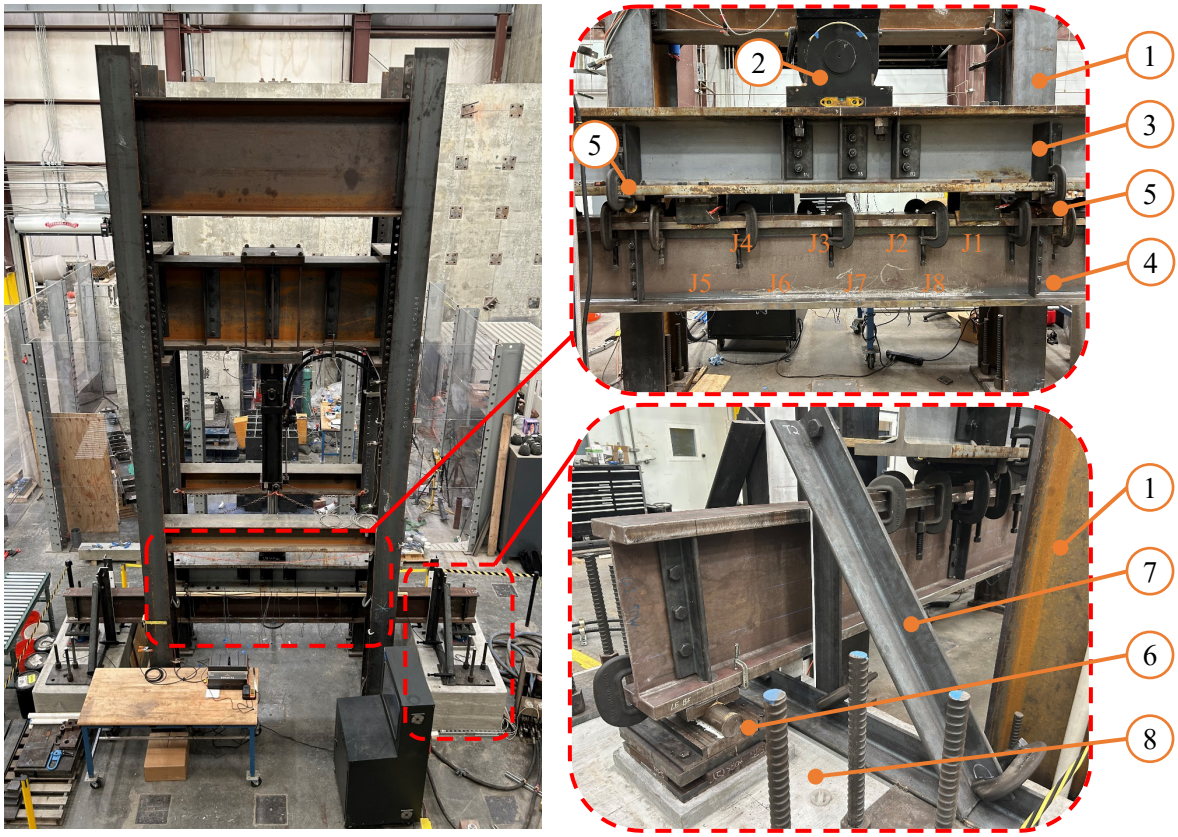


**Figure 6-8. Multiple Photos. Photos of the large-scale fatigue testing setup. (1) load frame, (2) hydraulic actuator, (3) loading beam, (4) test girder, (5) internal boundary condition, (6) exterior boundary condition, (7) end lateral bracing system, (8) concrete pedestal**

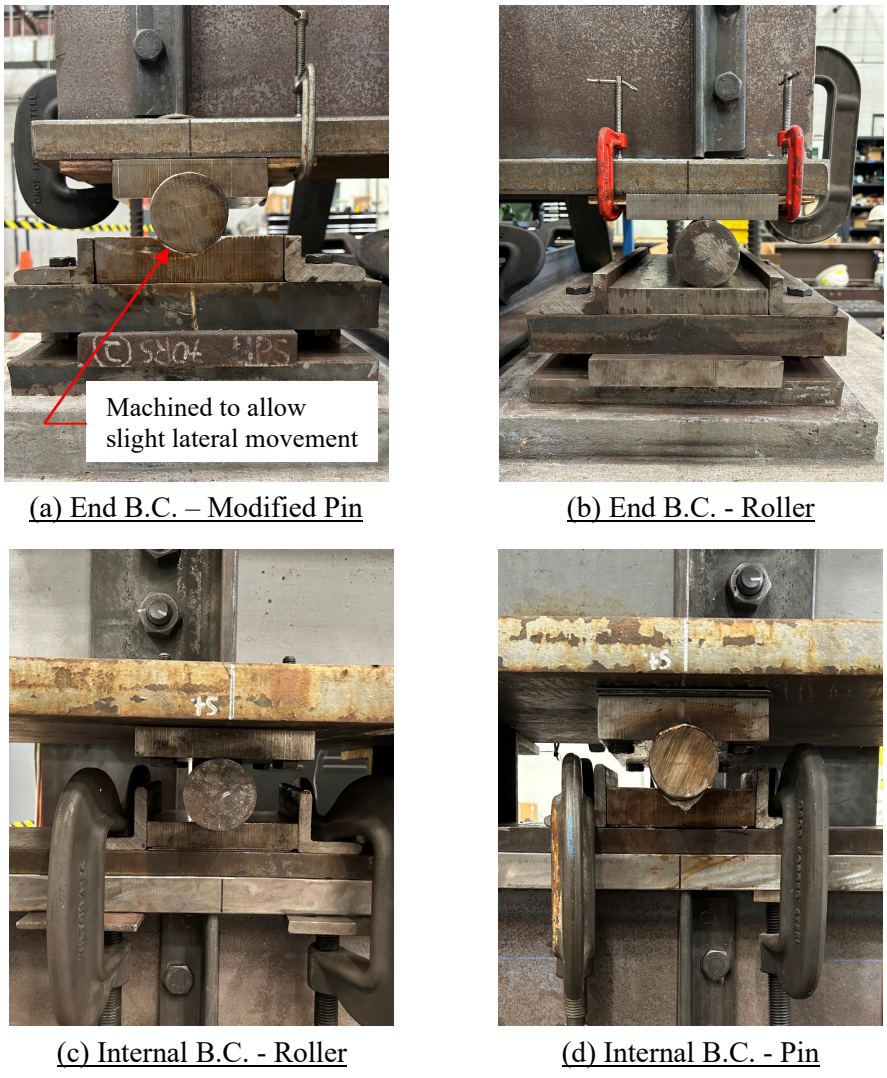


(a) End B.C. – Modified Pin

(b) End B.C. - Roller

(c) Internal B.C. - Roller

(d) Internal B.C. - Pin

**Figure 6-9. Multiple Photos. Photos showing the boundary conditions (B.C.) used. (a) End B.C. – Modified Pin, (b) End B.C. – Roller, (c) Internal B.C. – Roller, and (d) Internal B.C. - Pin**

## 6.5. Experimental Testing Setup Validation

The experimental testing setup was validated in two ways to ensure that the targeted stress range was achieved throughout testing: (a) strain gages were installed and monitored throughout testing, and (b) static tests were performed on the test girders prior to cycling to verify that the measured stresses correlated with the theoretical stresses. Strain gages were installed at discrete locations along the centerline of the tension flanges and at each CJP joint tested. The strain gages collected data at a sampling rate of 40 Hz, and the maximum and

minimum strains were measured over five seconds and recorded. The measured strains were converted to stresses using Hooke's Law and an assumed modulus of elasticity of 29,000 ksi. The strain gages enabled continuous monitoring of the CJP joints, allowing the stress ranges to be adjusted and maintained within a constant +/- 0.5 ksi range throughout testing. The strain gage layout and the measured peak–valley stresses recorded throughout testing for each test girder are provided and discussed in Chapter 7.

Before cycling, each girder was quasi-statically loaded to approximately 80–90% of the testing load: approximately 70 kips for Girders 2 / 4 and 150 kips for Girders 1 / 3. The measured stresses from the strain gages were then compared against the theoretical stresses determined using classical mechanics and the nominal cross-section of each test girder. The moments and axial forces were calculated using a first-order elastic analysis, and the resulting stresses throughout the middle section of the girder are the sum of the resulting flexural and axial stresses. The results from one static test from each test girder are shown in Table 6-8. Note that for the reasons discussed in Chapter 7, a 6 in. x 1 in. top cover plate was included in all calculations and measurements.

**Table 6-8. Results from the static experimental validation tests.**

| | | Location | | |
|---|---|---|---|---|
| | *Stress (ksi)* | *1* | *2* | *3* |
| Girder 1 | Theoretical | 23.2 | 19.8 | -19.3 |
| | Measured | 23.4 | 19.4 | -19.3 |
| Girder 2 | Theoretical | 17.6 | 16.3 | -14.3 |
| | Measured | 18.3 | 17.2 | -13.6 |
| Girder 3 | Theoretical | 23.2 | 19.8 | -19.3 |
| | Measured | 22.9 | 18.9 | -17.8 |
| Girder 4 | Theoretical | 17.6 | 16.3 | -14.3 |
| | Measured | 18.4 | 16.6 | -12.8 |

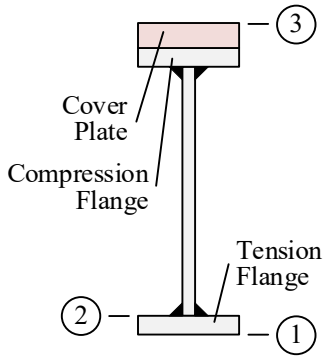


Girder 1 & 3: Area = 31.5 $in^2$ || $I_x$ = 1808 $in^4$

Girder 2 & 4: Area = 22.5 $in^2$ || $I_x$ = 1307 $in^4$

As shown in the table, the measured and calculated nominal theoretical stresses for all girders were in good agreement. The measured stresses in the bottom flange are within 5% of the theoretical stresses, and the measured stresses throughout the rest of the beam are within 10% of the theoretical stresses. The difference in measured and theoretical stresses is most likely due to: (a) differences between nominal and actual cross sections, (b) unaccounted for complexities due to the top cover plate being clamped, and (c) unaccounted for load-height effects since the girder was not braced at the points of load application. The close correlation validated the experimental setup, proving that the targeted testing stress range can be achieved and maintained.

### 6.6. Crack Detection and Repair Procedures

Throughout the testing program, cracks were checked for using a combination of visual inspection (using a 10x magnifying glass), fast-drying cleaner solvent, and MT NDT techniques. Using these inspection techniques, fatigue cracks were found on all flanges tested, with some being at joint locations and others in the base metal or fillet weld joints. To continue testing until all four CJP butt-spliced joints in each flange were complete, cracks were arrested and repaired. Note that the repairs discussed in this section are not related to the shop repair welds performed on the CJP joints being tested. All the fatigue crack repairs discussed below were performed at the laboratory during the fatigue life tests to address cracks that appeared from fatigue.

Two main crack repair techniques were used to address fatigue cracks: (a) mechanical grinding to remove the crack and (b) bolted splices using cover plates. Mechanical grinding was the preferred crack repair technique when feasible, as it leaves the flange mostly intact and limits additional fatigue-related concerns. However, grinding was not viable for many cracks, in which case a bolted splice repair was used. Note that no cracks were repaired using welding repair

techniques. While welding repair techniques would have been feasible for some of the cracks, these techniques were not used because the repairs would have involved complicated welding joints and processes (because the girder was in the testing bay and had no weld access holes) and to avoid adding additional welded fatigue details to the girders being tested.

Mechanical grinding was primarily used to repair fillet weld cracks and, if caught very early, the occasional base metal flange edge crack. A die grinder was used to mechanically grind out the crack and the nearby surrounding area, and the gouged-out region was checked with MT and PT to ensure the crack was fully removed. This repair method was very effective for toe-fillet weld cracks, often resulting in a repair that lasted throughout the rest of the testing. Grinding was less effective for root-fillet weld cracks, often lasting only approximately 400,000 cycles before a fatigue crack reappeared. The reason for this difference is the extent of gouging required to remove the cracks, with root-fillet weld cracks requiring a much deeper excavation than toe-fillet weld cracks. Regardless, the repairs were usually sufficient to complete testing without needing the more intrusive bolted splice repair if the fillet weld crack was caught early. Figure 6-10 shows photos illustrating the mechanical grinding repair process.

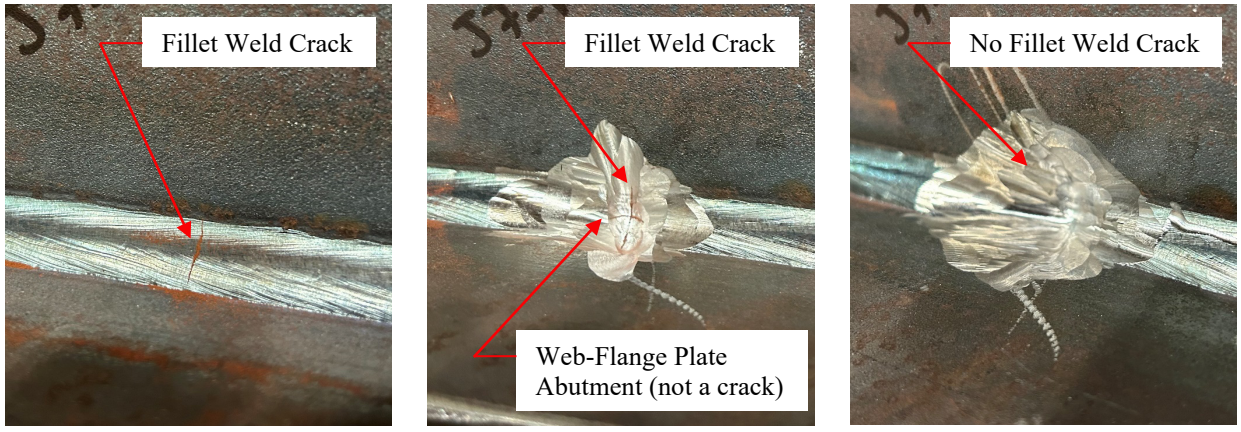


(a) Detection (b) Partial Excavation (c) Final Excavation

**Figure 6-10. Multiple Photos. Photos showing the mechanical grinding repair process. (a) Detection, (b) Partial excavation, and (c) Final excavation.**

Bolted splice repairs were typically used to repair flange-edge cracks and root-fillet weld cracks that extended beyond the practical limits of mechanical grinding repair. For these repairs, a magnetic base drill was used to drill out the crack tip locations in the flange and web to prevent further crack growth. A properly sized pretensioned bolt was installed in the web hole to make this bolt hole a Category B fatigue detail, which was usually sufficient to complete testing without additional cracks forming at this location. Bolt holes were then drilled in the flange, and top and bottom cover plates were attached. The cover plates always extended a minimum of two rows of bolts in each direction beyond the crack and contained a minimum of five rows of bolts, with each row containing two bolts. The cover plates were secured to the flange using pretensioned 1 in. A325 grade bolts (ASTM 2023) to create a slip-critical joint that covered the crack. The bottom cover plates used were 6 in. x 1 in. or 6 in. x 1-1/2 in. plates, depending on the girder, and all top cover plates were 2-1/2 in. x 1 in. plates. All cover plates were either grade A36 or A572 steel. The repairs introduced a new Category B fatigue detail to the girder flanges (i.e., all flange holes with pretensioned bolts installed), and it was not uncommon for the last row of the bolted splice joints to fail from fatigue during testing. In these cases, the cover plates were removed, the crack tips and additional bolt hole rows were drilled, and a longer cover plate was reinstalled. Figure 6-11 shows photos illustrating the bolted splice repair process. Note that the photos shown are not all from the same crack repair; they were selected from multiple crack repairs to showcase different scenarios.

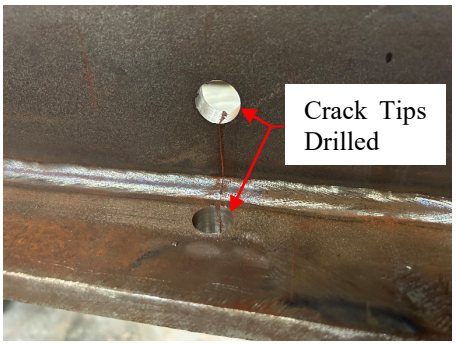


(a) Crack Tip(s) Arrested

(b) Bolt Holes Drilled in Flange

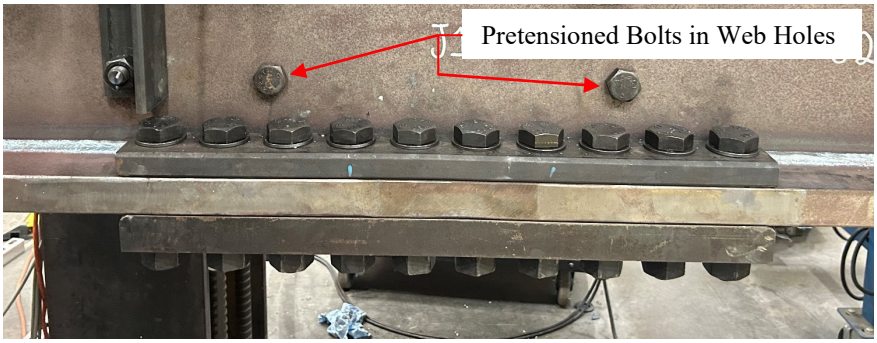


(c) Cover Plates Installed with Pretensioned Bolts

**Figure 6-11. Multiple Photos. Photos showing the bolted splice repair process. (a) Crack tips arrested, (b) Bolt holes drilled in flanges, and (c) Cover plates installed with pretensioned bolts.**

## 6.7. Testing Procedure and Joint Failure Classification

The test girders were cycled in a full-tension loading procedure ($R > 0$) at a constant amplitude stress range of 24 ksi ($\Delta\sigma = 24$ ksi), which is 8 ksi above the CAFT and well into the finite fatigue life design region for a Category B detail. The actuator was operated under force control to maintain a constant stress range even as fatigue cracks formed. Due to the full-tension loading procedure, the bottom flange was always subjected to tensile flexural stresses, and the top flange was always subjected to compressive flexural stresses. In general, the testing procedure was as follows:

1. Install the test girder in the fixture and install all strain gages. A detailed instrumentation layout for each test flange is provided in the subsequent sections.

2. Perform a static validation test, then begin cycling the beam.
3. Continue cycling until a crack is detected on the tension flange. Assess, document, and temporarily repair the crack using one of the procedures detailed in Section 6.6. Continue cycling until all CJP joints on the tension flange have failed or reached their runout life.
4. Remove the girder from the testing bay and flip it over so that the previously untested compression flange is now the tension flange.
5. Repeat Steps 1 to 3 until all the CJP joints have failed or reached the runout life.
6. Change the test girder and repeat Steps 1 to 5 until all CJP joints are tested.

In the current study, the failure of a joint was defined as the cycle count at which the crack at the joint had expanded to 1-1/2 inches from the flange edge. For fillet weld cracks, this roughly corresponded to performing a crack repair when the crack had propagated approximately 1-1/2 inches towards the flange edge. For flange edge cracks, this roughly corresponded to performing a crack repair when the crack had propagated approximately 1-1/2 inches towards the web. The failure point 1-1/2 inches from the flange edge was chosen because it represented a reasonable median between cracks caught close to initiation and those not detected until well into propagation. Furthermore, since welding repairs were not feasible, the procedure allowed cracks to be repaired before they became too severe. All cracks that led to the failure of a joint were destructively examined after testing to determine the point of crack initiation and properly classify whether the joint failed due to the CJP weld or fillet weld. If the crack initiated in the CJP weld in the flange, the joint is classified as a "CJP Weld Failure." If the crack initiated in the fillet weld, the joint is classified as an "Early Stoppage," signifying that the joint did not fail due to the CJP weld but that testing could not be continued. Additionally, although undesirable, there were occasions when a crack did not occur near a CJP joint, but testing could not continue

because of nearby base metal/fillet weld cracks that had to be repaired. In these cases, the maximum cycle count achieved before the repair was recorded, and the joint was marked as an "Early Stoppage."

The runout life for this testing program is classified as the fatigue life corresponding to approximately four standard deviations above the AASHTO S-N fatigue life design curves in LRFD-10, which corresponds to approximately two standard deviations above the mean experimental data on which the AASHTO S-N fatigue resistance design curves are founded. For a Category B fatigue detail at a stress range of 24 ksi, the design and runout cycle counts were 868,000 and 2,600,000 cycles, respectively (Modjeski and Masters, Inc. et al. 2014). The runout life of 2,600,000 cycles was chosen because it is roughly three times the number of cycles required by the design manual, and any relevant trends between fatigue life and the number of repair welds should be observed before this runout limit.

# CHAPTER 7. FATIGUE LIFE TESTING RESULTS

Before testing, the cross-sectional dimensions of all girders were measured and recorded, as shown in Table 7-1. Because the girders were doubly symmetric, the measured flange dimensions of the top and bottom flanges were averaged into a single value. All flange edges and fillet welds on the girders were visually inspected to identify any defects or abnormalities (e.g., abrasions on the flange edges or rough fillet weld transitions). Any identified defects and abnormalities were recorded and, if possible, ground and polished to prevent fatigue cracks from forming outside of the CJP joints. Once inspected, the test girder was loaded into the testing bay and aligned with the loading points, then tilted so that the web was plumb (i.e., perpendicular to the loading beam and the strong floor). Notably, both flanges had a slight fabrication-induced tilt, which was compensated for by installing steel shims at the boundary condition plates. To accommodate minor inconsistencies from the flange tilts, the stress ranges measured along the centerline of the tension flange were used for testing.

**Table 7-1. Measured cross-sectional dimensions of all girders.**

| | *Component* | *Width (in.)* | *Thickness (in.)* |
|---|---|---|---|
| Girder 1 | Flanges | 6.06 | 1.506 |
| | Web | 15.06 | 0.504 |
| Girder 2 | Flanges | 6.07 | 0.749 |
| | Web | 15.03 | 0.503 |
| Girder 3 | Flanges | 6.05 | 1.518 |
| | Web | 14.98 | 0.511 |
| Girder 4 | Flanges | 6.02 | 0.757 |
| | Web | 15.00 | 0.507 |

Following the testing of Girder 2 – Flange 1, the first test conducted, four large cracks were found in the top flange (i.e., Girder 2 – Flange 2), which was theoretically subjected only to compressive loading during the Flange 1 testing. The compression flange cracks likely resulted

from tensile residual stresses induced by the fillet at the web-flange juncture, which can approach the yield strength of the plate at the weld. The high tensile residual stresses, which are additive to the compressive loading stresses, resulted in a portion of the top flange experiencing cyclic tensile stresses and developing fatigue cracks at the fillet welds.

To prevent similar issues in subsequent tests, a 6 in. x 1 in. cover plate was installed along the compression flange of the remaining girders. When the compression flange of the girder had not yet been tested (e.g., Flange 1 was being tested but Flange 2 had not), the top cover plate was installed using bridge clamps to avoid damaging the top flange of the girder before testing. The top cover plate resulted in a singly symmetric cross section, allowing the bottom flange to be loaded to the targeted stress range while keeping the stress in the top flange below the threshold value of 16 ksi for a Category B detail. Strain gages were used to confirm the reduction in top flange stress range for the remainder of the tests, and no additional cracks developed on the compression flanges or fillet welds after the first girder.

All girders were cyclically loaded in two different tests: Flange 1 to test CJP joints J5, J6, J7, and J8; and Flange 2 to test CJP joints J1, J2, J3, and J4. As a reminder, J5 and J1 had zero weld repairs (R0), and J6 and J2 had one weld repair (R1). J7 and J3 had three weld repairs (R3), and J8 and J4 had five weld repairs (R5). A detailed description of each tested flange is provided in the following subsections, including an instrumentation layout, a detailed description of the test process, and a breakdown of the test results. Once all the joints on Flanges 1 and 2 of a girder were tested to completion, cracks that led to joint failure (i.e., cracks within 1-1/2" of the center of a welded joint) were destructively examined to evaluate the fatigue crack initiation point and confirm the failure classification of the joint. Figures and tables present the fatigue

cracks and the resulting fatigue life for each CJP joint tested. All fatigue cracks shown and discussed were not influenced by any crack repair procedures performed throughout testing.

## 7.1. Girder 1 (1-1/2 in. – 50W)

Including the top flange cover plate, Girder 1 has a nominal flexural capacity of 9,800 kip-in. The flexural capacity of the girder was determined using an iterative inelastic nonlinear buckling analysis (INBA) procedure to help account for the irregular bracing and boundary conditions. Girder 1 – Flanges 1 and 2 were tested by cycling Girder 1 at a constant amplitude load range from approximately 5 kips to 85 kips at the load points, resulting in flexural stresses along the flanges ranging from 1.5 ksi to 25.5 ksi. The loads resulted in a maximum applied moment of approximately 4,600 kip-in, less than half the allowable capacity. All loads and displacements were tracked throughout the test using the internal load cell and LVDT in the MTS actuator. The tests were conducted at 1.2 Hz, resulting in a daily cycle count of approximately 100,000. Strain gages were used to ensure the 24 ksi stress range was maintained. Additional test details and results for Flanges 1 and 2 are discussed in the following subsections.

### *7.1.1. Flange 1 (G1-J5, G1-J6, G1-J7, G1-J8)*

The strain gage layout used for Girder 1 – Flange 1 is shown in Figure 7-1. Three strain gages were placed at the center of the tension flange along the middle section to monitor the stress range during testing. Additionally, a strain gage was placed near the flange edges at each CJP joint to monitor joint stresses and support crack detection. Additional strain gages were placed on the flanges near the top and bottom fillet welds and on the cover plate to monitor stress ranges throughout the cross section.

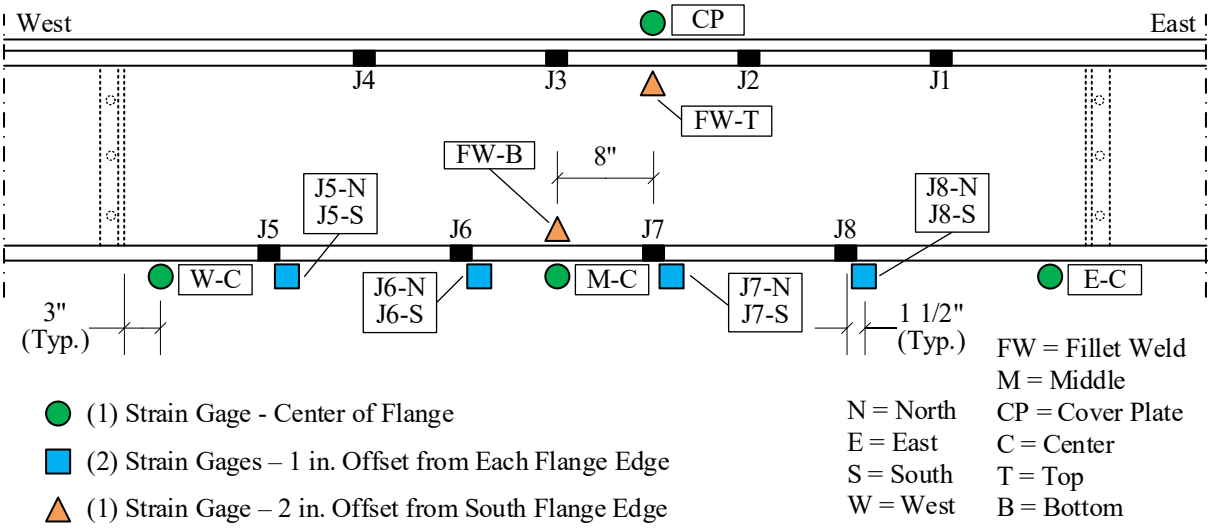


**Figure 7-1. Illustration. Instrumentation layout for Girder 1 - Flange 1 (looking north).**

The testing process followed the procedure outlined in Section 6.7. The fatigue cracks detected during testing are listed in Table 7-2. In this table, cracks are listed in order of detection, along with descriptions of the crack type, location, and the type of repair used. Each crack is named to reflect the test girder and the order of crack detection. For example, G1-1 is the first crack detected on Girder 1. Additionally, the cycle counts corresponding to the first detection and failure (i.e., when a crack repair was performed) are provided. Figure 7-2 illustrates the locations of all the fatigue cracks and shows photos of the cracks that led to joint failures or early stoppages.

**Table 7-2. Cracks detected during fatigue testing of Girder 1 - Flange 1.**

| *Crack* | *Crack Type* | *Crack Location* | *Detection Date* | *Cycle Count @ Detection* | *Cycle Count @ Failure* | *Crack Repair* |
|---|---|---|---|---|---|---|
| G1-1 | Flange Edge | J5 | 6/21/2025 | 1,038,400 | 1,087,500 | Bolted Splice |
| G1-2 | Flange Edge | J8 | 7/1/2025 | 1,558,400 | 1,558,400 | Bolted Splice |
| G1-3 | Fillet Weld | 4 in West of J7 | 7/16/2025 | 2,338,200 | 2,363,400 | Bolted Splice |
| G1-4 | Fillet Weld | 2 in. East of J7 | 7/16/2025 | 2,338,200 | 2,363,400 | Bolted Splice |

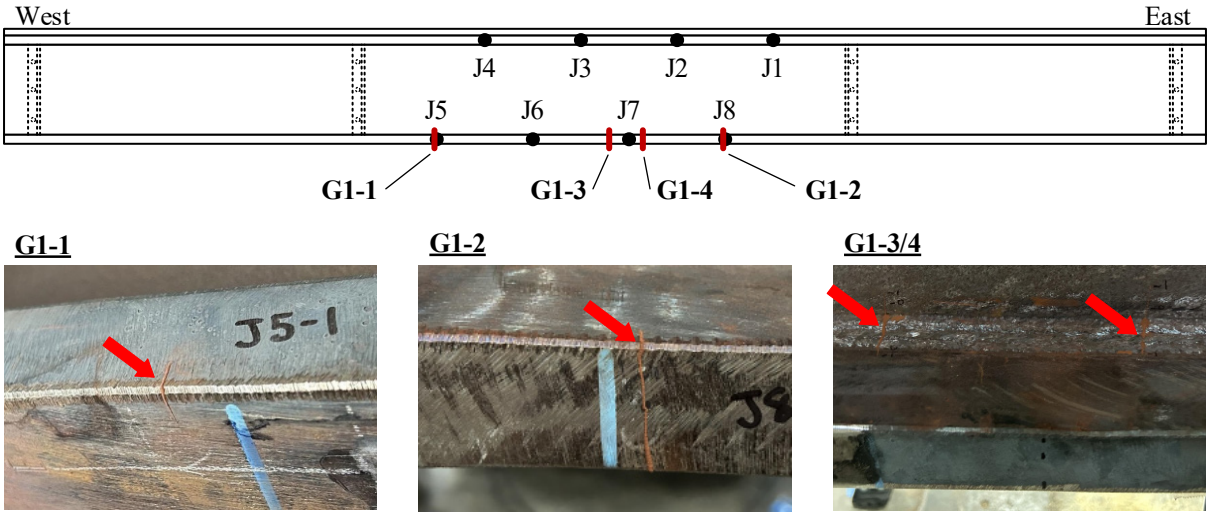


**Figure 7-2. Illustration. Overview showing the different fatigue cracks for Girder 1 – Flange 1.**

Cracks G1-1 and G1-2 were flange-edge cracks that initiated from the bottom flange tip. Crack G1-1 led to the joint failure of J5 (R0) at 1.09 million cycles, and crack G1-2 led to the joint failure of J8 (R5) at 1.56 million cycles. Cracks G1-1 and G1-2 were destructively examined after testing to confirm the points of crack initiation and failure classification of the joints. Cracks G1-3 and G1-4 were fillet weld cracks that initiated from the root of the fillet weld. While these cracks were more than 1-1/2 inches from J7 (R3), they propagated and required repair, resulting in the early stoppage of J7 (R3) at 2.36 million cycles. No cracks were detected at J6 (R1). The joint cycled to a runout life of 2.6 million cycles and was declared a runout.

After testing was completed for Girder 1, Cracks G1-1 and G1-2 were isolated and cut open using a vertical band saw to expose the internal crack planes and crack initiation points. Figures 7-3 and 7-4 show the crack initiation point and general crack growth behavior of Cracks G1-1 and G1-2, respectively. These figures confirm that Cracks G1-1 and G1-2 started at the bottom of the flange edge, so joints J5 (R0) and J8 (R5) are classified as CJP weld failures. A summary of the fatigue-life test results for the four CJP joints tested is shown in Table 7-3,

including the joint and fatigue life corresponding to joint failure, early stoppage, or runout life. Note that all CJP joints tested exceeded the minimum AASHTO design life.

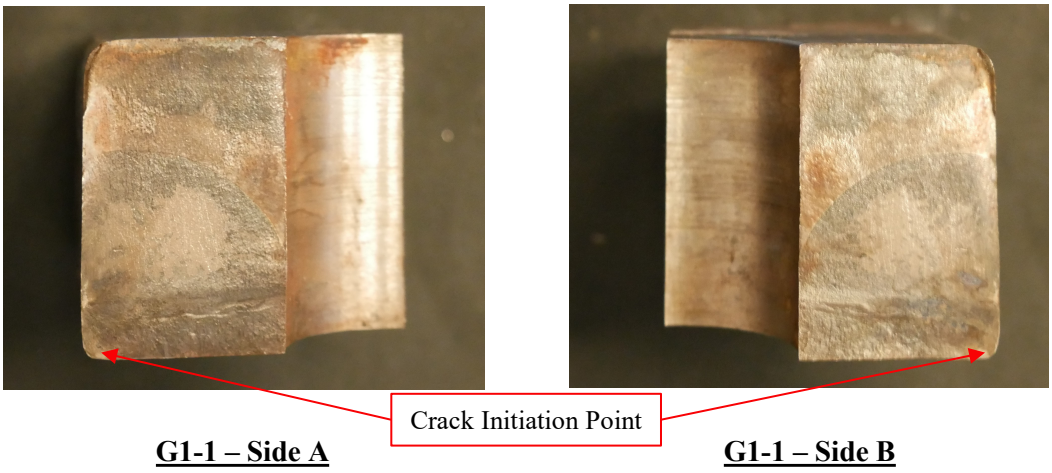


Crack initiation point at bottom of flange edge.

**Figure 7-3. Photo. Destructive evaluation of Crack G1-1, which led to the failure of G1-J5.**

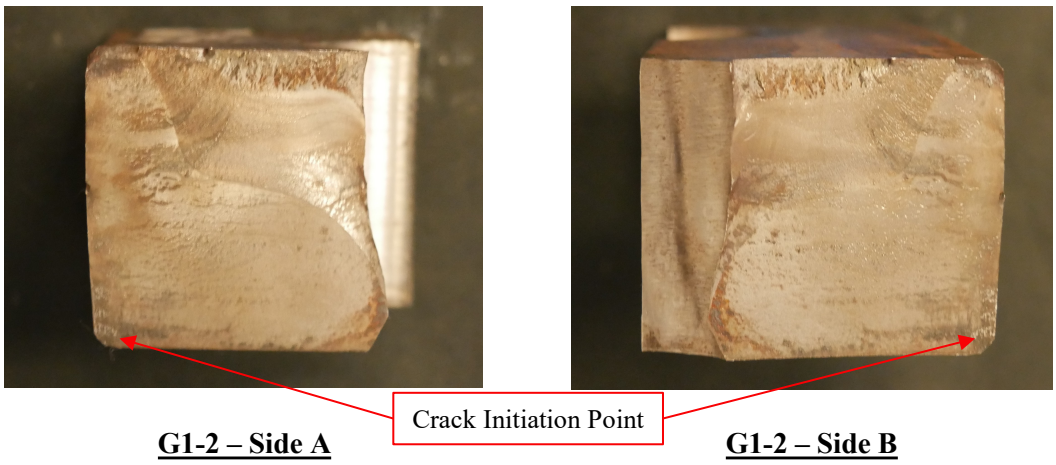


Crack initiation point at bottom of flange edge.

**Figure 7-4. Photo. Destructive evaluation of Crack G1-2, which led to the failure of G1-J8.**

**Table 7-3. Fatigue life test results for G1-J5, G1-J6, G1-J7, and G1-J8.**

| *Joint* | *Joint Results* | *Crack at Joint* | *Fatigue Life* |
|---|---|---|---|
| G1-J5 (R0) | CJP Weld Failure | Flange Edge | 1,087,500 |
| G1-J6 (R1) | Runout | - | 2,600,000 |
| G1-J7 (R3) | Early Stoppage | - | 2,363,400 |
| G1-J8 (R5) | CJP Weld Failure | Flange Edge | 1,558,400 |

Additionally, data from each strain gage were analyzed, and an average stress for the strain gage was determined for each test day. The average stresses for the centerline gages and CJP joint gages for each day are shown in Figures 7-5 and 7-6, respectively. In these plots, the abscissa shows the dates the girder was tested, and the ordinate shows the measured stress ranges. Note that some gages were removed prematurely for crack repairs, which is why some strain gages do not have data for the entire test. In the figures, a sharp change in stress usually correlates to the first detection of a fatigue crack, where the stress range at that particular strain gage steadily increased or decreased as a crack grew nearby.

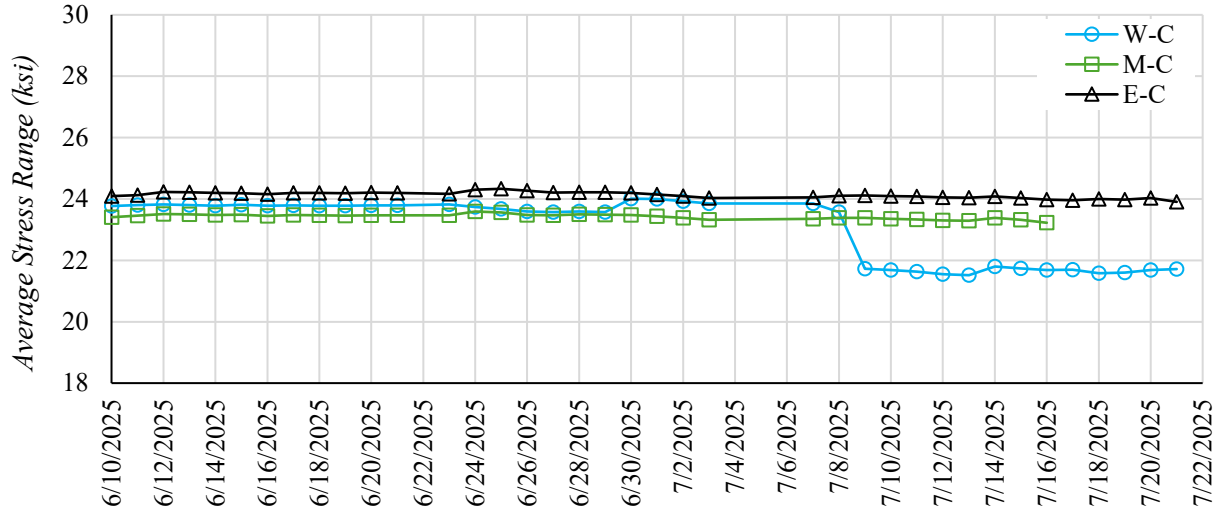


**Figure 7-5. Graph. Average daily stress range for Girder 1 – Flange 1 measured with strain gages along the bottom flange centerline.**

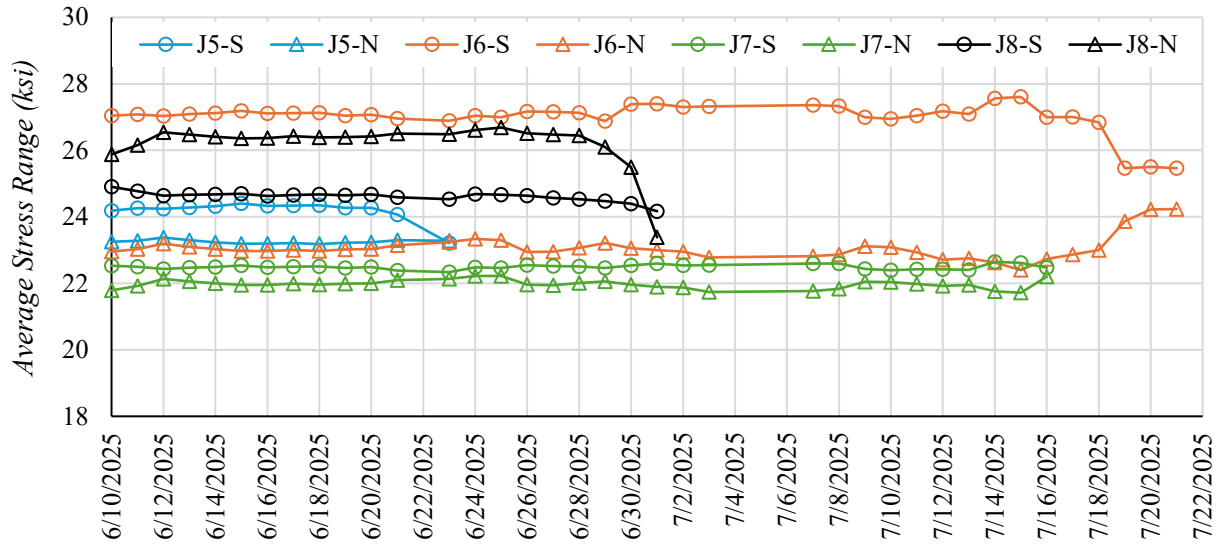


**Figure 7-6. Graph. Average daily stress range for Girder 1 – Flange 1 measured with strain gages at CJP butt-splice joints.**

Figure 7-5 demonstrates that the 24 ksi stress range was maintained along the centerline of the girder throughout testing. Figure 7-6 shows that the stress ranges along the flange edges were less consistent at each CJP butt-splice welded joint, with the measured stress ranges typically being within 4 ksi of the targeted 24 ksi. Discussions explaining why these stresses varied at the individual joints are provided in Section 7.5. In all cases, the measured stresses remained consistent until a crack formed near the joint/strain gage.

### *7.1.2. Flange 2 (G1-J1, G1-J2, G1-J3, G1-J4)*

The strain gage layout used for Girder 1 – Flange 2 is shown in Figure 7-7. Three strain gages were placed at the center of the tension flange along the middle section to monitor the stress range during testing. Additionally, a strain gage was placed near the flange edges at each CJP joint to monitor joint stresses and support crack detection. Additional strain gages were placed on the flange near the bottom fillet weld and on the cover plate to monitor stress ranges throughout the cross section.

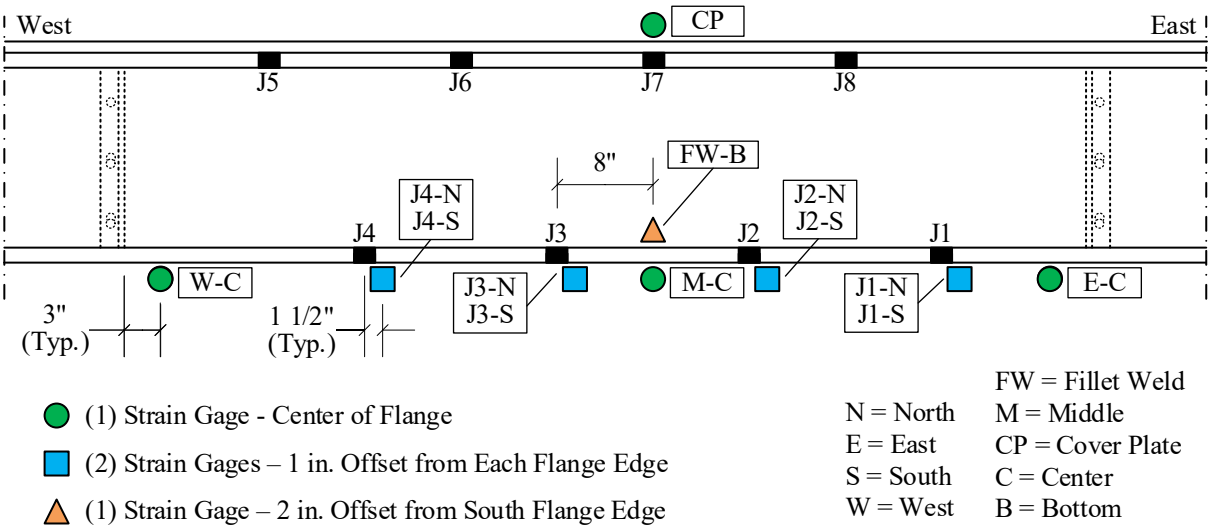


**Figure 7-7. Illustration. Instrumentation layout for Girder 1 - Flange 2 (looking north).**

The testing process followed the procedure outlined in Section 6.7. The fatigue cracks detected during testing are listed in Table 7-4. In this table, cracks are listed in order of detection, along with descriptions of the crack type, location, and the type of repair used. Each crack is named to reflect the test girder and the order of crack detection. For example, G1-5 is the fifth crack detected on Girder 1. Additionally, the cycle counts corresponding to the first detection and failure (i.e., when a crack repair was performed) are provided. Figure 7-8 illustrates the locations of all the fatigue cracks and shows photos of the cracks that led to joint failures or early stoppages.

**Table 7-4. Cracks detected during fatigue testing of Girder 1 - Flange 2.**

| *Crack* | *Crack Type* | *Crack Location* | *Detection Date* | *Cycle Count @ Detection* | *Cycle Count @ Failure* | *Crack Repair* |
|---|---|---|---|---|---|---|
| G1-5 | Flange Edge | J1 | 9/9/2025 | 1,119,500 | 1,459,000 | Bolted Splice |
| G1-6 | Fillet Weld | 26 in. West of J4 | 9/30/2025 | 2,548,200 | - | - |

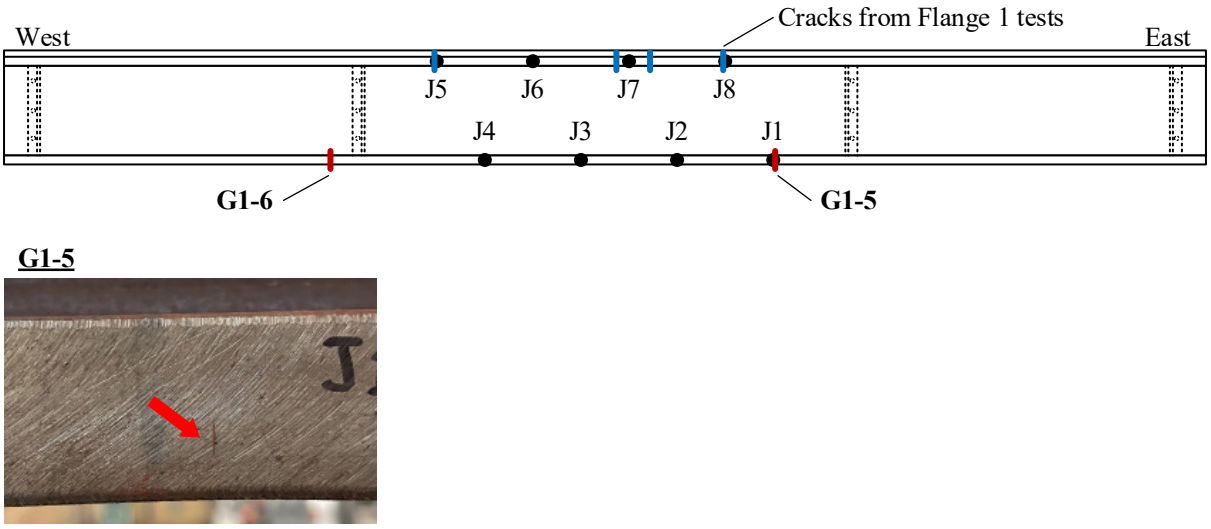


**Figure 7-8. Illustration. Overview showing the different fatigue cracks for Girder 1 – Flange 2.**

Crack G1-5 was a flange edge crack that initiated on the flange side wall, leading to the joint failure of J1 (R0) at 1.46 million cycles. Crack G1-5 was destructively examined after testing to confirm the point of crack initiation and failure classification of the joint. Crack G1-6 was a fillet weld crack that initiated from the root of the fillet weld, but it was not near a joint; therefore, no repairs were performed, and testing concluded before a repair was needed. No cracks were detected at J2 (R1), J3 (R3), or J4 (R5). The joints cycled to a runout life of 2.6 million cycles and were declared runouts.

After testing was completed for Girder 1, Crack G1-5 was isolated and cut open using a vertical band saw to expose the internal crack plane and crack initiation point. Figure 7-9 shows the crack initiation point and general crack growth behavior of Crack G1-5, confirming the crack initiated on the side of the flange edge. As such, Joint J1 (R0) is classified as a CJP weld failure. A summary of the fatigue-life test results for the four CJP joints tested is shown in Table 7-5, including the joint and fatigue life corresponding to joint failure, early stoppage, or runout life. Note that all CJP joints tested exceeded the minimum AASHTO design life.

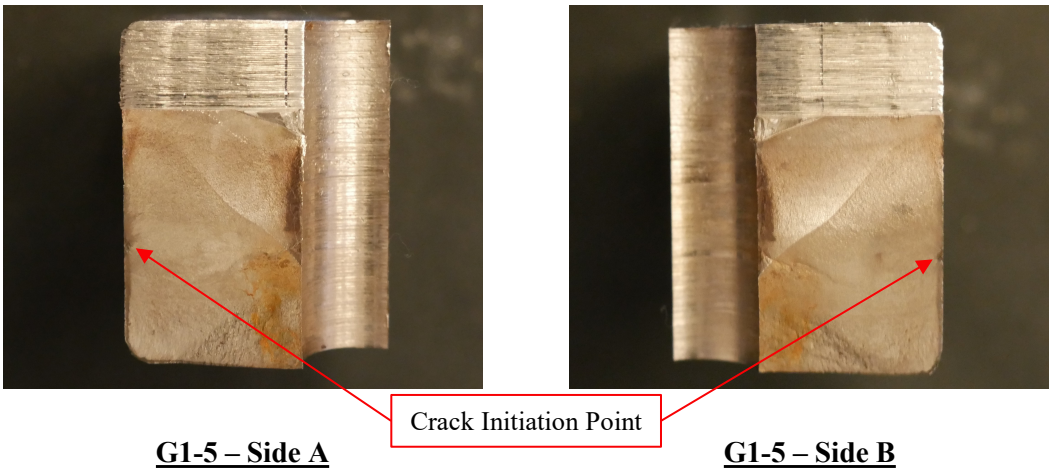


Crack initiation point on side of flange edge.

**Figure 7-9. Photo. Destructive evaluation of Crack G1-5, which led to the failure of G1-J1.**

**Table 7-5. Fatigue life test results for G1-J1, G1-J2, G1-J3, and G1-J4.**

| *Joint* | *Joint Results* | *Crack at Joint* | *Fatigue Life* |
|---|---|---|---|
| G1-J1 (R0) | CJP Weld Failure | Flange Edge | 1,459,000 |
| G1-J2 (R1) | Runout | - | 2,600,000 |
| G1-J3 (R3) | Runout | - | 2,600,000 |
| G1-J4 (R5) | Runout | - | 2,600,000 |

Additionally, data from each strain gage were analyzed, and an average stress for the strain gage was determined for each test day. The average stresses for the centerline gages and CJP joint gages for each day are shown in Figures 7-10 and 7-11, respectively. In these plots, the abscissa shows the dates the girder was tested, and the ordinate shows the measured stress ranges. Note that some gages were removed prematurely for crack repairs, which is why some strain gages do not have data for the entire test. In the figures, a sharp change in stress usually correlates to the first detection of a fatigue crack, where the stress range at that particular strain gage steadily increased or decreased as a crack grew nearby.

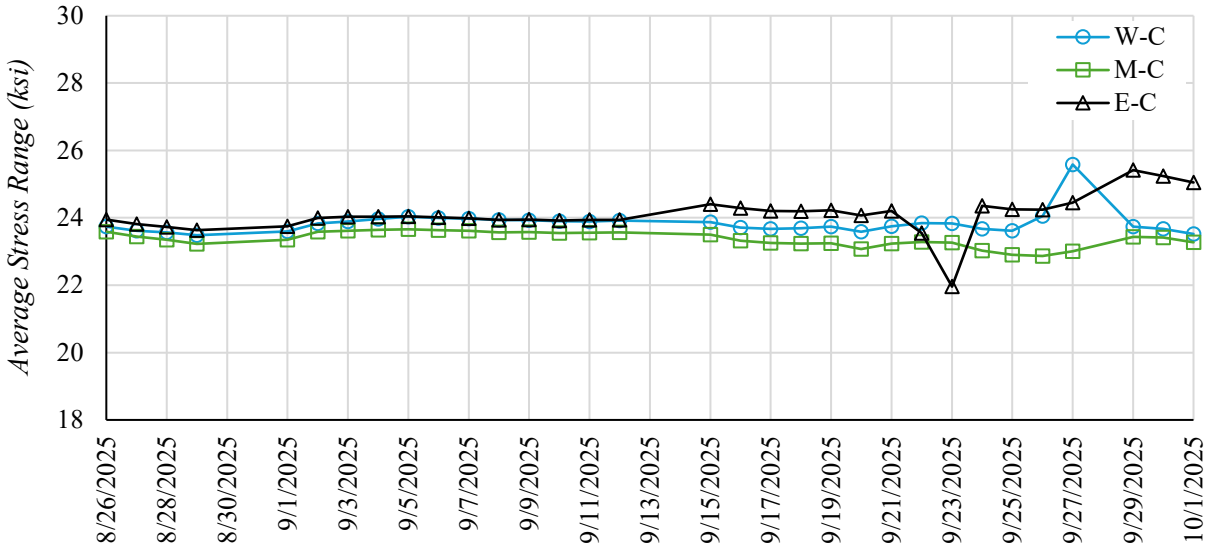


**Figure 7-10. Graph. Average daily stress range for Girder 1 – Flange 2 measured with strain gages along the bottom flange centerline.**

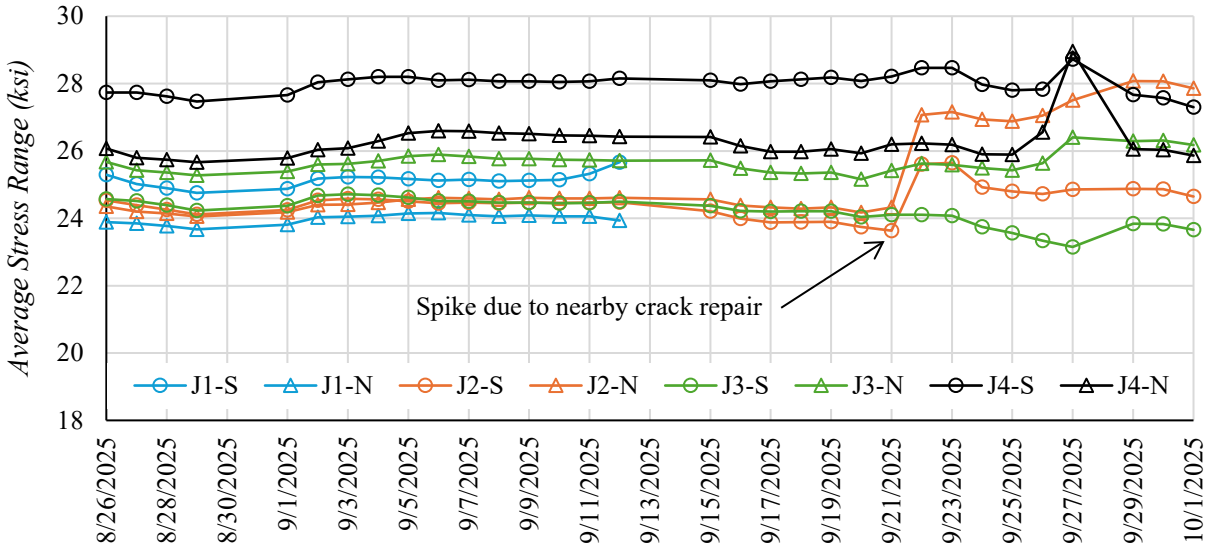


**Figure 7-11. Graph. Average daily stress range for Girder 1 – Flange 2 measured with strain gages at CJP butt-splice joints.**

Figure 7-10 demonstrates that the 24 ksi stress range was maintained along the centerline of the girder throughout testing. Figure 7-11 shows that the stress ranges along the flange edges were less consistent at each CJP butt-splice welded joint, with J4 being almost 4 ksi above the targeted 24 ksi. J1, J2, and J3 were much closer to the targeted 24 ksi, but there is still some variation. Discussions explaining why these stresses varied at the individual joints are provided

in Section 7.5. In all cases, the measured stresses remained consistent until a crack formed near the joint/strain gage.

## 7.2. Girder 2 (3/4 in. – 50W)

As discussed at the beginning of Chapter 7, a top flange cover plate was not used for the Girder 2 tests. Without the top cover plate, Girder 2 has a nominal flexural capacity of 3,500 kip-in. The flexural capacity of the girder was determined using an iterative inelastic nonlinear buckling analysis (INBA) procedure to help account for the irregular bracing and boundary conditions. The test details and results for flanges 1 and 2 are discussed in the following subsections.

### *7.2.1. Flange 1 (G2-J5, G2-J6, G2-J7, G2-J8)*

Girder 2 – Flange 1 was tested by cycling Girder 2 at a constant amplitude load range from approximately 3 kips to 45 kips at the load points, resulting in flexural stresses along Flange 1 ranging from 1.5 ksi to 25.5 ksi. The loads resulted in a maximum applied moment of 2,400 kip-in, approximately 70% of the allowable capacity. All loads and displacements were tracked throughout the test using the internal load cell and LVDT in the MTS actuator. The tests were conducted at 2.4 Hz, resulting in a daily cycle count of approximately 200,000. Strain gages were installed and monitored to verify that the 24 ksi stress range was maintained.

The strain gage layout used for Girder 2 – Flange 1 is shown in Figure 7-12. Three strain gages were placed at the center of the tension flange along the middle section to monitor the stress range during testing. Additionally, a strain gage was placed near the flange edges at each CJP joint to monitor joint stresses and support crack detection. Unlike the other tests, additional

strain gages were not placed near the fillet welds or the top flange, which was modified for all subsequent tests due to unexpected complications during the testing of Girder 2 – Flange 1.

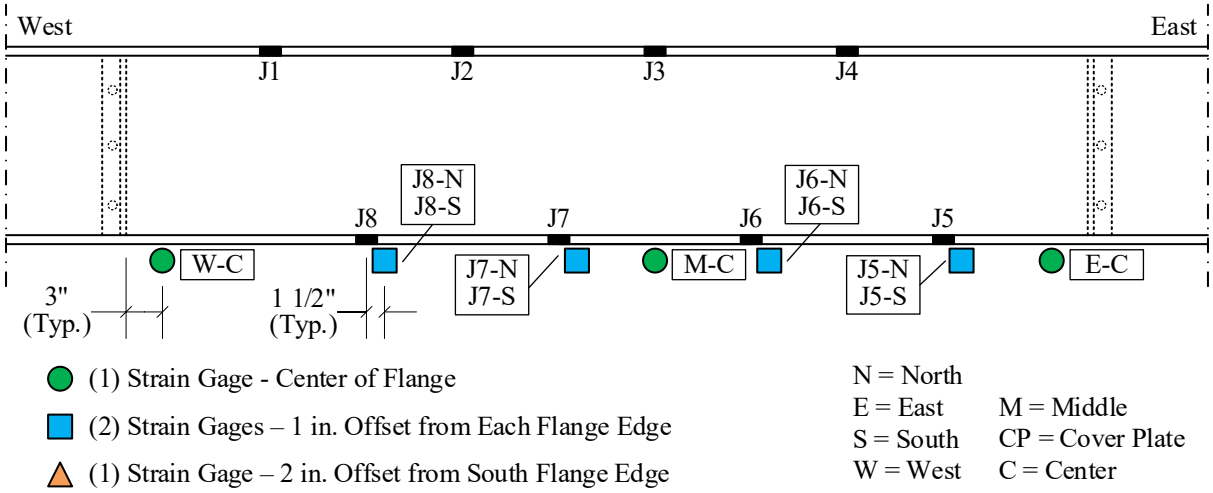


**Figure 7-12. Illustration. Instrumentation layout for Girder 2 - Flange 1 (looking north).**

The testing process followed the procedure outlined in Section 6.7. The fatigue cracks detected during testing are listed in Table 7-6. In this table, cracks are listed in order of detection, along with descriptions of the crack type, location, and the type of repair used. Each crack is named to reflect the test girder and the order of crack detection. For example, G2-1 is the first crack detected on Girder 2. Additionally, the cycle counts corresponding to the first detection and failure (i.e., when a crack repair was performed) are provided. Figure 7-13 illustrates the locations of all the fatigue cracks and shows photos of the cracks that led to joint failures or early stoppages.

**Table 7-6. Cracks detected during fatigue testing of Girder 2 - Flange 1.**

| *Crack* | *Crack Type* | *Crack Location* | *Detection Date* | *Cycle Count @ Detection* | *Cycle Count @ Failure* | *Crack Repair* |
|---|---|---|---|---|---|---|
| G2-1 | Fillet Weld | J5 | 2/24/2025 | 1,116,600 | 1,116,600 | Bolted Splice |
| G2-2 | Fillet Weld | 3 in. West of J5 | 2/24/2025 | 1,116,600 | 1,116,600 | Bolted Splice |
| G2-3 | Fillet Weld | 2 in. West of J7 | 2/24/2025 | 1,116,600 | 1,175,200 | Bolted Splice |
| G2-4 | Flange Edge | 3 in. East of J7 | 3/6/2025 | 1,175,200 | 1,175,200 | Bolted Splice |
| G2-5 | Fillet Weld | 2 in. East of J8 | 3/16/2025 | 1,680,000 | 1,796,100 | Bolted Splice |
| G2-6 | Fillet Weld | 24 in. East of J4 | 3/27/2025 | 2,600,000 | - | - |
| G2-7 | Fillet Weld | 6 in. West of J4 | 3/27/2025 | 2,600,000 | - | - |
| G2-8 | Fillet Weld | 6 in. West of J3 | 3/27/2025 | 2,600,000 | - | - |
| G2-9 | Fillet Weld | 4 in. East of J2 | 3/27/2025 | 2,600,000 | - | - |

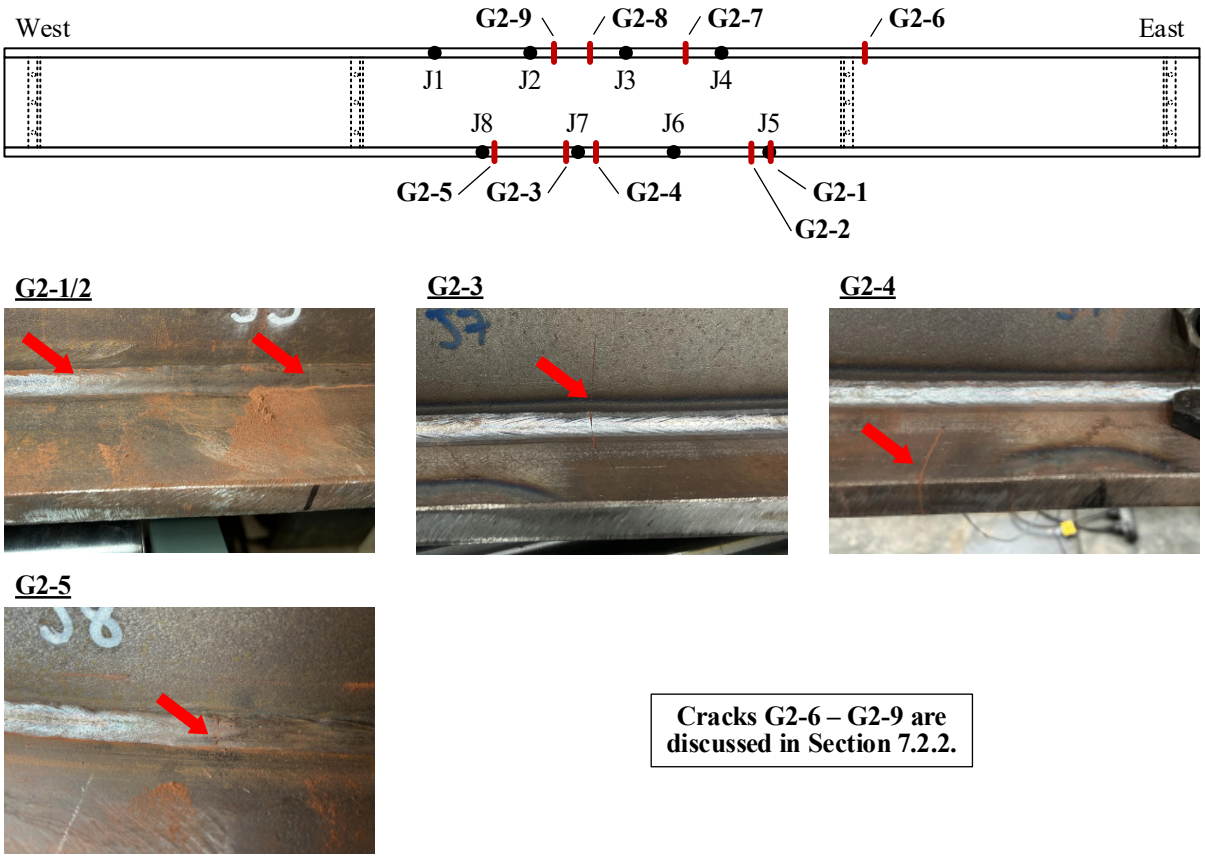


**Figure 7-13. Illustration. Overview showing the different fatigue cracks for Girder 2 – Flange 1.**

Cracks G2-1 and G2-2 were fillet weld cracks that initiated from the root of the fillet weld. Crack G2-1 led to the joint failure of J5 (R0) at 1.12 million cycles, and it was destructively examined after testing to confirm the point of crack initiation and failure classification of the joint. Crack G2-3 was a fillet weld crack that initiated from the root of the

fillet weld, and crack G2-4 was a base metal flange edge crack. These cracks were more than 1-1/2 inches from J7 (R3), but they propagated and required repairs, resulting in the early stoppage of J7 (R3) at 1.18 million cycles. Crack G2-5 was a fillet weld crack that initiated from the root of the fillet weld and led to the joint failure of J8 (R5) at 1.80 million cycles. Cracks G2-6 through G2-9 are discussed in Section 7.2.2. No cracks were detected at J6 (R1). The joint was a runout, cycling to the 2.6 million cycle limit.

After testing was completed for Girder 2, Crack G2-1 was isolated and cut open using a vertical band saw to expose the internal crack plane and crack initiation point. Figure 7-14 shows the crack initiation point and general crack growth behavior of Crack G2-1, confirming that the crack initiated from the root of the fillet weld at the flange-web juncture. As such, Joint J5 (R0) is classified as an early stoppage since the joint failed due to a fillet weld rather than the CJP weld. A summary of the fatigue-life test results for the four CJP joints tested is shown in Table 7-7, including the joint and fatigue life corresponding to joint failure, early stoppage, or runout life. Note that all CJP joints tested exceeded the minimum AASHTO design life.

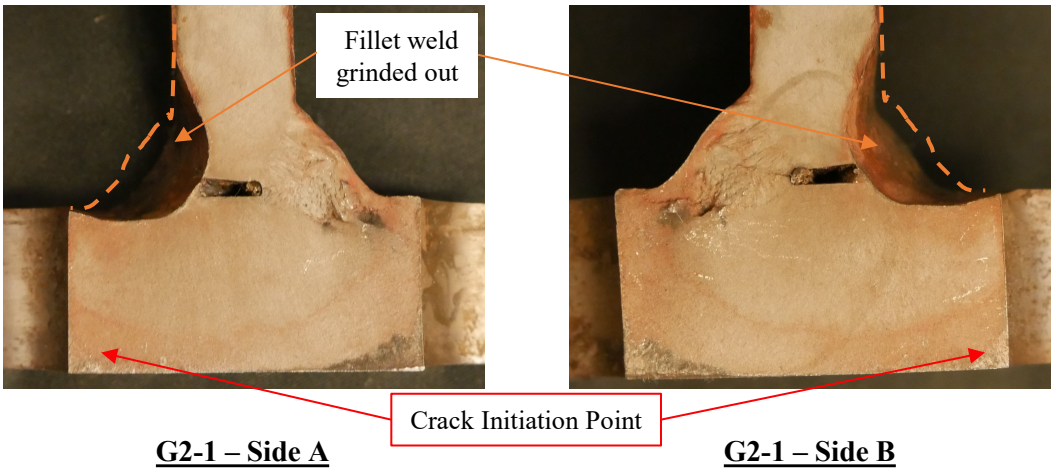


Crack initiation point at root of fillet weld at flange-web juncture.
Note: Area partially excavated from mechanical grinding repair attempt.

**Figure 7-14. Photo. Destructive evaluation of Crack G2-1, which led to the failure of G2-J5.**

**Table 7-7. Fatigue life test results for G2-J5, G2-J6, G2-J7, and G2-J8.**

| *Joint* | *Joint Results* | *Crack at Joint* | *Fatigue Life* |
|---|---|---|---|
| G2-J5 (R0) | Early Stoppage | Root Fillet Weld | 1,116,600 |
| G2-J6 (R1) | Runout | - | 2,600,000 |
| G2-J7 (R3) | Early Stoppage | - | 1,175,200 |
| G2-J8 (R5) | Early Stoppage | - | 1,796,100 |

Additionally, data from each strain gage were analyzed, and an average stress for the strain gage was determined for each test day. The average stresses for the centerline gages and CJP joint gages for each day are shown in Figures 7-15 and 7-16, respectively. In these plots, the abscissa shows the dates the girder was tested, and the ordinate shows the measured stress ranges. Note that some gages were removed prematurely for crack repairs, which is why some strain gages do not have data for the entire test. In the figures, a sharp change in stress usually correlates to the first detection of a fatigue crack, where the stress range at that particular strain gage steadily increased or decreased as a crack grew nearby.

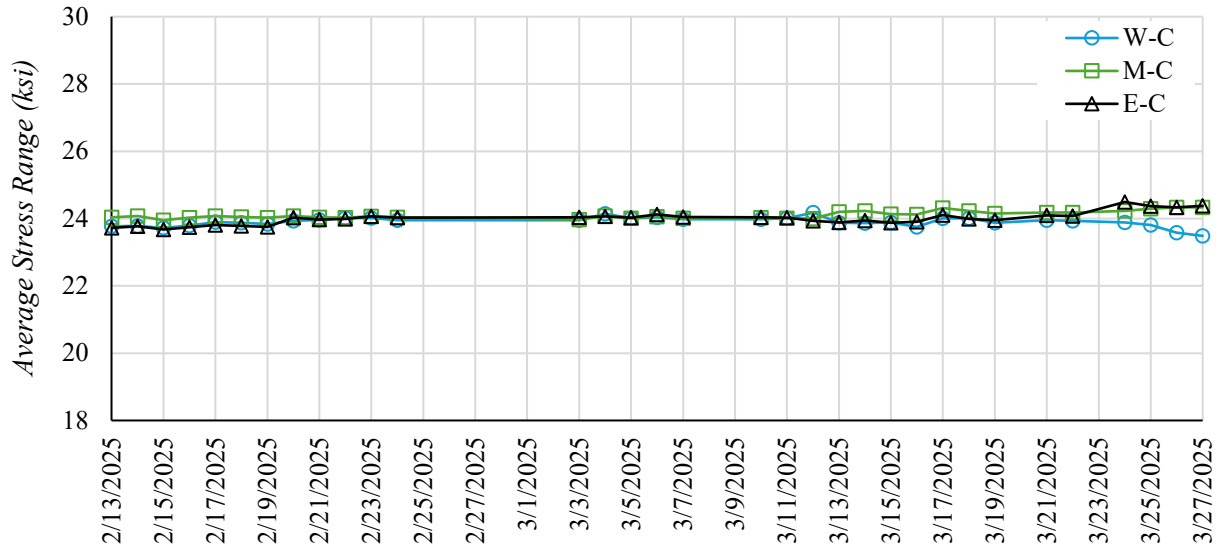


**Figure 7-15. Graph. Average daily stress range for Girder 2 – Flange 1 measured with strain gages along the bottom flange centerline.**

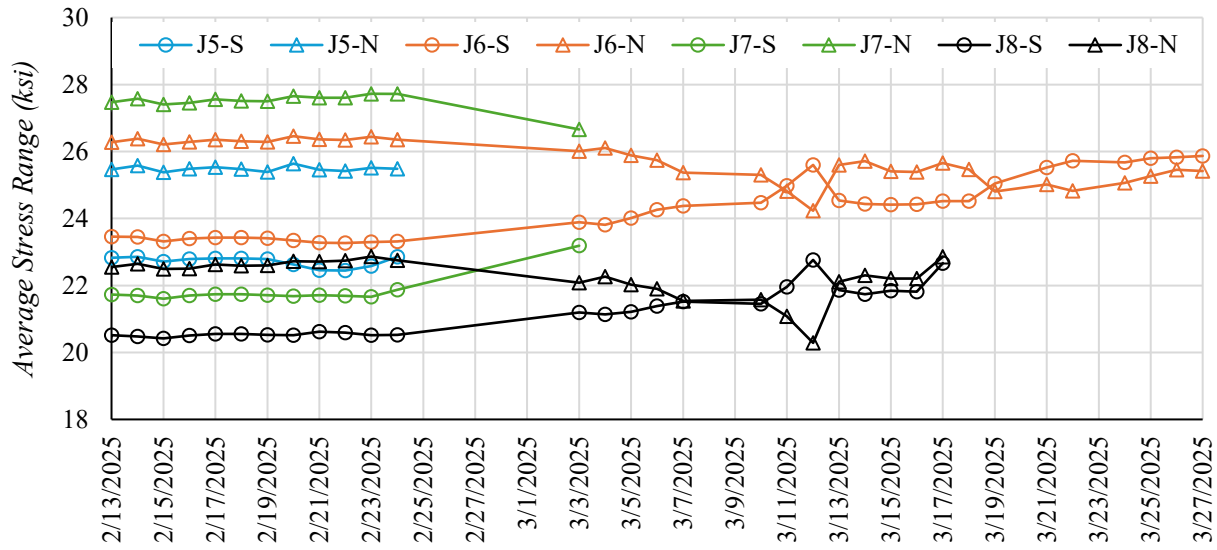


**Figure 7-16. Graph. Average daily stress range for Girder 2 – Flange 1 measured with strain gages at CJP butt-splice joints.**

Figure 7-15 demonstrates that the 24 ksi stress range was maintained along the centerline of the girder throughout testing. Figure 7-16 shows that the stress ranges along the flange edges were less consistent at each CJP butt-splice welded joint, with the measured stress ranges typically being within 4 ksi of the targeted 24 ksi. Discussions explaining why these stresses varied at the individual joints are provided in Section 7.5. In all cases, the measured stresses remained consistent until a crack formed near the joint/strain gage.

### *7.2.2. Flange 2 (G2-J1, G2-J2, G2-J3, G2-J4)*

As discussed in detail at the beginning of Chapter 7 and shown in Section 7.2.1, four compression flange cracks were found in Girder 2 – Flange 2 at the end of the Girder 2 – Flange 1 test. The cracks initiated from the root of the fillet weld and propagated during the testing of Flange 1; however, they were not detected until propagating approximately 1-1/2 in. into the web and 1-1/2 in. each direction along the flange width, resulting in a total crack length of 3 in. in the center of the flange. The exact crack locations are listed in Table 7-6 and shown in

Figure 7-13 (see Section 7.2.1). Additionally, representative photos of cracks G2-8 and G2-9 are provided in Figure 7-17. As none of the cracks were directly on top of a CJP joint, bolted splice repairs were performed on cracks G2-7 – G2-10 in an effort to test the four CJP joints on Flange 2. However, even after repairs, further cycling of Flange 2 was not feasible due to the fatigue damage accumulated in the fillet welds. As such, G2-J1 (R0), G2-J2 (R1), G2-J3 (R3), and G2-J4 (R5) could not be tested, and these data were not used to draw any conclusions. When applicable, the Girder 1 – Flange 2 CJP joints are marked as "unable to test" to indicate that they were not tested due to the unintended fatigue damage.

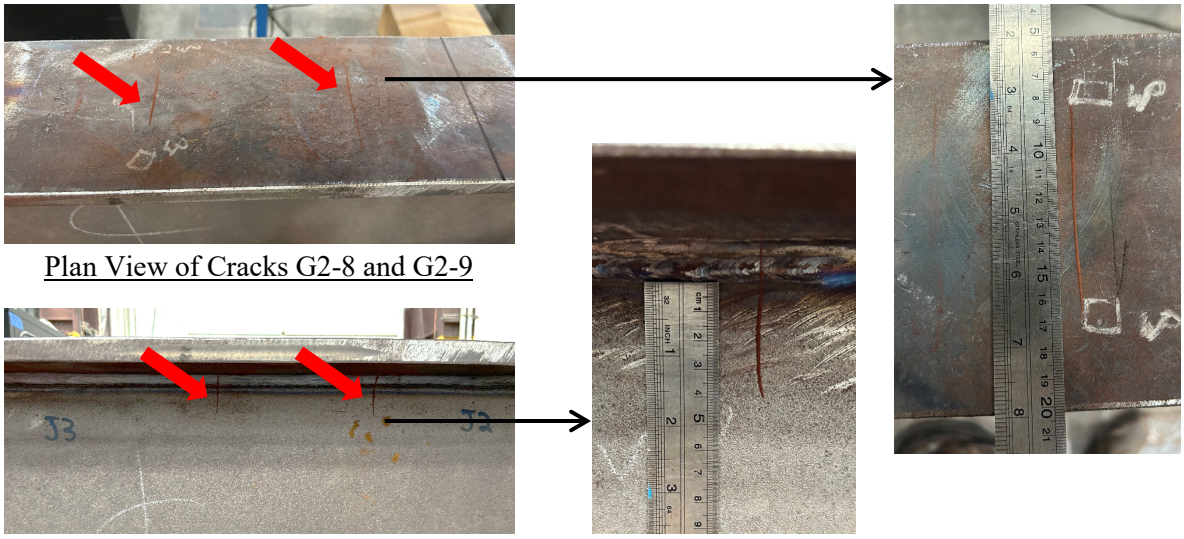


**Figure 7-17. Multiple Photos. Photos showing cracks G2-8 and G2-9 developed in Girder 2 - Flange 2 during testing of Flange 1.**

### 7.3. Girder 3 (1-1/2 in. – HPS70W)

Including the top flange cover plate, Girder 3 has a nominal flexural capacity of 12,100 kip-in. The flexural capacity of the girder was determined using an iterative inelastic nonlinear buckling analysis (INBA) procedure to help account for the irregular bracing and boundary conditions. Girder 3 – Flanges 1 and 2 were tested by cycling Girder 3 at a constant amplitude

load range from approximately 5 kips to 85 kips at the load points, resulting in flexural stresses along the flanges ranging from 1.5 ksi to 25.5 ksi. The loads resulted in a maximum applied moment of approximately 4,600 kip in, less than half the allowable capacity. All loads and displacements were tracked throughout the test using the internal load cell and LVDT in the MTS actuator. The tests were conducted at 1.2 Hz, resulting in a daily cycle count of approximately 100,000. Strain gages were used to ensure the 24 ksi stress range was maintained. Additional test details and results for Flanges 1 and 2 are discussed in the following subsections.

### *7.3.1. Flange 1 (G3-J5, G3-J6, G3-J7, G3-J8)*

The strain gage layout used for Girder 3 – Flange 1 is shown in Figure 7-18. Three strain gages were placed at the center of the tension flange along the middle section to monitor the stress range during testing. Additionally, a strain gage was placed near the flange edges at each CJP joint to monitor joint stresses and support crack detection. Additional strain gages were placed on the flanges near the top and bottom fillet welds and on the cover plate to monitor stress ranges throughout the cross section.

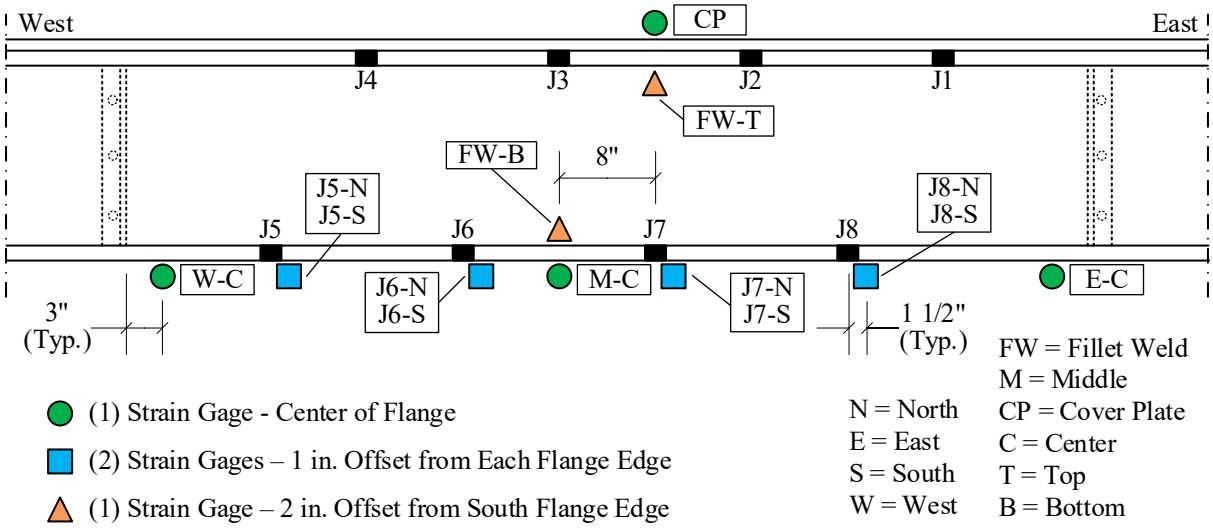


**Figure 7-18. Illustration. Instrumentation layout for Girder 3 - Flange 1 (looking north).**

The testing process followed the procedure outlined in Section 6.7. The fatigue cracks detected during testing are listed in Table 7-8. In this table, cracks are listed in order of detection, along with descriptions of the crack type, location, and the type of repair used. Each crack is named to reflect the test girder and the order of crack detection. For example, G3-1 is the first crack detected on Girder 3. Additionally, the cycle counts corresponding to the first detection and failure (i.e., when a crack repair was performed) are provided. Figure 7-19 illustrates the locations of all the fatigue cracks and shows photos of the cracks that led to joint failures or early stoppages.

**Table 7-8. Cracks detected during fatigue testing of Girder 3 - Flange 1.**

| *Crack* | *Crack Type* | *Crack Location* | *Detection Date* | *Cycle Count @ Detection* | *Cycle Count @ Failure* | *Crack Repair* |
|---|---|---|---|---|---|---|
| G3-1 | Fillet Weld | 23 in. East of J8 | 8/11/2025 | 1,898,200 | 1,898,200 | Mechanical Grinding |
| G3-2 | Fillet Weld | 32 in. East of J8 | 8/12/2025 | 1,936,900 | 1,936,900 | Mechanical Grinding |
| G3-3* | Flange Edge | J8 | 8/14/2025 | 2,041,800 | - | - |
| G3-4 | Fillet Weld | 6 in. East of J7 | 8/14/2025 | 2,080,600 | 2,080,600 | Mechanical Grinding |
| G3-5 | Fillet Weld | J7 | 8/16/2025 | 2,194,200 | 2,339,700 | Bolted Splice |
| G3-6 | Fillet Weld | 36 in. East of J8 | 8/20/2025 | 2,461,700 | 2,461,700 | Mechanical Grinding |

* Crack never propagated beyond detection size.

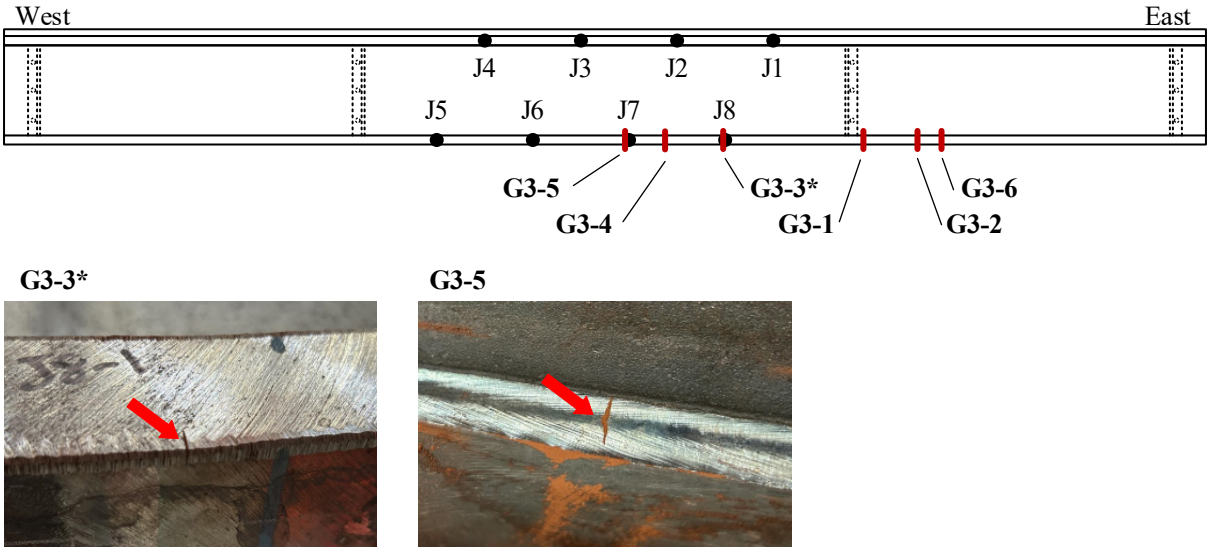


**Figure 7-19. Illustration. Overview showing the different fatigue cracks for Girder 3 – Flange 1.**

Cracks G3-1, G3-2, G3-4, and G3-6 were fillet weld cracks that initiated from the root of the fillet weld. These cracks were not near any joints; hence, repairs were performed without influencing the CJP butt-splice welded joints. Crack G3-3 was a flange edge crack that initiated at the bottom flange tip. After the first detection, the joint ran to a runout life of 2.6 million cycles without any additional crack growth; as such, J8 (R5) was declared a runout. Crack G3-5 was a fillet weld crack that initiated from the root of the fillet weld, leading to the joint failure of J7 (R3) at 2.34 million cycles. Crack G3-5 was destructively examined after testing to confirm the point of crack initiation and failure classification of the joint. No cracks were detected at J5 (R0) and J6 (R1). The joints cycled to the runout life of 2.6 million cycles and were declared runouts.

After testing was completed for Girder 3, Crack G3-5 was isolated and cut open using a vertical band saw to expose the internal crack plane and crack initiation point. Figure 7-20 shows the crack initiation point and general crack growth behavior of Crack G3-5, confirming that the crack initiated at the root of the fillet weld at the flange-web juncture. As such, Joint J7 (R3) is

classified as an early stoppage since the joint failed due to a fillet weld rather than the CJP weld. A summary of the fatigue-life test results for the four CJP joints tested is shown in Table 7-9, including the joint and fatigue life corresponding to joint failure, early stoppage, or runout life. Note that all CJP joints tested exceeded the minimum AASHTO design life.

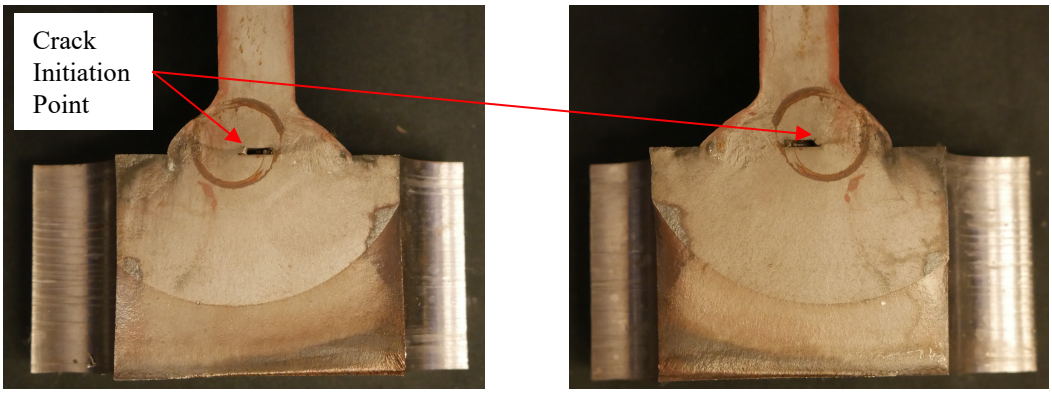


**G3-5 – Side A** **G3-5 – Side B**

Crack initiation point at root of fillet weld at flange-web juncture.

**Figure 7-20. Photo. Destructive evaluation of Crack G3-5, which led to the failure of G3-J7.**

**Table 7-9. Fatigue life test results for G3-J5, G3-J6, G3-J7, and G3-J8.**

| *Joint* | *Joint Results* | *Crack at Joint* | *Fatigue Life* |
|---|---|---|---|
| G3-J5 (R0) | Runout | - | 2,600,000 |
| G3-J6 (R1) | Runout | - | 2,600,000 |
| G3-J7 (R3) | Early Stoppage | Root Fillet Weld | 2,339,800 |
| G3-J8 (R5) | Runout* | - | 2,600,000 |

* Small flange edge crack was found, but it never propagated.

Additionally, data from each strain gage were analyzed, and an average stress for the strain gage was determined for each test day. The average stresses for the centerline gages and CJP joint gages for each day are shown in Figures 7-21 and 7-22, respectively. In these plots, the abscissa shows the dates the girder was tested, and the ordinate shows the measured stress ranges. Note that some gages were removed prematurely for crack repairs, which is why some strain gages do not have data for the entire test. In the figures, a sharp change in stress usually

correlates to the first detection of a fatigue crack, where the stress range at that particular strain gage steadily increased or decreased as a crack grew nearby.

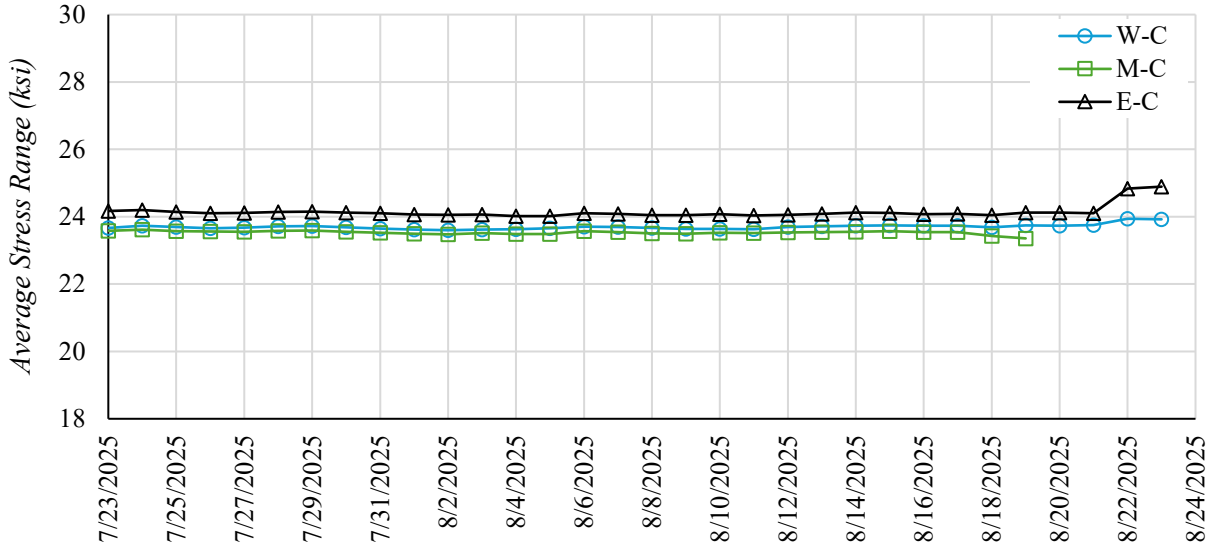


**Figure 7-21. Graph. Average daily stress range for Girder 3 – Flange 1 measured with strain gages along the bottom flange centerline.**

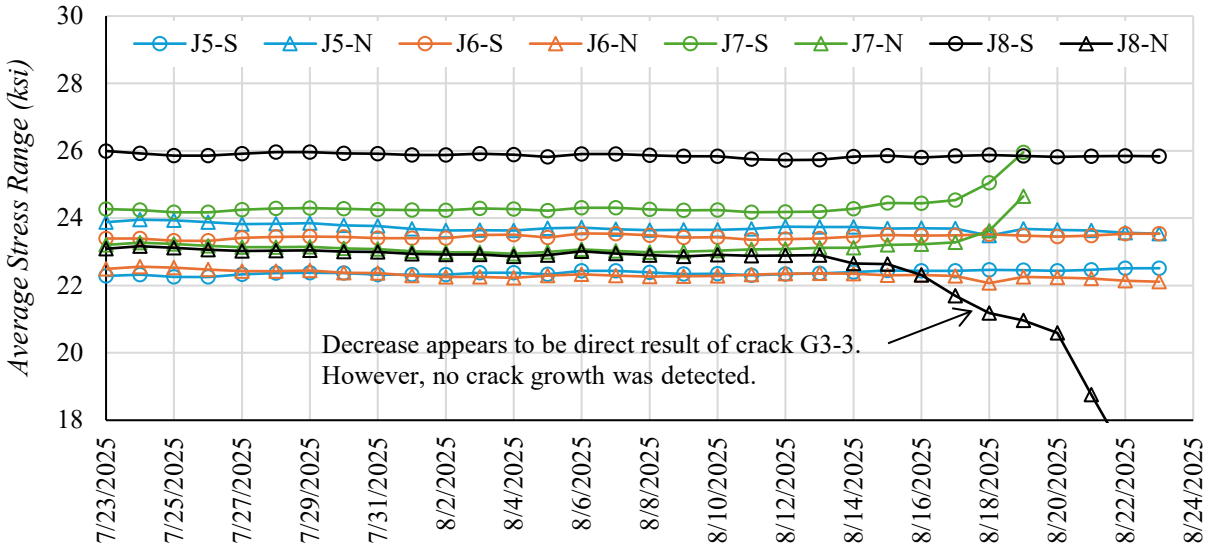


**Figure 7-22. Graph. Average daily stress range for Girder 3 – Flange 1 measured with strain gages at CJP butt-splice joints.**

Figure 7-21 demonstrates that the 24 ksi stress range was maintained along the centerline of the girder throughout testing. Figure 7-22 shows that the stress ranges along the flange edges

were less consistent at each CJP butt-splice welded joint, with the measured stress ranges typically within 2 ksi of the targeted 24 ksi. Discussions explaining why these stresses varied at the individual joints are provided in Section 7.5. Notably, J8-N shows a large decrease in the stress range towards the end of the test, coinciding with the detection of crack G3-3. As J8-S does not reciprocate this decrease, it is likely due to a combined influence from crack G3-3 and the nearby fillet weld cracks G3-1, G3-2, and G3-6, which did have fatigue cracks reinitiate in the ground regions towards the end of testing. In all cases, the measured stresses remained consistent until a crack formed near the joint/strain gage.

### *7.3.2. Flange 2 (G3-J1, G3-J2, G3-J3, G3-J4)*

The strain gage layout used for Girder 3 – Flange 2 is shown in Figure 7-23. Three strain gages were placed at the center of the tension flange along the middle section to monitor the stress range during testing. Additionally, a strain gage was placed near the flange edges at each CJP joint to monitor joint stresses and support crack detection. Additional strain gages were placed on the flange near the bottom fillet weld and on the cover plate to monitor stress ranges throughout the cross section. Note that strain gage E-C was moved ~13 in. east (i.e., 10 in. past the east interior stiffener) during testing due to nearby repairs. At the new location, the target stress range for strain gage E-C became: $\Delta\sigma = 24 \text{ ksi} * (1 - (10 \text{ in.} / 54 \text{ in.}) ) = 19.6 \text{ ksi}$.

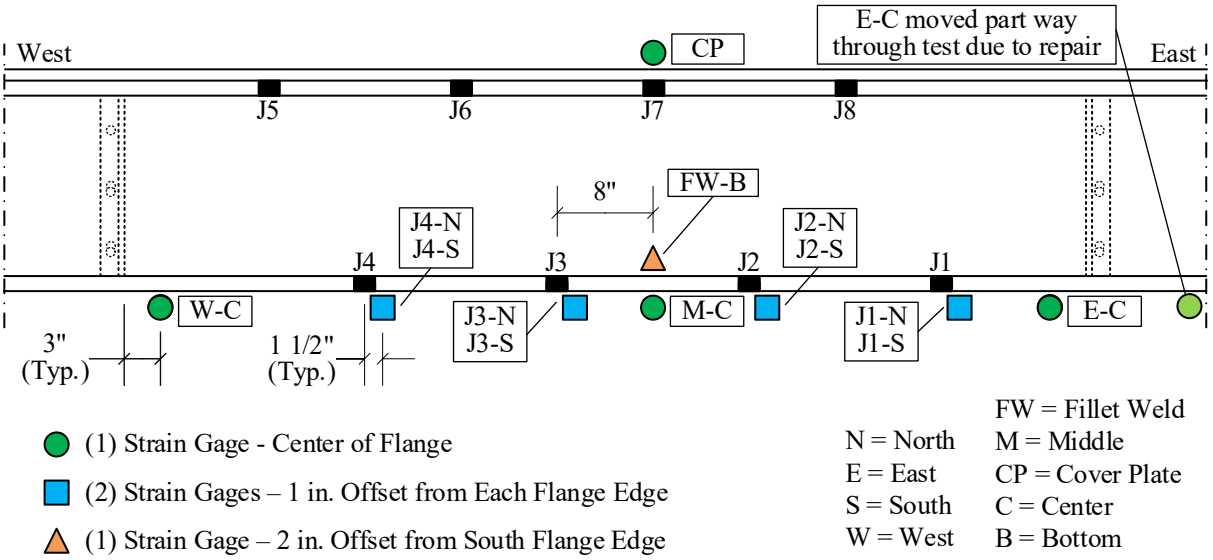


**Figure 7-23. Illustration. Instrumentation layout for Girder 3 - Flange 2 (looking north).**

The testing process followed the procedure outlined in Section 6.7. The fatigue cracks detected during testing are listed in Table 7-10. In this table, cracks are listed in order of detection, along with descriptions of the crack type, location, and the type of repair used. Each crack is named to reflect the test girder and the order of crack detection. For example, G3-7 is the seventh crack detected on Girder 3. Additionally, the cycle counts corresponding to the first detection and failure (i.e., when a crack repair was performed) are provided. Figure 7-24 illustrates the locations of all the fatigue cracks and shows photos of the cracks that led to joint failures or early stoppages.

**Table 7-10. Cracks detected during fatigue testing of Girder 3 - Flange 2.**

| *Crack* | *Crack Type* | *Crack Location* | *Detection Date* | *Cycle Count @ Detection* | *Cycle Count @ Failure* | *Crack Repair* |
|---|---|---|---|---|---|---|
| G3-7 | Flange Edge | 10 in. East of J1 | 10/5/2025 | 237,100 | 237,100 | Bolted Splice |
| G3-8 | Fillet Weld | J2 | 10/18/2025 | 1,103,200 | 1,195,100 | Bolted Splice |
| G3-9 | Flange Edge | J2 | 10/18/2025 | 1,134,800 | - | Bolted Splice |
| G3-10 | Fillet Weld | 15 in. West of J4 | 11/4/2025 | 1,865,100 | 1,865,100 | Bolted Splice |
| G3-11 | Fillet Weld | 23 in. West of J4 | 11/4/2025 | 1,896,300 | 1,896,300 | Bolted Splice |
| G3-12 | Fillet Weld | J4 | 11/9/2025 | 2,292,200 | 2,316,300 | Bolted Splice |

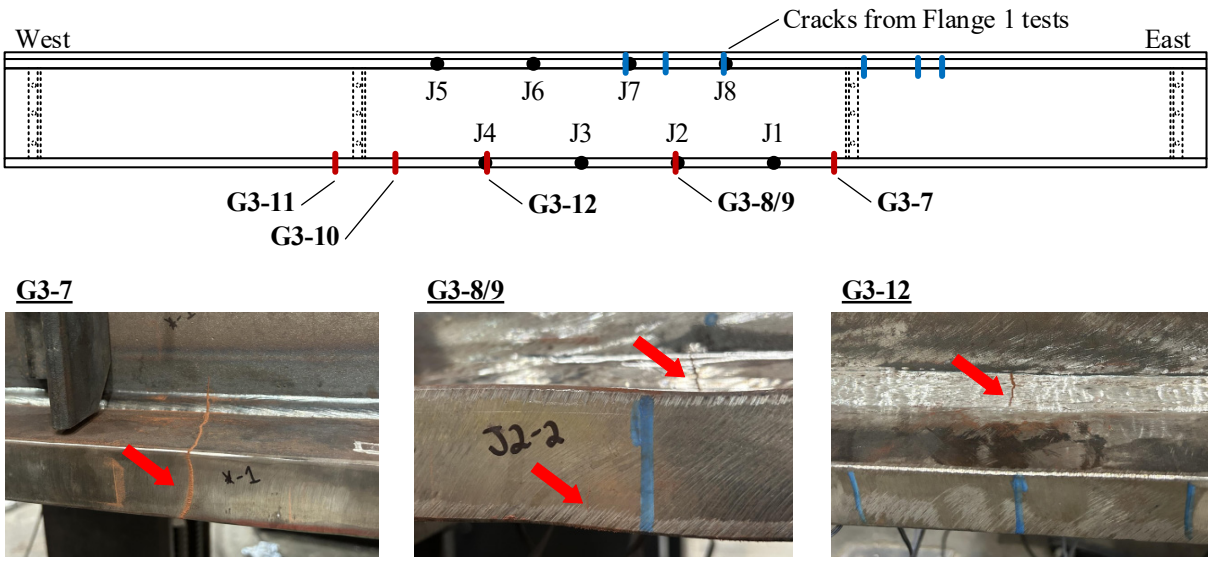


**Figure 7-24. Illustration. Overview showing the different fatigue cracks for Girder 3 – Flange 2.**

Crack G3-7 was a flange edge crack in the base metal that appeared unexpectedly early. After multiple bolted splice repair attempts, the repairs required to continue testing began interfering with J1 (R0); hence, it was declared an early stoppage at 429,000 cycles. Crack G3-8 was a fillet weld crack that initiated from the root of the fillet weld, and it led to the joint failure of J2 (R1) at 1.20 million cycles. Interestingly, crack G3-9, a flange edge crack, was also detected at J2 (R1) shortly after crack G3-8. While crack G3-9 did start propagating, it did not propagate to failure before crack G3-8. As such, the joint failure of J2 (R1) was controlled by crack G3-8. Crack G3-8 was destructively examined after testing to confirm the point of crack initiation and failure classification of the joint. Crack G3-10 was a fillet weld crack that initiated from the toe of the fillet weld. Crack G3-11 was a fillet weld crack that initiated from the root of the fillet weld. Neither crack was near a joint, so repairs were performed without affecting the CJP butt-splice welded joints. Crack G3-12 was a fillet weld crack that initiated at the root of the fillet weld and led to joint failure of J4 (R5) at 2.30 million cycles, and it was destructively examined after testing to confirm the point of crack initiation and failure classification of the

joint. No cracks were detected at J3 (R3), and the joint cycled to a runout life of 2.6 million cycles, at which point it was declared a runout.

After testing was completed for Girder 3, Cracks G3-8 and G3-12 were isolated and cut open using a vertical band saw to expose the internal crack planes and crack initiation points. Figures 7-25 and 7-26 show the crack initiation point and general crack growth behavior of Cracks G3-8 and G3-12, respectively. These figures confirm that Cracks G3-8 and G3-12 started at the root of the fillet weld at the flange-web junctures. As such, joints J2 (R1) and J4 (R5) are classified as early stoppages since the joints failed due to fillet welds rather than the CJP welds. A summary of the fatigue-life test results for the four CJP joints tested is shown in Table 7-11, including the joint and fatigue life corresponding to joint failure, early stoppage, or runout life. Note that all CJP joints tested except J1 (R0) exceeded the minimum AASHTO design life. However, J1 (R0) was an early stoppage due to nearby base metal cracks; hence, the premature "failure" is not indicative of the welded joint performance.

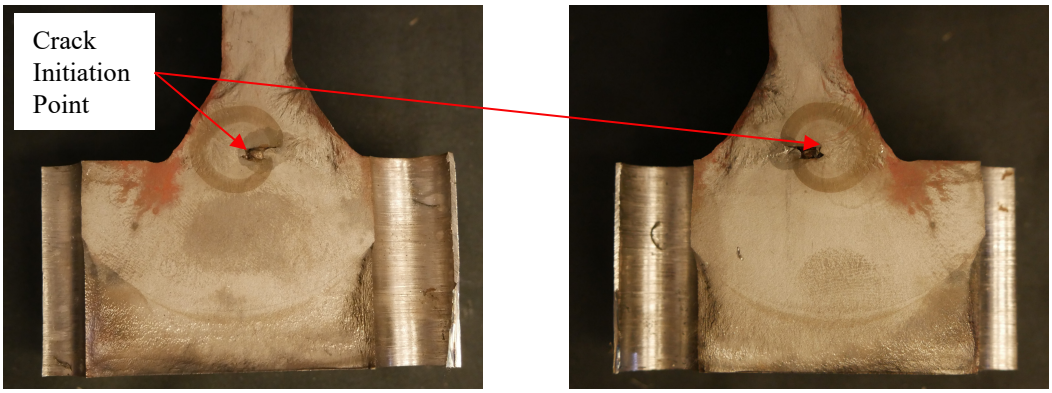


**G3-8 – Side A** **G3-8 – Side B**

Crack initiation point at root of fillet weld at flange-web juncture.

**Figure 7-25. Photo. Destructive evaluation of Crack G3-8, which led to the failure of G3-J2.**

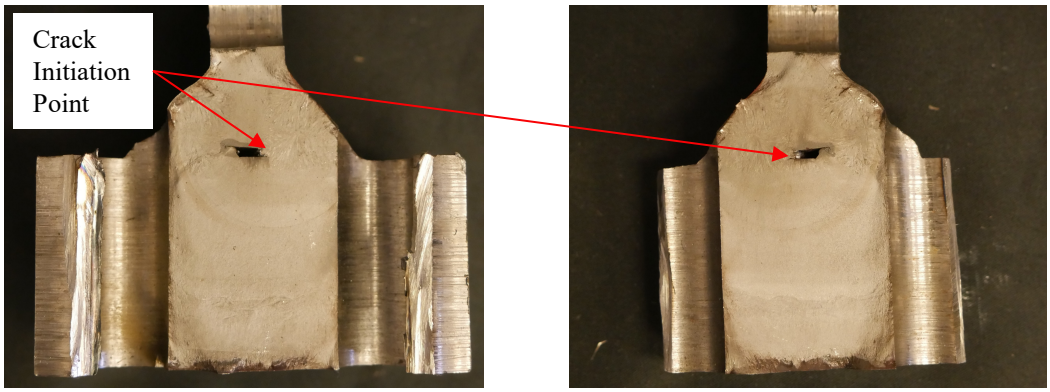


**G3-12 – Side A** **G3-12 – Side B**

Crack initiation point at root of fillet weld at flange-web juncture.

**Figure 7-26. Photo. Destructive evaluation of Crack G3-12, which led to the failure of G3-J4.**

**Table 7-11. Fatigue life test results for G3-J1, G3-J2, G3-J3, and G3-J4.**

| *Joint* | *Joint Results* | *Crack at Joint* | *Fatigue Life* |
|---|---|---|---|
| G3-J1 (R0) | Early Stoppage | - | 429,000 |
| G3-J2 (R1) | Early Stoppage | Root Fillet Weld | 1,195,100 |
| G3-J3 (R3) | Runout | - | 2,600,000 |
| G3-J4 (R5) | Early Stoppage | Root Fillet Weld | 2,302,200 |

Additionally, data from each strain gage were analyzed, and an average stress for the strain gage was determined for each test day. The average stresses for the centerline gages and CJP joint gages for each day are shown in Figures 7-27 and 7-28, respectively. In these plots, the abscissa shows the dates the girder was tested, and the ordinate shows the measured stress ranges. Note that some gages were removed prematurely for crack repairs, which is why some strain gages do not have data for the entire test. In the figures, a sharp change in stress usually correlates to the first detection of a fatigue crack, where the stress range at that particular strain gage steadily increased or decreased as a crack grew nearby.

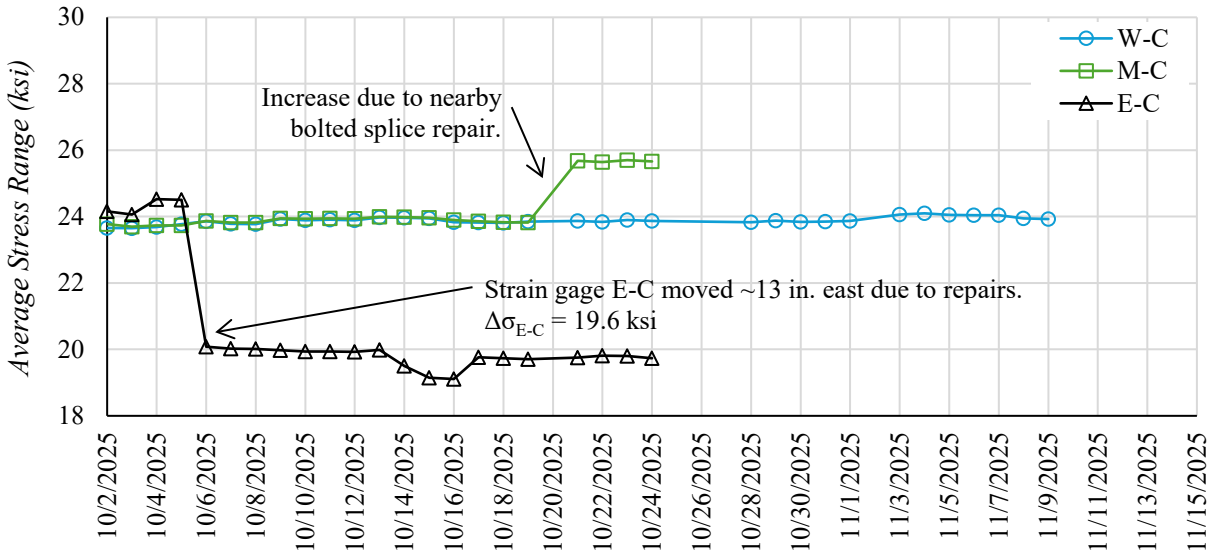


**Figure 7-27. Graph. Average daily stress range for Girder 3 – Flange 2 measured with strain gages along the bottom flange centerline.**

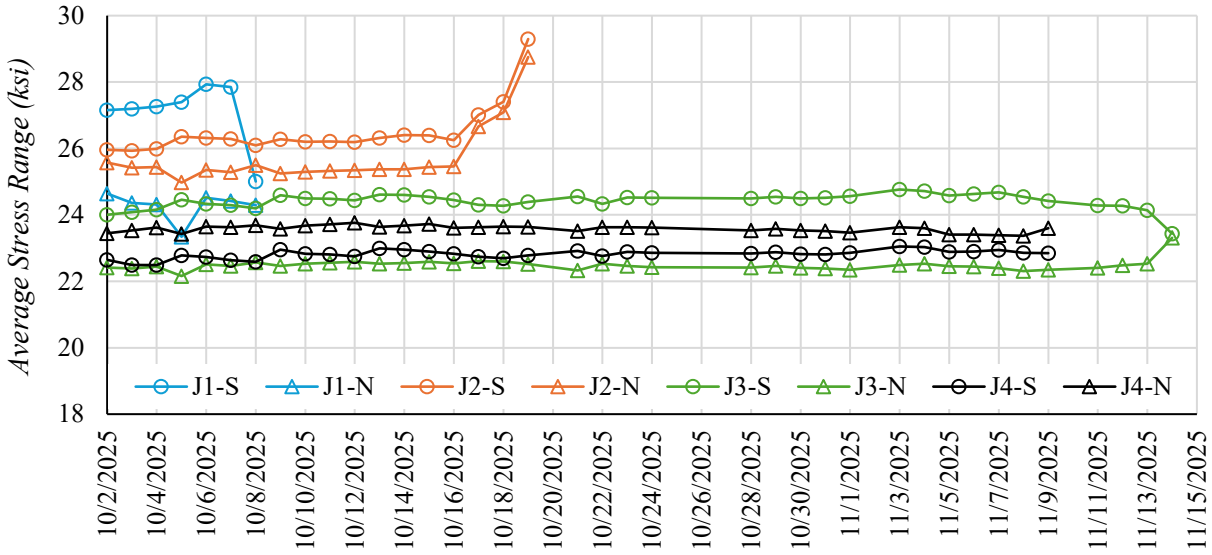


**Figure 7-28. Graph. Average daily stress range for Girder 3 – Flange 2 measured with strain gages at CJP butt-splice joints.**

Figure 7-27 demonstrates that the 24 ksi stress range was maintained along the centerline of the girder throughout testing, except as noted in the figure. Additionally, none of the centerline strain gages on the tension flange survived the entire test, which is why the data for all three gages stops before the test concluded on 11/14/2025. Figure 7-28 shows that the stress ranges along the flange edges were less consistent at each CJP butt-splice welded joint, with the

measured stress ranges typically being within 2 ksi of the targeted 24 ksi. Discussions explaining why these stresses varied at the individual joints are provided in Section 7.5. In all cases, the measured stresses remained consistent until a crack formed near the joint/strain gage.

## 7.4. Girder 4 (3/4 in. – HPS70W)

Including the top flange cover plate, Girder 4 has a nominal flexural capacity of 6,700 kip-in. The flexural capacity of the girder was determined using an iterative inelastic nonlinear buckling analysis (INBA) procedure to help account for the irregular bracing and boundary conditions. Girder 4 – Flanges 1 and 2 were tested by cycling Girder 4 at a constant amplitude load range from approximately 3 kips to 48 kips at the load points, resulting in flexural stresses along the flanges ranging from 1.5 ksi to 25.5 ksi. The loads resulted in a maximum applied moment of approximately 2,600 kip in, less than half the allowable capacity. All loads and displacements were tracked throughout the test using the internal load cell and LVDT in the MTS actuator. The tests were conducted at 2.4 Hz, resulting in a daily cycle count of approximately 200,000. Strain gages were used to ensure the 24 ksi stress range was maintained. Additional test details and results for Flanges 1 and 2 are discussed in the following subsections.

### *7.4.1. Flange 1 (G4-J5, G4-J6, G4-J7, G4-J8)*

The strain gage layout used for Girder 4 – Flange 1 is shown in Figure 7-29. Three strain gages were placed at the center of the tension flange along the middle section to monitor the stress range during testing. Additionally, a strain gage was placed near the flange edges at each CJP joint to monitor joint stresses and support crack detection. Additional strain gages were

placed on the flanges near the top and bottom fillet welds and on the cover plate to monitor stress ranges throughout the cross section.

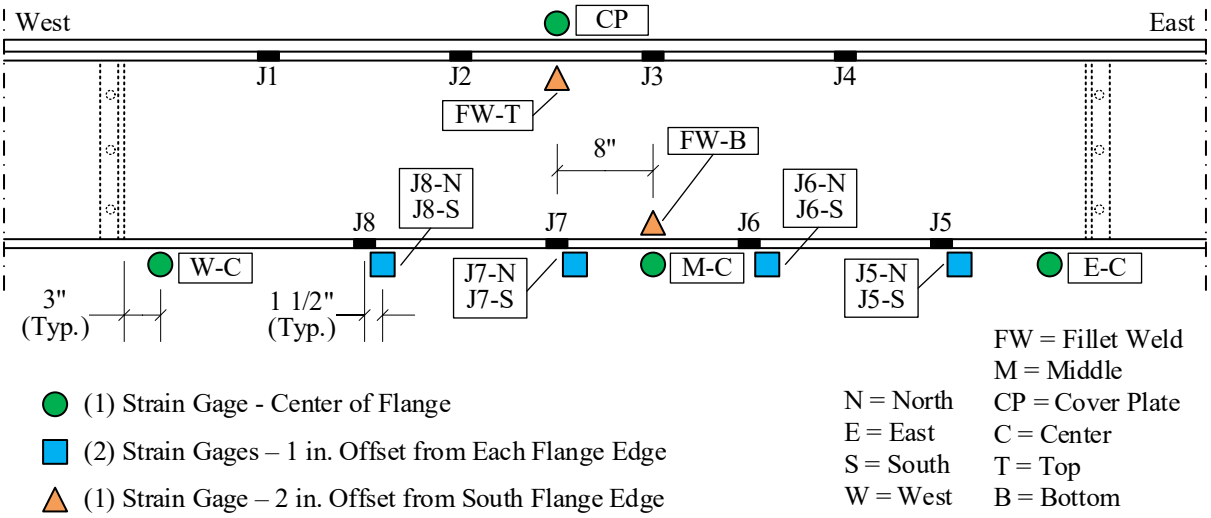


**Figure 7-29. Illustration. Instrumentation layout for Girder 4 - Flange 1 (looking north).**

The testing process followed the procedure outlined in Section 6.7. The fatigue cracks detected during testing are listed in Table 7-12. In this table, cracks are listed in order of detection, along with descriptions of the crack type, location, and the type of repair used. Each crack is named to reflect the test girder and the order of crack detection. For example, G4-1 is the first crack detected on Girder 4. Additionally, the cycle counts corresponding to the first detection and failure (i.e., when a crack repair was performed) are provided. Figure 7-30 illustrates the locations of all the fatigue cracks and shows photos of the cracks that led to joint failures or early stoppages.

**Table 7-12. Cracks detected during fatigue testing of Girder 4 - Flange 1.**

| *Crack* | *Crack Type* | *Crack Location* | *Detection Date* | *Cycle Count @ Detection* | *Cycle Count @ Failure* | *Crack Repair* |
|---|---|---|---|---|---|---|
| G4-1 | Fillet Weld | J7 | 4/5/2025 | 979,400 | 1,065,800 | Bolted Splice |
| G4- 2 | Fillet Weld | 5 in. West of J8 | 4/10/2025 | 1,414,600 | 1,414,600 | Mechanical Grinding |
| G4-3 | Fillet Weld | 8 in. East of J7 | 4/10/2025 | 1,453,600 | 1,681,000 | Bolted Splice |
| G4-4 | Fillet Weld | J5 | 4/11/2025 | 1,539,600 | 1,617,200 | Bolted Splice |
| G4-5 | Fillet Weld | 3 in. East of J6 | 4/11/2025 | 1,581,900 | 1,747,200 | Bolted Splice |
| G4-6 | Fillet Weld | 6 in. East of J6 | 4/11/2025 | 1,613,200 | 1,747,200 | Bolted Splice |
| G4-7 | Fillet Weld | J8 | 4/25/2025 | 2,590,100 | 2,590,100 | - |

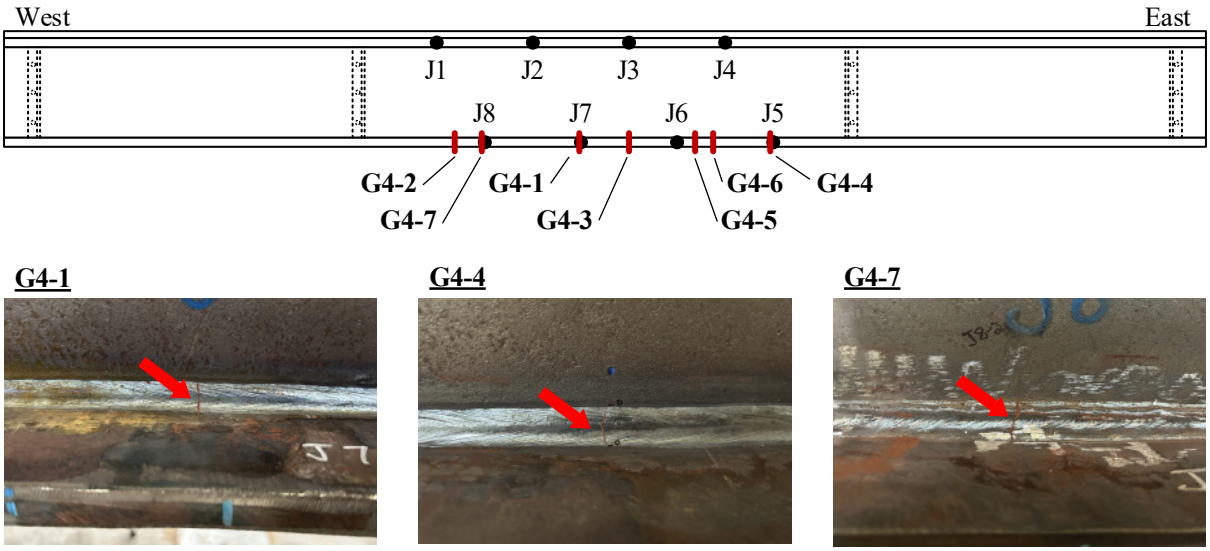


**Figure 7-30. Illustration. Overview showing the different fatigue cracks for Girder 4 – Flange 1.**

Crack G4-1 was a fillet weld crack that initiated from the root of the fillet weld, leading to the joint failure of J7 (R3) at 1.07 million cycles. Crack G4-1 was destructively examined after testing to confirm the point of crack initiation and failure classification of the joint. Cracks G4-2 and G4-3 were fillet weld cracks that initiated from the toe and root of the fillet welds, respectively. Both cracks were repaired without affecting the CJP welded-butt splice joints. Crack G4-4 was a fillet weld crack that initiated from the root of the fillet weld, leading to the joint failure of J5 (R0) at 1.62 million cycles. Crack G4-4 was destructively examined after testing to confirm the point of crack initiation and failure classification of the joint. Cracks G4-5

and G4-6 were fillet weld cracks that initiated at the root of the fillet weld but propagated and had to be repaired, resulting in the early stoppage of J6 (R1) at 1.75 million cycles. Crack G4-7 was a fillet weld crack that initiated from the root of the fillet weld, leading to the joint failure of J8 (R5) at 2.59 million cycles. As this crack occurred so close to the runout limit, no repairs were made, and testing was concluded once the runout limit of 2.6 million cycles was reached. Crack G4-7 was destructively examined after testing to confirm the point of crack initiation and failure classification of the joint.

After testing was completed for Girder 4, Cracks G4-1, G4-4, and G4-7 were isolated and cut open using a vertical band saw to expose the internal crack planes and crack initiation points. Figures 7-31 to 7-33 show the crack initiation point and general crack growth behavior of Cracks G4-1, G4-4, and G4-7, respectively. These figures confirm that Cracks G4-1, G4-4, and G4-7 started at the root of the fillet weld at the flange-web juncture. As such, joints J7 (R3), J5 (R0), and J8 (R5) are classified as early stoppages since the joints failed due to fillet welds rather than the CJP welds. A summary of the fatigue-life test results for the four CJP joints tested is shown in Table 7-13, including the joint and fatigue life corresponding to joint failure, early stoppage, or runout life. Note that all CJP joints tested exceeded the minimum AASHTO design life.

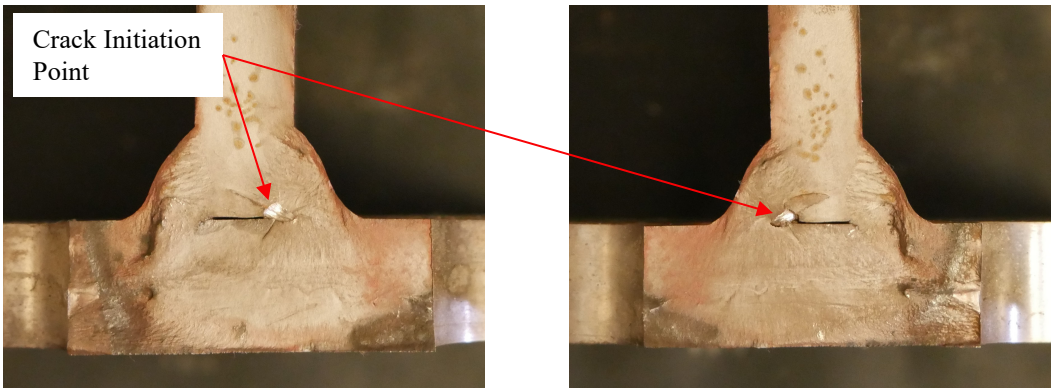


**G4-1 – Side A** **G4-1 – Side B**

Crack initiation point at root of fillet weld at flange-web juncture. Inclusion found.

**Figure 7-31. Photo. Destructive evaluation of Crack G4-1, which led to the failure of G4-J7.**

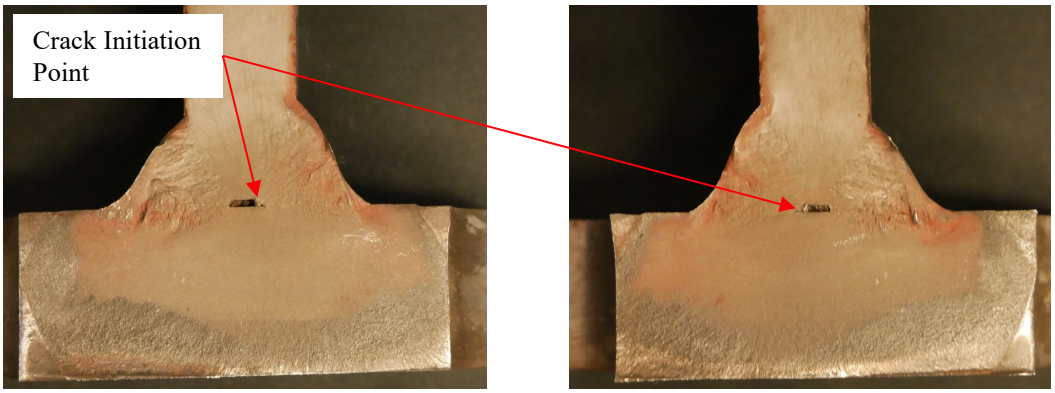


**G4-4 – Side A** **G4-4 – Side B**

Crack initiation point at root of fillet weld at flange-web juncture.

**Figure 7-32. Photo. Destructive evaluation of Crack G4-4, which led to the failure of G4-J5.**

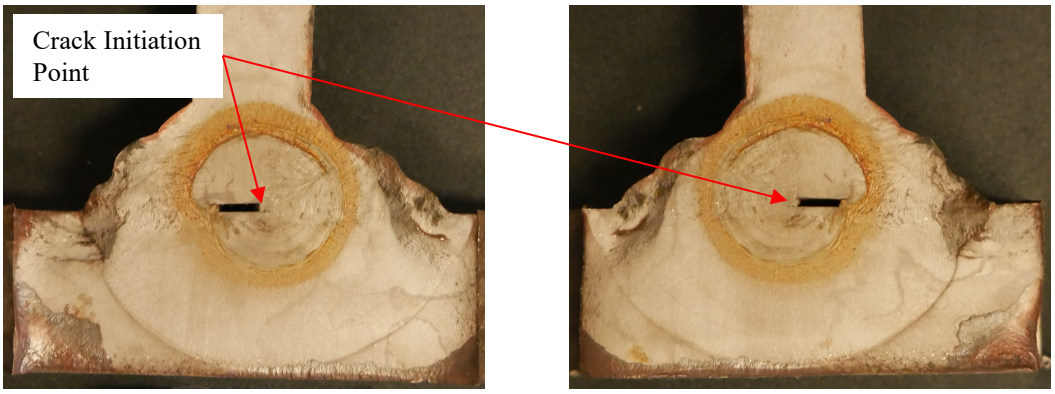


**G4-7 – Side A** **G4-7 – Side B**

Crack initiation point at root of fillet weld at flange-web juncture.

**Figure 7-33. Photo. Destructive evaluation of Crack G4-7, which led to the failure of G4-J8.**

**Table 7-13. Fatigue life test results for G4-J5, G4-J6, G4-J7, and G4-J8.**

| *Joint* | *Joint Results* | *Crack at Joint* | *Fatigue Life* |
|---|---|---|---|
| G4-J5 (R0) | Early Stoppage | Root Fillet Weld | 1,617,200 |
| G4-J6 (R1) | Early Stoppage | - | 1,747,200 |
| G4-J7 (R3) | Early Stoppage | Root Fillet Weld | 1,065,800 |
| G4-J8 (R5) | Early Stoppage | Root Fillet Weld | 2,590,100 |

Additionally, data from each strain gage were analyzed, and an average stress for the strain gage was determined for each test day. The average stresses for the centerline gages and CJP joint gages for each day are shown in Figures 7-34 and 7-35, respectively. In these plots, the abscissa shows the dates the girder was tested, and the ordinate shows the measured stress ranges. Note that some gages were removed prematurely for crack repairs, which is why some strain gages do not have data for the entire test. In the figures, a sharp change in stress usually correlates to the first detection of a fatigue crack, where the stress range at that particular strain gage steadily increased or decreased as a crack grew nearby.

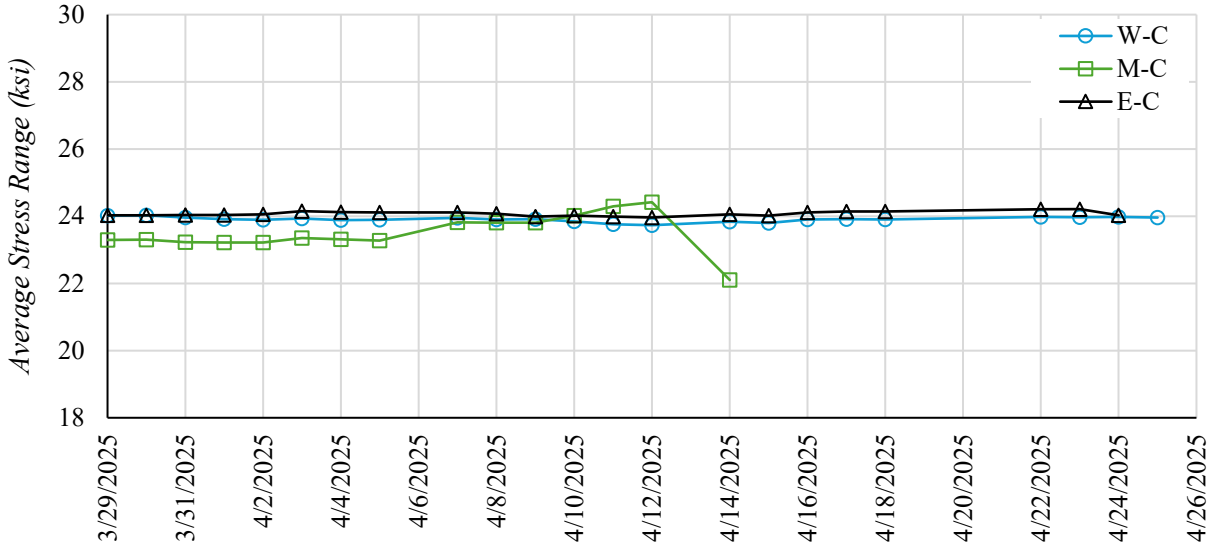


**Figure 7-34. Graph. Average daily stress range for Girder 4 – Flange 1 measured with strain gages along the bottom flange centerline.**

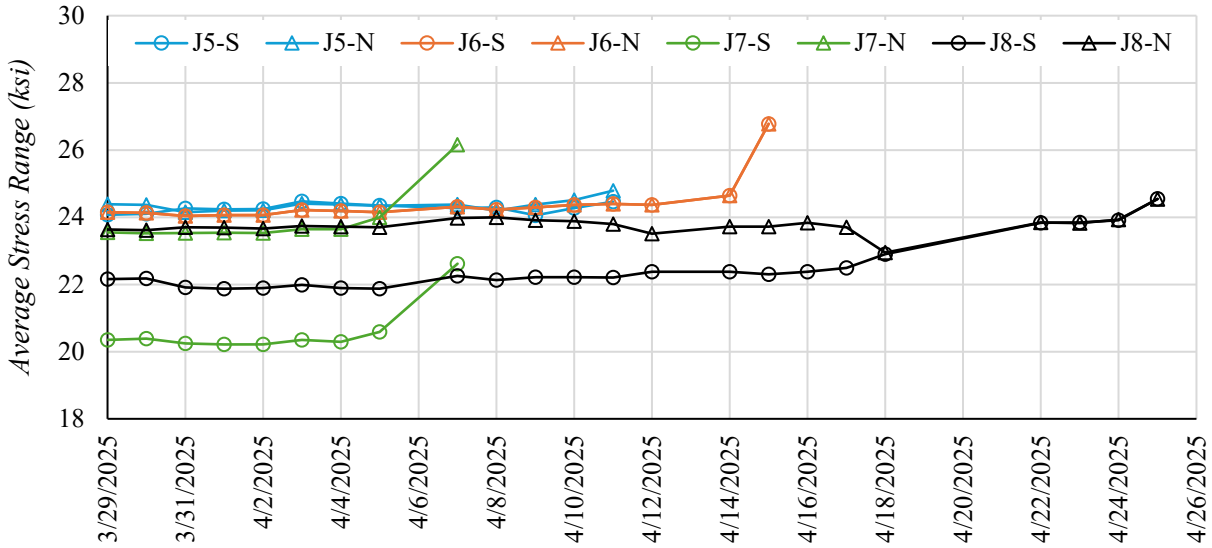


**Figure 7-35. Graph. Average daily stress range for Girder 4 – Flange 1 measured with strain gages at CJP butt-splice joints.**

Figure 7-34 demonstrates that the 24 ksi stress range was maintained along the centerline of the girder throughout testing. Figure 7-35 shows that the stress ranges along the flange edges were less consistent at each CJP butt-splice welded joint, with the measured stress ranges typically being within 4 ksi of the targeted 24 ksi. Discussions explaining why these stresses varied at the individual joints is provided in Section 7.5. In all cases, the measured stresses were generally consistent until a crack formed near the joint/strain gage.

### *7.4.2. Flange 2 (G4-J1, G4-J2, G4-J3, G4-J4)*

The strain gage layout used for Girder 4 – Flange 2 is shown in Figure 7-36. Three strain gages were placed at the center of the tension flange along the middle section to monitor the stress range during testing. Additionally, a strain gage was placed near the flange edges at each CJP joint to monitor joint stresses and support crack detection. Additional strain gages were placed on the flange near the bottom fillet weld and on the cover plate to monitor stress ranges throughout the cross section.

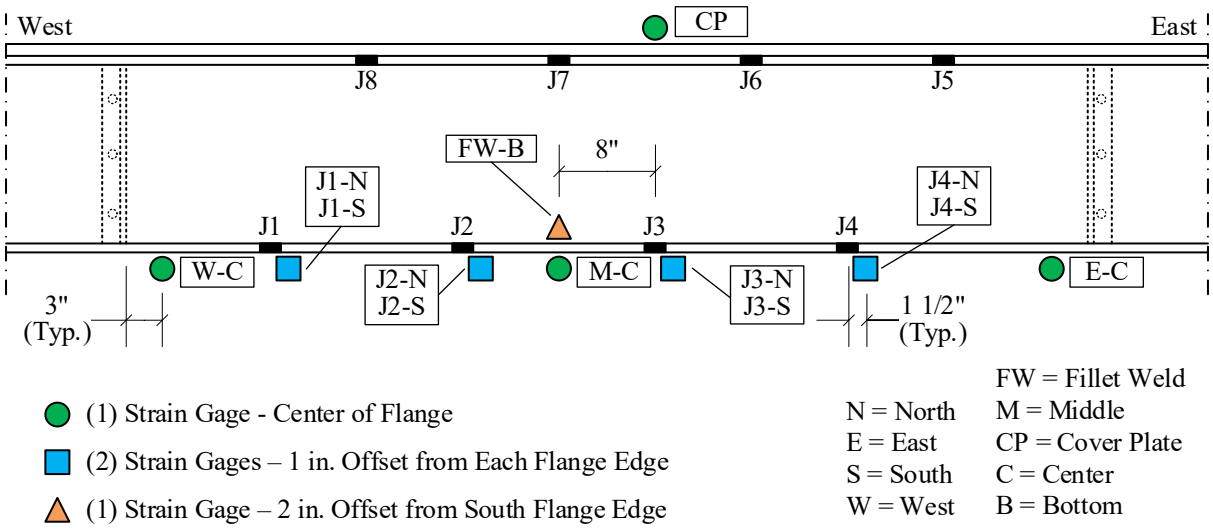


**Figure 7-36. Illustration. Instrumentation layout for Girder 4 - Flange 2 (looking north).**

The testing process followed the procedure outlined in Section 6.7. The fatigue cracks detected during testing are listed in Table 7-14. In this table, cracks are listed in order of detection, along with descriptions of the crack type, location, and the type of repair used. Each crack is named to reflect the test girder and the order of crack detection. For example, G4-8 is the eighth crack detected on Girder 4. Additionally, the cycle counts corresponding to the first detection and failure (i.e., when a crack repair was performed) are provided. Figure 7-37 illustrates the locations of all the fatigue cracks and shows photos of the cracks that led to joint failures or early stoppages.

**Table 7-14. Cracks detected during fatigue testing of Girder 4 - Flange 2.**

| *Crack* | *Crack Type* | *Crack Location* | *Detection Date* | *Cycle Count @ Detection* | *Cycle Count @ Failure* | *Crack Repair* |
|---|---|---|---|---|---|---|
| G4-8 | Flange Edge | 48 in. East of J4 | 5/9/2025 | 1,231,300 | 1,231,300 | Bolted Splice |
| G4-9 | Fillet Weld | 23 in. East of J4 | 5/17/2025 | 2,250,000 | 2,274,110 | Bolted Splice |
| G4-10 | Fillet Weld | J1 | 5/17/2025 | 2,250,000 | 2,339,200 | Bolted Splice |

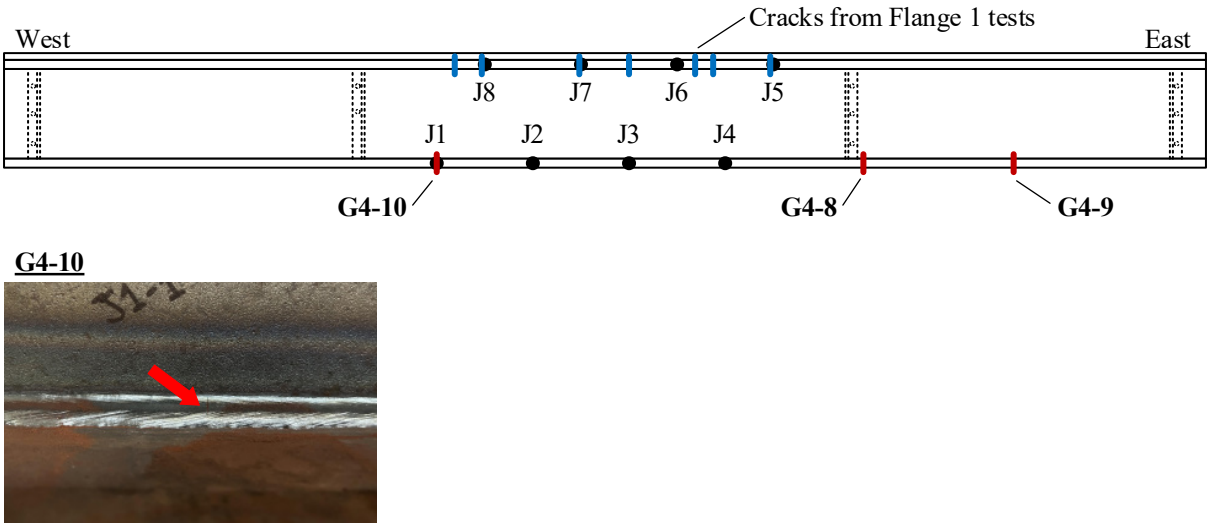


**Figure 7-37. Illustration. Overview showing the different fatigue cracks for Girder 4 – Flange 2.**

Crack G4-8 was a flange edge crack in the base metal that appeared unexpectedly in the eastern end section. Crack G4-9 was a fillet weld crack that initiated from the root of the fillet weld. Neither crack was near a joint, so repairs were performed without affecting the CJP butt-splice welded joints. Crack G4-10 was a fillet weld crack that initiated from the root of the fillet weld, leading to the joint failure of J1 (R0) at 2.34 million cycles. Crack G4-10 was destructively examined after testing to confirm the point of crack initiation and failure classification of the joint. No cracks were detected at J2 (R1), J3 (R3), and J4 (R5). The joints cycled to a runout life of 2.6 million cycles and were declared runouts.

After testing was completed for Girder 4, Crack G4-10 was isolated and cut open using a vertical band saw to expose the internal crack plane and crack initiation point. Figure 7-38 shows the crack initiation point and general crack growth behavior of Crack G4-10, confirming that the crack initiated at the root of the fillet weld at the flange-web juncture. As such, Joint J1 (R0) is classified as an early stoppage since the joint failed due to a fillet weld rather than the CJP weld. A summary of the fatigue-life test results for the four CJP joints tested is shown in Table 7-15,

including the joint and fatigue life corresponding to joint failure, early stoppage, or runout life. Note that all CJP joints tested exceeded the minimum AASHTO design life.

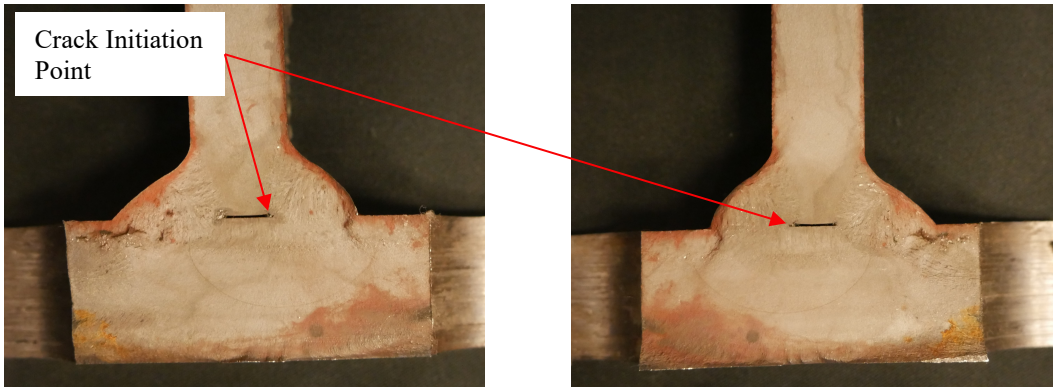


**G4-10 – Side A** **G4-10 – Side B**

Crack initiation point at root of fillet weld at flange-web juncture.

**Figure 7-38. Photo. Destructive evaluation of Crack G4-10, which led to the failure of G4-J1.**

**Table 7-15. Fatigue life test results for G4-J1, G4-J2, G4-J3, and G4-J4.**

| *Joint* | *Joint Results* | *Crack at Joint* | *Fatigue Life* |
|---|---|---|---|
| G4-J1 (R0) | Early Stoppage | Root Fillet Weld | 2,339,200 |
| G4-J2 (R1) | Runout | - | 2,600,000 |
| G4-J3 (R3) | Runout | - | 2,600,000 |
| G4-J4 (R5) | Runout | - | 2,600,000 |

Additionally, data from each strain gage were analyzed, and an average stress for the strain gage was determined for each test day. The average stresses for the centerline gages and CJP joint gages for each day are shown in Figures 7-39 and 7-40, respectively. In these plots, the abscissa shows the dates the girder was tested, and the ordinate shows the measured stress ranges. Note that some gages were removed prematurely for crack repairs, which is why some strain gages do not have data for the entire test. In the figures, a sharp change in stress usually correlates to the first detection of a fatigue crack, where the stress range at that particular strain gage steadily increased or decreased as a crack grew nearby.

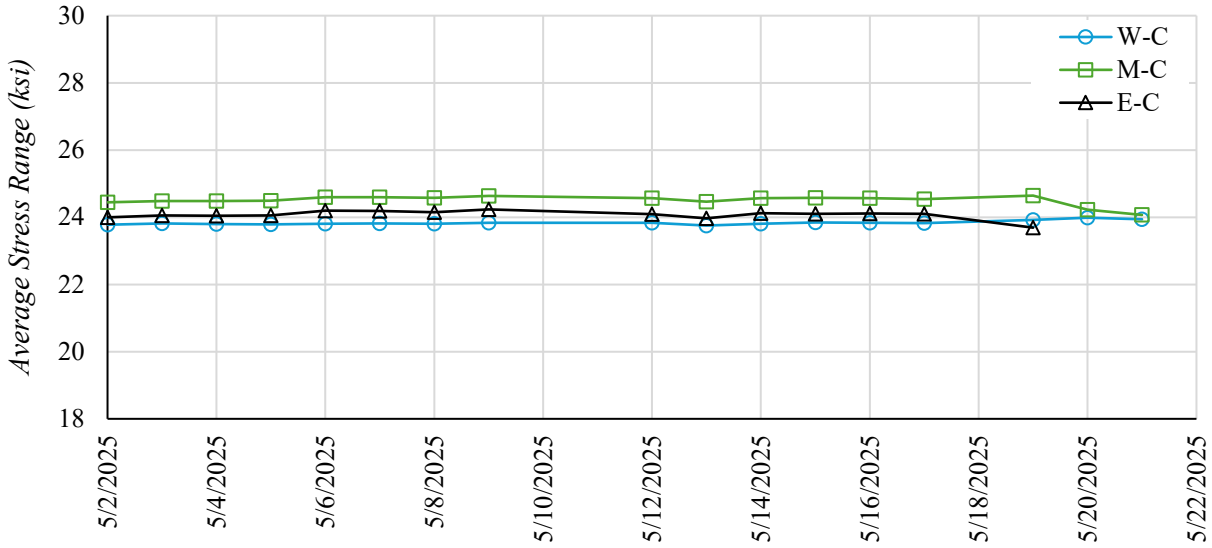


**Figure 7-39. Graph. Average daily stress range for Girder 4 – Flange 2 measured with strain gages along the bottom flange centerline.**

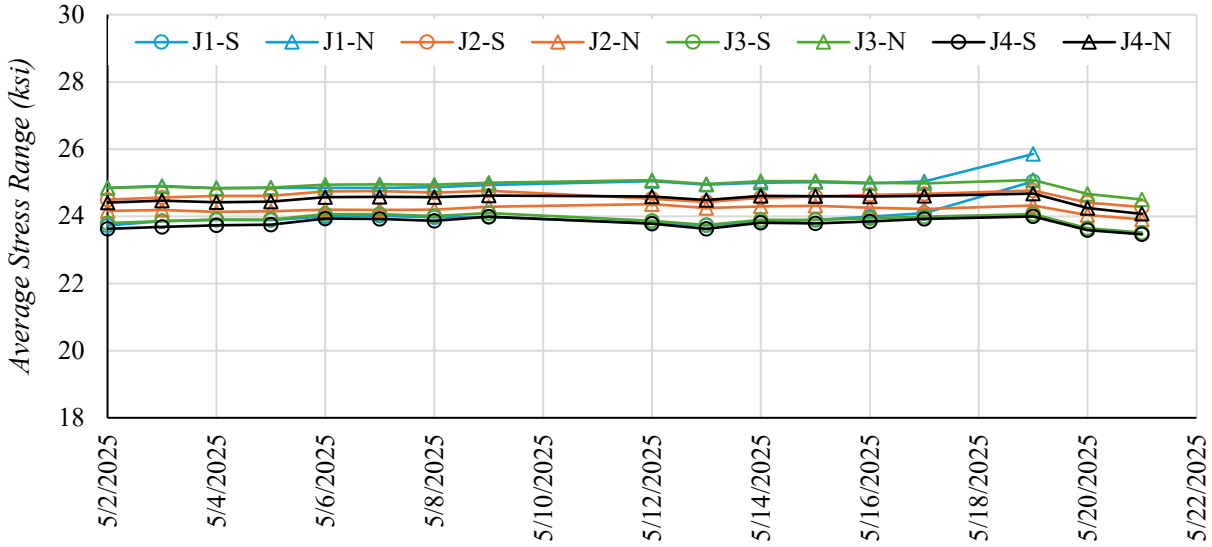


**Figure 7-40. Graph. Average daily stress range for Girder 4 – Flange 2 measured with strain gages at CJP butt-splice joints.**

Figure 7-39 demonstrates that the 24 ksi stress range was maintained along the centerline of the girder throughout testing. Figure 7-40 shows that the stress ranges along the flange edges were slightly less consistent at each CJP butt-splice welded joint, with the measured stress ranges typically within 1 ksi of the targeted 24 ksi. Discussions explaining why these stresses varied at

the individual joints are provided in Section 7.5. In all cases, the measured stresses remained consistent until a crack formed near the joint/strain gage.

### 7.5. Discussion of Results

In total, 28 of the 32 CJP welded butt-splice joints targeted in the current study were successfully tested for fatigue. For all flanges tested, the average daily stress range plots demonstrated that the 24 ksi stress range was well maintained along the centerline of the girder for the entirety of the tests. However, these same plots also showed that the stress ranges along the flange edges were slightly less consistent, often varying by +/- 4 ksi from the targeted 24 ksi. Furthermore, the pair of strain gages at a given CJP joint were frequently complementary to each other and over / under the targeted 24 ksi stress range by reciprocal stress range magnitudes, potentially indicating: (a) influence from geometrical imperfections and/or (b) compounding flange lateral bending stresses. Although the reciprocal stress behavior mimics the typical effects of lateral bending, flange lateral bending stresses are typically induced by applied out-of-plane loads or buckling of the flange. As neither scenario is relevant to the tested tension flange, it can be concluded that flange lateral bending need not be considered. As such, the measurement variation along the flange edges is most likely due to flange tilt and slight geometry differences along the cross-section resulting from the fabrication process, especially near the CJP butt-splice joints where grinding was performed after all final repairs. As four CJP joints were being tested concurrently on each flange, basing the testing stress range on the centerline strain gages of the flange rather than the specific CJP joint gages was justified, given the slight variances along the flange edges.

To evaluate the effects of multiple repair welds on the fatigue life of CJP butt-splice welds, the fatigue life test results for all CJP joints tested have been compiled and are discussed below. Table 7-16 summarizes the different types of fatigue failures observed for each girder tested. This table lists the different girders tested and tallies the fatigue failures, early stoppages, and runouts corresponding to non-CJP joints (i.e., base metals/fillet welds) and CJP butt-splice welded joints. The non-CJP joint failures are further broken down into either flange edge or fillet weld failure groups. The CJP butt-splice welded joint failures are further broken down into flange edge failures, fillet weld failures, early stoppages, runouts, and unable to test groups.

**Table 7-16. Summary of fatigue life test results for each test girder.**

| | | | **Base Metals / Fillet Welds** | | **CJP Butt-Splice Welded Joints** | | | | |
|---|---|---|---|---|---|---|---|---|---|
| | | | *Failures* | | *Failures* | | | | |
| *Girder* | *Flange Material* | $t_f$ *(in.)* | *Flange Edge* | *Fillet Weld* | *Flange Edge* | *ES (CJP)* | *ES (Non-CJP)* | *Runouts* | *Unable to Test* |
| 1 | 50W | 1-1/2 | 0 | 3 | 3 | 0 | 1 | 4 | 0 |
| 2 | 50W | 3/4 | 1 | 7 | 0 | 1 | 2 | 1 | 4 |
| 3 | HPS70W | 1-1/2 | 1 | 6 | 0 | 3 | 1 | 4 | 0 |
| 4 | HPS70W | 3/4 | 0 | 5 | 0 | 4 | 1 | 3 | 0 |
| | | Totals: | 2 | 21 | 3 | 8 | 5 | 12 | 4 |

ES (CJP) = Early stoppage from fillet weld cracks at the CJP joint
ES (Non-CJP) = Early stoppage from nearby fillet weld cracks not at the CJP joint

As the table shows, there were a significant number of failures that occurred outside of the CJP joints (i.e., in the base metal/fillet welds not at the CJP joints), totaling more than twice the number of failures that occurred at the CJP joints. Looking at the 32 CJP joints tested: 11 joints failed from fatigue, 5 joints were stopped early due to nearby non-joint fatigue failures, 12 joints met the runout limit, and 4 joints were unable to be tested. The joint failures were a combination of flange edge and fillet weld crack failures, with the majority of the failures being

fillet weld crack failures. Regardless of the failure type, these joint failures can be compared to assess trends in the number of repair welds performed, member thickness, and resulting fatigue life. While the early stoppages and runouts do not provide directly comparable data points, they are still valuable, as they can serve as a baseline for performance and help identify trends.

As a large portion of the data points were runouts or early stoppages,, a traditional regression analysis is not particularly insightful for identifying trends or a baseline level of fatigue performance. Instead, fatigue life test results for all the CJP joints tested are compared with one another and the AASHTO fatigue life design curves using a traditional log–log fatigue life (S–N) plot. The S–N plot is supplemented by a subplot showing the fatigue life test results for the CJP joints as a function of the number of repair welds. Figures 7-30 and 7-31 show the plots for the 50-grade and 70-grade specimens, respectively. In Figures 7-30a and 7-31a, the abscissa is the number of cycles ($N$), and the ordinate is the stress range. Additionally, the AASHTO fatigue design curve for a Category B detail and the resistance curves corresponding to the mean and runout limits are plotted. A runout is indicated by a black arrow that is attached to the data point marker, and the number of runouts is shown next to the arrow. In Figures 7-30b and 7-31b, the abscissa is the number of repair welds, and the ordinate is the number of cycles ($N$). Additionally, the cycle counts for a stress range of 24 ksi for the three resistance curves discussed above are shown in the plots. Note that the early stoppage data points are also plotted in these figures. Although the early stoppage data are shown, they do not represent fatigue failure and should not be used to draw any specific conclusions.

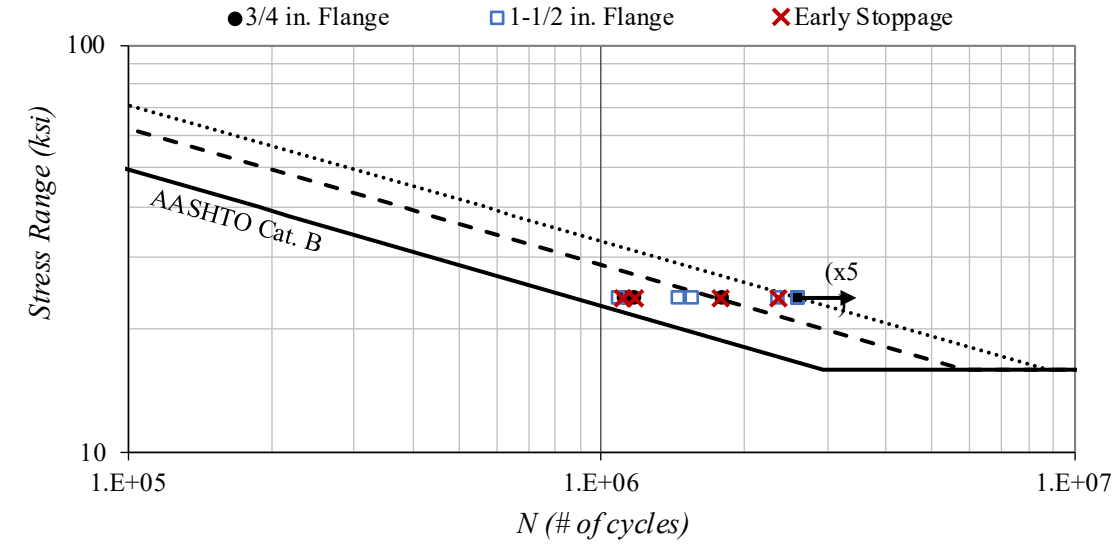


(a) S-N Plot Showing Fatigue Test Results

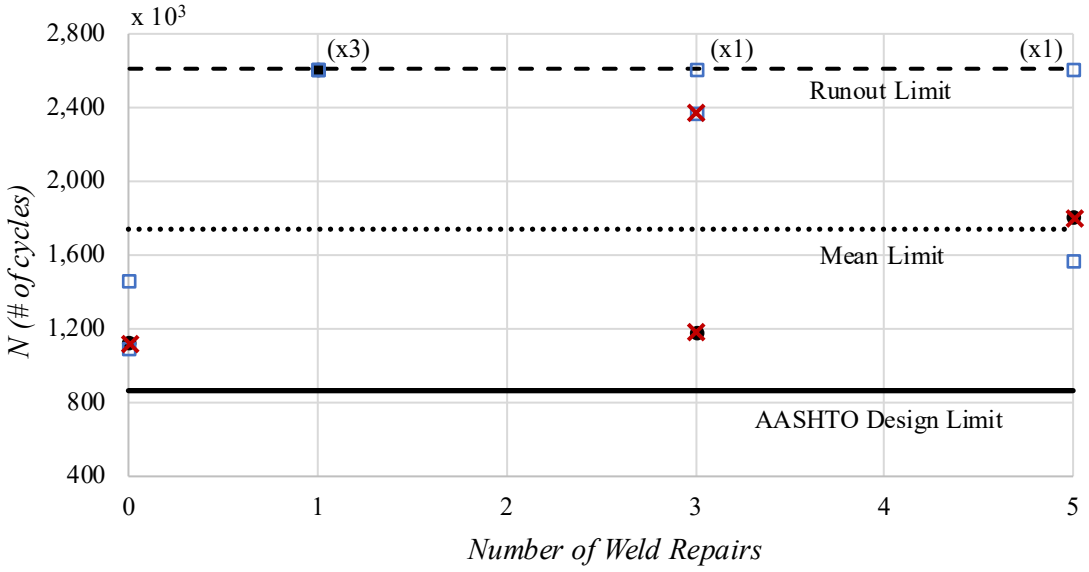


(b) Comparative Plot Showing Number of Weld Repairs

**Figure 7-41. Multiple Graphs. Fatigue life test results for all 50-grade specimens. (a) S–N plot showing fatigue test results and (b) Comparative plot showing the number of weld repairs.**

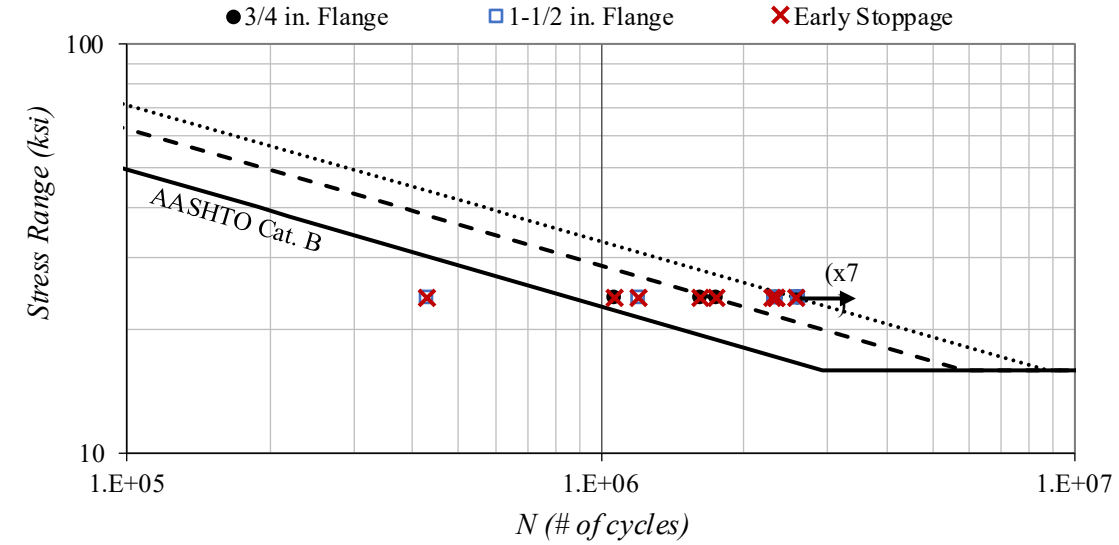


(a) S-N Plot Showing Fatigue Test Results

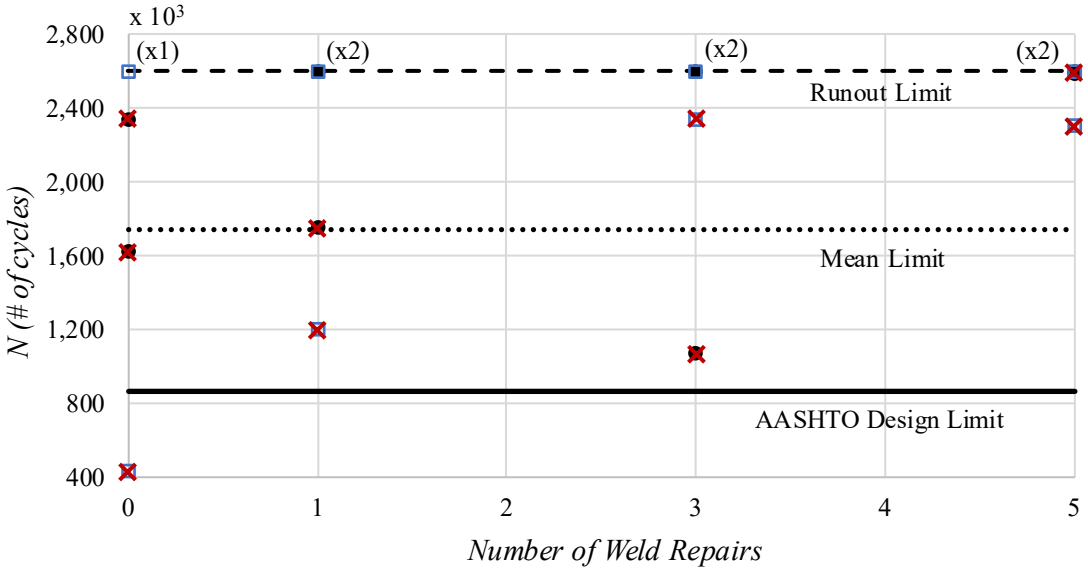


(b) Comparative Plot Showing Number of Weld Repairs

**Figure 7-42. Multiple Graphs. Fatigue life test results for all 70-grade specimens. (a) S–N plot showing fatigue test results and (b) Comparative plot showing the number of weld repairs.**

As the figures show, all the CJP joints tested (excluding the one early stoppage 70-grade joint) exceeded the design-life predictions from AASHTO LRFD-10, regardless of the number of weld repairs. Specifically, Figures 7-30b and 7-31b show that the same fatigue life test data are plotted as a function of the number of weld repairs to provide insights into the influence that weld repairs may have on the fatigue life of the joints. The figures demonstrate that joints with

one or more repairs generally performed similarly or better than those with no repairs, with numerous runouts even at five repairs. Additionally, these figures show data scatter commonly observed in fatigue testing, and there appears to be no discernible trend between the material grade, flange thickness, or number of weld repairs and the fatigue life of the joint. As such, the fatigue life test data show that there is no significant change in the fatigue behavior of CJP butt-splice joints up through five weld repairs for 50- and 70-grade A709 steels.

# CHAPTER 8. CONCLUSIONS

## 8.1. Summary

Welding is a common process used in the steel bridge fabrication industry to create built-up steel members. Even with guidance and standard documents such as AASHTO/AWS D1.5, welding nonconformances will occasionally be found during fabrication that must be repaired, with some nonconformances requiring multiple repair attempts before passing all inspection requirements. Currently, no standards or guidance documents specify how many repair attempts should be allowed at a joint, and no studies have investigated the effects that multiple repair welds may have on bridge members typical of the bridge industry. This lack of guidance and data leads to ambiguity and disagreements between owners and fabricators over how many repairs are allowed and, in the most extreme cases, can result in the entire member being rejected for seemingly excessive repair welds at a given joint, adding significant cost and time to the project. To address the knowledge gap, the current study has: (a) gathered existing data and practices commonly used in the steel bridge industry to detect and address welding nonconformances and (b) performed a suite of material characterization and large-scale fatigue life tests to generate novel experimental data that investigates if multiple repair welds have a significant effect on the material properties or fatigue life of a joint and the member as a whole.

An AASHTO Committee on Materials and Pavement survey and fabricator interviews were conducted to: (a) gain a better understanding of current practices implemented by owners across the US and (b) gather resources and industry knowledge regarding the effects of multiple weld repairs. The survey responses were compiled and analyzed to determine the resources

owners use for QA/QC and whether any limits are currently placed on repair welds during the fabrication process.

For the material characterization tests, 12 plates were fabricated for testing. All plates were A709-50W or A709-HPS70W and welded together with a single V-groove CJP butt-splice weld using SAW. A hypothetical defect was assumed to be in the welded joint at 0.5T, and each material characterization plate was repaired up to five times using repair weld techniques common to the bridge industry, mimicking a typical butt-splice joint repaired numerous times during fabrication. The result was 12 material characterization plates, each representing a unique combination of material and the number of weld repairs. Specimens were then extracted from the material characterization plates for tension, side-bend, CVN impact, and microhardness/macroetch tests to evaluate the influence of varying numbers of repair welds on the material properties of the CJP joints.

Concurrent to the material characterization tests, large-scale fatigue life tests were conducted on four built-up I-section members. The flanges of the members were either 3/4 in. or 1-1/2 in. thick and comprised of A709-50W or A709-HPS70W plates. Each flange contained four single V-groove CJP butt-splice joints, welded using SAW. Similar to the material characterization plates, a hypothetical defect was assumed at 0.5T, and each CJP joint was repaired either 0, 1, 3, or 5 times, resulting in eight CJP joints for testing on each girder that represented a unique combination of material, flange thickness, and number of weld repairs. The girders were loaded in a four-point bending configuration such that the tension flange was subjected to a pure tension constant amplitude stress range of 24 ksi ($R > 0$). The girders were cycled until all four joints on the tension flange either failed or met the runout limit. This loading configuration and pattern enabled the independent testing of each flange, resulting in eight

fatigue tests that evaluated 32 different CJP joints. Fatigue life test results from each CJP joint were compared with one another and with the AASHTO design life criteria to evaluate the effects of varying numbers of repair welds on the fatigue life of the CJP joints.

### 8.2. Research Objectives and Findings

This research has presented new experimental data on the effects of multiple repair welds on the material characterization and fatigue life of a welded CJP joint. The objectives targeted by the research are as follows:

1. Gather data from national standards, governing owner agencies, and fabricators to determine the current standards, practices, and restrictions used in the steel bridge industry to detect and address various fabrication nonconformances.
2. Generate and synthesize data from a suite of experimental material property tests to characterize any changes in the material properties of CJP welded joints that have been subjected to a varying number of repair welds.
3. Generate and synthesize data from large-scale experimental fatigue tests to characterize any changes in the fatigue performance of CJP welded joints that have been subjected to a varying number of repair welds.
4. Develop recommendations regarding quality acceptance and limits for repairing welding nonconformances and implement said recommendations in the first draft of the GDOT Steel Fabrication Quality Manual (SFQM).

The findings from the research program are as follows:

- The literature review and AASHTO member survey showed that approximately half of the states use a state-specific quality manual for the fabrication and QA/QC of steel

bridge members and implement some form of restriction on the number of repair welds allowed at a single location. However, no standard or guidance documents explicitly recommend one.

- The tension tests showed that there is no significant change in the ductility, yield strength, or tensile strength of the CJP butt-splice welded joints up through five repairs. All tests exceeded the A709 minimum strength requirements.
- All specimens passed the side-bend tests, showing that the CJP butt-splice welded joints with up to five repairs all meet the minimum ductility required to pass typical WPS qualification tests.
- The CVN impact tests showed that there is no significant change in the impact energy of the HAZ near the repaired CJP butt-splice welded joints up through five repairs. All specimens exceeded the A709 minimum impact energy requirements for all relevant temperature zones.
- The macroetches of the material characterization plate welds showed that the weld profile maintained a consistent geometry across all weld repairs, and, on average, the HAZ did not expand by more than 1–2 mm across all five repairs.
- The microhardness tests showed an observable relationship between HAZ hardness and the number of weld repairs, suggesting a potential link between tensile strength and the number of repair welds. The 50-grade specimens generally showed an increase in hardness, and the 70-grade materials generally showed a decrease in hardness. However, these observable relationships were not observed in the tension tests; therefore, they do not translate into meaningful changes in the overall joint material properties. Notably, the

280 Vickers hardness limit in AASHTO/AWS D1.5 was exceeded by Specimens 50-R3, 50-R4, and 50-R5, but all other specimens were below this requirement.

- The fatigue life tests showed that the repaired CJP joints met or exceeded the design-life predictions from AASHTO LRFD-10, regardless of the number of repair welds.
- No trend was discernable between the material grade, flange thickness, or number of repair welds and the fatigue life of the CJP joints, and the fatigue life data showed that there is no significant change in the fatigue behavior of CJP butt-splice joints up through five weld repairs.

Each of the findings listed above is discussed in more detail below.

For the tension tests, 36 tension specimens were tested to rupture. These tests showed that the weld repairs have little effect on the overall ductility of the joint, with the ductility of the repaired joints never decreasing more than 5% compared to the baseline CJP joint with no repairs. The measured yield and tensile strengths of all joints tested exceeded the A709 minimum requirements, but a negative relationship was observed between the yield/tensile strength and the number of weld repairs. However, these trends showed an insignificant decrease in strength with increasing number of weld repairs. On average, the 50-grade specimens decreased by approximately 12% and 17% from R0 to R5 for yield and tensile strength, respectively. However, the lowest-strength specimen still exceeded the A709 minimum yield and tensile strength by at least 17%. The 70-grade specimens exhibited no change in yield or tensile strength from R0 to R5, and the lowest-strength specimen exceeded the A709 minimum yield and tensile strengths by at least 7% and 9%, respectively.

For the CVN impact tests, 252 CVN specimens were tested at temperatures ranging from -110°F [-79°C] to 120°F [49°C]. The resulting impact test energies were then used to generate

full temperature transition curves for each material characterization plate. The CVN impact tests showed substantial scatter in the collective datasets for the 50-grade and 70-grade specimens, likely due to small variations in the notch location across the different weld profiles. On average, the welded 50-grade specimens exhibited higher impact energy than the base metal, whereas the welded 70-grade specimens exhibited impact energies similar to those of the base metal. Comparing the collective datasets at each test temperature showed that the number of weld repairs had little effect on impact energy, and, on average, there was no significant increase or decrease in impact energy due to weld repairs. The only notable decrease occurred at 60°F for the 70-grade specimen dataset, where a consistent reduction in impact energy of approximately 10% per repair was observed. However, this trend was not observed at -60°F in the 50-grade specimen dataset, nor was it present at any of the other 70-grade testing temperatures. Regardless, all CVN specimens exceeded the A709 minimum impact energy requirements for all relevant temperature zones.

For the microhardness tests, hardness shots were taken across the weld of each material characterization plate at 0.5T (i.e., half thickness). The microhardness tests yielded hardness values that clearly distinguished the three weld regions (weld metal, HAZ, base metal), with the HAZ generally exhibiting higher hardness than the weld metal and base metal. Comparing the measured HAZ hardness values for the 50-grade and 70-grade material groups showed an observable relationship between the number of repair welds and HAZ hardness. For the 50-grade materials, a positive relationship was observed, indicating an increase in hardness with each weld repair beyond three. The largest hardness values were within 3 mm of the fusion line, and Specimen 50-R4 showed the largest increase in hardness, reaching a maximum of 320 Vickers hardness (the average measured Vickers hardness of the 50-grade base metal was approximately

240). For the 70-grade materials, a negative relationship was observed, indicating a decrease in hardness with each weld repair. The lowest hardness values were within 4 mm of the fusion line, and Specimen 70-R5 showed the largest reduction in hardness, reaching a minimum of 190 Vickers hardness (the average measured Vickers hardness of the 70-grade base metal was approximately 220). However, this trend was not observed in the other material property tests, indicating that this relationship may not be substantial or indicative of performance in larger specimens.

For the large-scale fatigue life tests, 32 welded CJP butt-splice joints were tested: 11 joints failed from fatigue, five joints were stopped early due to nearby non-joint fatigue failures, 12 joints met the runout limit, and four joints were unable to be tested. Of the 11 joint failures, eight failed due to a fillet weld crack, and three failed due to a flange edge crack. All joints tested (except one early stoppage 70-grade joint) exceeded the design-life predictions from AASHTO LRFD-10. Additionally, comparing the fatigue life as a function of the number of repair welds showed a fair amount of scatter in the data, which is not uncommon in all fatigue tests. There appears to be no discernable relationship between the flange thickness, grade of material, and number of repair welds to the fatigue life of the joint.

The material characterization tests have shown that regardless of the number of repairs, all joints tested met or exceeded the minimum material property requirements of A709 and exhibited material properties comparable to those of a CJP joint with no repairs. Similarly, the fatigue life tests have shown that regardless of the number of repairs, all joints tested (excluding one early stoppage) met or exceeded the design life predictions from AASHTO LRFD-10 and exhibited a fatigue life comparable to a CJP joint with no repairs. As such, there appears to be no

significant change in the material performance or fatigue behavior of CJP butt-splice welded joints up through five repairs.

### 8.3. Further Research Needs

The current experimental research program focused exclusively on welded CJP butt-splice joints because they are very common in the bridge industry, susceptible to welding nonconformances, and can be easily replicated, which was essential for the current program. However, another joint in the bridge industry that is susceptible to welding nonconformances is the flange-to-web CJP joint. While the findings regarding material properties and fatigue life from the current study are directly applicable to the flange-to-web CJP joints, the different joint geometries result in the joints not being completely synonymous. One particular question concerns lamellar tearing. Due to the geometry, performing and repairing flange-to-web joints may result in through-thickness ductility issues in the flange, potentially leading to lamellar tearing concerns for the joint. Further investigation into the effects of multiple weld repairs on web-to-flange joints may be warranted.

Additionally, the welded joints and fabrication techniques studied in this research are primarily used on bridge members; however, welding is also extensively used in the fabrication of other transportation-related structures, such as high-mast poles, sign supports, and ancillary highway structures. These structures use joints, fabrication practices, and materials that can differ significantly from those of bridge members. Furthermore, their loading conditions make them highly susceptible to fatigue from wind- and truck-induced gusts. As such, further investigations into fabrication, inspection, and installation practices for high mast poles, sign

supports, and ancillary highway structures are essential, as is the development of similar fabrication quality guidance documents for GDOT.

## REFERENCES


AASHTO (2017). *LRFD Bridge Construction Specifications* (4th edition). AASHTO, American Association of State Highway and Transportation Officials.

AASHTO. (2023). *LRFD Steel Bridge Fabrication Specifications* (1st Edition). American Association of State Highway and Transportation Officials.

AASHTO. (2024). *LRFD Bridge Design Specifications* (10th Edition). American Association of State Highway and Transportation Officials.

AASHTO/AWS. (2020). *D1.5—Bridge Welding Code* (8th Edition). American Association of State Highway and Transportation Officials; American Welding Society.

AASHTO/NSBA. (2006). *G4.4—Sample Owners Quality Assurance Manual*. American Association of State Highway and Transportation Officials; National Steel Bridge Alliance.

AASHTO/NSBA. (2016). *G2.2—Guidelines for Resolutions of Steel Bridge Fabrication Errors*. American Association of State Highway and Transportation Officials; National Steel Bridge Alliance. https://doi.org/10.4135/9781483346526.n55

AASHTO/NSBA. (2018). *S2.1—Steel Bridge Fabrication Guide Specification*. American Association of State Highway and Transportation Officials; National Steel Bridge Alliance.

AASHTO/NSBA. (2019). *G4.1—Steel Bridge Fabrication QC/QA Guidelines*. American Association of State Highway and Transportation Officials; National Steel Bridge Alliance.

AghaAli, I., Farzam, M., Golozar, M. A., & Danaee, I. (2014). The effect of repeated repair welding on mechanical and corrosion properties of stainless steel 316L. *Materials & Design (1980-2015)*, *54*, 331–341. https://doi.org/10.1016/j.matdes.2013.08.052

AISC. (2022a). *Code of Standard Practice for Steel Buildings and Bridges*. American Institute of Steel Construction.

AISC. (2022b). *Specification for Structural Steel Buildings*. American Institute of Steel Construction.

ASME. (2023). *ASME Boiler and Pressure Vessel Code—Section VIII - Division 1*. American Society of Mechanical Engineers.

ASTM. (2018). *E23-18: Test Methods for Notched Bar Impact Testing of Metallic Materials*. ASTM International. https://doi.org/10.1520/E0023-18

ASTM. (2019). *A131-19: Specification for Structural Steel for Ships*. ASTM International. https://doi.org/10.1520/A0131_A0131M-19

ASTM. (2021a). *A6-21: Specification for General Requirements for Rolled Structural Steel Bars, Plates, Shapes, and Sheet Piling*. ASTM International. https://doi.org/10.1520/A0006_A0006M-21

ASTM. (2021b). *A709-21: Specification for Structural Steel for Bridges*. ASTM International. https://doi.org/10.1520/A0709_A0709M-21

ASTM. (2021c). *E190-21: Test Method for Guided Bend Test for Ductility of Welds*. ASTM International. https://doi.org/10.1520/E0190-21

ASTM. (2022a). *E8-22: Test Methods for Tension Testing of Metallic Materials*. ASTM International. https://doi.org/10.1520/E0008_E0008M-22

ASTM. (2022b). *E384-22: Test Method for Microindentation Hardness of Materials*. ASTM International. https://doi.org/10.1520/E0384-22

ASTM. (2023). *F3125-23: Specification for High Strength Structural Bolts and Assemblies*. ASTM International. https://doi.org/10.1520/F3125_F3125M-22

AWS. (2020). *D1.1—Structural Welding Code—Steel* (24th edition, second printing). AWS, American Welding Society.

AWS. (2021). *A5.23—Specification for Low-Allow High Manganese Steel Electrodes and Fluxes for Submerged Arc Welding* (6th Edition). American Welding Society.

AWS. (2025). *A Practical Guide to Submerged Arc Welding*. AWS Welding Digest. https://www.aws.org/magazines-and-media/welding-digest/2025/july/wd-july-2025-a-practical-guide-to-submerged-arc-welding/

Bannantine, J. A., Comer, J. J., & Handrock, J. L. (1990). *Fundamentals of metal fatigue analysis*. Prentice Hall.

Carpenter, K. R., Dissanayaka, P., Sterjovski, Z., Li, H., Donato, J., Gazder, A. A., Van Duin, S., Miller, D., & Johansson, M. (2021). The effects of multiple repair welds on a quenched and tempered steel for naval vessels. *Welding in the World*, *65*(10), 1997–2012. https://doi.org/10.1007/s40194-021-01150-y

Collins, W., & Yount, T. (2023). *Toughness Requirements for Heat-Affected Zones of Welded Structural Steels for Highway Bridges* (p. 101). Transportation Research Board. https://doi.org/10.17226/27250

Easterling, K. E. (1992). *Introduction to the Physical Metallurgy of Welding* (2nd ed). Butterworth Heinemann.

FHWA. (2019). *Bridge Welding Reference Manual* (Technical Report FHWA-HIF-19-088; p. 348). Federal Highway Administration.

Jiang, W., Luo, Y., Zhang, G., Woo, W., & Tu, S. T. (2013). Experimental to study the effect of multiple weld-repairs on microstructure, hardness and residual stress for a stainless steel clad plate. *Materials & Design*, *51*, 1052–1059. https://doi.org/10.1016/j.matdes.2013.05.027

Keating, P. B., & Fisher, J. W. (1986). *Review of fatigue tests and design criteria on welded details, Final Report* (NCHRP Report 286; p. 180). Lehigh University. http://preserve.lehigh.edu/engr-civil-environmental-fritz-lab-reports/524

Kelly, B. (1997). *Fatigue Performance of Repair Welds* [Masters Thesis]. Lehigh University.

Lin, C.-M., Tsai, H.-L., Cheng, C.-D., & Yang, C. (2012). Effect of repeated weld-repairs on microstructure, texture, impact properties and corrosion properties of AISI 304L stainless steel. *Engineering Failure Analysis*, *21*, 9–20. https://doi.org/10.1016/j.engfailanal.2011.11.014

Modjeski and Masters, Inc., University of Nebraska, Lincoln, University of Delaware, & NCS Consultants, LLC. (2014). *Bridges for Service Life Beyond 100 Years: Service Limit State*

*Design* (Report S2-R19B-RW-1; p. 521). Transportation Research Board. https://doi.org/10.17226/22441

Schasse, R., Kannengiesser, Th., Kromm, A., & Mente, T. (2015). Residual stresses in repair welds of high-strength low-alloy steels. *Welding in the World*, *59*(6), 757–765. https://doi.org/10.1007/s40194-015-0257-9

Wallin, K. (2011). *Fracture Toughness of Engineering Materials: Estimation and Application*. EMAS Publishing.

Wilson, A. D. (1999). *Properties of recent production of A709 HPS 70W bridge steels*. 41–49.

# APPENDIX A.

# AASHTO SURVEY INFORMATION

**From:** Allen, Patrick <paallen@dot.ga.gov>
**Sent:** Monday, March 6, 2023 1:53 PM
**To:** comp@aashto.org
**Cc:** Mark Felag; Soneira, Casey; pwu@dot.ga.gov; Sherman, Ryan J; Lee, Reginald; Wright, Cornelius; Phillips, Matthew L
**Subject:** AASHTO Survey for Quality Manual for Steel Brid
**Attachments:** GDOT Steel Quality Manual.pdf

AASHTO Members:

As the first step in a Georgia Department of Transportation (GDOT) project to create a Quality Manual for Steel Bridge Fabrication, GDOT and Georgia Institute of Technology (GA Tech) are conducting a survey of owners. The goal of the survey is to gain a better understanding of the approaches and systems utilized by other owner agencies regarding quality assurance/quality control (QA/QC) and nonconformances in steel bridge fabrication. An emphasis is placed on the documents and resources used by other owner agencies to develop their own QA/QC systems and any limitations associated with the repair procedures for nonconformances.

The GA Tech team, which includes Dr. Ryan Sherman, Dr. Lauren Stewart, and Matthew Phillips, would be grateful if you would complete the short survey concerning your experience and insight regarding quality processes for steel bridge fabrication.

*The survey should take about 10-15 minutes.*

## Link to Survey

https://gatech.co1.qualtrics.com/jfe/form/SV_8v9PxdEp7ldp2aq

Thank you for your time and input, and please feel free to reach out using the contact information below if you have any questions, concerns, or problems accessing the survey.

Patrick Allen, PE
State Materials Engineer
Georgia Department of Transportation

Dr. Ryan J. Sherman, PE
Assistant Professor
School of Civil and Environmental Engineering
Georgia Institute of Technology
ryan.sherman@ce.gatech.edu

Matthew Phillips
Graduate Research Assistant
School of Civil and Environmental Engineering
Georgia Institute of Technology
mphillips87@gatech.edu

# GDOT Steel Quality Manual Survey

**Contact Information** Please provide your contact information below.

- ○ Name: _____
- ○ Affiliation - Position: _____
- ○ Email: _____
- ○ Phone: _____

**Followup** Are you available for any follow-up questions pending the results of this survey?

- ○ Yes.
- ○ No.

**Q1** Does your organization have a quality assurance/quality control (QA/QC) manual (or similar) for the fabrication of steel bridge superstructure components (i.e., girders, cross frames, etc.)?

- ○ Yes, we have a QA/QC manual.
- ○ No, we do not have a QA/QC manual, but we have other documents that provide guidance and/or restrictions.
- ○ No.

*Display This Question:*

*If Q1 = Yes, we have a QA/QC manual.*

**Q1-1-1** Are you able to share your QA/QC manual with us? Please note that you are able to select multiple options below simultaneously.

- ☐ Yes, it is publicly available (please provide website) _____
- ☐ Yes (with a url link) _____
- ☐ Yes (with an attachment)
- ☐ Unable to Share / Not Interested

*Display This Question:*

*If Q1-1-1 = Yes (with an attachment)*

**Q1-1-2** Please attach the document below. If multiple documents are being uploaded, please compile them and upload a single .zip folder.

*Display This Question:*

*If Q1 = Yes, we have a QA/QC manual.*

**Q1-1-3** Who is the intended audience for your QA/QC manual (e.g., fabricator, inspector, both, internal use only, etc.)?

_____

_____

_____

_____

_____

*Display This Question:*

*If Q1 = Yes, we have a QA/QC manual.*

**Q1-1-4** Which resources and/or research did your organization use to develop your QA/QC manual? Please check all boxes that apply and fill in the "Other / Not Listed" box with any resources and/or research not listed.

- ☐ AWS D1.1 - Structural Welding Code--Steel
- ☐ AASHTO/AWS D1.5 - Bridge Welding Code
- ☐ AASHTO S2.1 - Bridge Fabrication Guide Specification
- ☐ AASHTO/NSBA G4.1 or S4.1 - Steel Bridge Fabrication QC/QA Guidelines
- ☐ AASHTO G2.2 - Guidelines for Resolution of Steel Bridge Fabrication Errors
- ☐ AISC 360 - Steel Construction Manual
- ☐ AISC 303 - Code of Standard Practice
- ☐ Other / Not Listed _____

*Display This Question:*

*If Q1-1-4 = Other / Not Listed*

**Q1-1-5** Are you able to share the unlisted document(s) with us?

☐ Yes, it is publicly available (please provide the name of the resource and website) _____

☐ Yes, with a url link (please provide the name of the resource and a url link) _____

☐ Yes (with an attachment)

☐ Unable to Share / Not Interested

*Display This Question:*

*If Q1-1-5 = Yes (with an attachment)*

**Q1-1-6** Please attach the document below. If multiple documents are being uploaded, please compile them and upload a single .zip folder.

*Display This Question:*

*If Q1 = No, we do not have a QA/QC manual, but we have other documents that provide guidance and/or restrictions.*

**Q1-2-1** What documents are utilized in lieu of a QA/QC manual? Please list all applicable documents, such as standard operating procedures, guidelines, and/or other manuals.

_____

_____

_____

_____

_____

*Display This Question:*

*If Q1 = No, we do not have a QA/QC manual, but we have other documents that provide guidance and/or restrictions.*

**Q1-2-2** Are you able to share these documents with us? Please note that you are able to select multiple options below simultaneously.

- ☐ Yes, it is publicly available (please provide the name of the resource and website) _____
- ☐ Yes, with a url link (please provide the name of the resource and a url link) _____
- ☐ Yes (with an attachment)
- ☐ Unable to Share / Not Interested

*Display This Question:*

*If Q1-2-2 = Yes (with an attachment)*

**Q1-2-3** Please attach the document below. If multiple documents are being uploaded, please compile them and upload a single .zip folder.

*Display This Question:*

*If Q1 = No, we do not have a QA/QC manual, but we have other documents that provide guidance and/or restrictions.*

**Q1-2-4** Who is the intended audience for these documents (e.g., fabricator, inspector, both, internal use only, etc.)?

_____

_____

_____

_____

_____

*Display This Question:*

*If Q1 = No, we do not have a QA/QC manual, but we have other documents that provide guidance and/or restrictions.*

**Q1-2-5** Which resources and/or research did your organization use to develop these documents? Please check all boxes that apply and fill in the "Other / Not Listed" box with any resources and/or research not listed.

- [ ] AWS D1.1 - Structural Welding Code--Steel
- [ ] AASHTO/AWS D1.5 - Bridge Welding Code
- [ ] AASHTO S2.1 - Bridge Fabrication Guide Specification
- [ ] AASHTO/NSBA G4.1 or S4.1 - Steel Bridge Fabrication QC/QA Guidelines
- [ ] AASHTO G2.2 - Guidelines for Resolution of Steel Bridge Fabrication Errors
- [ ] AISC 360 - Steel Construction Manual
- [ ] AISC 303 - Code of Standard Practice
- [ ] Other / Not Listed _____

*Display This Question:*

*If Q1-2-5 = Other / Not Listed*

**Q1-2-6** Are you able to share the unlisted document(s) with us?

☐ Yes, it is publicly available (please provide the name of the resource and website) _____

☐ Yes, with a url link (please provide the name of the resource and a url link) _____

☐ Yes (with an attachment)

☐ Unable to Share / Not Interested

*Display This Question:*

*If Q1-2-6 = Yes (with an attachment)*

**Q1-2-7** Please attach the document below. If multiple documents are being uploaded, please compile them and upload a single .zip folder.

*Display This Question:*

*If Q1 = No.*

**Q1-3-1** If no QA/QC requirements are directly given to the fabricator from your organization, what processes are in place to ensure quality fabrication?

_____

_____

_____

_____

_____

**Q2** Regarding steel member fabrication nonconformances, please complete the grid below to indicate which codes, standards, and/or procedures a fabricator must follow to repair the specified nonconformances as well as indicate which nonconformances (if any) have restrictions on the number of allowable repairs.

Examples of each major nonconformance category:

IMPROPER / ERRANT HOLES: misaligned holes, improper hole location, etc.
ERRONEOUS WELDS / MINOR WELD DEFECTS: improper weld location, misaligned welded component, excessive slag, etc.
MAJOR WELD DEFECTS: overlap, undersized welds, excessive porosity, incomplete fusion, cracking, etc.
BASE MATERIAL DEFECTS: member distortion, base material cracks/notches, etc.
OTHER DEFECTS: any other defect that does not fit into the other four major categories

| | Improper / Errant Holes | Erroneous Welds / Minor Weld Defects | Major Weld Defects | Base Material Defects | Other Defects |
|---|---|---|---|---|---|
| AWS D1.1 - Structural Welding Code--Steel | ☐ | ☐ | ☐ | ☐ | ☐ |
| AASHTO/AWS D1.5 - Bridge Welding Code | ☐ | ☐ | ☐ | ☐ | ☐ |
| AASHTO G2.2 - Guidelines for Resolution of Steel Bridge Fabrication Errors | ☐ | ☐ | ☐ | ☐ | ☐ |
| Approved Repair Plan from Engineer of Record | ☐ | ☐ | ☐ | ☐ | ☐ |
| Other / Not Listed | ☐ | ☐ | ☐ | ☐ | ☐ |
| Is there a limit on the number of repairs that are allowed? | ☐ | ☐ | ☐ | ☐ | ☐ |

*Display This Question:*

*If Q2 [ Other Defects] (Count) > 0*

**Q2-1** Please describe the nonconformance(s) indicated as "Other Defects" and the applicable codes, standards, and/or procedures a fabricator must follow for their repair, if not already indicated in the previous question.

_____

_____

_____

_____

_____

*Display This Question:*

*If Q2 [ Other / Not Listed ] (Recode) Is Not Empty*

**Q2-2** Are you able to provide us with the codes, standards, and/or standard operating procedures (SOPs) that were not previously listed?

☐ Yes, it is publicly available (please provide the name of the resource and website) _____

☐ Yes, with a url link (please provide the name of the resource and a url link) _____

☐ Yes (with an attachment)

☐ Unable to Share / Not Interested

*Display This Question:*

*If Q2-2 = Yes (with an attachment)*

**Q2-2-1** Please attach the document below. If multiple documents are being uploaded, please compile them and upload a single .zip folder.

*Display This Question:*

*If Q2 [ Is there a limit on the number of repairs that are allowed? ] (Recode) Is Not Empty*

**Q2-3** Please state the nonconformance(s) that is allowed a limited number of repairs and specify why. Please be specific as possible regarding the specific nonconformance(s), the number of allowable repairs, and (if known) why the number of repairs for this particular nonconformance is limited.

_____

_____

_____

_____

_____

**Q3** Regarding the QA/QC process for welding, please fill out the grid below to indicate which nondestructive testing (NDT) methods are used to inspect the specified weld types.

| | Partial Joint Penetration (PJP) | Complete Joint Penetration (CJP) | Longitudinal Fillet Weld (i.e., weld parallel with the direction of stress flow, such as a web-to-flange junction) | Transverse Fillet Weld (i.e., weld perpendicular with the direction of stress flow, such as a transverse stiffener) |
|---|---|---|---|---|
| Radiographic Testing (RT) | ☐ | ☐ | ☐ | ☐ |
| Ultrasonic Testing (UT) | ☐ | ☐ | ☐ | ☐ |
| Phased-Array Ultrasonic Testing (PAUT) | ☐ | ☐ | ☐ | ☐ |
| Magnetic Particle Testing (MT) | ☐ | ☐ | ☐ | ☐ |
| Dye Penetrant Testing (PT) | ☐ | ☐ | ☐ | ☐ |
| Visual Inspection | ☐ | ☐ | ☐ | ☐ |
| Other / Not Listed | ☐ | ☐ | ☐ | ☐ |
| Other / Not Listed | ☐ | ☐ | ☐ | ☐ |

**Q3-1** Of the NDT methods selected, which one is most commonly used/recommended by your organization for groove welds? Why?

_____

_____

_____

_____

**Q3-2** Of the NDT methods selected, which one is most commonly used/recommended by your organization for fillet welds? Why?

**Q4** What QA/QC procedures does your organization implement to ensure that the fabricator does not deviate from the welding parameters contained within the welding procedure specification (WPS)? If these parameters are violated, what actions are taken (e.g., repairs, member rejection, etc.), and what are the consequences for the fabricator?

**Q5** In your experience, are there any areas (in relation to steel fabrication nonconformances) that you feel would benefit from additional study? In particular, has your agency experienced any situations where excessive repairs of a nonconformance ultimately led to other problems (i.e., performance issues, total member replacement, etc.)?

**Q6** In relation to steel fabrication nonconformances, are there any reports, articles, codes, standards, or standard operating procedures not mentioned yet that you believe are useful?

- ○ Yes
- ○ No

*Display This Question:*
*If Q6 = Yes*

**Q6-1** Are you able to share these resources with us?

- ☐ Yes, it is publicly available (please provide the name of the resource and website) _____
- ☐ Yes, with a url link (please provide the name of the resource and a url link) _____
- ☐ Yes (with an attachment)
- ☐ Unable to Share / Not Interested

*Display This Question:*
*If Q6-1 = Yes (with an attachment)*

**Q6-2** Please attach the document below. If multiple documents are being uploaded, please compile them and upload a single .zip folder.

**Survey Contact Info**

Thank you for taking our survey. If you have any questions, concerns, or would like to discuss anything in more detail, please feel free to contact:

Dr. Ryan J. Sherman, PE
Assistant Professor
School of Civil and Environmental Engineering
Georgia Institute of Technology
ryan.sherman@ce.gatech.edu

Matthew Phillips
Graduate Research Assistant
School of Civil and Environmental Engineering
Georgia Institute of Technology
mphillips87@gatech.edu

# APPENDIX B.

# WELDING PROCEDURE SPECIFICATIONS (WPS)

HIGH STEEL STRUCTURES LLC
An Affiliate of High Industries Inc.

HSSI Project: State Cont:
Owner:
Location:

**Material Characterization Plates - 50W**

**Welding Procedure for Prequalified Joint:**

# WP90X

| | |
|---|---|
| Material Specification | **ASTM A709 Grade 36, 50, 50W** |
| Welding Process | **Submerged Arc Welding** |
| Manual, Semiautomatic or Machine | **Semiautomatic or Machine** |
| Filler Metal Specification | **AWS 5.23** |
| Weld Metal Classification | **F8A2-ENI1K-NI1-H8** |
| Single/Multiple Arc | **Single Arc** |
| Root Treatment | **Remove all scale, rust & contaminants and grind to sound metal** |
| Electrical Stickout | **1"** |
| Shielding Gas | **N/A** |
| Required Preheat | **See preheat chart** |
| kilojoules per inch | **31.6-96.6** |

Revision:
Original Issue: **4/19/2018**

| pass # | Position | Amps | Wire Feed Speed (In.Min.) | Volts | travel speed (IPM) | polarity | wire & flux combo. | wire dia. | gas flow (CFH) |
|---|---|---|---|---|---|---|---|---|---|
| ALL | 1G | 400-550 | 80-125 | 29-41 | 14-22 | DC+ | Lincoln LA-75 / 960 | 3/32" | N/A |

**Used for TC-P4-S. Joint details and dimensions as per approved shop drawings.**

| Qualified in accordance with PQR: | | |
|---|---|---|
| AWS-13-55 | expiration: | 7/10/2018 |
| AWS-13-56 | expiration: | 7/10/2018 |
| | | |
| | | |
| | | |
| | | |

(approval stamp)

Authorized for use by Chris Lausch, CWI HSSL.

HIGH STEEL STRUCTURES LLC
An Affiliate of High Industries Inc.

HSSI Project: State Cont:
Owner:
Location:

**Material Characterization Plates - HPS70W**

**Welding Procedure for Prequalified Joint:**

# WP10X-HPS

| | |
|---|---|
| Material Specification | **ASTM A709 Grade HPS 70W** |
| Welding Process | **Submerged Arc Welding** |
| Manual, Semiautomatic or Machine | **Semiautomatic or Machine** |
| Filler Metal Specification | **AWS 5.23** |
| Weld Metal Classification | **F9A4-ENi5-G-H2** |
| Single/Multiple Arc | **Single Arc** |
| Root Treatment | **Remove all scale, rust & contaminants and grind to sound metal** |
| Electrical Stickout | **1"** |
| Shielding Gas | **N/A** |
| Required Preheat | **See preheat chart** |
| kilojoules per inch | **33.0- 89.6** |

Revision: **3/10/2017**
Original Issue: **3/10/2003**

| pass # | Position | Amps | Wire Feed Speed (In.Min.) | Volts | travel speed (IPM) | polarity | wire & flux combo. | wire dia. | gas flow (CFH) |
|---|---|---|---|---|---|---|---|---|---|
| ALL | 1G | 410-550 | 83-125 | 29.5-38 | 14-22 | DC+ | Lincoln LA-85 /MIL800 | 3/32" | N/A |

**May be used for FCM and non-FCM welding applications**

**Used for Web to Flange Splicing**

Backgouge and grind to sound weld. May be used for approved repair welds.

| Qualified in accordance with PQR: | | |
|---|---|---|
| AWS-14-11 | expiration: | 5/2/2019 |
| AWS-14-12 | expiration: | 5/6/2019 |
| | | |
| | | |
| | | |
| | | |

(approval stamp)

Authorized for use by Chris Lausch, CWI/ WPC HSS.

HIGH STEEL STRUCTURES LLC
An Affiliate of High Industries Inc.

HSSI Project: 1240999H State Cont:

Owner: Georgia Tech

Location:

**Built-Up I-Girders - 50W Flange-to-Web Fillet Weld**

**Welding Procedure for AWS D1.5 Prequalified Joints:**

# WP13X

| | |
|---|---|
| Material Specification | **ASTM A709 Grade 50, 50W** |
| Welding Process | **Submerged Arc Welding** |
| Manual, Semiautomatic or Machine | **Machine** |
| Filler Metal Specification | **AWS A5.23** |
| Weld Metal Classification | **F8A2-ENi1K-Ni1-H4** |
| Single/Multiple Arc | **Single Arc** |
| Root Treatment | **Remove all mill scale, rust & contaminants** |
| Electrical Stickout | **1"** |
| Required Preheat | **See preheat chart** |
| K. Joules (per in.) | **41.1-90.8** |

| | |
|---|---|
| Revision: | **8/8/2024** |
| Original Issue: | **9/7/2017** |

| Pass # | position | amps | approx. wire feed speed | volts | travel speed (IPM) | Polarity | wire & flux combo. | wire dia. |
|---|---|---|---|---|---|---|---|---|
| 1 | 2F | 530-550 | 185-195 | 37.4-39.5 | 17-21 | DCEN | Lincoln LA-75 / 960 | 3/32" |

**Web to Flange 5/16" Single Pass Fillet Welds.**

JOINT DETAIL
FILLET WELDS

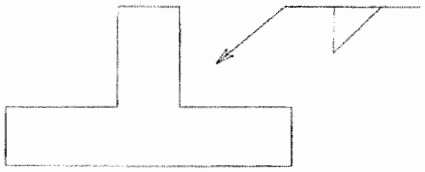

Minimum Preheat Requirements.

| Thickness at thickest part at point of welding. (Inches) | ASTM A709 Grade 50, 50W |
|---|---|
| To 3/4 inclusive | 50°F |
| Over 3/4 to 1-1/2 inclusive | 70°F |
| Over 1-1/2 to 2-1/2 inclusive | 150°F |
| Over 2-1/2 | 225°F |
| Maximum Preheat = 450°F | |
| Maximum Interpass = 550°F | |

QC APPROVED

AWS

Christopher D Lausch
CWI 17021851
QC1 EXP. 2/1/2026

Authorized for use by Chris Lausch, CWI HSSL.

HIGH STEEL STRUCTURES LLC
An Affiliate of High Industries Inc.

HSSI Project: 1240999H State Cont:

Owner: Georgia Tech

Location: **Built-Up I-Girders - HPS70W Flange-to-Web Fillet Weld**

**Welding Procedure for AWS D1.5 Prequalified Joints:**

# WP13XHPS

| | |
|---|---|
| Material Specification | **ASTM A709 Grade 50/50W to HPS70W, HPS70W to HPS70W** |
| Welding Process | **Submerged Arc Welding** |
| Manual, Semiautomatic or Machine | **Machine or Semiautomatic** |
| Filler Metal Specification | **AWS A5.23** |
| Weld Metal Classification | **F8A2-ENi1K-Ni1-H4** |
| Single/Multiple Arc | **Single Arc** |
| Root Treatment | **Remove all mill scale, rust & contaminants** |
| Electrical Stickout | **1"** |
| Required Preheat | **See preheat chart** |
| Kilojoules Per Inch | **41.1-90.8** |

Revision: **6/20/2023**
Original Issue: **3/15/2021**

| Pass # | Position | Amps | Wire feed speed (IPM) | Volts | Travel speed (IPM) | Polarity | Wire & flux combo. | Wire dia. (IN.) |
|---|---|---|---|---|---|---|---|---|
| 1 | 2F | 530-550 | 185-195 | 37.4-39.5 | 17-21 | DCEN | Lincoln LA-75 / 960 | 3/32" |

**Web to Flange 5/16" Single Pass Fillet Welds.**

JOINT DETAIL
FILLET WELDS

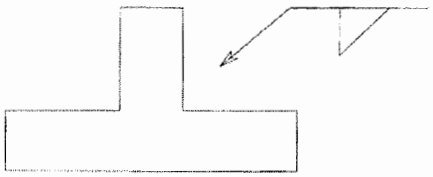

Minimum Preheat Requirements.

| Thickness at thickest part at point of welding. (Inches) | ASTM A709 Grade 50W, HPS70W |
|---|---|
| To 3/4 inclusive | 50°F |
| Over 3/4 to 1-1/2 inclusive | 125°F |
| Over 1-1/2 to 2-1/2 inclusive | 175°F |
| Over 2-1/2 | 225°F |
| Maximum Preheat = 450°F | |
| Maximum Interpass = 450°F | |

QC APPROVED
(approval stamp)
AWS
Christopher D Lausch
CWI 17021851
QC1 EXP. 2/1/2026

Authorized for use by Chris Lausch, CWI HSSL.

HIGH STEEL STRUCTURES LLC
An Affiliate of High Industries Inc.

HSSI Project: 1240999H State Cont:

Owner: Georgia Tech

Location:

**Built-Up I-Girders - 50W Flanges**

## Welding Procedure for AWS D1.5 Prequalified Joints:

# WP71X

| | |
|---|---|
| Material Specification | **ASTM A709 Grade 50, 50W** |
| Welding Process | **Submerged Arc Welding** |
| Manual, Semiautomatic or Machine | **Semiautomatic or Machine** |
| Filler Metal Specification | **AWS A5.23** |
| Weld Metal Classification | **F8A2-ENi1K-Ni1-H4** |
| Single/Multiple Arc | **Single Arc** |
| Root Treatment | **Remove all scale, rust & contaminants and grind to sound metal** |
| Electrical Stickout | **1"** |
| Required Preheat | **See preheat chart** |
| kilojoules per inch | **31.6-96.6** |

| | |
|---|---|
| Revision: | **4/13/2023** |
| Original Issue: | **4/19/2018** |

| pass # | Position | Amps | Wire Feed Speed (In.Min.) | Volts | travel speed (IPM) | polarity | wire & flux combo. | wire dia. |
|---|---|---|---|---|---|---|---|---|
| ALL | 1G | 400-550 | 80-125 | 29-41 | 14-22 | DCEP | Lincoln LA-75 / 960 | 3/32" |

**Used for Web and Flange Splicing and Repair**

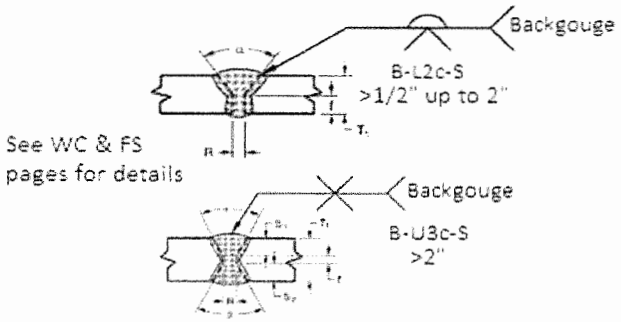


Minimum Preheat Requirements.

| Thickness at thickest part at point of welding. (Inches) | ASTM A709 Grade 50, 50W |
|---|---|
| To 3/4 inclusive | 50°F |
| Over 3/4 to 1-1/2 inclusive | 70°F |
| Over 1-1/2 to 2-1/2 inclusive | 150°F |
| Over 2-1/2 | 225°F |
| Maximum Preheat = 450°F | |
| Maximum Interpass = 550°F | |

QC APPROVED

AWS®
Christopher D Lausch
CWI 17021851
QC1 EXP. 2/1/2026

Authorized for use by Chris Lausch, CWI HSSL.

HIGH STEEL STRUCTURES LLC
An Affiliate of High Industries Inc.

HSSI Project: 1240999H State Cont:

Owner: Georgia Tech

Location:

**Built-Up I-Girders - HPS70W Flanges**

## Welding Procedure for AWS D1.5 Prequalified Joints:

# WP71XHPS

| | |
|---|---|
| Material Specification | **ASTM A709 Grade HPS70W** |
| Welding Process | **Submerged Arc Welding** |
| Manual, Semiautomatic or Machine | **Semiautomatic or Machine** |
| Filler Metal Specification | **AWS A5.23** |
| Weld Metal Classification | **F9A4-ENi5-G-H2** |
| Single/Multiple Arc | **Single Arc** |
| Root Treatment | **Remove all scale, rust & contaminants and grind to sound metal** |
| Electrical Stickout | **1"** |
| Required Preheat | **See preheat chart** |
| kilojoules per inch | **40.3-84.9** |

| | |
|---|---|
| Revision: | **2/2/2023** |
| Original Issue: | **1/16/2018** |

| pass # | Position | Amps | Wire Feed Speed (In.Min.) | Volts | travel speed (IPM) | polarity | wire & flux combo. | wire dia. |
|---|---|---|---|---|---|---|---|---|
| ALL | 1G | 410-550 | 83-125 | 29.5-36 | 14-18 | DCEP | Lincoln LA-85 /MIL800HPNi | 3/32" |

**Used for Web and Flange Splicing and Repair**

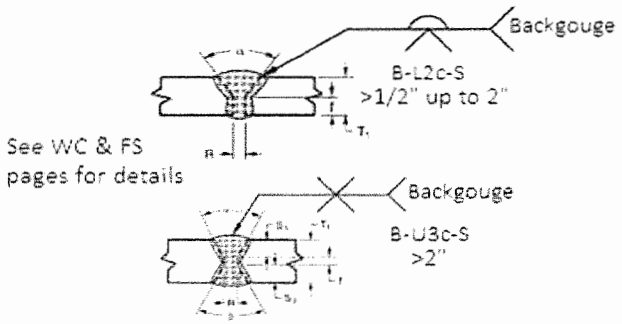


Minimum Preheat Requirements.

| Thickness at thickest part at point of welding. (Inches) | ASTM A709 Grade HPS70W |
|---|---|
| To 3/4 inclusive | 50°F |
| Over 3/4 to 1-1/2 inclusive | 125°F |
| Over 1-1/2 to 2-1/2 inclusive | 175°F |
| Over 2-1/2 | 225°F |
| Maximum Preheat = 450°F | |
| Maximum Interpass = 450°F | |

Q C APPROVED

AWS® Christopher D Lausch
CWI 17021851
QC1 EXP. 2/1/2026

Authorized for use by Chris Lausch, CWI HSSL.

# APPENDIX C.

# SIDE-BEND TEST PHOTOS

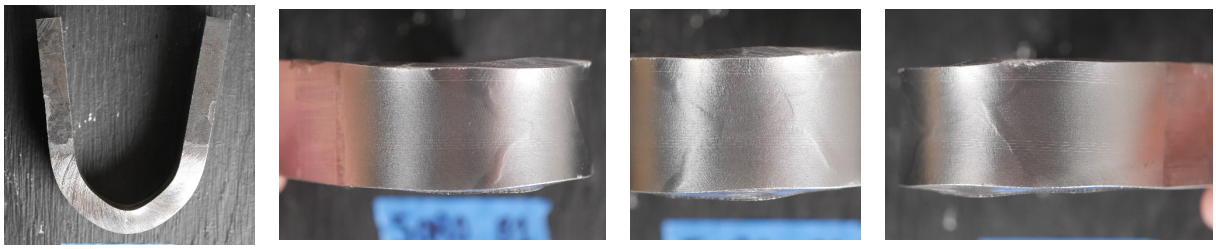

50-R0-B1

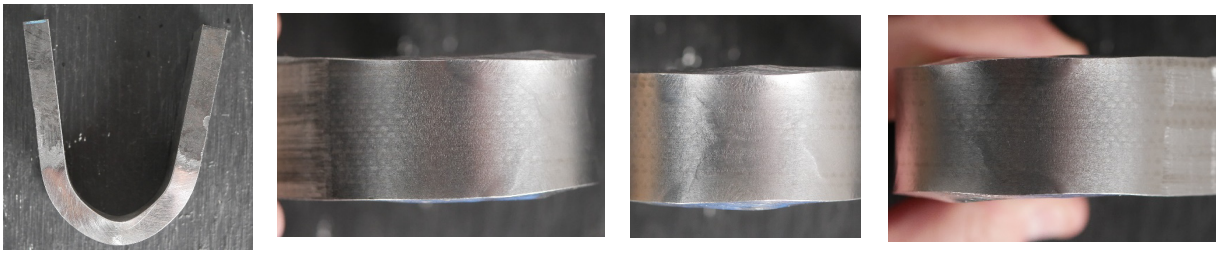

50-R0-B2

**Figure C-1. Multiple Photos. Side-Bend Test Photos for 50-R0.**

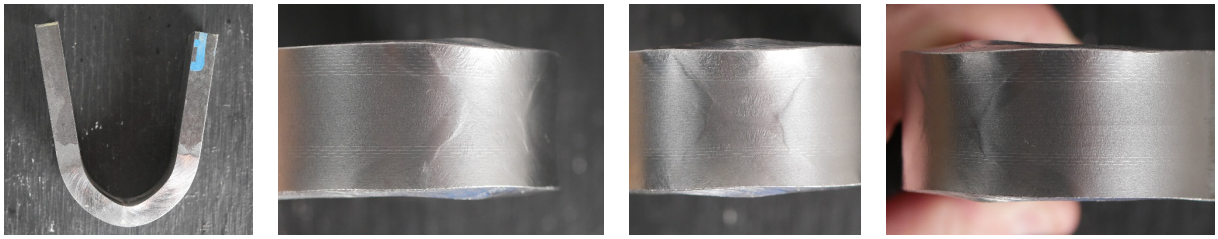

50-R1-B1

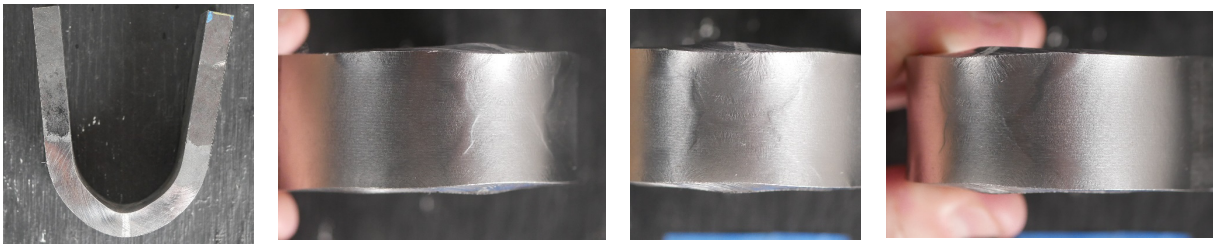

50-R1-B2

**Figure C-2. Multiple Photos. Side-Bend Test Photos for 50-R1.**

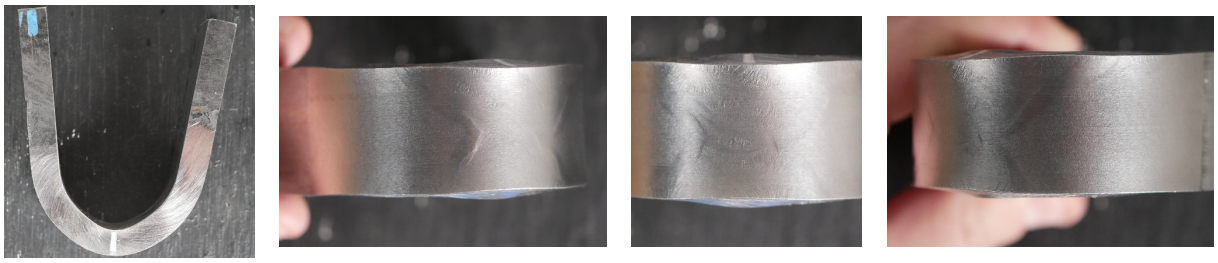

50-R2-B1

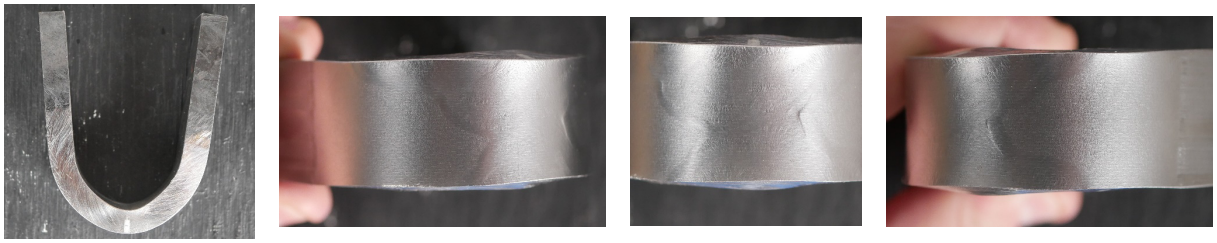

50-R2-B2

**Figure C-3. Multiple Photos. Side-Bend Test Photos for 50-R2.**

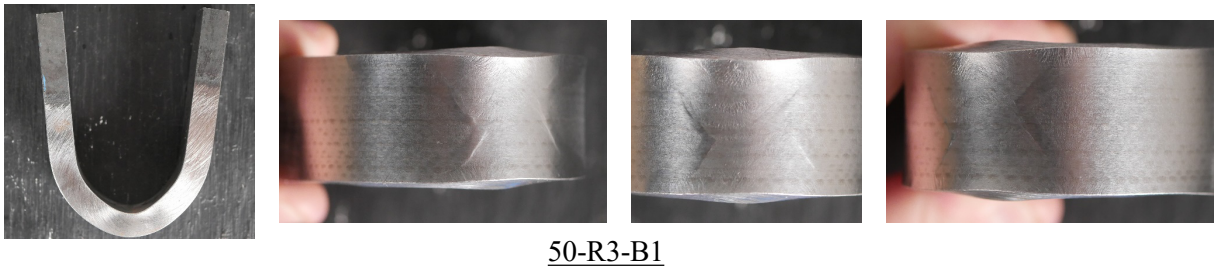

50-R3-B1

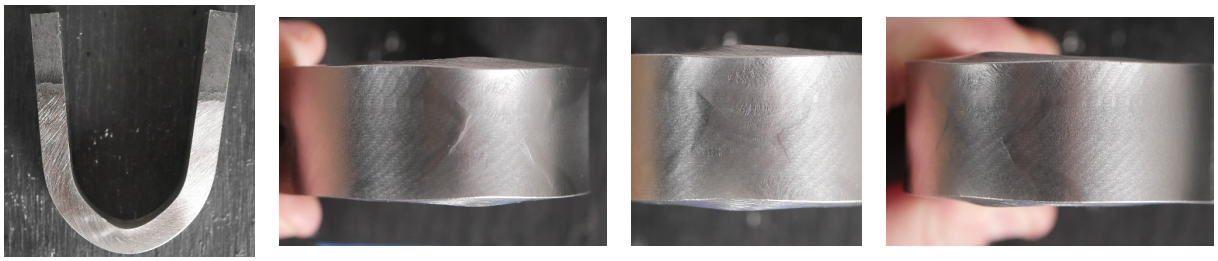

50-R3-B2

**Figure C-4. Multiple Photos. Side-Bend Test Photos for 50-R3.**

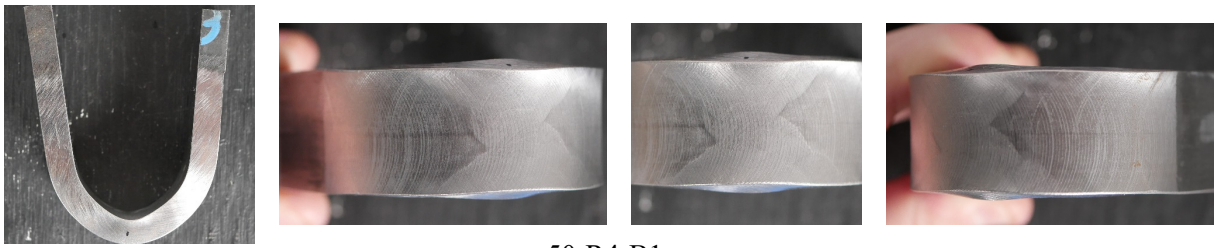

50-R4-B1

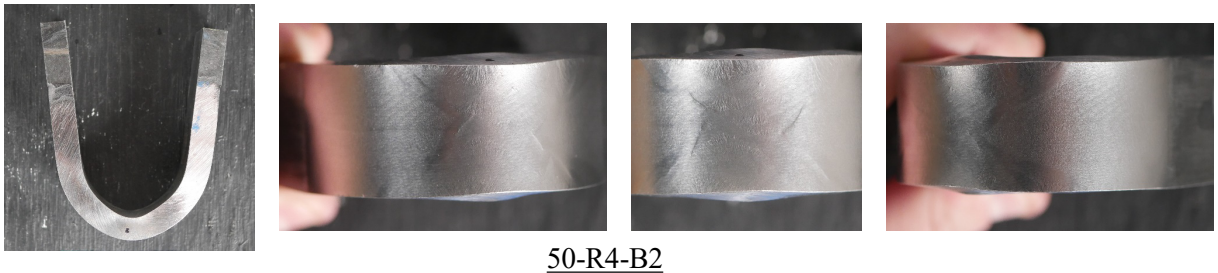

50-R4-B2

**Figure C-5. Multiple Photos. Side-Bend Test Photos for 50-R4.**

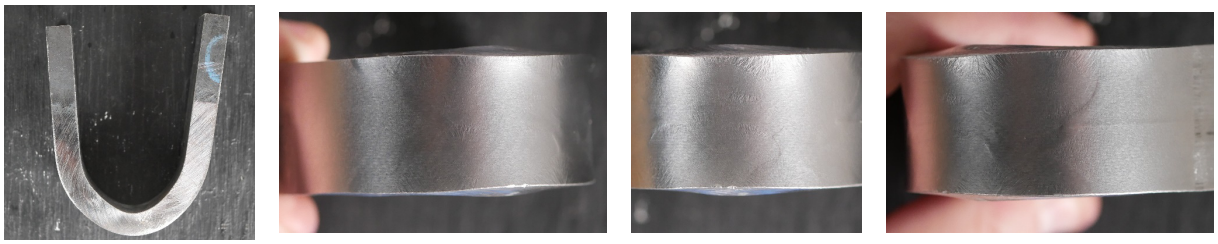

50-R5-B1

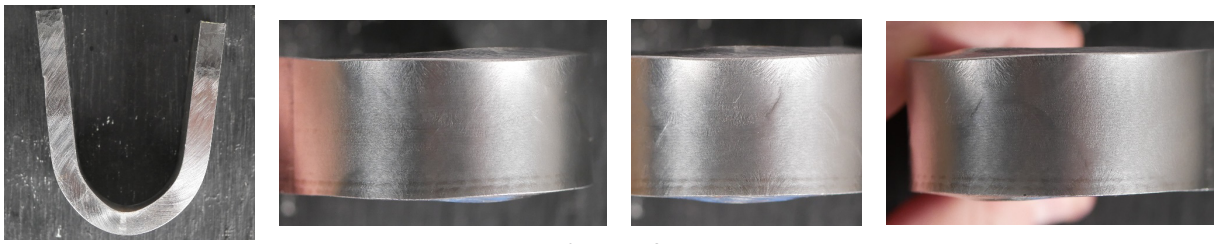

50-R5-B2

**Figure C-6. Multiple Photos. Side-Bend Test Photos for 50-R5.**

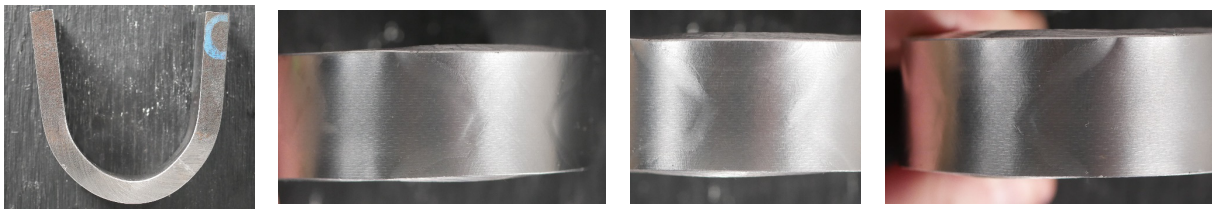

70-R0-B1

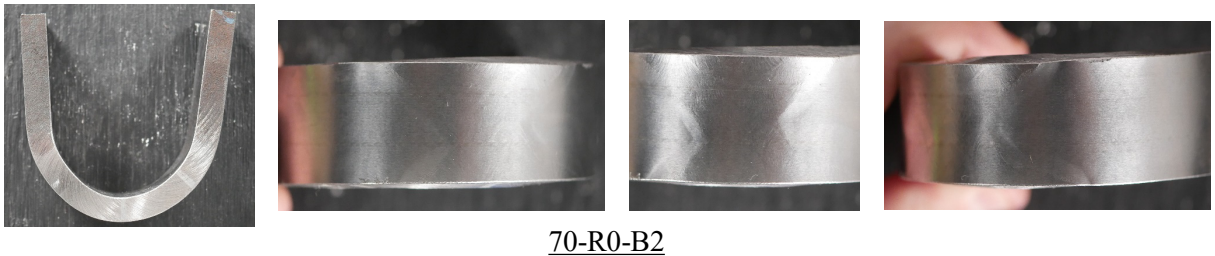

70-R0-B2

**Figure C-7. Multiple Photos. Side-Bend Test Photos for 70-R0.**

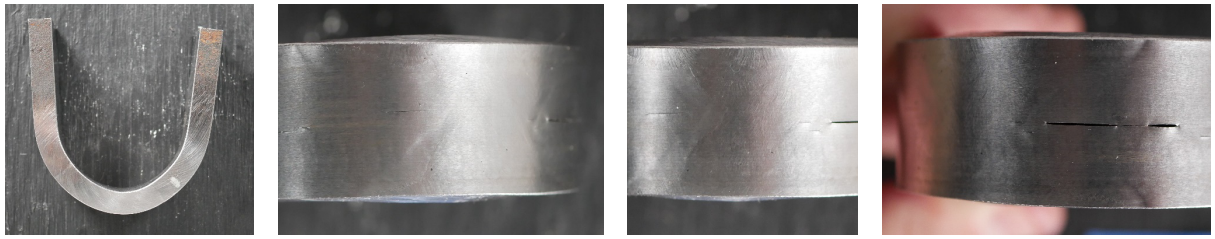

70-R1-B1

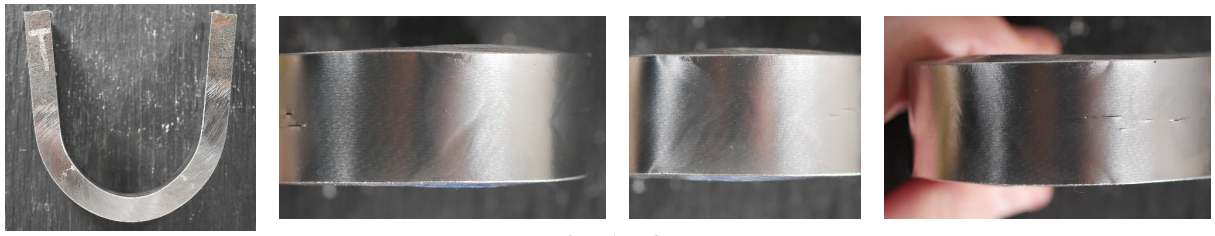

70-R1-B2

**Figure C-8. Multiple Photos. Side-Bend Test Photos for 70-R1.**

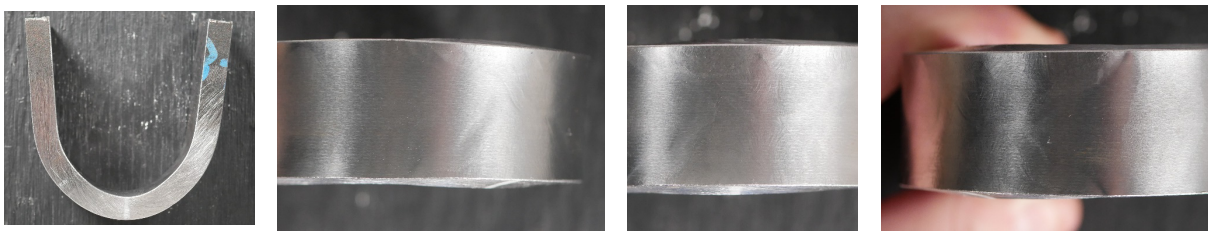

70-R3-B1

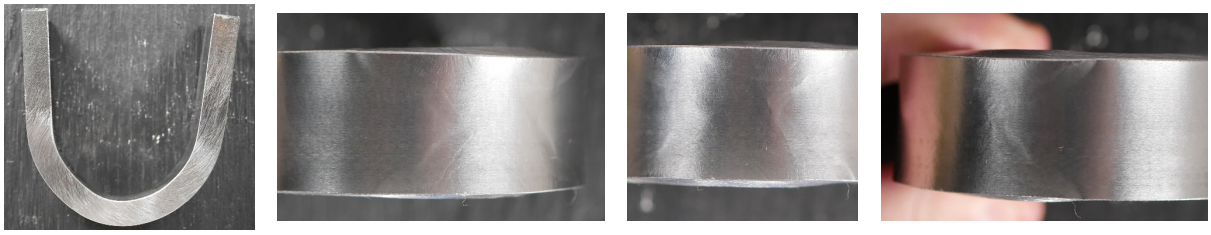

70-R3-B2

**Figure C-9. Multiple Photos. Side-Bend Test Photos for 70-R3.**

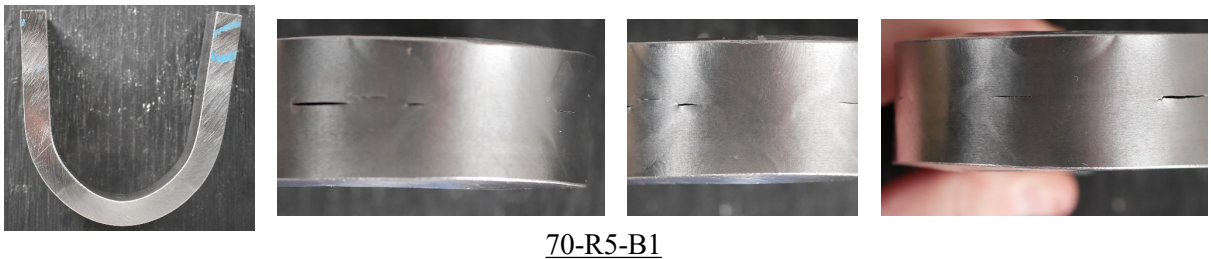

70-R5-B1

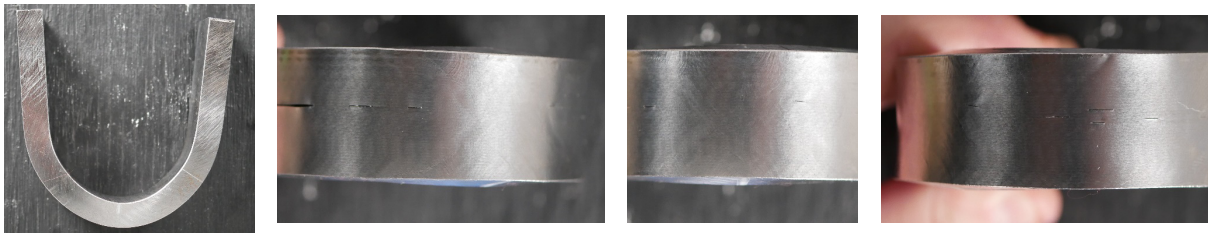

70-R5-B2

**Figure C-10. Multiple Photos. Side-Bend Test Photos for 70-R5.**

# APPENDIX D.

# GDOT STEEL FABRICATION QUALITY MANUAL – DEVELOPMENT AND LAYOUT INFORMATION

A primary deliverable of the research program was the development of the first draft of the GDOT Steel Fabrication Quality Manual (SFQM). The GDOT SFQM was created as a comprehensive document that supplements the fabrication and inspection requirements specified in the GDOT *Standard Construction Specifications* and is intended to supersede GDOT SOP8, the current standard operating procedure for fabricating, handling, transporting, storing, and field connections of bridge structural steel in Georgia. The purpose of the GDOT SFQM is to define a consistent set of standards and guidelines for the GDOT steel bridge quality assurance (QA) program and to provide guidance to the quality control (QC) and quality assurance inspectors. The GDOT SFQM establishes a baseline QA program for GDOT, and it conveys the minimum QC requirements and expectations to the fabricator. Due to the size and complexity of the document, the first draft of the GDOT SFQM is available as a standalone document titled *GDOT Steel Fabrication Quality Manual*. The resources used to develop the GDOT SFQM and some general layout information are discussed below.

As indicated in Section 3.2, one goal of the AASHTO member survey was to gather resources and sample quality manuals from other states to ensure that the GDOT SFQM meets or exceeds the quality of other manuals currently in use. In total, eight states provided example copies of their quality manuals. The state and the name of the quality documents are provided below (year of last revision and page count are shown in parentheses for reference):

- Colorado – QAP 5900 – Structural Steel QA Program – Bridges (2019 – 28 pages)
- Delaware – Fabrication Steel QC/QA Procedure (unknown – 5 pages)
- Indiana – Manual for Instructions for Structural Steel Shop Inspection (2007 – 55 pages)
- Michigan – Structural Fabrication Quality Manual (August 2021 – 124 pages)
- Minnesota – Structural Metals Manual and Quality Assurance Plan (2023 – 43 pages)

- Missouri – Quality Assurance Guidelines (2023 – 31 pages)
- Pennsylvania – Pub. 135: Inspection of Fabricated Structural Steel (2019 – 61 pages)
- Vermont – Quality Assurance Manual for Metal Fabrication (2020 – 10 pages)

Each of the documents listed above, and many of those listed in Section 3.1, were used during the development of the GDOT SFQM.

The GDOT SFQM is comprised of 14 main chapters:

- Chapter 1: GDOT Commitment to Quality
- Chapter 2: General Information
- Chapter 3: Reference Documents
- Chapter 4: Fabricator Plant Qualification Requirements
- Chapter 5: Inspector Qualifications and Equipment
- Chapter 6: Records and Reporting
- Chapter 7: Shop Fabrication, Workmanship, and Inspection
- Chapter 8: Field Connections
- Chapter 9: Request for Information Process
- Chapter 10: Nonconformances
- Chapter 11: Corrective Action Request Process
- Chapter 12: Calibration and Verification of Inspection Equipment
- Chapter 13: Handling, Storage, and Delivery of Products
- Chapter 14: Audits

The chapter content is self-evident from most of the chapter titles; however, an explanatory paragraph is provided at the beginning of each chapter in the GDOT SFQM that details exactly

what is covered in that chapter. Of note are Chapters 7 and 10. Chapter 7 has specific subsections that discuss the general requirements, inspection criteria, allowable repair procedures, and final acceptance criteria for base metals, welding, bolted connections, and coatings. Chapter 10 discusses the general procedure to be followed to address minor and major nonconformances, which blanketly covers all fabrication nonconformances.